CESPU
INSTITUTO UNIVERSITÁRIO
DE CIÊNCIAS DA SAÚDE

Therapeutic targeting of spindle assembly checkpoint silencing as a strategy to sensitize cancer cells to chemotherapy drugs

Ana Cristina do Espírito Santo Henriques

Tese conducente ao **Grau de Doutor** em **Ciências Biomédicas**

—

Gandra, **novembro de 2022**

CESPU
INSTITUTO UNIVERSITÁRIO
DE CIÊNCIAS DA SAÚDE

Ana Cristina do Espírito Santo Henriques

Tese conducente ao Grau de Doutor em Ciências Biomédicas

Therapeutic targeting of spindle assembly checkpoint silencing as a strategy to sensitize cancer cells to chemotherapy drugs

Trabalho realizado sob a Orientação de

Professor Doutor Hassan Bousbaa e Co-orientador Professor Doutor Bruno Sarmento

CESPU
INSTITUTO UNIVERSITÁRIO
DE CIÊNCIAS DA SAÚDE

DECLARAÇÃO DE INTEGRIDADE

Eu, acima identificada, declaro ter atuado com absoluta integridade na elaboração deste trabalho, confirmo que em todo o trabalho conducente à sua elaboração não recorri a qualquer forma de falsificação de resultados ou à prática de plágio (ato pelo qual um indivíduo, mesmo por omissão, assume a autoria do trabalho intelectual pertencente a outrem, na sua totalidade ou em partes dele). Mais declaro que todas as frases que retirei de trabalhos anteriores pertencentes a outros autores foram referenciadas ou redigidas com novas palavras, tendo neste caso colocado a citação da fonte bibliográfica.

Ana Cristina do Espírito Santo Henriques

(Ana Cristina do Espírito Santo Henriques)

Acknowledgments

I would like to express my gratitude to all the people that directly and indirectly contributed to my evolution during all the years of my Ph.D.

Ao meu orientador, Prof. Doutor Hassan Bousbaa, pelo acompanhamento pedagógico, e por todo o apoio, paciência, disponibilidade e dedicação. Por nunca ter desistido de mim e por me ter ajudado a crescer e a evoluir.

Ao meu co-orientador, Prof. Doutor Bruno Sarmento, pelo apoio e conhecimentos transmitidos.

À Patrícia Silva, por todo o apoio incondicional dentro e fora do laboratório. Por todos os conhecimentos transmitidos, pela dedicação. Pela amizade sincera, pela luz.

À Virgínia Gonçalves, por todo o apoio e pela amizade.

À Fernanda Garcez, por todo apoio, disponibilidade e conhecimentos transmitidos.

À D. Rosária, por todo o apoio e disponibilidade.

A todo o pessoal técnico da CESPU, por toda a disponibilidade e por todo o apoio, em especial: à Paula Oliveira, à Isabel Marques, à Zélia Ferreira, Paula Vinhas, à Paula Abreu e à D. Matilde.

Aos meus amigos e colegas de laboratório, a minha família CESPU. Em especial:

à Barbara Pinto, pela amizade incondicional e pelo carinho, pela alegria, pelo brilho;

ao João Silva, o meu "melguinha" :), pelo companheirismo e por todas as gargalhadas;

ao Pedro Novais, pelo companheirismo e pelos "brainstorms".

Àqueles que já passaram pela CESPU, em especial:

à Diana Ribeiro, pela amizade sincera, pelo apoio e carinho que permanecem muito para além do laboratório;

à Viviana Vasconcelos e à Sandra Marques, à Vanessa Nascimento e à Joana Fonseca, pela amizade e por todos os bons momentos passados:

à Marta Lourenço, por toda a amizade, companheirismo e apoio que permanecem;

ao Fábio França, por toda a amizade e companheirismo;

ao Joel Pedrosa e ao Ricardo Gonçalves, pela amizade, companheirismo, e por todas as gargalhadas.

A todos os amigos e a todas as pessoas da minha família que, de algum modo, sempre me apoiaram e me acompanharam.

À Vanessa Ribeiro, pela amizade sincera, pelo carinho, apoio, e compreensão ao longo de tantos anos.

Às minhas meninas Sílvia Andrade, Joana Neves, Letícia Costa e Mariline Gameiro, que me acompanham desde os tempos de Coimbra, e também à Diana Carvalho, que estejas bem.

À Maria Helena Oliveira, que me apoiou incondicionalmente durante minha integração no mundo académico, e cujo apoio foi tão importante para que eu conseguisse um dia fazer um doutoramento.

Aos meus pais e avó, por todo o amor, apoio, carinho e paciência incondicionais ao longo de toda a minha vida.

Em memória da minha tia Fernanda Silva, pelo teu amor, pela tua alegria e energia contagiantes, mesmo em momentos tão complicados para ti. Pela tua força e incentivo, pelas tuas orações, pela tua luz. Espero que estejas orgulhosa.

The work presented in this thesis was conducted at:

Cancer Research Group

IINFACTS – Institute of Research and Advanced Training in Health Sciences and Technologies |

CESPU – Cooperativa de Ensino Superior e Universitário

Rua Central de Gandra, 1317

4585-116 Gandra PRD, Portugal

iinfacts.cespu.pt

And

Nanomedicines & Translational Drug Delivery Lab

i3S - Instituto de Investigação e Inovação em Saúde

INEB - Instituto Nacional de Engenharia Biomédica

University of Porto, Porto, Portugal

Rua Alfredo Allen, 208

4200-135 Porto, Portugal

www.i3s.up.pt | www.ineb.up.pt

And

Natural Products and Medicinal Chemistry Group

CIIMAR-UP - Interdisciplinary Centre of Marine and Environmental Research,

University of Porto

Terminal de Cruzeiros do Porto de Leixões, Av. General Norton de Matos s/n

4450-208 Matosinhos, Portugal

ciimar.up.pt

CESPU
INSTITUTO UNIVERSITÁRIO
DE CIÊNCIAS DA SAÚDE

Financial Support

Ana Cristina do Espírito Santo Henriques was supported by a national PhD grant (SFRH/BD/116167/2016) from Fundação para a Ciência e a Tecnologia (FCT).

This dissertation was financed by CESPU (project references: ComeTarget_CESPU2017, CRISPRTech-CESPU-2018, ComeTax_CESPU2019), and by national Portuguese funding through FCT (030014 (Call: 02/SAICT/2017))

Publications

The following works already published resulted directly from the elaboration of the thesis and/or are integrant part of it:

- **Henriques, A.C.**; Silva, P.M.A.; Sarmento, B.; Bousbaa, H.. "Antagonizing the spindle assembly checkpoint silencing enhances paclitaxel and Navitoclax-mediated apoptosis with distinct mechanistic". Scientific Reports 11 1 (2021): http://dx.doi.org/10.1038/s41598-021-83743-7.

- **Henriques, A.C.**; Silva, P.M.A.; Sarmento, B.; Bousbaa, H.. "The Mad2-Binding Protein p31^{comet} as a potential target for human cancer therapy". Current Cancer Drug Targets 21 (2021): http://dx.doi.org/10.2174/1568009621666210129095726.

- Pinto, B.; **Henriques, A.C.**; Silva, P.M.A.; Bousbaa, H. "Three-dimensional spheroids as in vitro preclinical models for cancer research". Pharmaceutics 12 12 (2020): 1-38. https://doi.org/10.3390/pharmaceutics12121186

- **Henriques, A.C.**; Ribeiro, D.; Pedrosa, J.; Sarmento, B.; Silva, P.M.A.; Bousbaa, H. "Mitosis inhibitors in anticancer therapy: When blocking the exit becomes a solution". Cancer Letters 440-441 (2019): 64-81. https://doi.org/10.1016/j.canlet.2018.10.005

The following publications resulted from the participation in parallel projects, in the scope of the doctoral program and/or to develop expertise required for the elaboration of the thesis:

- De Marco, P.; **Henriques, A.C.**; Azevedo, R.; Sá, S.I.; Cardoso, A.; Fonseca, B.; Barbosa, J.; Leal, S.. "Gut microbiome composition and metabolic status are differently affected by early exposure to unhealthy diets in a rat model". Nutrients 2021,13, 3236. https://doi.org/10.3390/nu13093236

- Loureiro, D. R. P.; Magalhães, A. F.; Soares, J. X.; Pinto, J.; Azevedo, C.M.G.; Vieira, S.; **Henriques, A.C.**; *et al.* "Yicathins B and C and Analogues: Total Synthesis, Lipophilicity and Biological Activities". ChemMedChem 15 9 (2020): 749-755. http://dx.doi.org/10.1002/cmdc.201900735.

- França, F.; Silva, P.M.A.; Soares, J.X.; **Henriques, A.C.**; Loureiro, D.R.P.; Azevedo, C. M.G.; Afonso, C.M.M.; Bousbaa, H.. "A Pyranoxanthone as a Potent Antimitotic and Sensitizer of Cancer

Cells to Low Doses of Paclitaxel". Molecules (Basel, Switzerland) 25 24 (2020): https://doi.org/10.3390/molecules25245845

- Pinto, P.; Machado, C. Ma.; Moreira, J.; Almeida, J.D.P.; Silva, P.M.A.; **Henriques, A.C.**; Soares, J. X.; et al. "Chalcone derivatives targeting mitosis: Synthesis, evaluation of antitumor activity and lipophilicity". European Journal of Medicinal Chemistry (2019): 111752. http://dx.doi.org/10.1016/j.ejmech.2019.111752.

Abstract

Microtubule-targeting agents (MTAs) have been widely used in cancer treatment. By interfering with microtubules, MTAs activate the spindle assembly checkpoint (SAC), delaying cells in mitosis. SAC prevents metaphase to anaphase transition until all chromosomes are correctly attached to the spindle microtubules and bi-oriented in the metaphase plate. Hence, chronic activation of SAC induced by MTAs is expected to lead to cell death. However, resistance to MTAs, namely due to their effect on microtubules, limit their efficacy, allowing cells to escape cell death through premature mitotic exit, or slippage. Therefore, alternative antimitotics that do not interfere with microtubules have been investigated. Regulators of the SAC emerged as attractive targets, either individually or in combination with other drugs. Indeed, combination therapy has been used as a method to overcome drug resistance.

In this thesis, targeting of the SAC silencer p31^{comet} was investigated as a strategy to potentiate the efficacy of anticancer drugs.

First, p31^{comet} knockdown was assessed in combination with the MTA paclitaxel or with the pro-apoptotic Navitoclax, using cell non-small cell lung cancer (NSCLC) cells. Knockdown of p31^{comet} enhanced paclitaxel and Navitoclax cytotoxicity through distinct mechanistic. p31^{comet} knockdown increased mitotic block duration in cells challenged with nanomolar concentrations of paclitaxel, leading to an additive effect in terms of cell death which was predominantly anticipated during the first mitosis. On the other hand, when p31^{comet}-depleted mitotic-arrested cells were challenged with the apoptosis potentiator Navitoclax, cell fate was shifted to accelerated post-mitotic death. The efficacy of this strategy was further validated in 3D monotypic spheroids. Notably, p31^{comet} knockdown enhanced the cytotoxicity of clinically relevant doses of paclitaxel and Navitoclax in NSCLC spheroids.

Secondly, the clinical relevance of p31^{comet} was investigated in oral cancer. p31^{comet} expression was first screened across omics data on head and neck squamous carcinoma (HNSCC), and associated with other genes and relevant signaling pathways, as well as with clinicopathological features. p31^{comet} was overexpressed in HNSCC samples compared to normal tissues. Moreover, p31^{comet} overexpression coincided with changes in pathways that are frequently dysregulated in cancer, and with altered-chromatin status, highlighting its clinical relevance in oral cancer. p31^{comet} was also positively correlated with its interactors Mad2 and TRIP13. However, the isolated impact of

p31^{comet} expression on the survival of HNSCC patients was not conclusive. Remarkably, p31^{comet} knockdown potentiated the cytotoxicity of cisplatin in OSCC cells that displayed more resistance to cisplatin.

In conclusion, p31^{comet} inhibition is a promising strategy to enhance the lethality of antimicrotubule drugs and apoptosis-inducing small molecules in NSCLC, with distinct mechanisms. Moreover, p31^{comet} is a potential target with clinical relevance in oral cancer, and the combination of p31^{comet} inhibition with cisplatin deserves to be explored for oral cancer in the context of cisplatin resistance. Overall, this work reinforces the significance of SAC targeting in cancer treatment.

Keywords: p31^{comet}, spindle assembly checkpoint, slippage, antimitotic strategies, BH3-mimetics, cancer.

Resumo

Os agentes anti-microtúbulos (MTAs) têm sido amplamente usados no tratamento do cancro. Ao interferir com a dinâmica dos microtúbulos, levam à ativação do *checkpoint* mitótico (SAC), provocando uma paragem em mitose. O SAC impede a transição metafase-anafase até os cromossomas se encontrarem corretamente ligados aos microtúbulos do fuso mitótico e alinhados na placa metafásica. Assim, espera-se que a ativação do SAC induzida pelos MTAs resulte em morte celular. Contudo, a resistência aos MTAs, nomeadamente devido ao seu efeito sobre os microtúbulos, limita a sua eficácia, permitindo às células escaparem à morte celular através da saída prematura da mitose, ou *slippage*. Deste modo, têm sido investigados antimitóticos alternativos que não interfiram com os microtúbulos. Os reguladores do SAC têm emergido como alvos atrativos, individualmente, ou em combinação com outros fármacos. De facto, a terapia de combinação tem sido usada para contornar a resistência aos fármacos.

Na tese apresentada, a depleção da proteína silenciadora do SAC p31^{comet} foi investigada como estratégia para potenciar a eficácia de fármacos anticancerígenos.

Primeiro, o *knockdown* da p31^{comet} foi avaliado em combinação com o MTA paclitaxel ou com o pró-apoptótico Navitoclax em células de cancro do pulmão de não pequenas células (CPNPC). O *knockdown* da p31^{comet} aumentou a citotoxicidade do paclitaxel ou do Navitoclax através de mecanismos distintos. O *knockdown* da p31^{comet} aumentou a duração da mitose em células tratadas com concentrações nanomolares de paclitaxel, levando a um efeito aditivo em termos de morte celular, que foi predominantemente antecipada durante a primeira mitose. Por outro lado, o pro-apoptótico Navitoclax acelerou a morte pós-mitose em células depletadas de p31^{comet}. A eficácia desta estratégia foi posteriormente validada em esferóides 3D monotípicos. Assim, o *knockdown* da p31^{comet} aumentou a citotoxicidade de doses clinicamente relevantes de paclitaxel ou Navitoclax em esferóides de CPNPC.

Em segundo lugar, investigou-se a relevância clínica da p31^{comet} no cancro oral. A expressão da p31^{comet} foi averiguada em dados ómicos de carcinoma de células escamosas de cabeça e pescoço (CCECP), e relacionada com genes e vias de sinalização relevantes, bem como com características clínico-patológicas. A p31^{comet} encontrava-se em amostras de CCECP, comparativamente a tecidos normais. Adicionalmente, a expressão da p31^{comet} coincidiu com modificações em vias frequentemente desreguladas no cancro, e com alterações na cromatina, evidenciando a sua significância

clínica. Observou-se também uma correlação positiva entre a p31^{comet} e os seus parceiros Mad2 e TRIP13. Contudo, o impacto isolado da expressão da p31^{comet} na sobrevivência dos pacientes de CCECP foi inconclusivo. Notavelmente, o *knockdown* da p31^{comet} em células de carcinoma oral de células escamosas potenciou a citotoxicidade da cisplatina na linha mais resistência à cisplatina.

Em suma, a inibição da p31^{comet} é uma estratégia promissora que potencia a letalidade de fármacos antimitóticos e pro-apoptóticos em CPNPS, através de mecanismo distintos. Adicionalmente, a p31^{comet} apresenta potencial relevância clínica no cancro oral e a combinação da inibição da p31^{comet} com cisplatina merece ser explorada no cancro oral, num contexto de resistência à cisplatina. Este trabalho reforça a significância do uso do SAC como alvo no tratamento do cancro.

Palavras-chave: p31^{comet}, *checkpoint* mitótico, slippage, estratégias antimitóticas, miméticos de BH3; cancro.

Everything is theoretically impossible, until it is done.

Robert A. Heinlein

Table of Contents

List of Figures

List of Tables

Acronyms, Abbreviations and Symbols list

°C - Degree Celsius

µg - Microgram

µL – Microliter

µm - Micrometer

µM - Micromolar

AP2 - Adaptor Protein 2

APC/C - Anaphase promoting complex/-cyclosome

ATM - Ataxia Telangiectasia Mutated

ATP – Adenosine triphosphate

ATR - ATM and Rad3-related

Aurk – Aurora kinase

BRCA1 - Breast Cancer Type 1 Susceptibility Protein

Bub - Budding uninhibited by benzimidazole

Bub3 - Budding uninhibited by benzimidazole 3

BubR1 - Budding uninhibited by benzimidazole-related 1

C. elegans - *Caenorhabditis elegans*

CAFs - cancer-associated fibroblasts

Cdc - Cell division cycle

Cdc20 - Cell Division Cycle 20

$Cdc20^{MCC}$ - Cdc20 Subunit Intrinsic to the MCC

Cdh1 - Cdc20 Homologue-1

CDK1 - Cyclin-dependent Kinase 1

CDK - Cyclin-dependent kinase

cDNA – Complementary Deoxyribonucleic Acid

CENP-E - Centromere-associated protein E

CHK1 - Checkpoint kinase 1

CIN - Chromosomal instability

C-Mad2 - Closed Mad2

CMT2 - Caught by Mad2

CNS - Central Nervous System

CO_2 - Carbon dioxide

CPTAC - Clinical Proteomic Tumor Analysis Consortium

CRC1 - Central Region Component 1

CSC - Cancer stem cells

Ct – Cycle treshold

DAPI - 4',6-diamidino-2-phenylindole

DiM - Death in mitosis

DMEM - Dulbecco's Modified Eagle's Medium

DNA - Deoxyribonucleic Acid

DSBs - DNA double-strand breaks

E2F - E2 factor

ECL - Enhanced Chemiluminescence

ECM - Extracellular matrix

EDTA - Ethylenediamine tetraacetic acid

EGFR - Epidermal Growth Factor Receptor

EOC - Epithelial ovarian cancer

FBS - Fetal bovine serum

FITC - Fluorescein isothiocyanate

G0 - Gap0

G1 - Gap1

G2 - Gap2

GAPDH - Glyceraldehyde-3-Phosphate Dehydrogenase

gDNA - genomic DNA

GDP - Guanosine diphosphate

GFP - Green fluorescent protein

GTP - Guanosine triphosphate

h - Hours

HCC - Hepatocellular Carcinoma

HCl - Hydrochloric acid

HMG1 - Human high mobility group 1

HNSCC - Head and neck squamous cell carcinomas

HOK - Human oral keratinocytes

HORMA - for Hop1p, Rev7p and MAD2

HPAEpiC - Human pulmonary alveolar epithelial cells

HR - Homologous Recombination

HRP - Horseradish peroxidase

IC50 - Half maximal inhibitory concentration

ICL - Interstrand Cross-Link

IKKβ - Inhibitor of Nuclear Factor k-B Kinase-β

IR - Insulin Receptor

K-fiber - Kinetochore-fiber

KMN - KNL-1/Mis12 complex/Ndc80 complex

M - Phase Mitosis

Mad - Mitotic arrest deficient

Mad1 - Mitotic arrest-deficient 1

MAD1L1 - Mitotic arrest deficient 1 like 1

Mad2 - Mitotic Arrest Deficient 2

MAD2L1BP - Mad2-like 1 Binding Protein

MAD2L2 - Mitotic arrest deficient 2 like 2

MAPK - Mitogen activated protein kinase

MAPs - Microtubule-associated proteins

MBP1 - Mad2-Binding Peptide

MCC - Mitotic checkpoint complex

MDM2 - Murine double minute-2

min - Minutes

ml - Milliliter

mM - Millimolar

MMPs - Metaloproteases

MMS - Methyl-methane sulfonate

MOMP - Mitochondrial outer membrane permeabilization

MPF - Mitosis promotor factor

Mps1 – Monopolar spindle 1

mRNA - messenger RNA

MRP - Multidrug-resistance protein

MTAs - Microtubule targeting agents

MTOCs - Microtubule-organizing centers

mTOR - mammalian target of rapamycin

MTT - 3-(4,5-dimethylthiazolyl-2)-2,5-diphenyltetrazolium bromide

NaCl - Sodium chloride

NEB - Nuclear envelope breakdown

NF-κB - factor nuclear kappa B

nm - Nanometer

nM - Nanomolar

NRF2 - Nuclear factor erythroid 2-related factor 2

NSCLC - Non-small cell lung cancer

O-Mad2 - Open Mad2

OSCC - Oral squamous cell carcinoma

PARP-1- Poly [ADP-ribose] polymerase 1

PBS - Phosphate-buffered saline

PCH-2 - Pachytene Checkpoint Protein-2

PCM - Pericentriolar material

PCR – Polymerase chain reaction

PE - plating efficiency

Pearson-CC Pearson correlation coefficient

P-gp - P glycoprotein

PI - Propidium iodide

PI3K - Phosphatidylinositol 3-kinase

Plk1 - Polo-like Kinase 1

PMD - Postmitotic death

PP - Protein phosphatases

PTM - Post-translational modification

PTX - Paclitaxel

PUMA - p53 upregulated modulator of apoptosis

Q - Quadrant

qRT-PCR - Quantitative real-time polymerase chain reaction

RB - Retinoblastoma

RNA - Ribonucleic acid

RNAi - Ribonucleic acid interference

RNase - Ribonuclease

RPA - Replication protein A

RPMI - Roswell Park Memorial Institute

RT - Room temperature

RTK - Receptor tyrosine kinases

RZZ - ROD–Zwilch–ZW10

s - second

SAC - spindle assembly checkpoint

SC - Synaptonemal complex

SCC - Squamous cell carcinoma

SD - Standard deviation

SDS - Sodium dodecyl sulfate

SGO2 = Shugoshin 2

siRNA - Small interfering RNA

S-phase - Synthesis-phase

ssDNA - single-stranded DNA

SWI/SNF - SWItch/Sucrose Non-Fermentable

TCGA - Cancer Genome Atlas

TEM - Tumor microenvironment

TNF – Tumor necrosis factor

TRIP13 - Thyroid Hormone Receptor Interactor 13

Tris - Tris(hidroximetil)aminometano

TUNEL -Terminal deoxynucleotidyl transferase-mediated nick end labeling

ZW10 - Zeste White 10

CHAPTER I

General introduction

The information provided in this chapter was partially based on the following publications:

Henriques, A.C.; Ribeiro, D.; Pedrosa, J.; Sarmento, B.; Silva, P.M.A.; Bousbaa, H. "Mitosis inhibitors in anticancer therapy: When blocking the exit becomes a solution". Cancer Letters 440-441 (2019): 64-81. https://doi.org/10.1016/j.canlet.2018.10.005

Henriques, A.C.; Silva, P.M.A.; Sarmento, B.; Bousbaa, H. "The Mad2-Binding Protein $p31^{comet}$ as a potential target for human cancer therapy". Current Cancer Drug Targets 21 (2021): http://dx.doi.org/10. 2174/1568009621666210129095726.

1. Cancer

Cancer refers to a vast set of diseases which arise when the cells of an organ or tissue grow unrestrictedly and spread to neighboring tissues, and/or to other organs, through a process called metastization (1). Cancer have accounted for 10 million of deaths in 2020, according to World Health Organization (1). The incidence of an estimated 18 million new cases in 2018 is expected to double in 2040 (2). Although the incidence is stronger in developed countries, such as Australia, New Zealand, and United States of America, it kills mostly in poorer countries, as Mongolia, Serbia, Hungary and Montenegro. The most common cancers are lung and breast cancer, with the same incidence rate, followed by colorectal, prostate, skin and stomach cancers. Lung cancer is the deadliest, followed by colorectal, stomach, liver and breast.

Cancer tremendously affects health systems causing a remarkable socioeconomic effect, which is more prominent in underdeveloped countries. Therefore, several efforts are increasingly being made to develop more effective and less painful therapies. For this purpose, it is crucial to unravel the mechanisms underlying the formation and evolution of cancer.

1.1. Tumorigenesis

Tumorigenesis is a complex and multistep process by which normal cells transform and acquire malignant properties (3,4). Several factors may contribute to this process, such as the normal rates of incorrect DNA replication, the reduced control of DNA stability, epigenetic changes, the tissue of origin of the cell, the individual's age at the beginning of the process, as well as various environmental factors (4). The action of stimulators results in an evolutionary process where a set of transformations occur (4,5). Consequently, cells undergo genetic, epigenetic, and chromosomic alterations, through successive cycles of abnormal cell divisions. The acquisition of genetic diversity follows a clonal selection process, with the gain of malignant attributes (5).

Cancer grows and spreads in an intelligent and orchestrated process, behaving like a multicellular form of life within an organism (6,7). Cancer tissues, either metastatic or local, engender systemic pathogenic networks that affect the whole organism (7).

During malignant transformations, several capabilities are acquired. They were previously defined as the hallmarks of cancer by Hanahan and Weinberg (8,9) and comprise the following traits: sustaining proliferative signaling, evading growth suppressors, activating invasion and metastasis,

enabling replicative immortality, inducing angiogenesis, resisting cell death, deregulating cellular energetics, and avoiding immune destruction. In addition, genome instability and mutation, as well as tumor-promoting inflammation, two processes that emerge as a result of tumor formation, were further referred to as enabling characteristics that potentiate the mentioned hallmarks (9). These statements were later revisited by Fouad and colleagues (5), which refined the definition of the hallmarks of cancer as advantageous capabilities evolutionarily acquired, to not only potentiate malignant transformations but also trigger the progression of the malignant cells, in a complementary way. As such, the hallmarks were reorganized in the following way: selective proliferative advantage, altered stress response, vascularization, invasion and metastasis, metabolic rewiring, immune modulation, and abetting microenvironment.

Although the standard cancer cells may initiate the process and drive tumors forward, another type of cancer cells – the cancer stem cells (CSC) - have been reported in several tumors (9). CSC are frequently related to more aggressive phenotypic traits, such as improved metastization and therapeutic drug resistance (9,10). Beyond cancer cells and CSC, several types of non-cancer cells are active participants in tumorigenesis. In particular, the rearrangement of the tumor microenvironment (TEM) has a crucial role in the growth and transformation of the tumor. The crosstalk between the cancer cells and the components of TEM represents a high-level complexity mechanism that is preponderant for the establishment and dissemination of the disease.

1.2. Tumor Microenvironment

Tumors are complex structures that are composed not only of tumor cells but also of a wide variety of other elements (Figure 1). They also include the stromal cells in the vicinity of the tumor. TEM is, therefore, comprised of cancer cells and stroma (11,12). The stroma contains a complex of a heterogeneous set of cellular and non-cellular components (11,13). It includes fibroblasts, endothelial cells, pericytes, and immune cells, such as lymphocytes, macrophages, and microglia (11–13). Stroma also contains non-cellular components of extracellular matrix (ECM), such as collagen, elastine, fibronectin, laminin, hyaluronan, proteoglycans, matrix-degrading enzymes, cytokines, and epithelial growth factors (11,13,14). ECM plays an important role in tumorigenesis, as its modulation helps to sustain and promote tumor formation (14,15). For instance, cancer-associated fibroblasts (CAFs) can promote pro-tumorigenic changes in ECM, by remodeling the

expression of the ECM enzymes (16). As a result, tumor progression and invasiveness become enhanced.

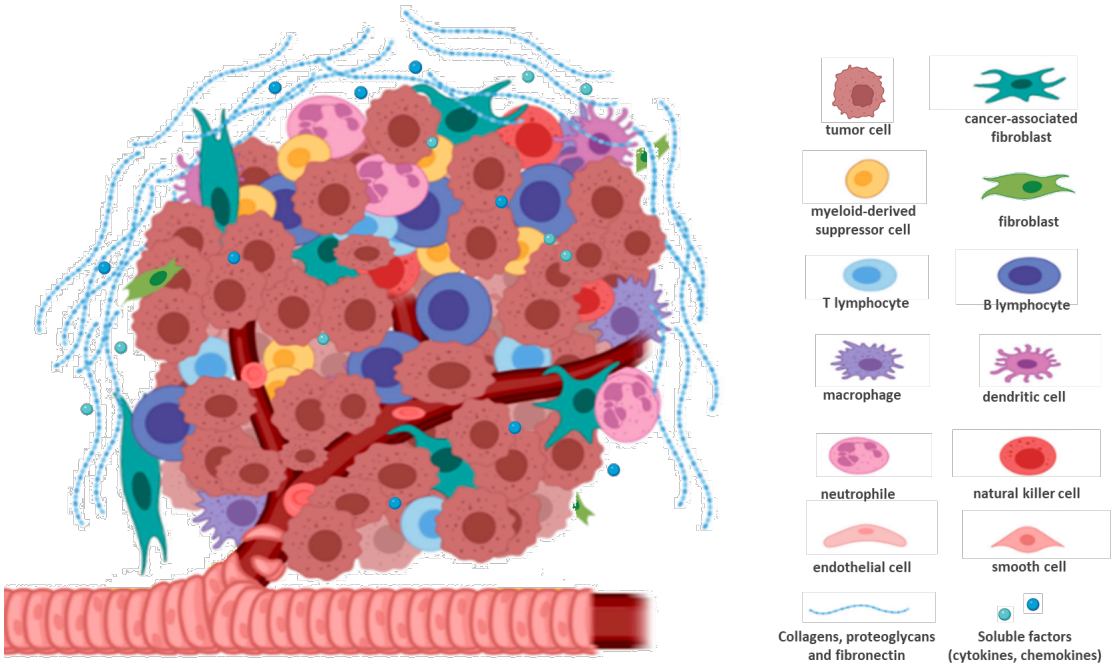

Figure 1. Schematic representation of the tumor microenvironment.

A vast and heterogeneous population of cells and proteins constitute the tumor ecosystem, which comprises not only comprises tumor cells but also tumor-associated fibroblasts and stromal cells, such as fibroblasts, endothelial cells, and immune cells. The tumor microenvironment also comprises a wide range of non-cellular components of the extracellular matrix (ECM), such as collagens, proteoglycans, fibronectins, and soluble factors, like cytokines and chemokines, which intermediate the cross-talk between those cells. Adapted from (17).

Cancer cells can influence the surrounding microenvironment, modulating and rearranging it to work for their benefit (10–12). For example, they can alter the expression of growth factors and evade the mechanisms of immune recognition through the production of immunosuppressive cytokines (14). Therefore, cancer and stromal cells intercommunicate through a complex signaling network to promote and strengthen the traits of malignancy, such as unrestricted growth, infiltration, and dissemination (10–12).

A factor that may influence the tumor microenvironment is the cell cycle activity. For example, some evidence suggests that the cell cycle activity may influence the ability of immune recognition and the infiltration of the immune cells in the tumor microenvironment (18). It was also suggested that the hyperactivation of cell cycle progression confers protection from

immunosurveillance and increases resistance to immune checkpoint inhibitors (18). Consequently, it was suggested that drugs that exert effects on the cell cycle may sensitize the tumors to immune modulators. Therefore, deregulation of the cell cycle may contribute not only to the transformation of healthy cells into cancer cells but also to the maintenance of a microenvironment favorable to tumor growth.

2. The cell cycle and mitosis

The cell cycle is the sequence of tightly regulated events through which a cell grows and divides into two genetically identic daughter cells.

The cell cycle of eukaryotic cells consists of a series of stages assembled in the interphase and in the mitotic (M) phase. During interphase, the cell duplicates its DNA content, some organelles, and other components, thus preparing for cell division. The interphase comprises the G_1, S, and G_2 phases. The G1 phase is the gap phase that goes from the end of a previous division to the interphase. During this phase, the cell grows and prepares for DNA replication. The S phase follows the G1 phase and is when DNA replication occurs. The G2 phase is the gap between the end of the S phase and the beginning of the M phase and is when RNA, proteins, and other components required for mitosis are synthesized. The M phase represents the stage during which the genetic material is partitioned between the two daughter cells. The M phase comprises the phases of mitosis (prophase, prometaphase, metaphase, anaphase, and telophase), and lastly cytokinesis. G0 is a quiescent stage from which cells exit from the cell cycle and do not grow or divide (19,20).

In order to ensure the fidelity of the entire process, the transition from one cell cycle stage to the next is tightly regulated by specific mechanisms.

2.1. Cell cycle regulation and control

The cell cycle comprises a set of events that are strictly organized in space and time and occur in a unidirectional way. Therefore, the cell only moves to the next cell cycle event after the earlier has been completed (21). This orchestration is under the regulation of the activity of the central cell cycle regulators cyclin-dependent kinases (CDKs).

Besides the regulation of the cell cycle, it is necessary to ensure the maintenance of genome integrity and to prevent cell transformation (22). This is guaranteed by control mechanisms known as cell cycle checkpoints.

2.2.1. Cell cycle regulation

The regulation of the cell cycle events is strictly dependent on CDKs, a family of threonine kinases that form complexes with cyclins (23). Cyclin binding stimulates CDK activation, which is completely achieved after the phosphorylation of the threonine residue 160 (Thr 160), catalyzed by the CDK-activating kinases (24,25). Since the concentration of the CDKs remains constant, their activation is influenced by oscillations in cyclin levels (23). Indeed, cyclins are constantly being synthesized and destroyed throughout the cell cycle, and different CDKs are activated at specific points of the cell cycle (Figure 2) (21,26). In this context, it is possible to consider four main classes of cyclins: G1, G1/S, S, and G2/M cyclins.

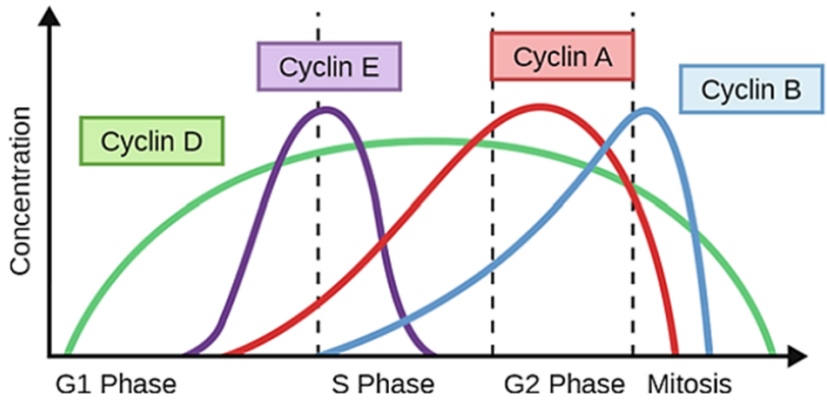

Figure 2. Cyclin expression throughout the cell cycle.

Cyclins are constantly being synthesized and destroyed throughout the cell cycle, and different CDKs are activated at specific points of the cell cycle. It is possible to consider four main classes of cyclins: G1 (D in vertebrates), G1/S (E in vertebrates), S (A in vertebrates), and G2/M cyclins (A and B in vertebrates). Adapted from (27).

G1 cyclins, (D in vertebrates), stimulate the entrance in the cell cycle, and remain in high levels through the cell cycle stages. In certain circumstances, such as nutrient deprivation or lack of growth factors, for example, cells may exit from the cell cycle, entering a stage known as the G0 phase (19,28). When cells are stimulated to reenter the cell cycle, D cyclins complex with CDK4 or CDK6 (in mammals), driving the successive phosphorylation of the retinoblastoma (Rb) proteins. When in a hypophosphorylated state, Rb proteins sequester members of the E2F family of

transcription factors (21,24,29). When Rb proteins become phosphorylated, E2F inhibition is alleviated, driving the transcription of cell cycle-related genes, which allows the progression of cells into the mid-G1 phase. Notably, this process allows the expression of the G1/S cyclin, cyclin E in vertebrates (28). E-type cyclins start to appear in late G1 and fall in the early S-phase. E cyclins form complexes with CDK2 (mammals), promoting the preparation for the entry in the S phase, by triggering centrosome duplication and chromosome replication (28). Cyclin E–CDK2 also helps to complete Rb phosphorylation, promoting the complete release of EF2 and the transcription of S-phase genes (28). Finally, the cyclin E–CDK2 complex induces the assembly of the pre-replication complex. S cyclins (A in vertebrates), remain throughout the S and G2 phase, as well as in early mitosis (A-type cyclins are also G2/M cyclins). Initially, A-type cyclins bind to CDK2, and allow the firing of replication origins, in a controlled way, driving the beginning of the DNA synthesis. At the beginning of the G2 phase, cyclin A-CDK1 complexes start to form. Although cyclin A-CDK2 remains until mitosis, probably having functions in spindle formation, cyclin A-CDK1 complexes only last until the late G2 phase. Cyclin A-CDK1 plays roles similar to cyclin A-CDK2 in avoiding the formation of multiple origin replication fires. Levels of G2/M cyclin B (in vertebrates) start to rise slowly in the late, reaching significant levels in the mid-G2 phase, and continuing to increase as cell reaches mitosis. At this moment, cyclin B1 starts to bind to CDK1, beginning to replace cyclin A (28). The complex between cyclin B1 and CDK1 constitutes the mitosis promotor factor (MPF), which is responsible for a set of transformations that drive cells into mitosis. The degradation of cyclin B1 occurs after ubiquitination by the E3 ubiquitin ligase Anaphase Promoting Complex (APC/C) and results in the inactivation of the CDK1. This event dictates the metaphase to anaphase transition, with the separation of the sister chromatids and, subsequently, the mitotic exit.

2.2.2 Cell cycle checkpoints

Cell cycle checkpoints detect errors occurring during the cell cycle to ensure the fidelity of the process. These mechanisms act before significant events of the cell cycle, inducing a cell cycle arrest until the errors are repaired. The main regulatory checkpoints are the G1 checkpoint, the intra-S checkpoint, the G2/M checkpoint, and the mitosis associated spindle assembly checkpoint (SAC) (Figure 3) (29).

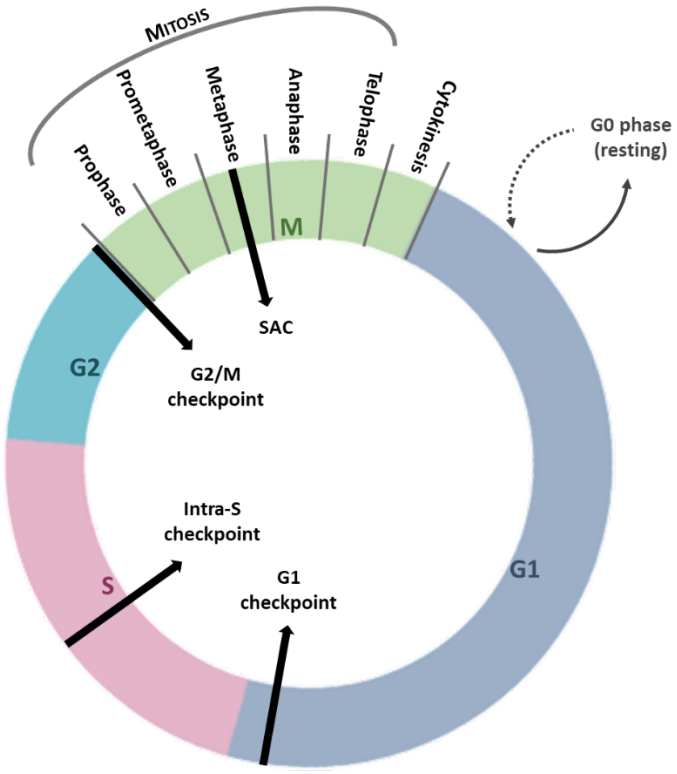

Figure 3. Diagram representation of the cell cycle and the major cell cycle checkpoints.

Cell cycle phases are represented: G1, S, G2, and M. Mitosis stages are also shown (prophase, metaphase, anaphase, and telophase), as well as cytokinesis. The cell cycle is controlled by four main checkpoints, G1 checkpoint, intra-S checkpoint, G2/M checkpoint, and spindle assembly checkpoint (SAC). This figure was created with BioRender.com.

The G1 checkpoint prevents the transition from G1 to S phase in the presence of DNA damage and involves the p53/p21/Mdm2 axis (29). p53 suppressor protein induces the transcription of the protein $p21^{CIP1/WAF}$, which precludes Rb phosphorylation and the progression to the S phase of the cell cycle. In addition, p53 is involved in the apoptosis-inducing mechanisms activated in a scenario of irreversible DNA damage (21), through the transcription of pro-apoptotic genes, such as *Puma*, *Noxa*, *BAX*, and *Apaf1* (30). The activity of p53 is impaired by the murine double minute-2 (MDM2) oncoprotein, which induces the p53 ubiquitination and represses p53 transactivation (31).

The intra-S checkpoint allows the cell to overcome the DNA damage episodes occurring during the S phase. This checkpoint is mediated by two main checkpoint kinases, Ataxia Telangiectasia Mutated (ATM) and ATM and Rad3-related (ATR). ATM is activated by the presence of DNA double-strand breaks (DSBs), and ATR senses single-stranded DNA (ssDNA) that accumulate at stalled replication forks (32,33). ATM and ATR act through their effector kinases CHK2 and CHK1, respectively (32,33).

The G2/M checkpoint controls the transition from G2 to mitosis (29). This is a more stringent checkpoint than the S-phase checkpoint. When active, the G2/M checkpoint completely halts the cell cycle (34). The G2/M checkpoint comprises the DNA damage G2 checkpoint and the decatenation G2 checkpoint (29). DNA damage G2 checkpoint prevents activation of the MPF through the ATM/CHK2/p53 (29). ATM drives the phosphorylation of CHK2, which in turn, phosphorylates and inactivates the phosphatases Cdc25A and Cdc25C (30). As the active Cdc25C activates CDK1 by dephosphorylation, the ATM/CHK2 activity precludes CDK1 activation via Cdc25C. In addition to Cdc25C inactivation, ATM/CHK2 also induce the activation of p53, through phosphorylation via CHK2 (30). The decatenation G2 checkpoint is activated by the catalytic inhibition of topoisomerase IIα (topo IIα), which is the main effector topoisomerase during DNA replication in humans (29,35,36).

Failures in any of the cell cycle checkpoints described above compromise the genome integrity and the accuracy of the chromosome segregation to the daughter cells, triggering an anomalous cell division. Consequently, the resulting abnormal daughter cells may drive unusual metabolic and replicative processes that meet the aforementioned cancer hallmarks, promoting tumor initiation and/or progression, and affecting the sensitivity of tumors to anticancer drugs (9,21,29). Mutations in the major players that regulate cell cycle checkpoints are frequently associated with cancer (21,29). For example, mutations in TP53 (the gene encoding p53 protein) may impair G1 and G2 checkpoints. As a consequence, the cell cycle may proceed in the presence of DNA damage, resulting in permanent damage or mutation in the genome. Indeed, TP53 mutations are widely common in human cancers.

Besides the cell cycle checkpoints described above, the SAC is the mechanism that halts cells in mitosis, preventing metaphase-to-anaphase transition if unattached and/or improperly attached kinetochores are detected (37). In the next sections, particular emphasis will be given to the mitotic process, the SAC mechanism, and the relation between SAC defects and cancer.

2.3. The event of mitosis

During the M phase, the cell contents duplicated in the previous phases of the cell cycle are rearranged and equally divided, generating two identical daughter cells (Figure 4) (38,39). The M phase consists of mitosis and cytokinesis. During mitosis, the cell faces a series of restructuring events that include chromosome condensation, nuclear envelope breakdown, mitotic spindle

formation, as well as chromosome congression and segregation. Due to the delicate nature of this process, mitosis is perhaps the most dramatic step of the cell cycle.

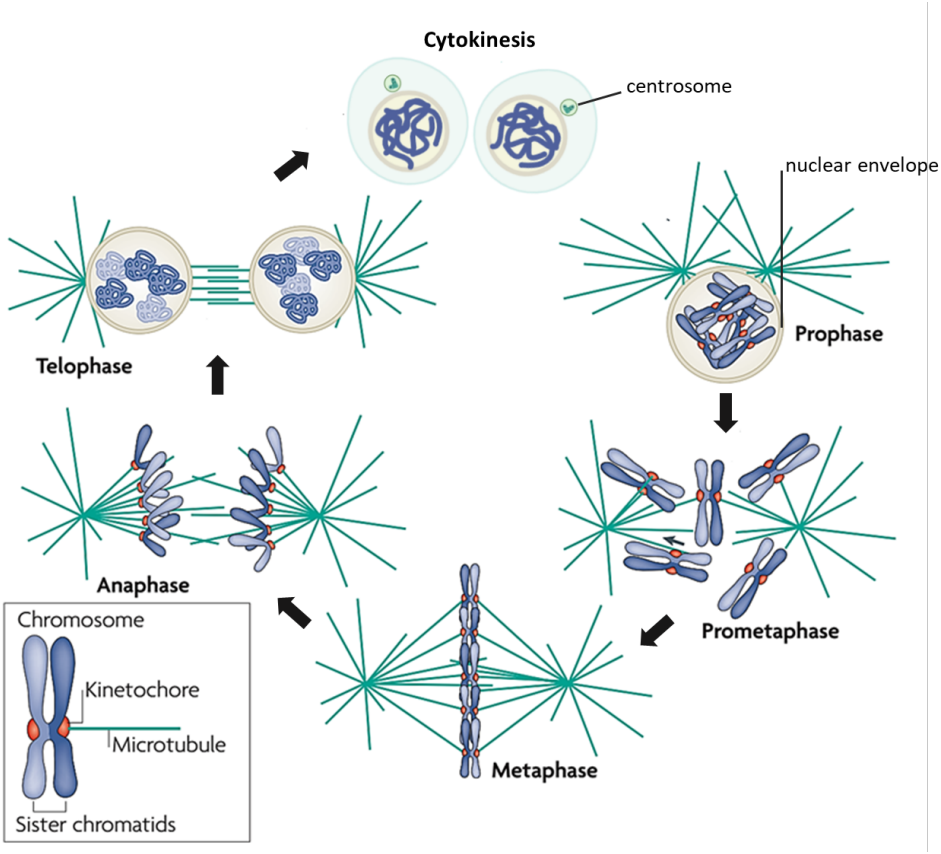

Figure 4. Schematic representation of the events of the M phase: the mitotic staged and cytokinesis.

During prophase, chromosomal DNA starts to condense and to generate well-defined chromosomes. Centrosomes begin to separate and to migrate to the opposite sides of the cell, to start to form the bi-polar spindle. Transition to prometaphase is set by nuclear envelope breakdown. At this point, chromosomes are no longer constrained in the nucleus, and microtubules from opposite poles can interact with chromosomes through the kinetochores. Metaphase occurs after all chromosomes have formed bipolar attachments with microtubules and are aligned at the equatorial plane of the cell. The cohesion between two sister chromatids is dissolved during anaphase, and they separate towards the poles. During telophase, chromosomes decondense, the nuclear envelope reorganizes, and the spindle is disassembled. Cytoplasm divides during cytokinesis, allowing the segregation of two individual cells. Adapted from (40).

2.3.1. The phases of mitosis

Mitosis comprises five main phases: prophase, prometaphase, metaphase, anaphase, and telophase. Next, these events will be described in more detail.

Prophase

Chromosome condensation is the event that marks the beginning of the prophase. During this process, the duplicated DNA molecules that correspond to the sister chromatids of each chromosome start to condensate and hold together at the centromere (38). As the compaction proceeds, the transcription shuts down, in part due to the displacement of the transcription factors. Other important events take place during prophase, such as nucleolus dispersion, the decrease in protein synthesis, as well as cytoplasmic and cytoskeletal changes (39). Changes in cytoplasm are responsible for the events conducting to initiate the formation of the mitotic spindle during prophase (38,39,41). In the centrosomes-containing cells, the maturation of these organelles, which were duplicated during interphase, also concludes. Centrosomes are crucial for the establishment of the mitotic spindle (38,41). In addition to these processes, cytoskeletal reorganization also occurs. In animal cells, is the dissolution of the interphase cytoskeleton and the acquirement of a rounded shape improves the distribution of the cell contents, promoting their equipartition at cytokinesis (39). In higher eukaryotes, the end of the prophase is marked by the breakdown of the nuclear envelope (38,41). The hyperphosphorylation of the laminin fibers of the inner surface of the nuclear envelope, probably by cyclin B1-CDK1, contributes to this process (39).

Prometaphase

Prometaphase is the phase that corresponds to the transition between prophase and metaphase. Once the nuclear envelope disperses, the microtubules grow toward the nuclear space (39). Throughout this period, the mitotic spindle assembly completes and chromosome congression (the movement of chromosomes to the spindle equator) takes place. During mitotic spindle assembly, chromosomes start to attach to the microtubules through centromeric proteinaceous complexes called kinetochores (37). Prometaphase concludes when all chromosomes congress to the spindle equator. All of these processes occur by a set of complex and coordinated mechanisms that will be described in more detail below.

Metaphase

Metaphase refers to the formation of the metaphase plate. This is achieved after all chromosomes have established bipolar attachments with microtubules from opposite poles. At this point, chromosomes become bi-oriented and aligned in the equatorial region (39). When that occurs,

the SAC, a control mechanism that prevents premature metaphase-anaphase transition, is silenced. Consequently, the activity of the anaphase promoting complex/-cyclosome (APC/C) is restarted, securin and cyclin B1 are degraded, and the sister chromatids start to separate, initiating anaphase (39,42,43).,

Anaphase

The anaphase begins when sister-chromatids start to separate and comprises two processes, designated as anaphase A and anaphase B (39). The first involves a decrease in the distance of each chromosome to each pole; the second refers to an increase in separation between the two poles. Both mechanisms are dependent on changes in lengths and dynamics of microtubules and the action of motor enzymes.

Telophase

During telophase, the nucleus reforms, and chromosomes decondenses. First, the still-condensed chromosomes associate with proteins of the inner nuclear envelope, in a process that leads to the formation of a new nuclear envelope and the reassembling of nuclear pores (39). Then, chromatin starts to decondense, transcription restarts, and nucleoli reform.

During mitosis, the mitotic spindle assembly and chromosome congression are crucial processes where the microtubules and kinetochores are key players. These concepts are discussed below.

2.3.2. Mitotic spindle assembly and chromosome congression

The assembly of the mitotic spindle is a crucial step in mitosis, that promotes the accuracy of chromosome congression and segregation.

The mitotic spindle starts to form during prophase (38,39,41) and, in cells containing centrosomes (Figure 5), such as human cells, these organelles represent the microtubule-organizing centers (MTOCs), playing a major role in the nucleation, anchoring, and organization of microtubules required for the mitotic spindle (41). Although acentrosomal pathways for spindle assembly have been found in *Drosophila* cells, as reviewed in (37), centrosome-dependent mechanisms revealed to be the main responsible for microtubule organization.

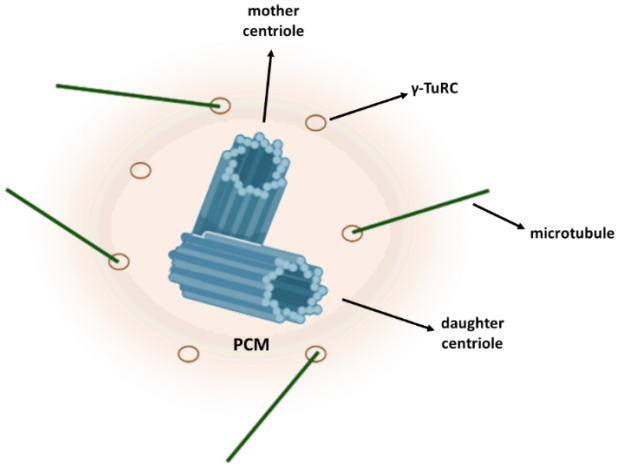

Figure 5. Simplified representation of the centrosome structure.

Centrosomes are composed of two centrioles (mother and daughter centriole), which are embedded in the pericentriolar material (PCM). γ-tubulin ring complex (γ-TuRC), the microtubule nucleating template, serves as a scaffold for microtubule formation. Created with Biorender

Centrosomes are cytoplasmic organelles composed of two centrioles and pericentriolar material (PCM). Centrosomes are duplicated during interphase and, in prophase, their maturation concludes. They separate immediately before or after NEB, moving towards opposite sides of the nucleus (37,38,41). Centrosome separation is dependent on the action of the proteins Nek2 kinase, the motor Eg5, and dynein - a nuclear-envelope-associated minus-end motor (41). Centrosome comprises about 400 proteins and the majority resides in PCM. Polo-kinase-1 (PLK1) and Aurora A are two major regulators of PCM recruitment and centrosome maturation. Their activity allows controlling the centrosomal and spindle pole localization of the microtubule-associated proteins (MAPs), which are important for spindle formation (41). Particularly important to improve the nucleation capacity of the mitotic PCM is the increase of the centrosomal levels of the microtubule nucleating template, the γ-tubulin ring complex (γ-TuRC), which serves as a scaffold for the formation of the microtubules (38).

Microtubules grow into the nuclear space once the nuclear envelope disperses (39). At this moment, the nucleoplasm and cytoplasm mix, and chromosomes are exposed to the microtubules of the mitotic spindle. The "search and capture" model (Figure 6) is the main accepted model for centrosome-dependent spindle assembly in animal cells (37,39,44). Microtubules display polarity, extending through the more dynamic plus-ends, while the minus-ends nucleate at the MTOCs. Due to the dynamic instability of microtubules, their plus ends experiment episodes of

lengthening and shortening, which allows the microtubules to probe the cytoplasm in different trajectories, to meet and bind chromosomes. Some kinetochores initially bind to the lateral surface of the microtubules. The chromosome moves then along the microtubule to a spindle pole, through the motor activity of dynein (recruited to kinetochores by RZZ complex through Spindly) (44,45). Then, the lateral attachments are converted into "end-on" attachments. Some factors have been proposed to contribute to this process, such as the high density of microtubules close to spindle poles, and the proteins Ska1, Ska2, and Ska3 (44). After the attachment of one kinetochore, the unattached sister kinetochore faces the microtubules from the opposing spindle pole, in a process that results in bi-orientation (44). However, this is not a static process. First, the microtubules of the mitotic spindle are dynamically unstable, alternating between phases of growing and shrinking. Second, the kinetochore-microtubule attachment only stabilizes when kinetochores are under tension, i.e., when both kinetochores are bound to microtubules from the opposing poles (39).

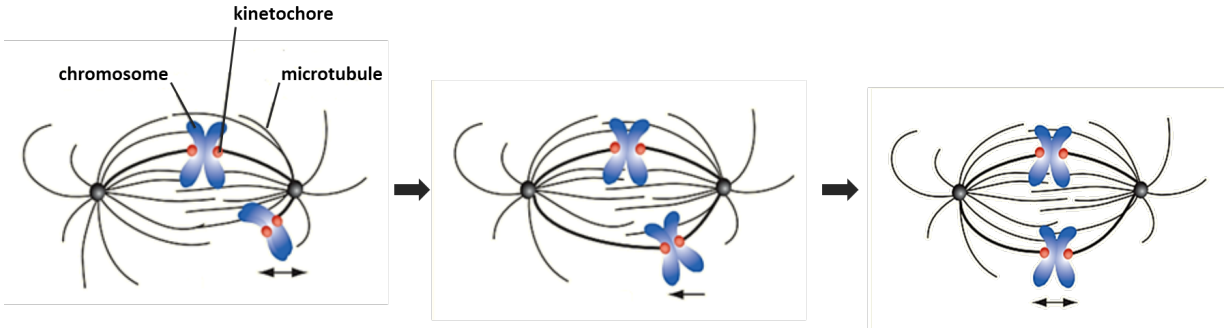

Figure 6. Schematic representation of the "search and capture model" in vertebrates.

Due to their dynamic instability, microtubules experiment episodes of lengthening and shortening, increasing their chances to meet and bind a chromosome. In the scheme, a mono-oriented chromosome (on the left) oscillates near the spindle pole (double-ended arrow), after the attachment of one kinetochore. On the right, the unattached sister kinetochore faces the microtubules from the opposing spindle pole, a process that results in the chromosome bi-orientation. The bi-oriented chromosome can now congress toward the metaphase plate. Adapted from (46).

In some cases, chromosome congression occurs naturally as a result of this bi-orientation process. However, sometimes, a coordinated set of active transport mechanisms are required to promote the movement of chromosomes to the spindle equator and to promote bi-orientation (37). One of these mechanisms involves plus end-directed microtubule motor CENP-E (Centromere-associated protein E), which acts in concert with dynein (Figure 7). The chromosomes that migrated to the spindle poles by the action of dynein may then be transported to the spindle equator by CENP-E, through tubulin detyrosination (37,39,44,45). Another mechanism of chromosome congression

involves the so-called "polar ejection forces", that act on chromosome arms and push chromosomes away from the poles. This mechanism is mediated by chemokinesins, such as kinesins-4 and -10 (37,39). that

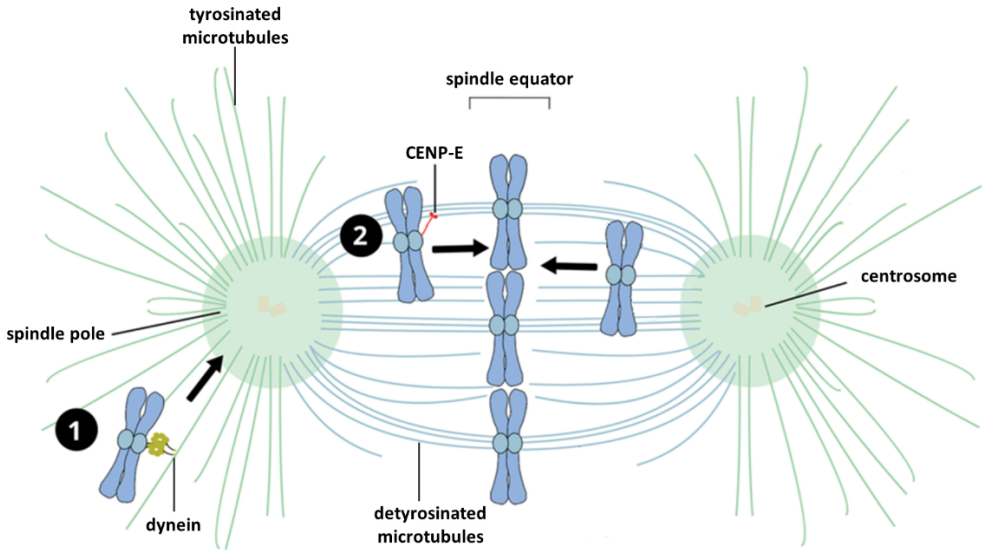

Figure 7. Schematic representation of CENP-E and dynein-dependent chromosome congression.

In this process, CENP-E acts in concert with dynein. Dynein mediates the poleward transport of chromosomes that fall outside the interpolar region (1), preferentially along tyrosinated microtubules (green). The plus-end directed motor CENP-E drives the transport of the unattached and mono-oriented chromosomes along detyrosinated microtubules (blue) towards the spindle equator (2). Adapted from (47).

Microtubule polymerization and the types of microtubules that arise during the assembly of the mitotic spindle are briefly discussed below.

2.3.3. Microtubules

As described in the previous section, microtubules play a determinant role in mitosis, namely through the mitotic spindle, indispensable for cell duplication. In addition, these structures are crucial for numerous cellular processes, as they integrate the cytoskeleton. Some of these processes include intracellular transport of organelles, proteins, and vesicles, as well as the maintenance of cell shape and polarity, and cell migration (48).

Microtubules are made of polymers of αβ-tubulin heterodimers, forming a lateral association of 13 protofilaments that assemble in a polarized tubular structure (Figure 8) (48). The minus end of a microtubule is less dynamic, while the plus end is more dynamic and exposes a β- tubulin

subunit (48). The intrinsic dynamic properties of microtubules are related to GTP hydrolysis. GTP binds to β-tubulin and is hydrolyzed during or shortly after polymerization, thus diminishing tubulin affinity for nearby molecules, and favoring depolymerization (38).

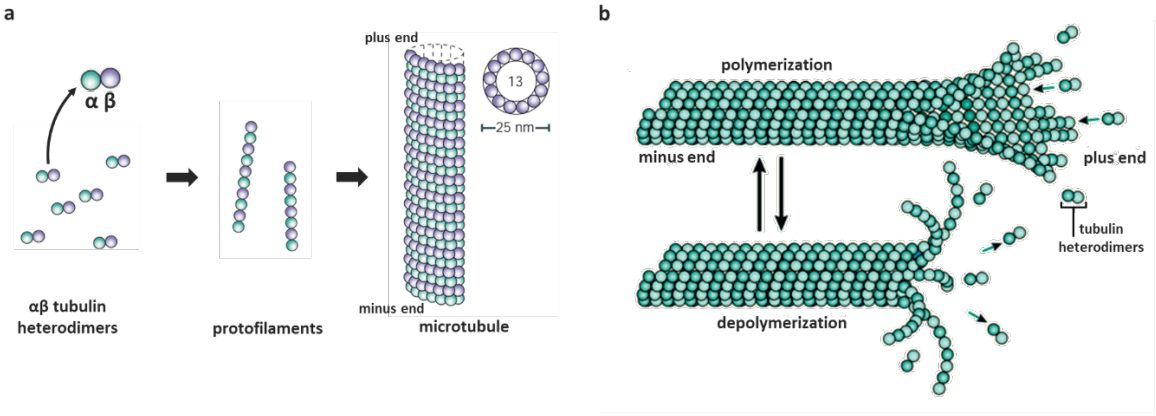

Figure 8. Microtubules are dynamic structures formed by tubulin heterodimers.

a) Microtubule structure. Microtubules are cylindric structures with an outer diameter of 25 nm, made of 13 protofilaments. Protofilaments result from the head-to-tail association of αβ heterodimers. Each protofilament, the heterodimers are oriented with α and β tubulin subunits exposed at the minus and plus ends, respectively. **b)** Microtubules exhibit dynamic instability, undergoing periods of polymerization and depolymerization. The plus end is more dynamic than the minus end. Adapted from (49,50).

The minus end of a microtubule is usually anchored in the MTOC, while the plus end is extended to the periphery. During mitosis, the formation of the mitotic spindle leads to the emergence of different types of microtubules: astral, kinetochore, and interpolar microtubules (Figure 9) (41,51). The astral microtubules originate mainly from the centrosome, extending toward the cell cortex, thereby connecting the centrosomes with the cell membrane and helping to the positioning of the spindle. Interpolar microtubules radiate from the centrosomes towards the mid-zone, where they interdigitate, to increase stability. Kinetochore microtubules, also referred as k-fibers, attach to the kinetochores at their plus end, and are crucial for the chromosomal movement.

The fidelity of the kinetochore-microtubule attachment is highly regulated by the kinetochore.

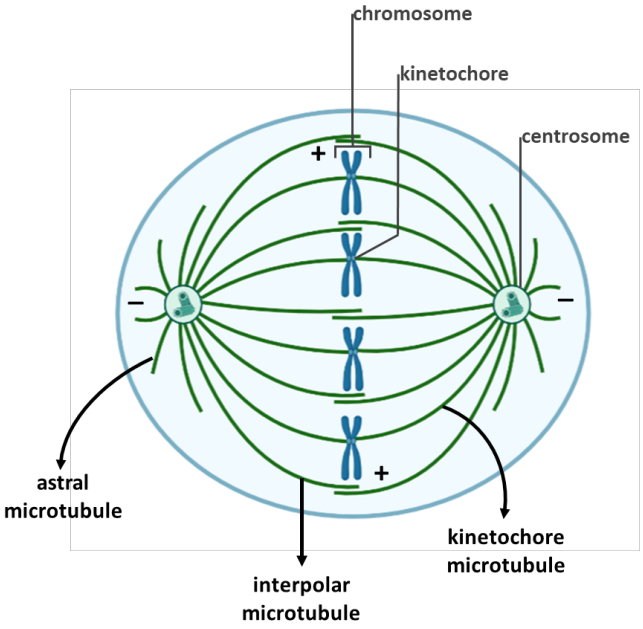

Figure 9. Schematic representation of the mitotic spindle in metaphase.

The slow-growing minus-ends (-) of microtubules are oriented toward the poles and the faster-growing plus-ends (+) are oriented to the cell cortex. Three major classes of microtubules of the mitotic spindle. K-fibers, interpolar microtubules, and astral microtubules are shown. Created with Biorender.

2.3.4. Kinetochores

Kinetochores are specialized protein-rich structures, assembled on centromeric chromatin of a sister chromatid. They represent the major mediators of the attachment of microtubule attachment to the chromosomes, acting as structural scaffolds, and ensuring the fidelity of the process (39,52).

The vertebrate kinetochore has a trilaminar structure, as revealed by electron microscopy studies: an outer electron-dense plate (outer kinetochore), an inner electron-dense plate (inner kinetochore), and an electron-translucent middle layer (53). Moreover, an additional structure, known as the fibrous corona, expands in a crescent-shaped structure from the distal surface of the outer plate, surrounding the unattached kinetochores (Figure 10) (45,53).

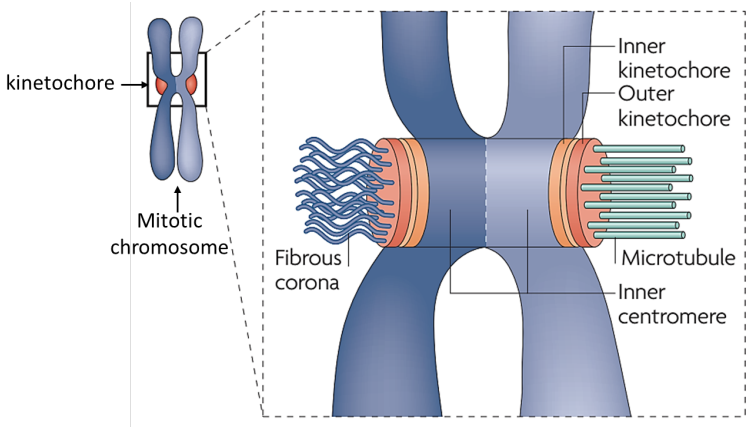

Figure 10. Structure of the vertebrate kinetochore.

Schematic representation of a mitotic chromosome. The chromatid on the right is attached to microtubules, and the chromatid on the left is unattached. Inner kinetochore and outer kinetochore are represented. Fibrous corona is only detectable on the unattached kinetochore, which are highlighted. Adapted from (40)

Kinetochores comprise more than 100 proteins, that can be categorized into proteins that regulate the activities of the kinetochore, inner kinetochore proteins that interact with the centromeric DNA, and outer kinetochore proteins that interact with microtubules (39)(54). Specifically, the outer kinetochore contains the KMN complex, which is crucial to combine and coordinate the chromosome movement to microtubule dynamics. The KMN complex of vertebrates consists of Knl1 complex (KNL1 - or blinking in humans, and ZWINT), Mis-12 complex (Mtw1, NSL1, NNF1, and DSN1), and the Nd80 complex (NDC80 - or Hec-1 in humans, NUF2, SPC24, and SPC25) (55). In addition, fibrous corona contains motor proteins (CENP-E, dynein), Rod–Zw10–Zwilch complex (RZZ), SAC proteins, and microtubule-associating proteins. Fibrous corona works as a platform that facilitates the attachment of microtubules (45,52,53).

During mitosis, the morphology of the kinetochore changes significantly. This process alters the localization of several proteins, being crucial for the effectiveness of the kinetochore-microtubule attachments (53).

Correct kinetochore-microtubule attachments are crucial to chromosome bi-orientation in the metaphase plate. However, different types of kinetochore-microtubule mis-attachments may occur, before correct attachments are formed (35).

2.3.5. Correction of kinetochore-microtubule mis-attachments

The correct attachment of sister-chromatids to microtubules that results in chromosome bi-orientation in the metaphase plate is called amphitelic attachment and ensures the correct segregation of chromosomes to the daughter cells (Figure 11). However, until kinetochore-microtubule attachment stabilizes, other types of attachments may occur, resulting in improper kinetochore-microtubule attachments (44). The kinetochore-microtubule mis-attachments can be classified as monotelic, when only one sister-chromatid is connected to a spindle pole, while the other is unattached; syntelic, if both sister kinetochores are attached to microtubules from a single spindle pole; merotelic if one sister kinetochore is attached to microtubules from both spindle poles, instead of one (Figure 11). The imbalanced tension across sister kinetochores produced by mis-attachments, is sensed by Aurora B (44). Aurora B regulates the interactions between kinetochores and microtubules through the phosphorylation of kinetochore proteins. The presence of inappropriate tension at kinetochores promotes a higher spatial closeness between Aurora B and their substrates, which results in the weakening of kinetochore-microtubule interactions. For example, although monotelic and syntelic attachments activate SAC, the merotelic attachments do not directly produce a SAC response, as they do not produce unattached kinetochores. However, the unbalanced tension weakens kinetochore-microtubule attachments through Aurora B activity. The resulting free kinetochore then triggers the SAC, helping to prevent an anticipated SAC release, as well as providing the opportunity to form new and accurate kinetochore-microtubule attachments (44,54).

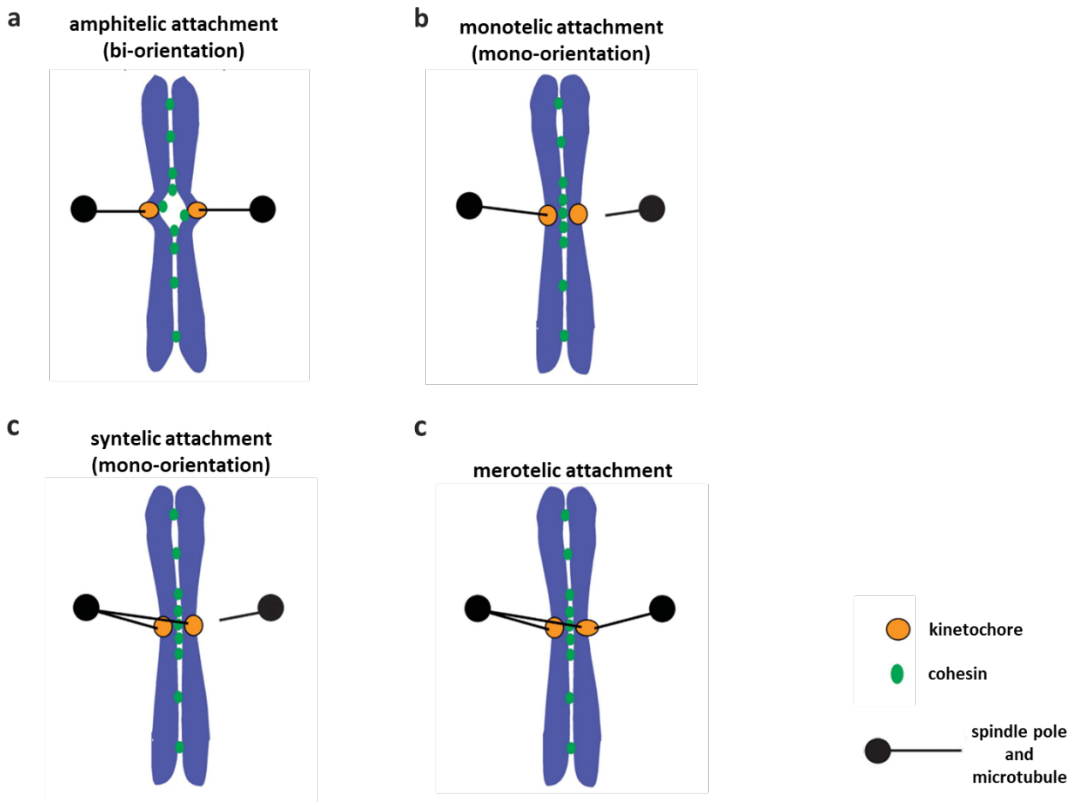

Figure 11. Modes of kinetochore-microtubule interactions: bi-orientations and attachment errors.

(**a**) In amphitelic attachment, sister kinetochores attach correctly to the microtubules from opposite spindle poles. As a result, sister kinetochores become bi-oriented. (**b**) In monotelic attachment, one kinetochore is attached to the microtubules from one pole, and the sister kinetochore is unattached, so the chromosome is mono-oriented. (**c**) In syntelic attachment, the chromosome is also mono-oriented, as the sister kinetochores are both attached to microtubules from the same pole. (**d**) In merotelic attachment, one of the kinetochores is simultaneously attached to microtubules that extended from both spindle poles. Adapted from (56).

The action of SAC is crucial to ensure the fidelity of the kinetochore-microtubule attachment, and SAC silencing only occurs when all the kinetochores are correctly attached to microtubules and aligned in the metaphase plate.

2.3.6. The spindle assembly checkpoint (SAC)

Correct bipolar kinetochore-microtubules attachments are crucial to accurate chromosome segregation at anaphase, and this process is under the surveillance of the spindle assembly checkpoint (SAC). Unattached and/or improperly attached kinetochores activate the SAC, which halts cells in mitosis until the errors are corrected (57,58) (Figure 12a).

SAC signaling proteins include mitotic arrest-deficient 1 (Mad1), Mad2, budding uninhibited by benzimidazole-related 1 (BubR1), budding uninhibited by benzimidazole 3 (Bub3), and monopolar spindle 1 (Mps1) (44). Mps1 is recruited to the unattached kinetochores, subsequently promoting the recruitment of the remaining SAC proteins (54). SAC acts through the generation of a diffusible "wait anaphase" signal, called mitotic checkpoint complex (MCC). The MCC forms between Mad2, Bub3, BubR1, and cell division cycle 20 (Cdc20), an activator of the E3 ubiquitin ligase anaphase promoting complex/-cyclosome (APC/C) (57,59,60). MCC assembly is mediated by the Mad2 template model. According to this model, Mad1 bound to Mad2 in its closed conformation (C-Mad2), or Mad1-C-Mad2, serves as a template to convert the open and inactive form of Mad2 (O-Mad2) into C-Mad2 bound to Cdc20. By sequestering Cdc20, the MCC inhibits APC/C: on the one hand, the MCC can act as a pseudo-substrate, blocking the access of the substrates to the active site; on the other hand, the MCC alters the APC/C conformation, preventing its association with the E2 enzyme UBE2C/UBCH10, and precluding substrate ubiquitination (54,61–63). Once inactivated, the APC/C is not able to drive ubiquitination and consequent degradation of securin and cyclin B1. Cyclin B1 plays an important role in sustaining the mitotic state through the activation of CDK1. Securin, in turn, inhibits separase, a protease responsible for cleaving the cohesins that keep the sister chromatids together. Therefore, APC/C inactivation by MCC delays mitotic exit by preventing the anaphase to metaphase transition.

Once the last kinetochore is properly connected to spindle microtubules, the SAC must be silenced to allow the anaphase onset (42,43). Several mechanisms have been proposed to contribute to this process. SAC silencing implies stopping the assembly of new MCC and promoting disassembly of existing ones, both mediated by structural and compositional changes at kinetochores upon microtubule attachment (Figure 12b) (64). Halting MCC assembly requires the motor protein dynein which actively mediates the transport of SAC components, namely Mad1-Mad2 complexes, from kinetochores towards the spindle poles, a process termed streaming or stripping (43,65). This dynein-mediated stripping is mainly dependent on spindly, a protein involved in dynein recruitment to the kinetochore (66–68). Alternatively, the protein p31^{comet} silences SAC by two different mechanisms: on the one hand, p31^{comet} prevents further SAC activation by inhibiting O-Mad2 to C-Mad2 conversion and, thus, further MCC formation; on the other hand, p31^{comet} induces SAC inactivation by promoting preformed MCC disassembly. (69–71). One of the main mechanisms of p31^{comet}-mediated MCC disassembly involves the AAA + family ATPase thyroid hormone receptor interactor 13 (TRIP13). p31^{comet} and TRIP13 cooperatively convert active C-Mad2

to the unbound O-Mad2 conformation, thereby promoting MCC dissociation and APC/C^{Cdc20} reactivation (72,73). $p31^{comet}$ may also have a role in cohesin degradation required for anaphase onset (74). In addition, ubiquitination-mediated protein degradation of Cdc20 subunit intrinsic to the MCC ($Cdc20^{MCC}$) was reported to contribute to MCC turnover and reactivation of inhibited APC/C-Cdc20 (75,76). In particular, the APC15 subunit induces APC/C^{MCC} conformation changes that are able to auto-ubiquitinate and degrade MCC-bound Cdc20 (76). Dephosphorylation of kinetochore and SAC proteins has also recently been reported as an essential mechanism for SAC silencing. PP1 and PP2A-B56 are the main protein phosphatases which, through negative feedback loops with Mps1 and Aurora B kinases, allow rapid dissociation of the MCC and SAC silencing upon proper microtubule attachment (69,77).

A defective SAC may fail to detect and correct erroneous attachments, which can lead to precocious chromosome segregation and aneuploidy, a hallmark of cancer cells (71,78,79). In fact, mutation or dysregulation of MCC proteins has been observed in several cancers (21).

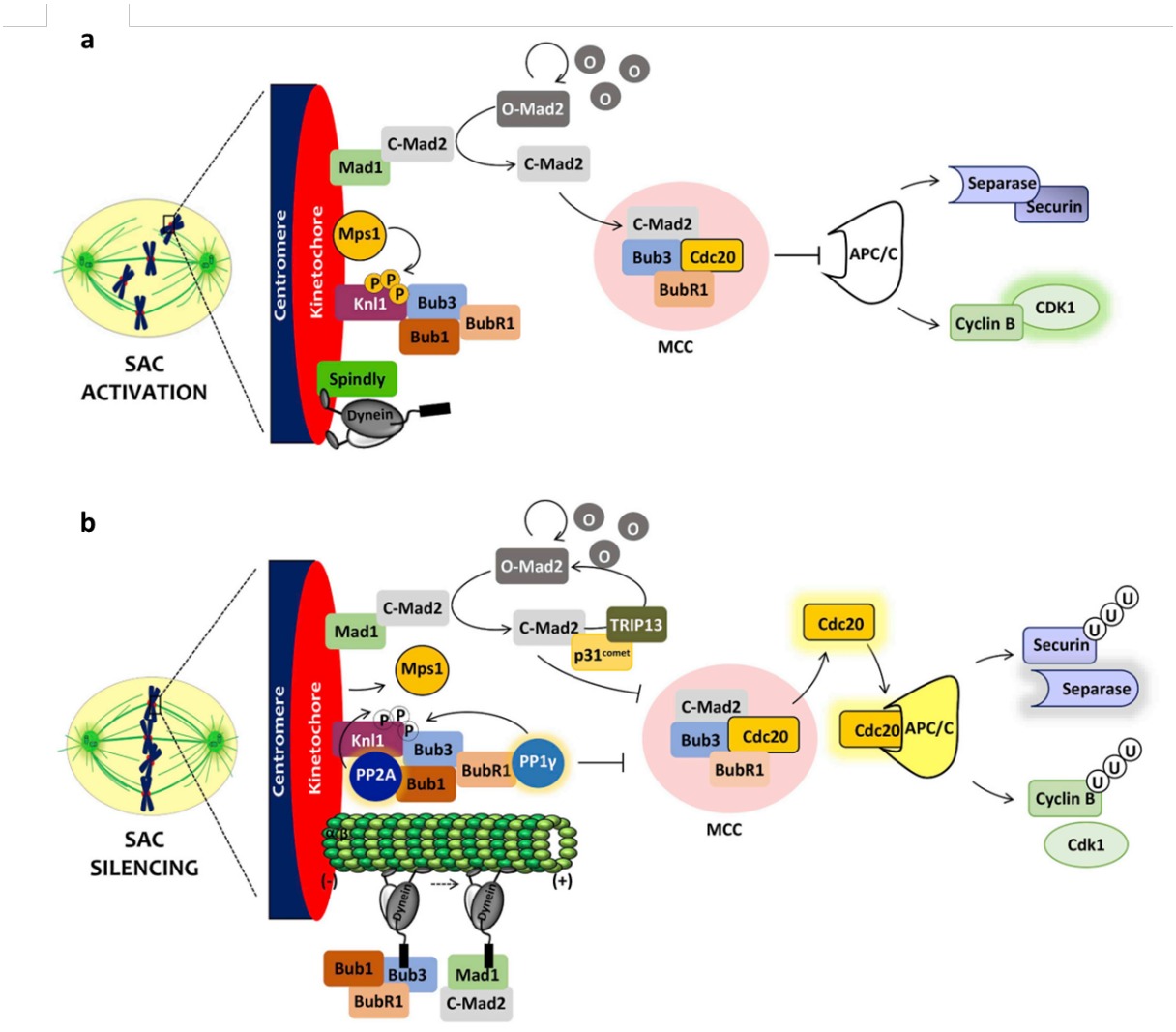

Figure 12. Spindle assembly checkpoint activation and silencing.

(**a**) The SAC is turned on in the presence of unattached kinetochores (red) where the Mad1/C-Mad2 complex actively recruits and converts cytosolic O-Mad2 into C-Mad2, which together with Bub3, BubR1, and Cdc20 constitute the MCC, resulting in APC/C inhibition. Consequently, cyclin B1 and securin are not degraded and remain associated with CDK1 and separase, respectively, leading to mitotic arrest. At the kinetochore, Mps1 is responsible for Knl1 phosphorylation promoting the recruitment of Bub3, Bub1 and BubR1. Also, spindly is essential for dynein recruitment to the kinetochore. (**b**) Different mechanisms have been proposed for SAC silencing, namely (i) through Mad2 inhibition by $p31^{comet}$ and TRIP13, which convert active C-Mad2 to the unbound O-Mad2 conformation, thereby promoting MCC dissociation and APC/C-Cdc20 reactivation; (ii) through the release of Mps1 from the kinetochore and dephosphorylation of Knl1 motifs by PP2α or PP1γ phosphatases, resulting in MCC inhibition; and (iii) through dynein-mediated stripping of SAC components, from kinetochores towards the spindle poles, promoting MCC disassembly. The consequence is the APC/C activation by Cdc20, resulting in ubiquitination-mediated protein degradation of cyclin B1 and securin, and mitotic exit. Moreover, ubiquitination-mediated protein degradation of Cdc20 subunit intrinsic to the MCC, by APC15, contributes to reactivating the APC/C-Cdc20 (80).

3. The spindle assembly checkpoint and cancer

Mitosis is a high-fidelity process, allowing accurate segregation of the chromosomes to the daughter cells. However, despite the mechanisms safeguarding cell division, numerous mitotic errors may occur, resulting in chromosomal instability (CIN) and aneuploidy (81). Aneuploidy refers to an abnormal number of chromosomes (21,81). CIN is related to the acquisition of genomic alterations, involving increased rates in chromosomal abnormalities that comprise duplications, deletions, as well as chromosome gain and loss (21,81). Chromosomal instability (CIN) is a general characteristic of aneuploid cancer cells (81), and it is estimated that aneuploidy is present in almost 70% of human solid tumors (81,82). Mitotic errors are considered a major cause of changes in chromosome number and may also contribute to chromosomal rearrangements (81). Several sources of mitotic errors can be considered, such as SAC defects, cohesion defects, centrosome amplification, and timing of centrosome separation. The relationship between SAC defects and cancer will be focused with more detail.

3.1. Deregulation of spindle assembly checkpoint in cancer

SAC is a highly controlled process, but it is not an all-or-none response, and its intensity depends on the number of unattached kinetochores (83). A deficient SAC response can dramatically affect chromosome segregation and result in aneuploidy. While failure of SAC activity causes cell death (21,84), impairments in SAC machinery can be bypassed in some cases, being associated with CIN in cancer cells. Numerous proteins are involved in SAC response in an orchestrated manner. Dysregulation of the activity of any of these proteins, either through a decrease or an increase, affects SAC performance. These alterations may occur as a result of mutations in genes that encode SAC proteins, or due to altered gene expression, and may also involve additional pathways that interfere with the regulation of the expression of these proteins.

3.1.1. Gene mutations

Mutations in genes encoding SAC proteins are rare but can impair drastically SAC response. For example, mutations that diminish SAC activity may result in premature anaphase, before full kinetochore attachment, and cause chromosome mis-segregation. Mutations in genes that encode SAC-related proteins were found in several cancer samples or cell lines.

Mutations in Bub1 and BubR1 genes were reported in T-cell leukemia/lymphoma (21,85). Bub1 inactivating mutations were found to weaken SAC and cause CIN in colon cancer cell lines (83,84,86). Additional Bub1 missense mutations were also associated with lung cancer (cell line and primary tumor) and colon cancer-derived lymph node metastasis in a clinical study (83,85,87). Regarding the MAD1L1 gene, eight heterozygous mutations were found frequently in samples of cell lines and fresh cancer cells of prostate cancer (83,88,89). Moreover, missense variations of MAD1L1 and MAD2L2 were reported to weaken the SAC and to increase lung cancer susceptibility (83,90). Mad1 and Mad2 mutations were also prevalent in Indian patients with ovarian cancer (83), and two additional mutations in MAD1L1 were associated with a higher risk of colorectal carcinoma in the Chinese population (83,91). Furthermore, mutations in TRIP13 and BubR1 genes were found to cause mosaic variegated aneuploidy, which is associated with aneuploidy and increased tumorigenesis (81,92–94).

3.1.2. Altered gene expression

Dysregulation of the expression of SAC core components can significantly modify SAC activity. For instance, the overexpression of MAD1, MAD2, Cdc20, BUB1, and BUBR1, correlated with poor survival in cancer patients (83,95).

For example, Cdc20 was overexpressed in oral cancer cell lines and primary tumors and associated with premature anaphase and chromosomal abnormalities (83,96). Cdc20 overexpression was also related to high ovarian cancer related-tumor grade (83,97). Furthermore, Mad2 overexpression was observed in diverse types of cancer, such as osteosarcoma, endometrial, gastric, mucinous ovarian, nasopharyngeal, soft tissue sarcoma, testicular germ cell, hepatocellular, prostate, breast, and lung cancer (83,98–100). On the contrary, downregulation of Mad2 was found in cervical cancer (83,101). In addition, the SAC silencer $p31^{comet}$ was found to be overexpressed in several cancers at the mRNA level, such as breast, head and neck, lung, melanoma, and prostate (102,103).

Several works described the mechanistic changes induced by alterations in the expression of SAC-related proteins. siRNA-mediated knockdown of BubR1 resulted in decreased levels of securin, and BubR1 haploinsufficient mice presented higher and faster development of lung and intestinal adenocarcinomas (83,104). Mice with reduced levels of Mad2 and Bub1 revealed a significant increase of aneuploid fibroblasts (83,104). Furthermore, overexpression of Mad2 stabilized securin and cyclin B1 and inhibited cytokinesis, having promoted the formation of aneuploid and tetraploid cells (105,106).

3.1.3. Other deregulations

Dysregulation and mutation of SAC-related proteins disturb SAC response, thereby contributing to tumorigenesis. In fact, the expression of SAC components may be under the control of different pathways, whose alteration may indirectly affect SAC. For example, the expression of Mad2 and $p31^{comet}$ is under the control of the Rb/E2F pathway (83,107,108). Inactivating mutations in Rb result in Mad2 overexpression and CIN (83,107). Indeed, Rb mutation or inactivation is related with many cancers (109). Furthermore, E2F is responsible for $p31^{comet}$ overexpression in colorectal carcinoma cells (108). Mad2 is also under the control of Breast Cancer Type 1 Susceptibility Protein (BRCA1), whose mutations contribute to Mad2 downregulation (83,110). Moreover, the recruitment

of p53 consensus element induces Mad1 repression (83,111). On the other hand, Mad1 overexpression may destabilize p53 during interphase, contributing to tumorigenesis (83,112).

Additionally, it cannot be forgotten that many SAC components are also involved in additional processes, other than mitotic checkpoint. For example, p31^{comet} acts in concert with TRIP13 not only in SAC silencing but also in additional processes, such as cohesion degradation and DNA repair. Moreover, p31^{comet}, Mad2 and BubR1 are implicated in insulin-mediated metabolic regulation (113–115).

Mitosis is a critical event of the cell cycle, and dysregulation of the mechanisms that control mitosis may promote tumorigenesis Therefore, strategies targeting mitosis have been widely considered for cancer treatment. Antimitotic-based strategies for cancer treatment will be focused on with more detail in the next section, with particular emphasis on approaches involving SAC.

4. Antimitotic-based strategies

Sustained proliferation is a hallmark of cancer (9). As such, targeting mitosis has been a major goal in the research for anticancer therapies. Current antimitotic drugs consist mainly of microtubule targeting agents (MTAs), also called spindle poisons. MTAs remain amongst the most successful of classical chemotherapeutics, but still raise resistance issues related to their effect on microtubules (116). Therefore, a second generation of antimitotics has also been arising. Furthermore, different strategies have been explored, including combination approaches that allow to increase treatment efficacy and to diminish the effective doses of drugs. In addition, simultaneous targeting of mitosis and apoptosis pathways have been investigated.

4.1. Microtubule-targeting agents

MTAs are by far the most widely used antimitotic drugs for cancer treatment. These spindle poisons include the taxanes paclitaxel and docetaxel, as well as the vinca alkaloids vinblastine and vinorelbine. Paclitaxel and vinblastine are used in the treatment of several cancers, particularly breast, ovarian, non-small-cell-lung, and head-and-neck cancers (117). MTAs prevent the formation of a functional bipolar spindle, either by inhibiting microtubule depolymerization (*e.g.* paclitaxel) or polymerization (*e.g.* vinblastin) (116,118). Consequently, chromosomes of

dividing cells cannot establish proper attachments to spindle microtubules, which triggers a chronic activation of the SAC (44). As a result of a prolonged mitotic arrest, cells eventually die by apoptosis during mitosis.

4.1.1. Cell fate of mitotic-arrested cells

Although cancer cells may undergo death in mitosis (DiM) upon MTAs treatment, alternative outcomes are possible (Figure 13).

An MTA-arrested cell can also exit mitosis without division and become tetraploid (4N) in a process known as mitotic slippage (119). According to the competing networks model, after a prolonged mitotic arrest, cell fate is governed by two independent competing networks: one refers to the slow degradation of cyclin B1, due to incomplete inhibition of the APC/C; the other involves the accumulation of proapoptotic signals (120). Both networks have thresholds. If the increase of proapoptotic signals reaches its threshold first, then the cell dies. On the other hand, if cyclin B1 levels fall below a threshold first, the cell undergoes mitotic slippage.

The slipped cell may face different scenarios, depending on the status of genes TP53, PRb, or P38, and the degree of DNA damage induced by MTA (59). As such, slipped cells may arrest in interphase and undergo senescence, die (post-mitotic death), or continue cycling. Although a subsequent mitosis of a tetraploid cell would be expected to result in cell death, cancer cells can generate viable daughter cells by focusing multiple centrosomes into a bipolar spindle (120). Although not consensual, the fate of cells arrested in mitosis due to MTAs seems to be influenced by the duration of the mitotic arrest and varies greatly between cancer cells (121,122).

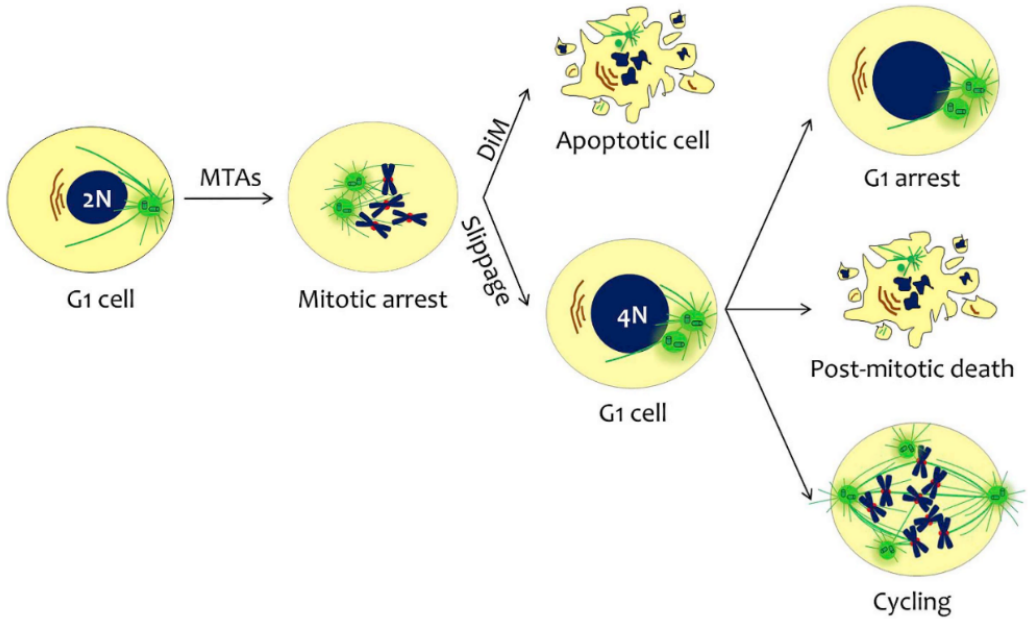

Figure 13. Cell fate after treatment with microtubule-targeting agents.

Diploid cells (2 N) treated with microtubule-targeting agents (MTAs) arrest in mitosis and may undergo death in mitosis (DiM), or mitotic slippage caused by a defective SAC and/or gradual degradation of cyclin B1. These tetraploid (4N) slipped cells may arrest in interphase (G1 arrest), undergo post-mitotic death, or continue cycling (80).

4.1.2. Drug resistance and adverse effects

Drug resistance is currently a major limiting factor in cancer treatment. It is estimated to be responsible for 90 % of failures in chemotherapy (123). Drug resistance can be intrinsic, normally associated with individual genetic variations, or acquired, which can be attributed to changes in drug targets and epigenetics, to alterations in drug metabolism, to multi-drug resistance, and to cell death inhibition (124). Resistance to MTAs is frequently associated with changes in the expression of membrane efflux pumps, such as P glycoprotein (P-gp), and mutations in tubulin sites affecting drug binding and/or GTPase activity (125). In addition to drug resistance, adverse effects also limit MTAs therapeutic efficacy. MTAs are commonly associated with neurotoxicity and myeloid toxicity owing to the role of microtubules in axonal transport and cycling bone marrow cells, respectively (70,126).

4.2. Targeting the spindle assembly checkpoint

Given the limitations associated with the use of MTAs, other antimitotic therapeutic possibilities have been explored. Therefore, it was suggested that alternative targets that disrupt mitosis without affecting microtubules would circumvent these issues, and SAC has emerged as an attractive option (127). Theoretically, both SAC activation and silencing provide a rational approach for the design of cancer cell killing strategies (128). Overriding SAC prompts cell death by inducing a premature mitotic exit due to massive chromosome misegregation. On the other hand, chronic activation of SAC stimulates DiM. As such, new antimitotic agents have been identified, namely small molecules targeting mitosis-specific kinases and microtubule-motor proteins, grouped into mitotic blockers and mitotic drivers, some have reached clinical trials (128). In addition, nucleotide-based strategies are being developed to target non-enzyme SAC-related proteins, also called "undruggable".

4.2.1. Chronic activation of the spindle assembly checkpoint

Chronic activation of SAC can be achieved by inhibiting the proteins responsible for the bipolar organization of the mitotic spindle, or by targeting SAC silencing. Several mitotic proteins that are involved in bipolar mitotic spindle organization can be considered as potential targets. These proteins are not required for microtubule formation, but their inhibition affects spindle bipolarity and creates misattached chromosomes, which results in SAC activation (129,130). Moreover, the function of these targets is mainly restricted to mitosis, which expectedly should result in better efficacy and lower toxicity compared to MTAs Examples of these targets include the kinesins CENP-E and Eg5, and the kinases Polo-like Kinase 1 (Plk1) and Aurora kinase A (62,131–142). Indeed, several small molecules have been developed - mitotic blockers, and some of these inhibitors have reached clinical trials, such as ispinesib (SB-715992) (Eg5 inhibitor), GSK913295 (CENP-E inhibitor); BI 2536 and BI 6727 (Plk-1 inhibitor); MLN8237 (Aurora A inhibitor) (132–134,141,142). In addition to these proteins, effectors of SAC silencing can also be targeted. SAC silencers under investigation include the spindly and p31^{comet} (mentioned in the preceding sections), as well as the phosphatase Fcp1, which dephosphorylates the kinase Wee-1, thereby promoting APC/C-dependent cyclin B degradation and subsequent mitotic exit (108,118,143–146). TRIP13 inhibition was also shown to abolish p31^{comet}-mediated SAC silencing (147), although TRIP13 is also required for sustaining the SAC response (148).

4.2.2. Inactivating the spindle assembly checkpoint

Targeting components of SAC activation constitutes a valid strategy to kill cancer cells by inducing lethal instability, as SAC is essential for cell survival (116,149,150). In addition, cancer cells should be more sensitive to this strategy as they already display certain degrees of chromosome instability (151). Potential targets include the core SAC signaling components Mad1, Mad2, Bub3, Bub1, BubR1, Aurora B, and Mps1. Inhibition of any of these SAC components overrides the SAC in cells arrested in mitosis by MTAs, leading to aberrant mitosis and subsequent cell death (152–155). For some of these putative targets, namely the Aurora kinases and Mps1, many small molecules have been developed and tested in different stages of pre-clinical and clinical studies (156–159). For example, the Mps1 inhibitors NCT03328494, NCT02366949, and NCT02138812 have reached phase I clinical trials (152).

Although small molecules targeting SAC components have been extensively investigated, in most cases, only partial responses were obtained in clinical trials (62,132–134,141,142,152,160,161). One possible reason may relate to the slower proliferation rate of tumors *in vivo*, relatively to *in vitro* cancer cells or to xenograft tumors in pre-clinical trials (81,162). In addition to these challenges, adverse effects still represent a limiting factor. For example, several side effects were reported with Plk-1 and aurora kinase (AURK) inhibitors (133,156,160,163). On the other hand, some encouraging outcomes have been emerging in combinatorial approaches, and several have reached clinical trials. Indeed, small molecules targeting mitotic proteins have been shown to sensitize cancer cells to several cytotoxic drugs, and radiotherapy. For example, small molecules targeting mitotic proteins have retrieved interesting results in combination strategies, such as antimitotics targeting Plk1, Aurora kinases, Mps1, and Bub1 (63,149,164–166).

4.3. Combination strategies

Combinatorial strategies have so far been explored in the field of clinical oncology with two main objectives: to minimize adverse effects by lowering drug effective doses and to overcome drug resistance.

4.3.1. Targeting SAC activation or SAC silencing in combination with Microtubule-targeting agents

Many combinatorial approaches have been investigated to maximize MTAs efficacy, and different outcomes have been observed. Targeting both SAC activation and silencing has the potential to improve the outcomes of MTA treatment (Figure 14).

Targeting SAC silencing delays mitotic slippage, thus favoring the apoptosis of an MTA-arrested cell. Indeed, cells depleted of $p31^{comet}$ required a 10-fold lower concentration of MTAs to trigger mitotic arrest and subsequent mitotic cell death than $p31^{comet}$ efficient cells, while overexpression of $p31^{comet}$ overrides hyperactivation of the SAC caused by MTAs leading to resistance to microtubule poisons (167–170). Additionally, spindly inhibition trapped cells in mitosis and dramatically sensitized cancer cells to clinically relevant doses of MTAs by exacerbating post-mitotic death (144). Furthermore, depletion of Fcp1 by siRNAs trapped cancer cells in mitosis in the presence of MTAs (143). Overall, those evidence support that targeting SAC slippage can be promising, and these *in vitro* results need to be verified in preclinical and clinical studies.

Targeting SAC activation, in turn, promotes aberrant mitosis with massive chromosome missegregation errors which may result in inviable cells that die or arrest in G1 phase. Some mitotic drivers have shown promising results. For instance, Mps1 inhibitors BOS172722 and BAY1217389 (ClinicalTrials.gov Identifiers: NCT03328494, NCT02366949) achieved phase I when administrated with paclitaxel. Mps1 is not only required for recruitment of SAC components to unattached kinetochores and subsequent MCC formation, but also for mitotic progression, centrosome duplication, chromosome alignment, error correction of kinetochore-microtubule attachment (171,172). Two small molecule inhibitors of Bub1, BAY-320 and BAY-524, have recently been developed and were also found to sensitize cancer cells to clinically relevant doses of paclitaxel, with only marginal impact on nontumor cells, although clinical trials are still lacking for these agents (166). On the other hand, Mad2-targeting miR-493–3p was associated with paclitaxel resistance and reduced survival of ovarian and breast cancer patients (173).. Moreover, the depletion of proteins involved in SAC activation was reported to be associated with MTA resistance (174). In fact, complete inactivation of SAC is difficult to achieve *in vivo*, which might favor mitotic slippage with chromosome aberrations that fuel chromosome instability and MTA resistance in cells surviving to post-mitotic death. In addition, the aberrant mitosis resulting from SAC overriding can also continue cycling, promoting MTAs resistance.

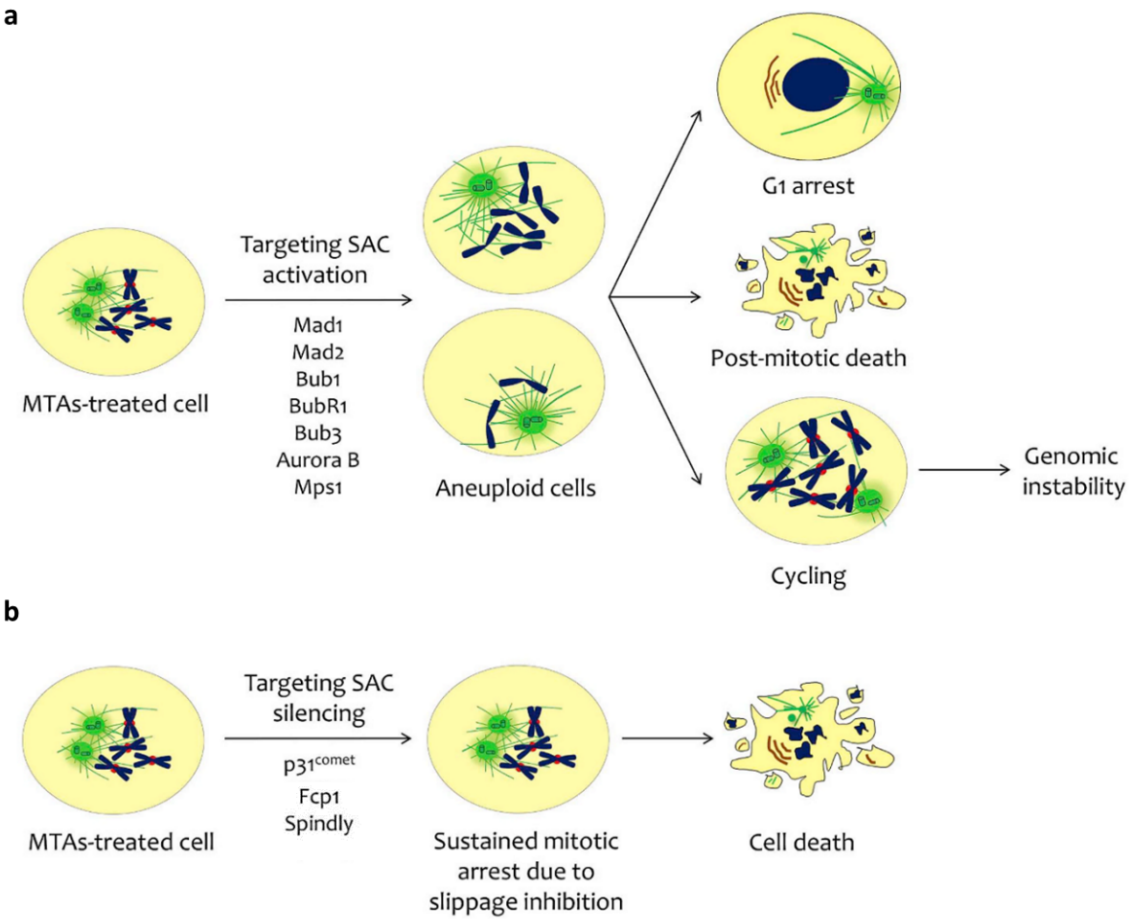

Figure 14. Effect of SAC activation or silencing on cell fate of an MTA-targeted cell.

(**a**) Targeting core SAC components (Mad1, Mad2, Bub1, BubR1, Bub3, Aurora B, Mps1) induces aberrant mitosis with massive chromosome missegregation, generating cells with increased chromosome instability (aneuploid cells) that may arrest in interphase (G1 arrest), undergo post-mitotic death or continue cycling, leading to genomic instability. (**b**) Targeting SAC silencing components ($p31^{comet}$, Fcp1, spindly) delays mitotic slippage and increases susceptibility to apoptosis, thereby tipping the balance in favor of death. Adapted from (80).

4.3.2. Strategies to force mitotic-arrested cells to die

One of the main mechanisms of resistance against MTAs is mitotic slippage (119,175). As referred above, slipped cells may keep on cycling. Indeed, some slipped multiploid cell survivors might re-enter the cell cycle and acquire increased instability and malignancy (78,176). Considering the two competitive networks model by Taylor et al., theoretically, it should be possible to have control over cell fate and influence the effectiveness of antimitotic drugs that arrest cells in mitosis, if

death signal accumulation is accelerated and/or mitotic slippage is retarded (Figure 15) (120,175). Strategies to accelerate apoptosis would lead to cell death before mitotic slippage occurs, while strategies to delay mitotic slippage would increase the time cells spend in mitosis, thereby allowing more time for apoptosis signals to accumulate. Both strategies, individually or in combination, should increase the sensitivity of cancer cells to antimitotics by shifting cell fates to death, which may be relevant to kill apoptosis-resistant, slippage-prone, or SAC-defective cancer cells.

Delaying mitotic slippage

Slippage can be delayed by slowing cyclin B proteolysis, which can be achieved by inhibiting the APC/C-Cdc20-proteasome axis, or by preventing SAC silencing.

Targeting the APC/C-Cdc20-proteasome axis can be achieved by targeting Cdc20, APC/C, or proteasome. Cdc20 ablation effectively arrested cells in metaphase and induced massive apoptosis in mouse models. Cdc20 inhibitor apcin acted synergistically with APC/C inhibitor TAME (tosyl-L-arginine methyl ester) in mitosis blocking (177). TAME binds APC/C and suppresses its activation by Cdc20 (178). TAME treatment enhances cell death in combination with MTAs or the alkylating agent melphalan (178–180). Another interesting antitumor target is the proteasome for which several inhibitors have reached clinical trials (181–183). Bortezomib (Velcade) became the first therapeutic proteasome inhibitor approved for multiple myeloma treatment, and subsequently, other proteasome inhibitors such as carflzomib (Kyprolis) and ixazomib (Ninlaro) were also approved (181,183). Altogether, these observations reveal that targeting APC/C-Cdc20-Proteasome axis to slow cyclin B degradation could be an effective way to fight cancer.

Other interesting targets to slow cyclin B degradation are the components involved in SAC silencing. This motivated studies that have shown that preventing SAC silencing increases the duration of mitosis and promotes cell death. As already referred to in a previous section, SAC silencing through downregulation of $p31^{comet}$, spindly, or Fcp1, sensitized cancer cells to paclitaxel (143,144,167–170). As such, these proteins emerge as potential drug targets candidates to delay mitotic slippage. Overall, targeting SAC slippage seems to be promising, and *in vitro* results need to be verified in preclinical and clinical studies.

Accelerating apoptosis: co-targeting mitosis and apoptosis

The so-called death in mitosis occurs in mitotic arrested cells mainly through the activation of the intrinsic caspase-dependent pathway of apoptosis (127). This is under the regulation of the Bcl-2 family, which comprises the proapoptotic BH3-only members, such as Bim, Bid, Bad, PUMA, and Noxa, and the antiapoptotic proteins Bcl2, Bcl-xL, and Mcl-1 (127,175,184,185). The oligomerization of the proteins BAX and BAK induce the formation of pores at the outer mitochondrial membrane - mitochondrial outer membrane permeabilization (MOMP), with the consequent release of cytochrome C and caspase activation (120,184). The anti-apoptotic proteins Bcl2, Bcl-xL, and Mcl-1 sequester BAX and BAK proteins, preventing MOMP and apoptosis. In the presence of death signals, BH3-only proteins bind to anti-apoptotic proteins, antagonizing their action, and some can also activate BAX and BAK through direct binding, which drive the intrinsic pathway of apoptosis (184). Considering the potential targets involved in this pathway, and the two competing networks model by Taylor *et al.*, several studies have emerged to evaluate the potential of targeting anti-apoptotic proteins in combination with antimitotic chemotherapy (120,175,186). Indeed, many cancers exhibit resistance to MTAs, deregulated SAC, or deregulated apoptosis that render them resistant to death (187,188). Therefore, the efficacy of antimitotics could be improved by combining them with pro-apoptotic drugs. The therapeutic relevance of this approach has proven to be efficient *in vitro* and in human tumor xenograft models by using BH3 mimetics (184,189,190). For instance, ABT-263/Navitoclax, a BH3 mimetic that inhibits the pro-survivals Bcl-2, Bcl-xL, and Bcl-w, precipitates apoptosis in cancer cells arrested in mitosis by MTAs or Eg5 inhibitors (191). Also, Navitoclax increased the sensitivity of taxane-based treatment in a panel of non-small cell lung cancer cell lines (192). The results of this study show that Navitoclax shifted the cell fate of paclitaxel-treated cells from slippage to DiM. This effect was particularly evidenced in cells presenting higher levels of Bcl-xL, which are normally more resistant to taxane therapy. Of note, inhibition of Bcl-xL, whether by RNAi or the BH3 mimetic ABT-737, triggered extensive cell death in otherwise slippage-prone cancer cells treated with MTAs, underlying the pro-survival proteins dependence of cancer cells during mitotic arrest (193). These results were recapitulated by RNAi-mediated depletion of pro-survival proteins such as Bcl-xL, which, from an antimitotic chemotherapy perspective, highlights the potential of the approach to reduce variation in death response between different cancers (175). Synergy in killing solid tumor cancer cells was also reported for the Bcl-xL inhibition-docetaxel combination, either in vitro or in tumor xenografts (190). Interestingly, most patients whose ovarian tumor tissue

expresses high Bcl-xL levels are less sensitive to taxane treatment, supporting the idea that the addition of Bcl-xL inhibitors could improve taxane-based therapy (194).

Works from Taylor's group indicate that exploring apoptosis inducer drugs may be more promising with mitotic blockers than mitotic drivers. They showed that treatment with WEHI-539, a potent and selective Bcl-xL inhibitor, sensitized cells to MTAs as well as to second-generation mitotic blockers, such as inhibitors of Eg5, CENP-E, and Plk1 (128). In this case, sensitization was largely by enhancing postmitotic death (PMD). On the other hand, the combination of WEHI-539 with mitotic drivers, such as inhibitors of Aurora B and Mps1, showed only minor impact unless the pro-survival Mcl-1 was also inhibited. These results suggest that Mcl-1 levels could serve to stratify patients that would benefit from the combination therapy (128). Also, combining apoptosis inducer drugs with SAC silencing inhibitors deserves to be explored. For instance, BH3-only mimetics in combination with inhibitors of SAC silencing components should, potentially, shift the fate of mitosis-arrested cells in favor of death. Yet, inhibitors that target SAC silencing proteins need to be developed.

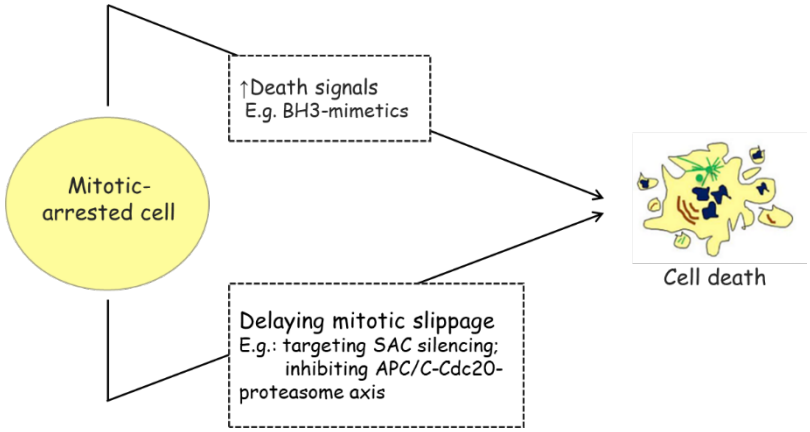

Figure 15. Shifting the fate of a mitotic-arrested cell to death.

Two main strategies can be considered, according to the competitive networks model (120): increasing death signals (e.g. through BH3-mimetics) and delaying mitotic slippage (e.g., by preventing SAC silencing, or inhibiting APC/C-Cdc20-proteasome axis).

Another possible strategy to promote the apoptosis of cancer cells is by using cisplatin (*Cis*-diamine-dichloroplatinum (II)). Once inside the cell, cisplatin turns into a powerful electrophile, being able of reacting with several nucleophilic sites, particularly with nitrogen donor atoms of

nucleic acids and sulfhydryl groups of proteins. Genomic DNA (gDNA) is considered the primary target of cisplatin and the covalent bonds generated between the platinum atom of cisplatin and purine bases give rise to a variety of adducts (195,196). Cisplatin-induced DNA damage can drive apoptosis in several ways (195) Furthermore, cisplatin induces ROS, which can not only result in gDNA damage but also affect mitochondrial function, resulting in apoptosis activation. Cisplatin is an important chemotherapeutic agent used in the treatment of several malignancies, such as ovarian, testicular, head and neck, lung, bladder, cervical, and colorectal cancer (196). Although cisplatin has been widely used in cancer treatment, there are many resistance and toxicity-related issues that limit its effectiveness.

To minimize the drawbacks associated with these issues, combination therapy of cisplatin with other drugs has been explored as an attractive strategy (195,197–199), and several drugs are already used in combination with cisplatin for cancer treatment (195). Despite the wideness of mechanisms underlying cisplatin resistance, the ability of cells to re-enter the cell cycle after a cisplatin-induced interphase arrest constitutes a relevant feature. Although the exact mechanisms underlying these events remain to be clarified, changes in mitotic regulation probably have a significant role in this process. Therefore, targeting mitosis in combination with cisplatin arises as an interesting approach in cancer therapy (197). Moreover, considering the competitive networks model Taylor and colleagues, cisplatin could be used in the logic of increasing death signals in mitotic arrested cells. In fact, combination therapy using cisplatin and paclitaxel is used in the treatment of ovarian, breast, head and neck, and lung cancer (195). However, many patients continue to develop resistance, even following a combination regimen (200). It has already been reported that cisplatin-resistant cells are cross-resistant to MTAs, and that microtubules are significant in cisplatin resistance (200–202), although the mechanisms underlying this hypothesis remain to be clarified, and other works share an opposite point of view (200,203). Recently, it was also suggested that cross-resistance may be related to an increase of pro-survival TNF/NF-kB signaling (200). Despite the lack of consensus regarding this issue, microtubules targeting could be avoided if the targeting of mitotic regulators was considered in this strategy, instead of MTAs. Silva and colleagues (199) demonstrated that the knockdown of Bub3 or spindly were able to sensitize oral squamous cell carcinoma (OSCC) cells to clinically relevant concentrations of cisplatin, which indicated that targeting mitosis, either by inducing precocious mitosis or preventing mitotic exit, deserves to be explored to sensitize OSCC cancer cells to cisplatin. In addition, the combination of cisplatin with the PLK-1 inhibitor volasertib

reached clinical trials [NCT00969761] with metastatic solid tumors (204). Indeed, APC/C dysfunction was found in epithelial ovarian cancer (EOC) resistant cells, which revealed a higher dependency on PLK-1 for mitotic exit, and became more sensitive to cisplatin therapy after PLK-1 inhibition (197). These findings highlight the relevance of investigating the potential of combining the targeting of mitotic regulators with cisplatin.

In conclusion, two main approaches have shown potential in forcing mitotic-arrested cells to die, either the induction of apoptosis or the delaying of the mitotic slippage. In this context, the use of apoptosis-inducing drugs in combination with the targeting of SAC silencing emerges as a potential research focus in cancer treatment. Therefore, SAC silencing molecules emerge as interesting targets, as is the case of p31^{comet}.

5. p31^{comet} as a potential target for human cancer therapy

As outlined in the previous section, slippage is a major cause of drug resistance. Therefore, delaying slippage through inhibition of SAC silencing has arisen as a promising strategy. In this context, p31^{comet} has been regarded as a potentially valid target to delay SAC silencing. Considering that p31^{comet} has a crucial role in SAC silencing, ensuring timely mitotic exit (Figure 16) (168,205), it emerges as an attractive target in the context of SAC-based antimitotic strategies. In the next sections the current status of p31^{comet} functions, with particular focus on SAC silencing, will be addressed, and its potential as a therapeutic target for cancer treatment will be discussed.

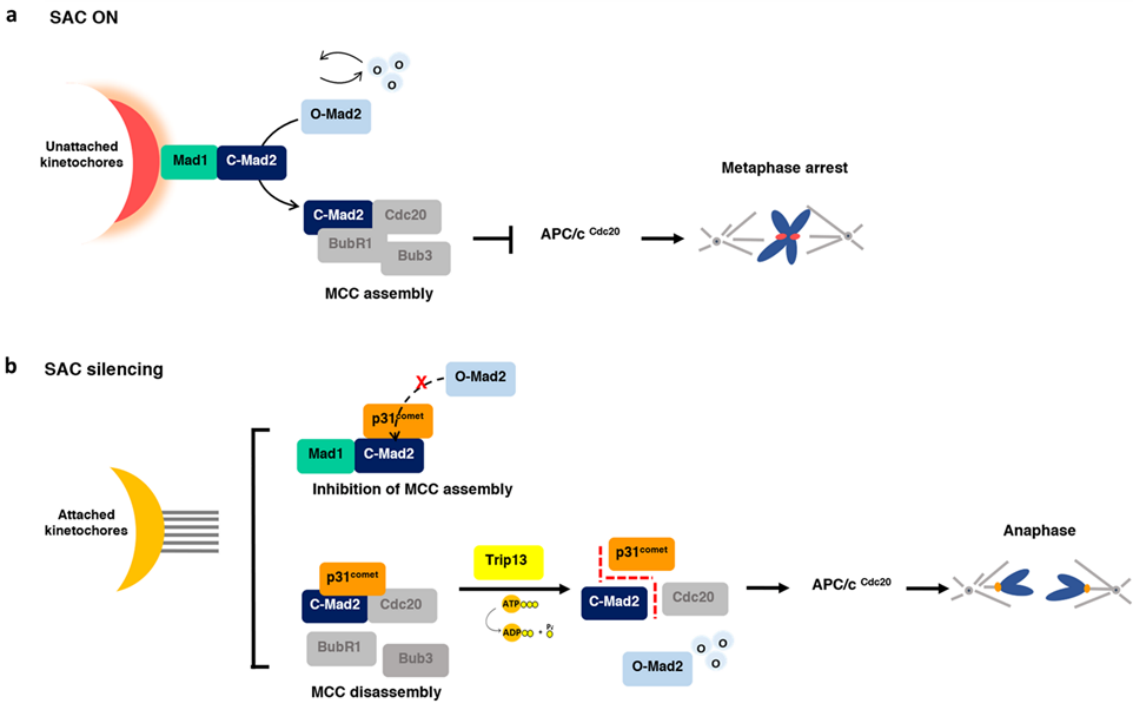

Figure 16. Spindle Assembly Checkpoint mechanism (SAC).

(**a**) SAC activation (SAC ON). At unattached kinetochores, the Mad1-closed Mad2 (-C-Mad2) template recruits cytosolic inactive open-Mad2 (O-Mad2) and catalyzes its conversion to active C-Mad2, which then forms the C-Mad2-Cdc20 complex. C-Mad2-Cdc20 interacts with BubR1-Bub3 to form a stable mitotic checkpoint complex (MCC) which, in turn, prevents Cdc20 from activating the anaphase promoting complex/cyclosome (APC/C^{Cdc20}), resulting in metaphase arrest. (**b**) SAC silencing. Upon kinetochore attachments, the SAC silencing results either from preventing new MCC assembly or disassembly of existing MCC, both are mediated by $p31^{comet}$ protein and lead to APC/C activation and mitotic exit: i) specific binding of $p31^{comet}$ to C-Mad2 of the Mad1-C-Mad2 complex inhibits the further conversion of O-Mad2 into C-Mad2 and, thus, further MCC production; ii) binding of $p31^{comet}$ to MCC-bound C-Mad2 disrupts BubR1-C-Mad2 interaction which promotes MCC disassembly, then Cdc20-C-Mad2 is disassembled upon the cooperative activity of $p31^{comet}$ and the ATPase TRIP13, resulting in the conversion of C-Mad2 to unbound O-Mad2 (206).

5.1. Molecular structure and subcellular localization

$p31^{comet}$ (also known as MAD2L1BP – MAD2L1- binding protein and, initially, as CMT2 – Caught by MAD Two) is encoded by the *MAD2L1BP* gene (Gene ID: 9587), located in chromosome 6p21.1 (207). This protein was initially identified in a yeast two-hybrid screen of HeLa cell complementary DNA (cDNA), using Mad2 as a bait (208). The cDNA encoded a predicted protein sequence of 31

kDa, but the bacterially expressed p31^{comet} protein had 34 kDa. Then, two human transcript isoforms were found, corresponding to variants 1 (NM_001003690.1) (209) and 2 (NM_014628.3) (210). When ectopically expressed, both variants bind endogenous Mad2 to silence the SAC (118). Nevertheless, variant 2 was the most expressed, corresponding to the endogenous 34 kDa p31^{comet} of HeLa cells.

The analysis of the p31^{comet} crystal structure revealed three central α helices inserted between a 7-stranded β sheet and a short helix (Figure 17) (72). p31^{comet} contains a HORMA domain, which is known to be involved in the regulation of multiple eukaryotic signaling pathways and is also present in the MCC subunit Mad2. HORMA domain proteins typically establish interactions through a characteristic "safety belt" mechanism (211). Accordingly, p31^{comet} also adopts a safety belt conformation, in which its C-terminal tail is trapped in the pseudo-ligand binding site (72). p31^{comet} sequence also contains two destruction box (D box) like motifs (208), indicative of an APC/C mediated degradation in anaphase. Indeed, the intensity of p31^{comet} immunofluorescence signal changes during the cell cycle, increasing as mitosis progresses, and dropping at the end of mitosis (208), suggesting p31^{comet} cycles of synthesis and degradation before and after mitosis, respectively. The strong dependence of APC/C activation on p31^{comet} levels also suggests that p31^{comet} should be regulated in some way (168). p31^{comet} levels were reported to be regulated throughout the cell cycle, most likely under the control of the retinoblastoma (RB)/E2 Factor (E2F) pathway (108). Nevertheless, the lack of information on the intracellular concentrations of p31^{comet} during mitosis led to the speculation that p31^{comet} activity could be regulated through posttranslational mechanisms (168). Indeed, p31^{comet} was reported to be a phosphoprotein (212), indicating that its activity is likely regulated by phosphorylation (213,214). Accordingly, Plk1 phosphorylation was proposed to have an inhibitory action on p31^{comet}, mainly through phosphorylation of Ser-102 (215).

Regarding cellular localization, early experiments on HeLa showed that p31^{comet} is present throughout the nucleoplasm during prophase and pro-metaphase, and accumulates at the kinetochores as the cell progresses to metaphase (208). During anaphase and telophase, p31^{comet} signal is found mainly in the spindle or in the mid zone, respectively. Other studies described p31^{comet} localization to the nuclear envelope during interphase and prophase, and to the kinetochores during prometaphase, with p31^{comet} levels decreasing at kinetochores after chromosome alignment (168,205). p31^{comet} traffics through kinetochores with the same kinetics as

Mad2 and localizes to unattached kinetochores in a Mad2-dependent manner (168,205). The binding of the two proteins is maximal during mitotic exit. This behavior highlights the functional relevance of p31^{comet}-Mad2 interaction in p31^{comet}-mediated SAC silencing.

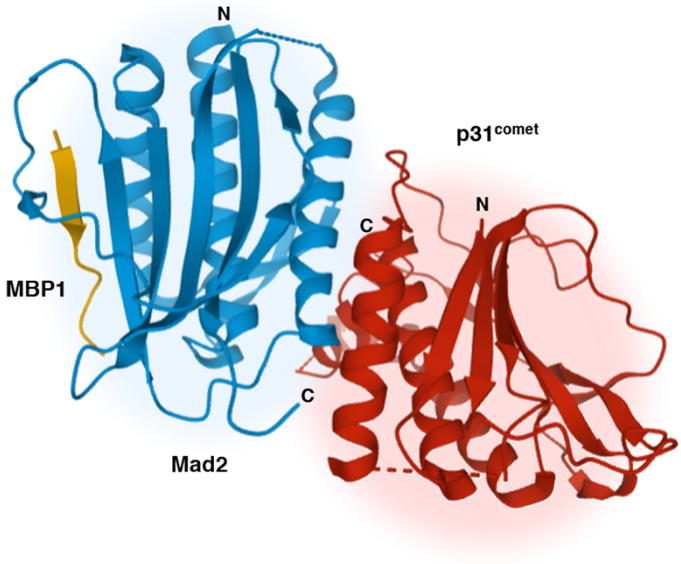

Figure 17. Structural representation (ribbon diagram) of the Mad2-p31^{comet} complex determined by Yang et al [29]. Blue, red and yellow chains represent Mad2, p31^{comet}, and Mad2-binding peptide (MBP1), respectively. The structure was retrieved from Protein Data Bank (PDB): 2qyf (https://www.rcsb.org/structure/2qyf) (206).

5.2. Functions

The Mad2-binding protein p31^{comet} plays an important role in mitosis, ensuring a timely mitotic exit (205,208,213,216–218). p31^{comet} antagonizes the role of Mad2 in SAC activation. Indeed, in the absence of p31^{comet}, SAC could not be silenced, and mitotic exit is drastically delayed. Conversely, p31^{comet} overexpression overrides SAC (208,218) in a manner dependent on its ability to bind Mad2 (205). p31^{comet} silences SAC by two different mechanisms: on the one hand, p31^{comet} prevents further SAC activation by inhibiting O-Mad2 to C-Mad2 conversion and, thus, further MCC formation; on the other hand, p31^{comet} induces SAC inactivation by promoting preformed MCC disassembly. p31^{comet} may also have a role in cohesin degradation required for anaphase onset (74). Other roles of p31^{comet} in important cellular processes, such as meiotic recombination, DNA repair, and insulin-mediated metabolic regulation, have also been reported (113,219–222). These p31^{comet} functions are discussed below.

5.2.1. Preventing Further SAC Activation by Preventing Further MCC Assembly

According to the Mad2 template model outlined in previous sections, the cytosolic inactive O-Mad2 is recruited to unattached kinetochores and binds to C-Mad2-Mad1 to be converted into active C-Mad2 that can bind to Cdc20 (223). Then, C-Mad2-Cdc20 binds to BubR1-Bub3 to form the MCC (205,224). $p31^{comet}$ was proposed to prevent SAC activation by blocking Mad2 activation. $p31^{comet}$ co-localizes with Mad2 at the kinetochores (168,205), and binds to Mad1-bound C-Mad2 at the dimerization interface between C-Mad2 and O-Mad2 (72,216). C-Mad2 displays the C-terminal safety belt region wrapped around the Mad2-interacting motif, while in the O-Mad2 the "safety belt" is folded back on this motif, blocking the ligand-binding site. $p31^{comet}$ binds specifically to C-Mad2 (205,208,216,218), interacting with Mad1- or Cdc20- bound C-Mad2. $p31^{comet}$ and C-Mad2 establish multiple contacts mediated by groups of charged and hydrophobic residues, and interaction of $p31^{comet}$ with C-Mad2 occurs at the dimerization interface between C-Mad2 and O-Mad2, through structural mimicry (Figure 7) (72).

In addition, $p31^{comet}$ competes with O-Mad2 for Mad1:C-Mad2 binding (72,216), with ~40 fold higher affinity to C-Mad2 compared to O-Mad2 (168,225). $p31^{comet}$ was suggested to act as a cap that inhibits the dimerization between O-Mad2 and Mad1-bound C-Mad2, thus preventing the conversion of O-Mad2 into C-Mad2 (216).

This model suggests that $p31^{comet}$ is recruited to the kinetochores along with Mad1:C-Mad2, and that Mad2 activation occurs after weakening the $p31^{comet}$-C-Mad2 interaction (216). Recent findings supported that $p31^{comet}$ counteracts SAC by preventing Mad2 activation (226). $p31^{comet}$ was shown to be critical for the timing of mitotic slippage, suggesting that $p31^{comet}$ leads to a gradual weakening of SAC, mainly by blocking Mad2 activation, allowing a progressive increase on the APC/C^{Cdc20}-mediated degradation of cyclin B1.

However, some aspects remain to be clarified. For example, there is a lack of evidence on how O-Mad2 would be recruited to the kinetochores. Furthermore, the modulation of $p31^{comet}$ levels did not influence the recruitment of O-Mad2 to the kinetochores on HeLa cells (205). Similarly, $p31^{comet}$ levels at the kinetochores did not change after blocking O-Mad2 recruitment to kinetochores. On the other hand, $p31^{comet}$ actively traffics throughout kinetochores along with Mad2 (168). This would implicate a rapid association and dissociation kinetics, contrasting with the notion that $p31^{comet}$ forms a stable cap on C-Mad2-Mad1 complexes at the kinetochores. Further work is needed to clarify this discrepancy.

5.2.2. SAC Silencing by Driving Disassembly of Preformed MCC

Several studies indicate that p31^{comet} has a role in SAC silencing through MCC disassembly. p31^{comet} binds to C-Mad2 bound to Cdc20, resulting in dissociation of Mad2-Cdc20 subcomplex (208). p31^{comet} forms a transient complex with APC/C-bound Mad2, enhancing the activity of Mad2-inhibited APC/C (218). Furthermore, p31^{comet} mediates the extraction of Mad2 from the MCC (205). Yet, p31^{comet} alone was unable to extract Mad2 from MCC bound to APC, and complete dissociation of MCC and SAC requires additional factors, suggesting that other mechanisms are involved in MCC disassembly (205,227).

p31^{comet} promotes MCC disassembly through at least two ATP-dependent mechanisms. First, the binding of p31^{comet} to Cdc20-bound C-Mad2 promotes a conformational change in Cdc20, which facilitates its phosphorylation and consequent dissociation from BubR1 (217). Second, p31^{comet} acts in concert with the AAA-ATPase TRIP13, targeting it to MCC, which triggers the dissociation of the Cdc20-C-Mad2 subcomplex, as well as C-Mad2 conversion back to O-Mad2, via ATP hydrolysis (73,148,213,228–232). As a result, Mad2 is released from MCC as O-Mad2. TRIP13 contains a substrate-binding site comprising two subsites for the interaction with p31^{comet} and C-Mad2 bound to MCC (229). p31^{comet} binding to TRIP13 promotes the engagement of the Mad2 N-terminus into TRIP13 pore loops, leading to Mad2 unfolding and conformational change in the presence of ATP (231,232). Further works revealed that TRIP13-p31^{comet} can prevent APC/C inhibition by MCC but cannot reactivate it per se after APC/C binding to MCC (233). Nevertheless, p31^{comet} ensures the timely metaphase-to-anaphase transition, as cells arrest in metaphase during longer periods in the absence of p31^{comet} (168). TRIP13 was demonstrated to be required for sustaining SAC activation, as unbound C-Mad2 was not sufficient to activate the SAC in TRIP13-deficient cells (148). Indeed, in the absence of TRIP13, the ability to form robust MCC was only restored in Mad2-overexpressing cells (234). Thus, TRIP13 might act in concert with p31^{comet} to replenish the O-Mad2 pool for Mad2 activation (148). Interestingly, the ability of TRIP13/ p31^{comet} to convert C-Mad2 to its open conformer is shared with their respective orthologous PCH-2/CMT-1 (Pachytene Checkpoint Protein-2) in *C. elegans* (73). In fact, the interaction between p31^{comet} and TRIP13 has been observed in different organisms (*C. elegans*, *Oryza sativa*, and *Arabidopsis thaliana*), with roles not only in SAC regulation but also in meiotic recombination, consistent with a conserved

role of p31^{comet} in assisting TRIP13 to disengage HORMA proteins from their "seatbelt" partners (73,219–221,235,236).

p31^{comet} was also suggested to mediate MCC dissociation, through Cdc20 ubiquitination. APC/C-dependent auto-ubiquitination of Cdc20 was proposed to be required for MCC disassembly (42,237). This suggests that p31^{comet} acts in concert with the APC-specific ubiquitin-conjugating enzyme (E2) UbcH10 to promote Cdc20 ubiquitination (42). However, p31^{comet} depletion was still efficient in delaying Mad2-Cdc20 dissociation and mitotic exit in HeLa cells expressing Cdc20 mutants for auto-ubiquitination (238). The exact involvement of p31^{comet} in Cdc20 autoubiquitination is still discussable.

Recently, it was reported that p31^{comet} can cooperate with the Cdc20 binding molecule apcin, to prevent the binding of MCC to the APC/C co-activator Cdc20, allowing APC/CCdc20 to remain active (239).

The data summarized here indicate that p31^{comet} is preponderant for SAC regulation, acting through different mechanisms, considered relevant for p31^{comet}-mediated SAC silencing (168)].

5.2.3. Cohesin Degradation

In addition to silencing the SAC, p31^{comet} was also recently proposed to contribute to cohesin degradation, acting in concert with TRIP13 to release separase from shugoshin 2 (SGO2) (74). It seems that human SGO2, previously known as a meiotic cohesin protector, acts in association with C-Mad2 to inhibit separase through a securin-independent mechanism. Accordingly, both p31^{comet} and TRIP13 were able to disassemble the separase–SGO2–Mad2 complex and to release separase on securin-depleted HeLa cells.

5.2.4. Meiotic Recombination

p31^{comet} was involved in meiotic processes in rice (*Oryza sativa* L.) (220). It co-localizes with ZEP1, a transverse filament protein of synaptonemal complex (SC), and interacts with the Central Region Component 1 (CRC1), which is essential for double-strand break (DBS) formation (220). CRC1 (the mammalian ATPase TRIP13 orthologous in rice) was proposed to bridge the connection between p31^{comet} and ZEP1, suggesting a key role of p31^{comet} in DSB and formation of the SC in rice.

p31^{comet} and TRIP13 orthologous in *C. elegans* (CMT-1 and PCH-2, respectively) also have a relevant function in meiosis. Interaction between the two proteins was found to be required to proofread meiotic homologous interactions (221).

A meiotic role of p31^{comet} was also found in *Arabidopsis* (219). The homologous of p31^{comet} in *Arabidopsis*, COMET, was proposed to mediate the removal of ASY1 (homolog of HORMAD1/2 in mammals and Hop1 in yeast) from the meiotic chromosome axis by PCH-2.

HORMA domain proteins play an important role in the formation of crossovers, ensuring accurate DSB and DNA recombination. TRIP13 was reported to negatively regulate this process, through a negative feedback response by removing HORMA domain proteins.

As far as we know, the role of p31^{comet}-TRIP13 in meiotic recombination has not been reported in humans and deserves to be elucidated.

5.2.5. DNA Repair

Homologous recombination (HR) is a high-fidelity pathway that takes place mainly in S, G2, and M phases (240). HR is dependent on the resection of DBS ends, which in turn is repressed by a signaling cascade that comprises, among others, REV7-Shieldin (SHLD1-3) complex (241). REV7 is a HORMA protein, as Mad2, and similarly to what occurs with the Cdc20-Mad2 subcomplex, the C-terminal "seatbelt" region of REV7 clamps down SHLD3, allowing the recruitment of SHLD1 and 2. Recent evidence demonstrated that p31^{comet} mediates the TRIP13-REV7 interaction, acting as an adaptor for the release of SHLD3 from the REV7-Shieldin complex in human osteosarcoma and embryonic kidney cells (222). This, in turn, would allow DBS end resection and HR, as mentioned above.

5.2.6. Insulin-Mediated Metabolic Regulation

p31^{comet} was involved in metabolic homeostasis through impairment of the insulin receptor (IR) endocytosis (230).

IR can be internalized through clathrin-mediated endocytosis, and this process depends largely on Adaptor Protein 2 (AP2), which interacts with clathrin and cargo. Based on the findings that BubR1 interacts with AP2 and Mad2 with IR (113–115), it was proposed that Mad2 may mediate

the connection between BubR1-AP and IR. p31^{comet} can prevent the interaction between BubR1-AP and Mad2-IR in vitro, which would probably prevent the IR internalization. This possibility is supported by the ability of p31^{comet} to bind to C-Mad2 at the same interface as BubR1 during SAC regulation (242). p31^{comet} knockout mice presented reduced glycogen stores and did not survive after birth. Moreover, p31^{comet} depletion in the liver caused reduced IR levels in the hepatocyte plasma membrane, insulin resistance, hyperglycemia, and hyperinsulinemia in mice (113). Further works are needed to elucidate the precise involvement of SAC-related proteins in metabolic regulation.

5.3. p31^{comet} expression in cancer

Given the important role of p31^{comet} in the control of SAC, dysregulation in the activity or expression of this protein is expected to affect normal cell division, which may lead to cancer. Only one work reported p31^{comet} mutation at the gene sequence levels, in the form of two nucleotide substitutions as potential, but phenotypically irrelevant, polymorphisms in hepatocellular carcinoma (HCC) (243). Altered p31^{comet} gene expression is the most frequently reported deregulation. p31^{comet} mRNA levels were shown to vary between normal tissues, with higher levels in bone marrow (103). When comparing cancer with normal tissues, the analysis of the data from mRNA screenings integrated into the oncomine database (102) revealed that p31^{comet} is overexpressed in an array of cancers. From 447 unique analyses, p31^{comet} mRNA was upregulated in 27, and downregulated in 1 (in pancreatic cancer) only, using the threshold values described in Table 1. p31^{comet} was significantly overexpressed in several types of cancer, including bladder, brain, and central nervous system (CNS), breast, head and neck, kidney, lung, melanoma, and prostate.

Table 1. p31^{comet} mRNA expression according to oncomine database.

p31^{comet} mRNA is upregulated in several cancers. Data were retrieved from the oncomine database (102) (www.oncomine.org), based on the array datasets of 447 unique analysis from several human cancer samples. The following parameters were used for the search in oncomine: threshold *p*-value 0.05; threshold fold change 1.5; threshold gene rank top 10%.

Organ	Cancer type	Upregulated / Downregulated	Dataset reference
Lung	Lung adenocarcinoma	Upregulated	(244)
	Squamous cell lung carcinoma		
	Large cell lung carcinoma		

	Small cell lung carcinoma		
	Lung adenocarcinoma	Upregulated	(245)
	Lung carcinoid tumor		
	Squamous cell lung carcinoma		
	Small cell lung carcinoma		
Breast	Mucinous breast carcinoma	Upregulated	(246)
	Tubular breast carcinoma		
	Ductal breast carcinoma		
	Invasive ductal and invasive lobular breast carcinoma		
	Breast phyllodes tumor		
	Breast carcinoma		
	Invasive ductal breast carcinoma		
Skin	Melanoma	Upregulated	(247)
	Non-neoplastic nevus		
	Cutaneous melanoma		(248)
Parathyroid gland	Parathyroid hyperplasia	Upregulated	(249)
	Parathyroid gland adenoma		
	Non-neoplastic nevus		
	Cutaneous melanoma		
Bladder	Superficial bladder cancer	Upregulated	(250)
Brain and CNS	Pilocytic astrocytoma	Upregulated	(251)
Head and neck	Floor of the mouth carcinoma	Upregulated	(252)
Kidney	Renal oncocytoma	Upregulated	(253)
Leukemia	B-cell acute lymphoblastic	Upregulated	(254)
Prostate	Prostatic intraepithelial neoplasia epithelia	Upregulated	(255)
Uterus	Uterine corpus leiomyoma	Upregulated	(256)
Pancreas	Pancreatic adenocarcinoma	Downregulated	(257)

Furthermore, the analysis of p31^{comet} expression was also performed in the web resource UALCAN (258), using the transcriptomic data from The Cancer Genome Atlas (TCGA). From the 24 types of cancer in analysis, p31^{comet} was overexpressed in 18 and underexpressed in 6 of them (table 2). Cholangiocarcinoma showed a more pronounced overexpression, 1.457 times higher than in normal samples. On the other hand, an opposite result was found to pancreatic adenocarcinoma, which was found to be upregulated when performing UALCAN analysis.

Table 2. p31^{comet} mRNA expression according to UALCAN analysis.

p31^{comet} mRNA is upregulated in 18 from 24 cancers. Data were retrieved from UALCAN web resource (http://ualcan.path.uab.edu/) (258), through the analysis of transcriptomics data from The Cancer Genome Atlas (TCGA) (258). The information is based on a pan-cancer analysis expressed as log_2(TPM+1), where TPM refers to transcripts per million.

Organ	Cancer type	TCGA code	Upregulated / Downregulated
Bile ducts	Cholangiocarcinoma	CHOL	Upregulated
Medulla	Pheochromocytoma and Paraganglioma	PCPG	Upregulated

Esophagus	Esophageal carcinoma	ESCA	Upregulated
liver	Liver hepatocellular carcinoma	LIHC	Upregulated
Head and neck	Head and Neck squamous cell carcinoma	HNSC	Upregulated
Stomach	Stomach adenocarcinoma	STAD	Upregulated
Bladder	Bladder urothelial carcinoma	BLCA	Upregulated
Cervical cancer	Cervical squamous cell carcinoma	CESC	Upregulated
Breast	Breast invasive carcinoma	BRCA	Upregulated
Lung	Lung adenocarcinoma	LUAD	Upregulated
	Lung squamous cell carcinoma	LUSC	Upregulated
Endometrium	Uterine Corpus Endometrial Carcinoma	UCEC	Upregulated
Brain and CNS	Glioblastoma multiforme	GBM	Upregulated
Soft tissues, connective tissues, bones	Sarcoma	SARC	Upregulated
Prostate	Prostate adenocarcinoma	PRAD	Upregulated
Rectus	Rectum adenocarcinoma	READ	Upregulated
Pancreas	Pancreatic adenocarcinoma	PAAD	Upregulated
Skin	Skin cutaneous melanoma	SKCM	Upregulated
Colon	Colon adenocarcinoma	COAD	Downregulated
Kidney	Kidney Choromophobe	KICH	Downregulated
	Kidney renal clear cell carcinoma	KIRC	Downregulated
	Kidney renal papillary cell carcinoma	KIRP	Downregulated
Thyroid	Thyroid carcinoma	THCA	Downregulated
Thymus	Thymoma	THYM	Downregulated

In addition, a recent work published a result based on the analysis of The Cancer Genome Atlas (TCGA) (222). Cancer subtypes presented the same abnormal protein expression pattern. Moreover, both TRIP13 and p31^{comet} overexpressing cancer cells harbored the HR mutational signature (mutational signature 3), suggestive of an inadequate HR. Also, the simultaneous overexpression of TRIP13 and p31^{comet} in breast cancer type 1 susceptibility protein (BRCA-1) deficient cancers seems to be associated with the worst prognosis. This is in agreement with resistance to PARP inhibitors in BRCA-1 mutant cells. Although BRCA-1 deficient cancers cannot activate HR, TRIP13 and p31^{comet} overexpression can balance the lack of BRCA-1 response and promote HR. Indeed, this had already been observed for TRIP13 overexpressing cells (259). These findings reinforce the clinical significance of p31^{comet}.

Moreover, changes in regulators of p31^{comet} expression may be associated with cancer development. p31^{comet} expression was suggested to be regulated by the RB-E2F pathway (108). RB inhibits the E2F family of transcription factors, thus limiting gene expression, being RB mutation or inactivation associated with many cancers (109). *In silico* investigation from oncomine data showed that E2F can bind to DNA regions close to the start codon of both p31^{comet} isoforms and

that the expression of E2F family members E2F5 and E2F4 is correlated with that of p31^{comet} in breast cancer and lung adenocarcinoma, respectively (108). In addition, E2F induces p31^{comet} overexpression in colorectal carcinoma cells, and the reduction of E2F activity resulted in p31^{comet} loss in osteosarcoma cells (108). The expression ratio p31^{comet}/Mad2 was suggested to be important in cancer development (108,118). Indeed, although the analysis of 51 HCC tissues did not reveal significant differences between tumor and non-tumor liver samples (243), it was found that p31^{comet}/Mad2 ratio was altered in HCC, as well as non-small cell lung cancer carcinoma cells, and such alteration was correlated with mitotic slippage (118). Like p31^{comet}, Mad2 expression is also regulated by Rb-E2F pathway and the analysis of mRNA screening data revealed that expression of p31^{comet} and Mad2 expression is coordinately increased in breast, lung, and cervical cancer (108). Higher p31^{comet}/Mad2 ratios were positively correlated with the resistance of human cancer cells to spindle poisons (169). As Mad2 overexpression is known to promote tumorigenesis in cancer, and considering the coordinated expression of p31^{comet} and Mad2, it was suggested that p31^{comet} promotes survival of Mad2 overexpressing cells by buffering increased Mad2 activity (108).

Therefore, p31^{comet} expression seems to be under the control of the RB/E2F pathway, and p31^{comet} upregulation is frequently linked to cancer development. Moreover, p31^{comet}/Mad2 ratio was found to be crucial for cell survival and its deregulation may be a preponderant factor for cancer development (108,118).

5.4. Targeting p31^{comet} as an anticancer strategy

SAC has a crucial role in ensuring the fidelity of chromosome segregation, motivating its recent targeting by new antimitotic strategies (127). Given its importance in SAC silencing, as well as its dysregulated expression in cancer cells, p31^{comet} has been regarded as a potential anti-tumoral target. For that, two strategies can be considered: i) overexpressing p31^{comet} to preciously silence the SAC; ii) inhibiting p31^{comet}, to delay SAC silencing. Both strategies are expected to lead to the death of cancer cells. In addition, modulation of p31^{comet}-derived peptides may be as an alternative approach to directly inactivate APC/C and, thus, to sustain mitotic arrest (260).

5.4.1. Overexpressing p31^{comet} for Cancer Therapy

Aberrant SAC inactivation frequently results in massive chromosome missegregation, which often triggers cell death and/or senescence (a permanent state of cell cycle arrest) (261). Indeed, p31^{comet} overexpression, expected to inactivate SAC, is cytotoxic to several cancer cell lines (lung, cervix, breast, liver, bone, kidney, and brain), in a Mad2-binding dependent manner, by driving senescence and/or apoptosis (261–263). p31^{comet}-induced senescence was found to be associated with mitotic catastrophe phenotypes, such as micronucleation, nuclear and chromosomal abnormalities, and anaphase bridges (261). In addition, senescence was not associated with p53 status (262), except in A549 p53-proficient cells, where it was also dependent on the tumor suppressor protein p21$^{Waf1/Cip1}$ (261).

Cellular senescence has been considered as a suppressive mechanism for tumorigenesis (264), making p31^{comet} overexpression a possible anti-cancer strategy (261). However, senescence may also play a role in tumorigenesis by promoting inflammation and remodeling the extracellular matrix, contributing to a pro-tumorigenic environment (265). p31^{comet} overexpression was reported in a variety of human cancers (Table 1), being associated with senescence (262). Also, p31^{comet} overexpression promotes resistance of cancer cells to spindle poisons by abolishing SAC-induced mitotic arrest (118,169,263).

In sum, while overexpressing p31^{comet} could be an attractive strategy for cancer intervention, the contribution of senescence to tumorigenesis, together with the development of resistance to MTAs, should not be ignored. In this sense, to our view, depletion or inhibition of p31^{comet} could be a better strategy.

5.4.2. Inhibiting p31^{comet} to Increase Sensitivity to Microtubule Poisons

p31^{comet} depletion was reported to sensitize cancer cells to microtubule-targeting agents (MTAs) at concentrations that could not sustain the SAC alone (118). Low concentrations of spindle poisons may still interfere with microtubule dynamics and activate SAC, although in a manner that allows the kinetochore-microtubule attachments to be corrected and the SAC satisfied. Depletion of p31^{comet} could, thus, potentiate the mitotic arrest induced by spindle poisons, by trapping cells in mitosis until death. This highlights the relevance of exploiting p31^{comet} depletion as a strategy to increase the efficacy of MTAs in cancer treatment.

Interestingly, the yeast homologous to human p31^{comet}, and a human p31^{comet}-derived peptide (from the homologous region to the yeast protein) can bind to APC/C (260). When these peptides were present in excess, they were able to inhibit APC/C in yeast, through competition with the APC/C co-factors Cdc20 or Cdc20 homologue-1 (Cdh1), thereby increasing sensitivity to the spindle poison benomyl. This suggests that p31^{comet}-derived peptides can serve as a strategy to inhibit APC/C in order to increase sensitivity to MTAs, which is particularly relevant to overcome resistance issues due to slippage.

6. Three-dimensional in vitro cell culture models for pre-clinical evaluation of therapies

Numerous drugs with anti-cancer potential emerge every day and constantly need to be screened. A common path is generally followed: drugs are first tested in a 2D model, usually a panel of cancer cell lines, followed by pre-clinical tests in animal models before clinical trials. The transition from a 2D to a more complex model is obviously required (266). Cell monolayers lack the three-dimensional organization, as well as the complexity of the tumor microenvironment. As such, it is undeniable the utility of animal models, that allows not only to rebuild a tumor architecture and a microenvironment but also to perform pharmacokinetic studies. However, it is not rare that drugs with promising results in pre-clinical studies fail to succeed in clinical trials (267). Indeed, animal models present some limitations (268). For example, human cancer cells usually grow at higher rates in xenograft models; there are also differences in TEM, as the stroma is different from the human. Furthermore, high-cost and ethical issues are frequently associated with animal models.

Considering all these concerns, 3D *in vitro* culture systems emerge as attractive models for drug assessment. Therefore, it is possible to recreate several traits of human tumors, like 3D structure and microenvironment.

As outlined before, the tumor microenvironment (TEM) is illustrated by the presence of a high diversity of stromal cells and ECM that acquire particular traits in the course of the tumorigenic process. For instance, the abnormal vasculature, in association with an unrestricted proliferation, leads to the insufficient blood supply to the inner regions of the tumor (14,269,270). Consequently, hypoxia leads to the emergence of necrotic regions, as well as to a metabolic adaptation, with a

shift to anaerobic metabolism. As such, lactate production leads to the acidification of the environment (Warburg effect). The lower pH impairs drug effectiveness, as they are converted into cationic substances ("ion trapping" process) that cannot transpose cell membrane. In addition, the rigid ECM of the tumor constitutes a physical barrier that hampers drug penetration.

Among 3D in vitro systems, spheroids and organoids have been increasingly regarded as promising models (266). Organoids are 3D structures made of organ-specific cells, normally derived from adult or embryonic stem cells. Organoids reflect the functionality and the architecture of the origin tissues. Organoids have been revealed useful in personalized medicine. As these structures can be formed from healthy or tumor tissues, they allow to test and to access the response to new drugs in a more specific and less toxic manner. However, organoids still face some limitations, due to the lack of human stromal components, although increasingly efforts have been made in this field (266). On the other hand, spheroids represent the most common *in vitro* 3D model in research. Spheroids are aggregates made of cells that assemble and develop into structures that reflect the TEM (Figure 18). Given the ease of handling and the versatility of spheroids, they have been revealed very useful in anti-cancer drug screening (14,266).

Tumor spheroids can be produced by self- or induced- aggregation of cells from a cell suspension (266). While cells assemble into a spheroid, cell-cell interactions are privileged through desmosomes and dermal junctions (271). In addition, as components of ECM are secreted and deposited, cells-ECM interactions are enhanced, and typical tumorigenic transformations of TEM take place. Spheroids of appropriate size (200-500 μm) are usually spherical and reflect the complexity of a tumor (272). Spheroids can be homotypic or heterotypic as if they are composed of single or multiple cell types, respectively (266). Heterotypical spheroids include not only cancer cells but may also comprise stromal cells, such as fibroblasts, endothelial cells, and immune cells.

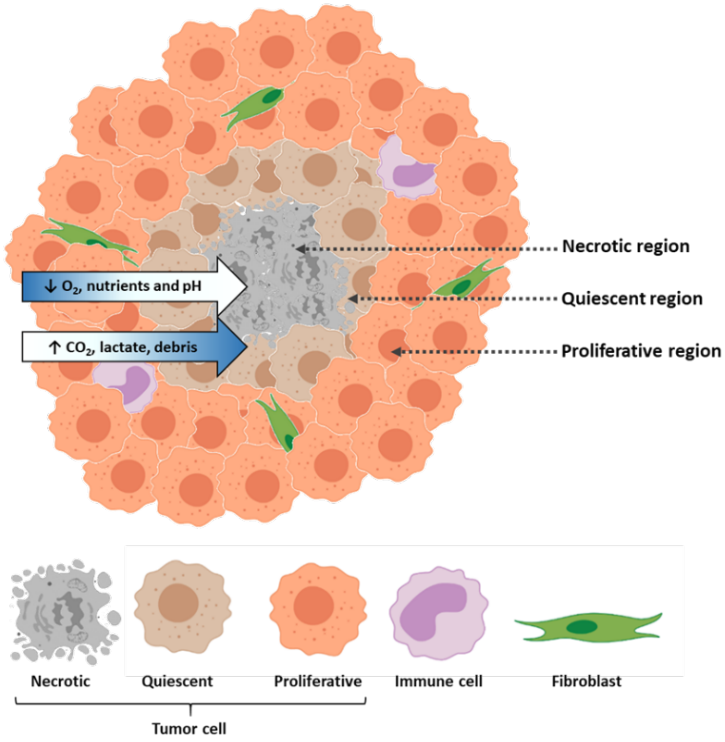

Figure 18. Schematic representation of a multicellular tumor spheroid.

Cells within a spheroid are typically organized in three regions: one more internal, necrotic; one intermediate, quiescent; and one more external, proliferative. Due to the arrangement of the cells, O_2, nutrients, and pH decrease from the outside to the inside, while the concentrations of CO_2, lactate, and waste are higher in most internal zones. Created with BioRender.com and adapted from (14).

The gradient of oxygen (O_2) and nutrients formed as a result of a limited diffusion to the most internal regions of the spheroids promotes the development of distinct layers of heterogeneous cell populations. The most external zone comprises high-proliferative cells, an intermediate layer is composed of quiescent and senescent cells, and the inner region contains necrotic and apoptotic cells. In parallel to what happens in tumors, the O_2 gradient promotes an anaerobic metabolism in internal zones, which results in an acidification of the environment and limits drug efficacy (14,266). In addition, an intensification of the interstitial fluid pressure is observed, as a result of an increased density and compaction, which also limits drug penetration. Changes in protein-expression patterns are also observed to enhance the resistance to drug treatment. For instance, an increase of anti-apoptotic proteins, such as BCL-2 family members, is commonly observed, as well as metaloproteases (MMPs) (266).

Considering the aforementioned reasons, spheroids are advantageous 3D models that allow not only to mimic tumor-specific traits more easily, but also to reduce the ethical and practical constraints associated with the use of animal models

CHAPTER II

Motivations and Aims

Cancer is the second leading cause of death worldwide (1). Mitosis is a crucial step in the cell cycle and an attractive target for anticancer therapies (39,81). The approved antimitotic drugs are mainly MTAs which are amongst the most successful class of chemotherapeutics (116). However, resistance mechanisms and adverse effects related to their action on microtubules limit their efficacy (70,125,126). As such, several proteins involved in the regulation of SAC have arisen as putative targets for antimitotic chemotherapy, without affecting microtubules (273). In addition, investigation on combination strategies has retrieved promising outcomes. An interesting approach consists of shifting the cell fate of a mitotic-arrested cell to death either by delaying slippage or promoting apoptosis (120,175). For instance, targeting some SAC-silencing effectors can increase the sensitivity to MTAs of tumors or cancer cells otherwise resistant (143,167–169,263,274). Furthermore, the combination of antimitotics with pro-apoptotic drugs, such as ABT-263/Navitoclax, or WEHI-539 can potentiate cell death (128,191,192). Additionally, the combination of cisplatin with antimitotic strategies that do not target microtubules have already been tested (197,199,204).

In the context of those therapeutic possibilities, the SAC-silencer p31^{comet} emerges as a potential target. p31^{comet} can impair SAC through different mechanisms (58,78,123–125,127–129,232,275), and its overexpression can override the mitotic arrest induced by MTAs in a variety of cancer cell lines, inducing resistance to spindle poisons (118,169,262,263). Also, p31^{comet} overexpression was reported in several human cancers (262).

Therefore, the first main aim of this work, covered in chapters III and IV, refers to the evaluation of the potential of p31^{comet} knockdown within the scope of anticancer strategies, in combination with clinically relevant doses of the MTA paclitaxel or the pro-apoptotic Navitoclax. Non-small cell lung cancer (NSCLC) was selected as a model, given its elevated mortality (1). Accordingly, the specific objectives are:

- To explore the anti-tumoral potential of p31^{comet} knockdown in NSCLC cells in combination with paclitaxel and Navitoclax;

- To validate this strategy in 3D-cancer models, through the generation of tumor spheroids.

The second main aim intends to evaluate the clinical relevance of p31^{comet} targeting to oral cancer. Impairment of SAC silencing through spindly silencing was previously shown to sensitize oral squamous carcinoma cells to clinically relevant doses of cisplatin (199). In addition, cisplatin is the

first-line chemotherapeutic drug used in the treatment of OSCC. As such, OSCC was chosen as a model. The specific objectives of this aim, covered in chapter V, are:

- to access the clinical relevance of $p31^{comet}$ as a biomarker in oral cancer, by assessing $p31^{comet}$ expression in head and neck squamous cell carcinoma and the correlation with clinicopathological features of patients;

- to investigate the effect of $p31^{comet}$ knockdown in combination with clinically relevant doses of cisplatin, in OSCC cells,

$p31^{comet}$ knockdown is expected to enhance the lethality of MTAs, and the pro-apoptotic drugs in NSCLC, as well as to improve the efficacy of cisplatin in OSCC cells. Therefore, it is anticipated that the inhibition of SAC silencing through $p31^{comet}$ targeting can open a new window of possibilities for anticancer strategies.

CHAPTER III

Antagonizing the spindle assembly checkpoint silencing enhances paclitaxel and Navitoclax-mediated apoptosis with distinct mechanistic

The information provided on this chapter was partially based in the following publication:

Henriques, A.C.; Silva, P.M.A.; Sarmento, B.; Bousbaa, H.. "Antagonizing the spindle assembly checkpoint silencing enhances paclitaxel and Navitoclax-mediated apoptosis with distinct mechanistic". Scientific Reports 11 1 (2021): http://dx.doi.org/10.1038/s41598-021-83743-7.

1. Abstract

Antimitotic drugs arrest cells in mitosis through chronic activation of the spindle assembly checkpoint (SAC), leading to cell death. However, drug-treated cancer cells can escape death by undergoing mitotic slippage, due to premature mitotic exit. Therefore, overcoming the slippage issue is a promising chemotherapeutic strategy to improve the effectiveness of antimitotics. Here, we antagonized SAC silencing by knocking down the MAD2-binding protein p31^{comet}, to delay mitotic slippage, and tracked cancer cells treated with the antimitotic drug paclitaxel, over 3 days live-cell time-lapse analysis. We found that in the absence of p31^{comet}, the duration of the mitotic block was increased in cells challenged with nanomolar concentrations of paclitaxel, leading to an additive effect in terms of cell death which was predominantly anticipated during the first mitosis. As accumulation of an apoptotic signal was suggested to prevent mitotic slippage, when we challenged p31^{comet}-depleted mitotic-arrested cells with the apoptosis potentiator Navitoclax (previously called ABT-263), cell fate was shifted to accelerated post-mitotic death. Interestingly, the results also hinted that the levels of Mcl-1 expression may help to select the cases that would benefit from p31^{comet} depletion during Navitoclax treatment. We conclude that inhibition of SAC silencing is critical for enhancing the lethality of antimitotic drugs as well as that of therapeutic apoptosis-inducing small molecules, with distinct mechanisms. The study highlights the potential of p31^{comet} as a target for antimitotic therapies.

2. Introduction

Microtubule targeting agents (MTAs) such as paclitaxel prevent the spindle assembly during mitosis, leading to chronic activation of the spindle assembly checkpoint (SAC), which results in the mitotic arrest of cancer cells until dead (44,116,117). However, the efficacy of these drugs is limited by neurotoxic and hematopoietic side effects, as well as by resistance mechanisms (70,125,276). Therefore, alternative antimitotic therapies that do not directly interfere with microtubules have led to the development of second-generation antimitotics (127). As such, SAC-related proteins have been regarded as potential targets for the development of new strategies to kill cancer cells or to increase their sensitivity to the current chemotherapeutics (63,144,149,164–166,277).

SAC is a mitotic surveillance mechanism that prevents metaphase to anaphase transition until all chromosomes are correctly attached to the spindle microtubules and bi-orientated in the metaphase plate (44,275,278). Improper chromosome-microtubule attachments that occur during normal mitosis, or artificially under MTA treatment, activate the SAC. The SAC activity is mediated by the mitotic checkpoint complex (MCC), which is formed between the SAC proteins Mad2 (mitotic arrest deficiency 2), Bub3 (budding uninhibited by benomyl 3) and Bub1-related 1 (BubR1), and Cdc20 (cell-division cycle protein 20). At unattached kinetochores, closed-Mad2 conformation (C-Mad2) bound to Mad1 recruits open-Mad2 conformation (O-Mad2), thereby promoting its conformational change to C-Mad2 (223,279), which in turn sequesters Cdc20, an activator of anaphase promoting complex/cyclosome (APC/C). Then, Cdc20-C-Mad2 binds to the BubR1-Bub3 complex, forming the MCC. As a result of Cdc20 sequestration, the APC/C is kept inactive, thereby preventing securin and cyclin B degradation by the 26S proteasome and, thus, mitotic exit (44,278,280). Once all chromosomes are properly aligned at the metaphase plate, the SAC must be silenced for the cell to proceed to anaphase. The Mad2-binding protein p31^{comet} (69,77) is crucial to this SAC silencing, by blocking further Mad2 activation and promoting MCC disassembly (72,216).

The fate of mitotic-arrested cells was reported to be dictated by two competing networks (175). One network determines cell death through accumulation of apoptotic signals during mitosis. The other network determines mitotic slippage through gradual degradation of cyclin B1. The network that reaches its threshold first determines the cell fate. Therefore, theoretically, it should be

possible to have a control over the cell fates and influence the effectiveness of antimitotics if mitotic slippage is retarded and/or death signal accumulation is accelerated (120,175).

In this context, and given its key role in SAC silencing and mitotic exit, p31^{comet} appears as an ideal target to delay mitotic slippage. On the other hand, the BH3-only proteins, Bim, Bid, Bad, and Noxa, have been shown to contribute to death in mitosis (281–284). Thus, using BH3-mimetic drugs, in a background of mitotic slippage delay, should shift the fate of mitosis-arrested cells in favor of death. Therefore, we tested these two possibilities by monitoring cell fates by single-cell tracking during three-day live-cell time-lapse analysis. Firstly, we investigated the relative contribution of delaying mitotic slippage (through p31^{comet} depletion) to cell death following exposure to nanomolar concentrations of paclitaxel. Secondly, we determined the relative contribution of BH3-mimetic-mediated apoptosis potentiation to cell death of cells delayed in mitosis by p31^{comet} depletion.

3. Materials and methods

3.1. Cell lines and culture conditions

Cells were grown and maintained as described (144). NCI-H460 (human non-small cell lung cancer) cells were grown in RPMI-1640 culture medium (Lonza, Basel, Switzerland) with 5% FBS. HPAEpiC (human pulmonary alveolar epithelial cells), A549 (human adenocarcinoma alveolar basal epithelial), and Calu-3 (human lung adenocarcinoma) cells were grown in DMEM medium with 10% fetal bovine serum (FBS, Biochrom) and 1% non-essential amino acids (Sigma Aldrich Co., Saint Louis, MO, USA). Cells were maintained in a 5% CO_2 humidified incubator, at 37 °C. The experiments were performed when cells were at exponentially growing and presented more than 95% viability. The NCI-H460, A549, and Calu-3 cell lines were obtained from American Type Culture Collection. HPAEpiC cell line was purchased from ScienCell Research Laboratories.

3.2. RNA isolation and quantitative real-time PCR

RNA isolation for quantitative real-time PCR was performed using the PureZOL RNA Isolation Reagent (Bio-Rad Laboratories, Hercules, CA, USA), according to the manufacturer's instructions. Quantification of RNA was achieved by spectrophotometry (NanoDrop 2000, Termo Scientifc, Waltham, MA, USA). cDNA was synthesized with the iScript cDNA Synthesis Kit (Bio-Rad),

according to the supplier's instructions. The iQ SYBR Green Supermix Kit (Bio-Rad) was used for amplification on iQ Termal Cycler (Bio-Rad) coupled to CFX Manager Sofware (version 3.1, Bio-Rad), as follows: initial denaturing step at 95.0°C for 3 min; 40 cycles at 94.0°C for 20 s; 65.0°C ($p31^{comet}$) or 56°C (Mcl-1, Bcl-2, and Bcl-xL) for 30 s and 72.0°C for 30 s. Temperatures from 65.0 to 95.0°C, with increments of 0.5°C for 5 s were included in the melt curves. Primers were used at a final concentration of 0.1 µM.

$p31^{comet}$-directed primers were designed in PerlPrimer software v1.1.21 (285) and tested for $p31^{comet}$ amplification, targeting transcript variants 1 and 2, using the following temperature values for the annealing step: 56, 57, 60 and 65°C (Supplementary figure S1). However, the amplification was only successful for variant 2 (annealing temperature of 65°C), which was previously shown to be the most expressed (118). Therefore, the primers 5'-AGTCCCTGATTTGGAGTGGT-3' (forward), 5'-GTAAACTGACAGCAGCCTTCC-3' (reverse) were used for $p31^{comet}$ amplification. For amplification of Mcl-1, Bcl-2, and Bcl-xL, the following primers were used: Mcl-1, 5'-CCAAGGCATGCTTCGGAAA-3' (forward), 5'-TCACAATCCTGCCCCAGTTT3' (reverse) (286); Bcl-2, 5'-ATCGCCCTGTGGATGACTGAGT-3' (forward), 5'-GCCAGGAGAAATCAAACAGAGGC-3' (reverse); Bcl-xL, 5'-GCCACTTACCTGAATGACCACC-3' (forward), 5'-AACCAGCGGTTGAAGCGTTCCT-3' (reverse) (287). In addition, the following primer sequences were employed for the amplification of actin and GAPDH: actin, 5'-AATCTGGCACCACACCTTCTA-3' (forward), 5'-ATAGCACAGCCTGGATAGCAA-3' (reverse) (274); GAPDH, 5'-ACAGTCAGCCGCATCTTC-3' (forward), 5'-GCCCAATACGACCAAATCC-3' (reverse) (288). For each data point, triplicated experiments were performed. The results were normalized against GAPDH and actin and expression levels and analyzed through the ΔΔCT method. Over- or underexpression of a gene was determined with basis on a fold value of mRNA level ≥ or ≤ 1.5 relative to that of normal cells.

3.3. siRNAs transfection

NCI-H460 cells were seeded at a density of 0.1275×10^6 cells per well, in 6-well plates containing complete culture medium. Cells were transfected after 24 h using INTERFERin siRNA Transfection Reagent (PolyPlus, New York, USA) following the manufacturer's instructions. Transfection was performed with 50 nM of a validated siRNA sequence against $p31^{comet}$ (289) or a validated negative control siRNA (AllStars Negative Control siRNA, Qiagen, Germantown MD, USA).

3.4. Cell extracts and Western blotting

Preparation of total cell protein extracts was performed as previously described (290). For Western Blot analysis, samples were separated by molecular weight using SDS-PAGE gels and transferred to a nitrocellulose membrane. The membrane was blocked with 0.05% Tween-20 with 5% w/v nonfat dry milk and the incubation with antibodies was performed within the same solution. The signal was detected using ECL detection of the HRP-conjugated secondary antibodies. Blots were visualized using X-ray films. Images of X-ray films were captured using Carestream BIOMAX Light Film (Sigma-Aldrich) and quantified by densitometry using ImageJ 1.4v software (http://rsb.info.nih.gov/ij/). The primary antibodies were used as follows: rabbit anti-$p31^{comet}$ (abcam) and mouse anti-α-tubulin (Sigma-Aldrich), diluted at 1:1000 and 1:5000, respectively. Horseradish peroxidase (HRP)-conjugated secondary antibodies were diluted at 1:4000 (anti-mouse, Sigma-Aldrich) or at 1:1000 (anti-rabbit, Sigma-Aldrich). ImageJ 1.4v software was used for the quantification of the intensity of the protein signal. α-Tubulin expression levels were used for normalization.

3.5. Mitotic index determination

NCI-H460 cells were seeded in 6-well plates containing a complete culture medium at a density of 0.1275×10^6 cells per well. Cells were counted 48 h after transfection with control- or p31comet siRNA, or 24 h after paclitaxel treatment. For the $p31^{comet}$ siRNA and paclitaxel cotreatment, paclitaxel was added 24 h after siRNA transfection. Cells were counted from random microscope fields ($n > 2000$ for each condition). Round-shaped mitotic cells were quantified over the total cell population for the determination of the mitotic index. Paclitaxel (Sigma-Aldrich) was used at a clinically relevant concentration of 10 nM.

3.6. Cell viability assay

The MTT (3-(4,5-dimethylthiazolyl-2)-2,5-diphenyltetrazolium bromide) assay (Sigma-Aldrich) was used to determine cell viability. Control and $p31^{comet}$ siRNA-treated cells (NCI-H460 or A540) were seeded in 96-well plates at the density of 5000 cells per well. After 6 h, paclitaxel was added at a clinically relevant range of concentrations (0–100 nM) (291,292). 48 h later, the culture medium was replaced with fresh FBS-free medium containing 20 µl of MTT reagent (5 mg/ml in PBS). Cells were at 37°C and 5% CO_2 for 4 h. Solubilization of the purple formazan crystals was

achieved with a detergent solution (89% (v/v) 2-Propanol, 10% (v/v) Triton X-100, 1% (v/v) HCl 3.7%), for 2 h. Results were analyzed based on optical density at 570 nm. Measurements were performed in a microplate reader (Biotek Synergy 2, Winooski, VT, USA) coupled with the Gen5 software (version 1.07.5, Biotek, Winooski, VT, USA). Cell viability values were normalized against control siRNA-treated cells.

3.7. Colony forming assay

Colony formation assays were performed as described (274). 24 h after control- or $p31^{comet}$ siRNA-transfection, NCI-H460 or A549 cells were seeded in six-well plates at the density of 500 cells per well. Cells were allowed to attach for 6 h and then treated with paclitaxel (2 and 4 nM and 10 nM) and/or Navitoclax (3.5 μM). 48 h later, the medium was removed, cells were washed gently with PBS, and fresh medium was added. Cells were allowed to grow for 10 days, and the recovered colonies were fixed with 3.7% (w/v) paraformaldehyde in PBS for 5 min and stained with 0.05% (w/v) violet crystal (Merck Millipore, Billerica, MA, USA) in distilled water for 20 min. Three independent experiments were performed on duplicate dishes for each condition. The number of colonies was counted and the plating efficiency (PE) was calculated as the percentage of the number of colonies over the number of cells seeded in control. The survival fraction (the number of colonies over the number of cells seeded × 1/PE) was determined for each condition.

3.8. Flow cytometry

NCI-H460 cells were plated in six-well plated at the density of 0.12750 x 10^6 cells per well. 24 h after control- or $p31^{comet}$ siRNA-transfection, cells were treated with 10 nM or 100 nM of paclitaxel. 24 or 48 h later, cells were harvested and prepared for flow cytometry, as previously described (274). Cell cycle analysis was performed after treatment with propidium iodide and RNase. Briefly, cells were harvested, washed twice in PBS, fixed in 70% ice-cold ethanol, and maintained at 4 °C for at least 30 min. Cells were then treated with 5 μg/ml propidium iodide and 100 μg/ml RNase in PBS for 30 min and analyzed in the flow cytometer. Apoptosis detection was performed with the Annexin V-FITC Apoptosis Detection Kit (eBioscience, Vienna, Austria) according to the manufacturer's instructions. Flow cytometry analysis was carried out using a BD Accuri C6 Flow cytometer (BD Biosciences, Qume Drive, San Jose, CA) with the analysis of 20,000 events per

sample. Data were analyzed with BD Accuri C6 Plus Sofware, version 1.0.27.1 (www.bdbiosciences.com).

3.9. TUNEL assay

In order to detect DNA breaks, Terminal deoxynucleotidyl transferase-mediated nick end labeling (TUNEL) assay was performed. Briefly, cells were plated and treated as above in six-well plates containing coverslips. Coverslips-attached cells were processed with DeadEnd Fluorometric TUNEL System (Promega, Madison, WI, USA), according to the manufacturer's instructions. For DNA staining, 2 µg/ml of DAPI was used in Vectashield mounting medium. TUNEL-positive cells were scored in a total of 500 cells, from at least ten random microscopic fields, under a fluorescence microscope, to determine the levels of cells undergoing cell death.

3.10. Live cell imaging

For live-cell imaging experiments, 5.5×10^6 NCI-H460 cells were seeded onto LabTek II chambered coverglass (Nunc, Penfeld, NY, USA). Cells were allowed to attach for 24 h at 37°C with 5% CO_2, and then transfected with control or $p31^{comet}$ siRNA or treated with 10 nM of paclitaxel, or 3.5 µM of Navitoclax. For cotreatment, paclitaxel or Navitoclax were added 24 h after siRNA-transfection. Time-lapse imaging was performed 24 h after siRNA transfection or immediately after the addition of paclitaxel or Navitoclax. RPMI without phenol red supplemented with 5% FBS was used in the experiments. Image capture was performed up to 72 h at intervals of 10 min under differential interference contrast (DIC) optics, with a 63× objective. An Axio Observer Z.1 SD inverted microscope (Carl Zeiss, Germany) coupled with an incubation chamber with the temperature set to 37°C and an atmosphere of 5% CO_2 was used in the experiments. ImageJ software (version 1.44, Rasband, W.S., ImageJ, US National Institutes of Health, Bethesda, MD, USA) was used to produce movies from the images captured during time-lapse imaging. The cells were followed through the entire imaging period and cell fates were tracked for each experimental condition. The number of cells was scored for mitosis and cell death based on changes in cell morphology by DIC imaging. Cell death was characterized by cell retraction and plasma membrane blebbing, and mitotic entry by cell rounding. Dead cells were categorized into death in mitosis (DiM) or post-mitotic death (PMD) when the death occurred before or following cell division, respectively.

3.11. Microscopy analysis and image processing

A Nikon TE 2000-U microscope (Amsterdam, Netherlands), with a DXM1200F digital camera (Amsterdam, Netherlands) and a Nikon ACT-1 software (version 2.62, Melville, NY, USA) was used for phase-contrast experiments, as described previously (274). The acquisition of fluorescence images was performed in a Plan Apochromatic 63x/NA 1.4 objective on an Axio Observer Z.1 SD microscope (Carl Zeiss, Germany), coupled to an AxioCam MR3. For Z-stacks generation, the AxioVision Release SPC software (version 4.8.2, Carl Zeiss, Germany), with 0.4 mm intervals and after image deconvolution was used. ImageJ (version 1.44, Rasband, W.S., ImageJ, US National Institutes of Health, Bethesda, MD, USA) was used for image processing.

3.12. Statistical analysis

Data were collected in the same experiments, being control siRNA and p31^{comet}-siRNA only conditions the same for all the data. For statistical analysis, Unpaired Student t-test or ordinary two-way ANOVA with Tukey's multiple comparisons test, or Kruskal–Wallis with Dunn's multiple correction test were performed in GraphPad Prism version 7 (GraphPad software Inc., CA, USA). Data are shown as the means ± standard deviation (SD) of at least three independent experiments.

4. Results

4.1. p31^{comet} expression and knockdown

In order to obtain a better understanding on the relevance of p31^{comet} as a potential target for cancer therapy, p31^{comet} expression was assessed in three non-small lung cancer cell lines (NSCLC): NCI-H460, A549 and Calu-3, and compared to the non-tumor cell line HPAEpiC. Primers for both p31^{comet} variants were tested (supplementary table S1). However, only variant 2 was successfully amplified (Supplementary figure S1), which is in line with experiments of Ma and colleagues (118) showing that variant 2 corresponds to the most expressed isoform. Therefore, variant 2-directed primers were used to evaluate the expression of p31^{comet}. Upregulation of p31^{comet} was observed both at mRNA and protein levels in all the NSCLC cells tested comparatively to HPAEpiC (Figure 19a and b). This highlights the importance of targeting p31^{comet}. Due to its suitability for quantitative evaluation of morphological changes in *in vivo* microscopy assays, NCI-H460 cell line was selected in this study. p31^{comet} knockdown was performed using siRNA duplexes previously

validated (289) and ascertained by qRT-PCR and immunoblotting against p31^{comet}. More than 70% depletion of p31^{comet} was achieved, both at mRNA and protein levels, 48 h after treatment of NCI-H460 cells with p31^{comet} siRNAs (sip31^{comet}), comparatively to cells treated with a negative control siRNA (Control siRNA) (Figure 19c and d). These depletion levels were not altered by extended transfection time. Furthermore, contrast-phase microscopy analysis revealed an accumulation of round shaped mitotic cells and an increase in the mitotic index (Figure 9e), in accordance with previously reported p31^{comet} depletion phenotype (208,218).

4.2. p31^{comet} depletion enhances lethality of nanomolar concentrations of paclitaxel by promoting massive cell death in mitosis.

We explored whether delaying mitotic slippage, by antagonizing SAC silencing through p31^{comet} depletion, could potentiate cancer cell killing to nanomolar concentrations of paclitaxel, ranging from 0 to 100 nM. This is relevant as paclitaxel is used as first-line chemotherapy for various cancers (116,293). In addition to NCI-H460, the A549 cell line was also used in this experiment, after determining a decrease in p31^{comet} mRNA levels > 50% with 48 hours of transfection (Supplementary figure S4).

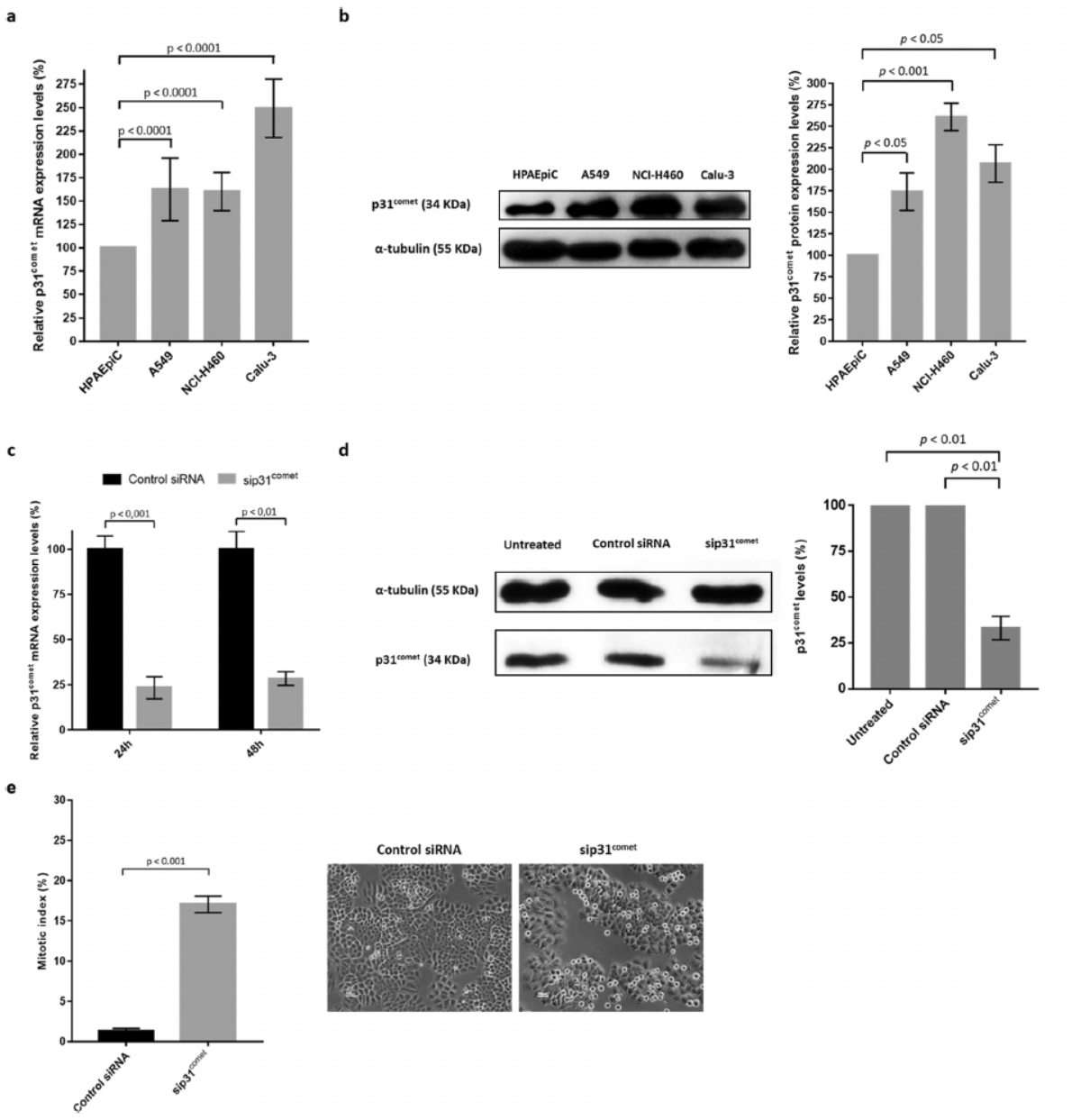

Figure 19. p31^{comet} expression and knockdown in lung cancer cells.

p31^{comet} is overexpressed in lung cancer cells, as shown in (**a**) and (**b**). (**a**) Relative expression of p31^{comet} mRNA as determined by qRT-PCR in the indicated tumor cell lines, comparatively to non-tumor HPAEpiC. (**b**) Representative western blot showing differential expression at protein levels in cell lines analyzed in (**a**) and the respective quantification on the right (full-length blot image in Supplementary Fig. S2). Tubulin served as a loading control. (**c**) Relative expression of p31^{comet} mRNA in control siRNA and in cells treated with p31^{comet} siRNAs (sip31^{comet}), as determined by qRT-PCR. RNA was extracted 24 h and 48 h after transfection. (**d**) Representative western blot for NCI-H460 extract showing effective protein depletion (left) and respective quantification (right) (full-length blot image in Supplementary Fig. S3). Tubulin served as a loading control. Protein extraction was performed 48 h after transfection. (**e**) p31^{comet} knockdown increases the mitotic index. Mitotic cells were quantified 48 h after transfection. Statistical analysis was performed through the Student t-test. The error bars represent mean ± SD.

We found that paclitaxel concentrations ≥ 50 nM or ≥ 100 nM were needed to induce a significant increase in cytotoxicity ($p < 0.0001$ or $p < 0.001$) in NCI-H460 or A549 cells, respectively, as determined by a 48 h MTT assays (Figure. 20 a and d). In contrast, in cells depleted of p31^{comet}, concentrations as low as 10 nM of paclitaxel were sufficient to significantly reduce cell viability ($p < 0.01$ or $p < 0.0001$ in NCI-H460 or A549 cells, respectively). Indeed, dose-response curves showed a threefold decrease in IC50 values for paclitaxel in NCH-H460 cells depleted of p31^{comet}, and a fourfold decrease in the case of A549 cells (Figure 20b,e). Importantly, in a 10-day clonogenic assay, p31^{comet} knockdown significantly affected NCI-H460 and A549 cell proliferation at much lower concentrations (4 nM) of paclitaxel ($p < 0.0001$), suggesting that long-term survival becomes compromised at very low concentrations of paclitaxel (Figure 20c and f). These results indicate that antagonizing SAC silencing by targeting p31^{comet} can enhance the lethality of cancer cells in the presence of low doses of paclitaxel. According to the data outlined in (Figure 10a, b, d, and e), we selected the concentration of 10 nM paclitaxel to further analyze the mechanism of its combination with p31^{comet} suppression. It represents the lowest concentration that still leads to maximal antitumor effect when combined with p31^{comet} suppression. From a therapeutic point of view, this is expected to reduce paclitaxel toxicity and resistance concerns.

To get insight into the mechanism underlying the lethality enhancement resulting from combining p31^{comet}-depletion with clinically relevant concentrations of paclitaxel, we first determined the mitotic index by phase-contrast microscopy and flow cytometry. We observed an increase in the mitotic index in p31^{comet}-depleted cells treated with paclitaxel for 24 h (23.92 ± 2.16%), when compared to untreated (1.33 ± 0.31%) and to paclitaxel-treated cells (6.00 ± 5.1%) (Figure 21a). Flow cytometry analysis not only confirmed these results (Figure 21b) but also revealed an increased sub-G1 population in p31^{comet}-depleted cells treated with 10 nM paclitaxel for 48 h, indicative of massive cell death. This suggests that p31^{comet} depletion is acting as a co-adjuvant of paclitaxel, namely at 10 nM, by retaining cells in mitosis through preventing SAC silencing and, thus, delaying mitotic slippage, which may explain the enhancement of cell killing obtained in the above cytotoxic assays.

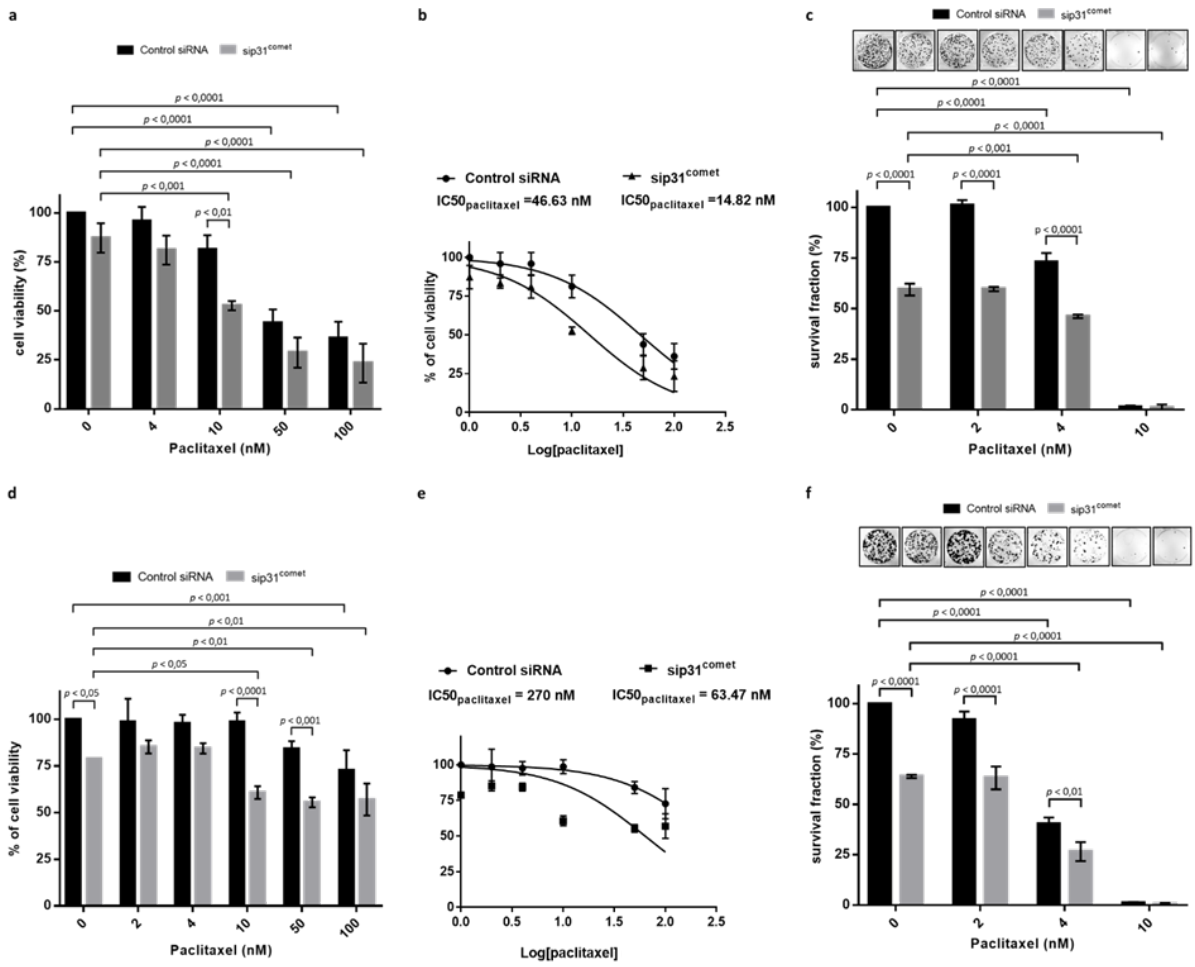

Figure 20. p31^{comet} inhibition enhances paclitaxel-mediated toxicity in NCI-H460 and A549 cells under low doses of paclitaxel.

(**a**) Cell viability, as determined by MTT assay in NCI-H460 and (d) A549 cells. Twenty-four hours post-transfection with control or p31^{comet} siRNAs, paclitaxel was added at the indicated concentrations (0–100 nM) and cells were incubated for an extra 48 h. (**b**) Dose-response curves and IC50 values relative to paclitaxel treatment of NCI-H460 or (**e**) A549 cells transfected with control or p31^{comet} siRNA. (**c**) NCI-H460 and (f) A549 cells were treated as in (**a**) and (**d**), washed, and allowed to grow for 10 days for colony formation assays. Results are the mean from three independent experiments, expressed as % of survival fraction. Representative images of surviving colonies (top) are shown for each condition. Statistical analysis was performed by two-way ANOVA with Tukey's multiple comparisons test. The error bars represent mean ± SD.

Then, we scored the duration of mitosis and the survival fate of each mitotic NCI-H460 cell by single-cell time-lapse imaging. For survival fate analysis, we considered three categories: cell death in mitosis (DiM), postmitotic death (PMD), and survivors (175). Control and p31^{comet}-depleted cells were incubated with a sublethal dose (10 nM) of paclitaxel and imaged over a 72h time course. We found that mitosis lasted 155.00 ± 199.86 min in paclitaxel-treated (n=30), and 150.40 ± 295.99 min in p31^{comet}-depleted (n = 30) cells, more than four times longer than control siRNA-

cells (31.33 ± 4.34 min, n = 30) (Figure 21c). Notably, the combination of p31^{comet}-depletion + paclitaxel resulted in a dramatic increase in mitosis duration (443.67 ± 365.92 min, n = 30), compared to control and to individual treatments (Figure. 21c), again suggesting that p31^{comet} downregulation, by preventing SAC silencing, delays mitotic slippage and retains low dose paclitaxel-treated cells in mitosis.

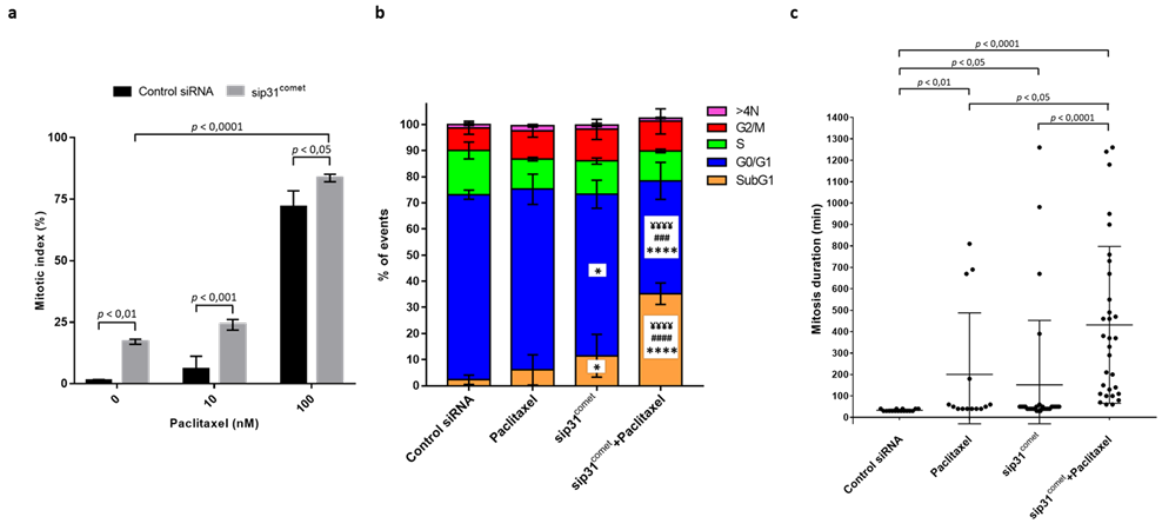

Figure 21. p31^{comet} knockdown increases the mitotic index and the duration of the mitotic block and enhances cancer cells death under low doses of paclitaxel treatment.

NCI-H460 cells were treated with control or p31^{comet} siRNAs for 48 h, then 10 nM of paclitaxel was added for further 24 h or 48 h. (**a**) Determination of the mitotic index 24 h after addition of paclitaxel, as determined phase-contrast microscopy. Two-way ANOVA with Tukey's multiple comparisons test was used for statistical analysis. (**b**) Cell cycle analysis. 48 h after the addition of paclitaxel, cells were treated with propidium iodide/RNase and analyzed by flow cytometry. *p < 0.05, ****p < 0.0001, sip31^{comet} or sip31^{comet} + paclitaxel *vs* control siRNA; ###p < 0.001, ####p < 0.0001, sip31^{comet} + paclitaxel *vs* sip31^{comet}; ¥¥¥¥ p < 0.0001, sip31^{comet} + paclitaxel *vs* paclitaxel, by two-way ANOVA with Tukey's multiple comparisons test. (**c**) Quantification of mitosis duration. 24 h after paclitaxel treatment and/or 48 h after siRNA transfection cells were followed by time-lapse imaging for 72 h. The scatter plot shows the time from mitosis entry to cell division. Each spot represents one cell. Statistical analysis was performed by Kruskal–Wallis with Dunn's multiple correction test. The error bars represent mean ± SD.

Cell survival profiling showed that the lethality of paclitaxel was increased after p31^{comet}-depletion (Figure 22a–c, and Movies 1, 2, 3 and 4). 10 nM paclitaxel resulted in only 56.67% cell death. At this low concentration, while only a small fraction underwent DiM (16.67%) or PMD (40.00%) after one to three cycles, the remainder (43.33%) continued cycling. After p31^{comet}-depletion, while 13.33% underwent DiM at the first mitosis, 86.67% divided. Of the dividers, 19.23% underwent DiM and 57.69% underwent PMD only after the first or second mitosis, while the survivors

(23.08%) remained at interphase suggesting cell cycle arrest. Notably, combining paclitaxel with p31^{comet} depletion shifted the fate to DiM during the first (80%) mitosis and, interestingly, time to death was accelerated by 5.94 h and by 0,92 h comparatively to that of DiM in p31^{comet}-depleted cells and paclitaxel-treated cells, respectively (Figure 22d). In the few PMD events that occurred, time to death was significantly shortened, compared to individual treatments. Apoptosis was the main mechanism of cell death as confirmed by the TUNEL assay and Annexin-V/propidium iodide costaining (Figure 22e and f).

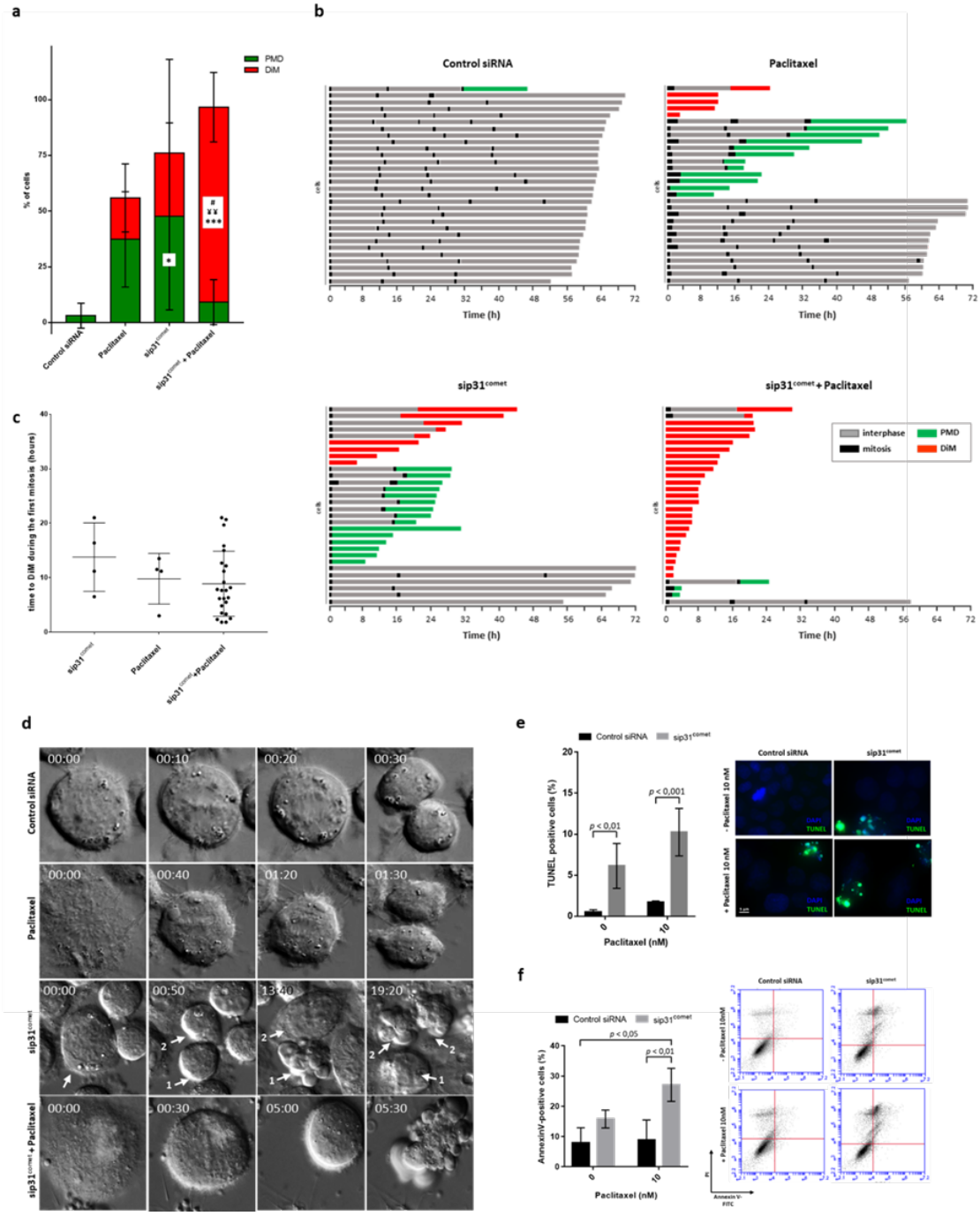

Figure 22. p31^{comet} knockdown enhances cell death in mitosis following the addition of nanomolar doses of paclitaxel. (**a**) Quantification of the percentage of cells undergoing post-mitotic death (green) and death in mitosis (red) over the total number of cells. Cells were transfected with control or p31^{comet} siRNAs for 48 h, then paclitaxel was added for 24 h, and cells imaged by time-lapse microscopy for 72 h. *p < 0.05, ***p < 0.001, sip31^{comet} or sip31^{comet} + paclitaxel *vs* Control siRNA; $^{\#}$p < 0.05, sip31^{comet} + paclitaxel vs sip31^{comet}, $^{¥¥}$p < 0.01, sip31^{comet} + paclitaxel *vs* paclitaxel, by two-way ANOVA with Tukey's multiple comparisons test. PMD postmitotic death, DiM death in mitosis. (**b**) Cell fate profiles, as determined by time-lapse microscopy. Cells were treated as in (**a**). The graphics represent the tracking from the time when cells entered mitosis (zero h). Individual cells are represented as horizontal bars. After mitosis, the time of cell death was determined by the time the first daughter cell dies. Thirty cells are represented per condition. (**c**) The scatter plot demonstrates the quantification of time from mitotic entry to death for cells that died during the first mitosis. Each spot represents one cell. (**d**) The panel shows time-lapse sequences representative of the cells characterized in (**b**). Paclitaxel and sip31^{comet}-treated cells have longer mitosis than that treated with Control siRNA, which spend only 30 min in mitosis. A sip31^{comet}-transfected cell (arrow) dies through PMD, and an increase of only 20 min in mitosis duration relative to the Control siRNA-treated cell is enough to trigger death (1). One of the daughter-cell survives and divides (2), but her daughter cells die after mitosis. A cell treated with sip31^{comet} plus paclitaxel is trapped in mitosis and undergoes membrane blebbing after 5 h. (**e**) Cell death by apoptosis was tested by TUNEL assay to detect DNA fragmentation. Representative images are shown (left). DNA (blue) was stained with DAPI. DNA fragmentation is represented as green. Quantification of TUNEL positive is shown (right). (**f**) Flow cytometry analysis of apoptosis by Annexin V/PI co-staining, 48 h after paclitaxel treatment. Quantification of Annexin V-positive cells (left) and representative cytogram (right) are shown. The quadrants Q were defined as Q1 = live (Annexin V- and PI-negative), Q2 = early stage of apoptosis (Annexin V-positive/PI-negative), Q3 = late stage of apoptosis (Annexin V- and PI-positive), and Q4 = necrosis (Annexin V-negative/PI-positive). Statistical analysis was performed by two-way ANOVA with Tukey's multiple comparisons test. For all the experiments, the error bars represent mean ± SD.

Overall, the results indicate that suppression of p31^{comet} prevents SAC silencing and delays mitotic slippage, thereby enhancing and accelerating cell death during the first mitosis, at clinically relevant doses of paclitaxel. Because the effect of the combination is close to the sum of the single effects, we conclude that the combined treatment has an additive effect.

4.3. p31^{comet}-siRNA mediated cell death can be accelerated by a BH3-mimetic drug

Variations in cell death sensitivity to antimitotics was attributed to two competitive and mutually exclusive networks, one controlling mitotic cell death through accumulation of apoptotic signals, and the other controlling mitotic slippage through gradual cyclin B1 degradation (120). Thus, one

way to force mitosis-arrested cells to die, rather than to slip, is to challenge them with small molecules that artificially stimulate apoptosis. We thought that by delaying premature SAC silencing and, simultaneously, stimulating apoptosis signal accumulation, one should create maximal conditions for maximal cytotoxicity. We explored this possibility by combining p31^{comet} knockdown with the BH3-mimetic drug Navitoclax, an antagonist of the Bcl-2 family of anti-apoptotic proteins Bcl-2, Bcl-XL, and Bcl-w (294).

First, we observed that the addition of Navitoclax further compromised the long-term survival of NCI-H460 cells depleted of p31^{comet} (Figure 23a). This effect was not too evident in A549 cells (Figure 13b). However, it should be noted that the decrease in cell viability induced by Navitoclax individual treatment was more accentuated in A549 cells (≈ 46% of viable cells) than in NCI-H460 cells (≈ 72% of viable cells) (Figure 23a and b).

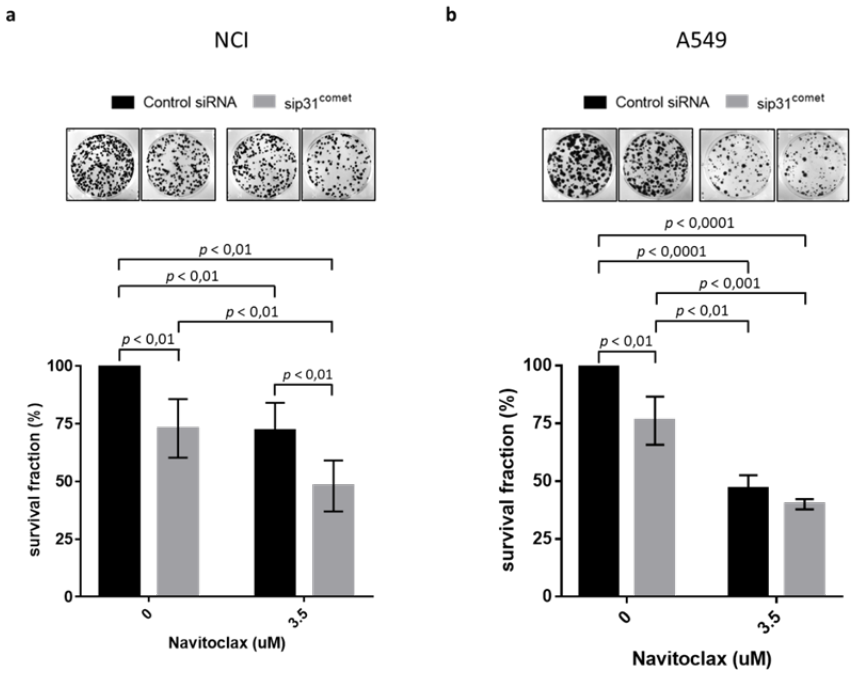

Figure 23. Navitoclax compromises the long-term survival of NCI-H460 cells depleted of p31^{comet}.

(**a**) Colony formation assays in NCI-H460 and (**b**) A549 cells, respectively. 24 h post-transfection with control or p31^{comet} siRNAs, Navitoclax was added at the indicated concentrations, and cells were incubated for an extra 48 h. Cells were then washed and allowed to grow for 10 days. Results are the mean from three independent experiments, expressed as % of survival fraction. Statistical analysis was performed by two-way ANOVA with Tukey's multiple comparisons test.

Furthermore, qRT-PCR experiments revealed that mRNA levels of Mcl-1, a prosurvival that is only weakly affected by Navitoclax (294) are upregulated in NCI-H460 cells and downregulated in A549 cells (Figure 24a).

This may explain, in part, why A549 cells were more affected by Navitoclax. Indeed, Mcl-1 is known as a resistant factor to Navitoclax and other Bcl-2 family inhibitors (190). Notably, Bcl-2 mRNA was highly overexpressed in NCI-H460 cells (Figure 24b), which is in line with previous evidence (295,296), and Bcl-xL was underexpressed in both tumoral cell lines (Figure 24c).

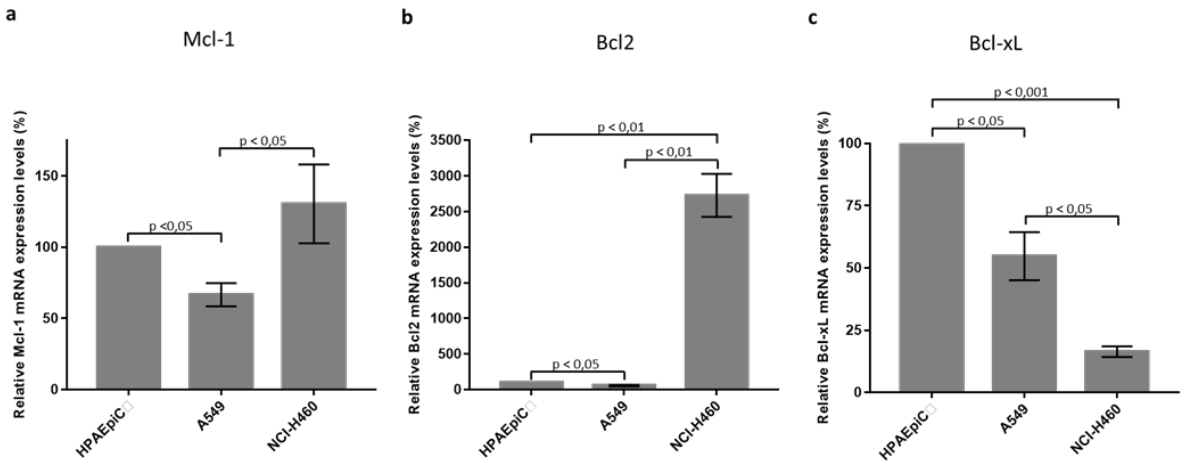

Figure 24. Relative expression of mRNA levels of Bcl1, Bcl-xL, and Mcl-1 genes in NCI-H460 and A549 NSCLC cell lines, compared to the non-tumor cell line HPAEpiC.

Mcl-1 is overexpressed in NCI-H460 and underexpressed in A549 cells (**a**). Bcl2 is highly overexpressed in NCI-H460 and underexpressed in A549 cells (**b**), while Bcl-xL is underexpressed in both NSCLC cell lines (**c**). Statistical analysis was performed through the Student t-test. The error bars represent mean ± SD.

After that, mitotic duration and cell fate were analyzed by live-time imaging, over 72 h experiments, in NCI-H460 cells, as above. As shown in Figure 25a, exposure of NCI-H460 cells to 3.5 μM Navitoclax alone did not alter mitosis duration in control siRNA cells. Interestingly, the addition of Navitoclax to $p31^{comet}$ siRNA transfected cells significantly reduced the duration of the mitotic block to 61.00 ± 65.51 min (n = 30), more than two times shorter compared to $p31^{comet}$ siRNA transfected only cells (150.40 ± 295.99 min (n = 30). Because no mitotic role was described, so far, for the anti-apototic proteins targeted by Navitoclax, we believe that the shortening of the observed mitotic arrest time is the result of precocious cell death, rather than a genuine reduction in mitotic arrest duration.

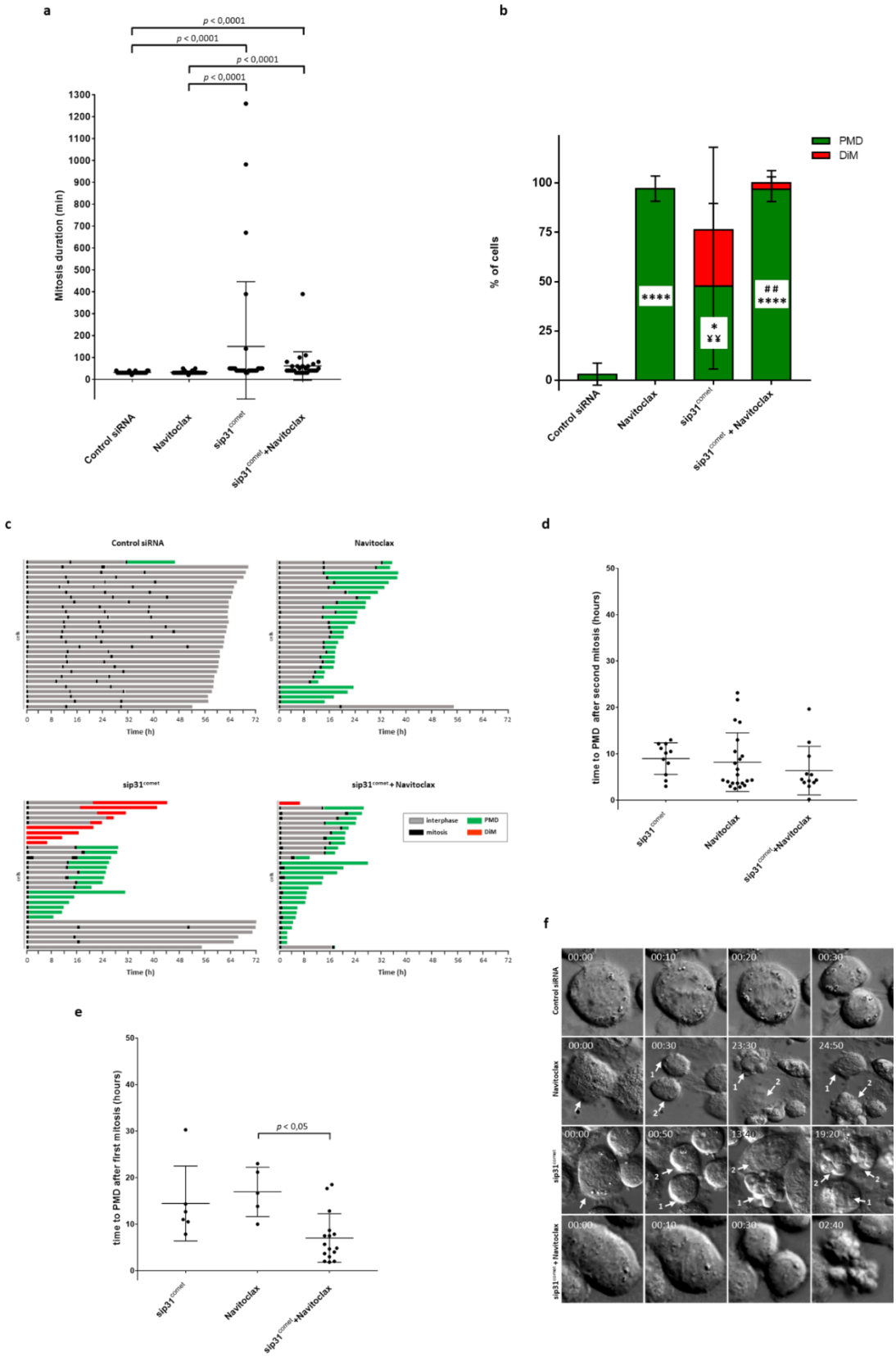

Figure 25. Navitoclax decreases mitosis duration and accelerates post-mitotic death in sip31^{comet}-treated NCIH460 cells

(**a**) Mitosis duration as determined by live-cell imaging. NCI-H460 cells were treated with control or p31^{comet} siRNA, either alone, or in combination with 3.5 μM of Navitoclax. For the combined treatment, Navitoclax was added 24 h after siRNA transfection, and cells were imaged for 72 h. The scatter plot shows the time from mitosis entry to cell division. Each spot represents one mitotic cell. Kruskal–Wallis with Dunn's multiple correction test was used for statistical analysis. (**b**) Quantification of the percentage of cells undergoing postmitotic death (PMD) and death in mitosis (DiM) over the total number of cells. Cells were treated as in (**a**). *$p < 0.05$, ****$p < 0.0001$, Navitoclax or sip31^{comet} or sip31^{comet} + Navitoclax *vs* Control siRNA; $^{\#\#}p < 0.01$, sip31^{comet} + Navitoclax *vs* sip31^{comet}; $^{¥¥}p < 0.01$, Navitoclax *vs* sip31^{comet}, by two-way ANOVA with Tukey's multiple comparisons test. (**c**) Cell fate profiles, as determined by time-lapse microscopy. Individual cells were tracked and represented as horizontal bars. The graphic represents the tracking from the time when cells entered mitosis (zero h). After mitosis, the time of cell death is determined by the time the first daughter cell dies. Thirty cells are represented per condition. (**d**) The scatter plot shows the time from mitotic exit to death for cells that died after the second mitosis. Each spot represents one cell. Statistical analysis was performed Krushkal–Wallis with Dunn's multiple correction test. (**e**) The same analysis as in (**d**), but for cells that died after the first mitosis. For all the experiments, the error bars represent mean ± SD. (**f**) The panel shows timelapse sequences representative of the cells characterized in (**c**). A Navitoclax-treated cell spends the same time in mitosis as the Control siRNA-treated cell (30 min), and the first daughter cell (1) dies 23 h after division. The cell treated with sip31^{comet} plus navitoclax spends only 30 min in mitosis (20 min less than the cell only transfected with sip31^{comet}), and both the daughter-cells die approximately 2 h after cell division, 21 h or 11 h less than cells individually treated with Navitoclax or sip31^{comet}, respectively.

As to cell survival profile (Figure 25b and c), Navitoclax alone induced PMD in 96.67% of treated cells, most of which (86.21%) occurred only after the second cell cycle, with an average of 7.81 h between mitotic exit and death (Figure 25d). When Navitoclax was added to p31^{comet}-depleted cells, PMD after the first mitosis became the predominate cell fate (56.67%) (Figure 25e), with death onset time significantly accelerated by approximately 8 h and 4 h, compared to Navitoclax ($p < 0.05$) and p31^{comet}-depletion individual treatments, respectively (Figure 25e and f), and (Movies 5 and 6). Interestingly, although some PMD (41.38%) still occurred only after the second cell cycle (Figure 25b and c), the death onset time was significantly accelerated by approximately 1.19 h relatively to Navitoclax alone, and 5.06 h relatively to p31^{comet}-depletion alone (Figure 25e), indicating that cells that escape cell death after the first cell cycle are committed to death after the second cell cycle.

In sum, the data demonstrate that the use of a BH3-mimetic in an antagonized SAC silencing background enhances and accelerates cancer cell death, largely by post-mitotic cell death after the first division.

5. Discussion

In this study, we demonstrated that modulating SAC silencing, by p31^{comet} depletion, can influence mitotic slippage and cell death in the presence of spindle poisons or apoptosis potentiators. While both spindle poisons and apoptosis potentiators exacerbate cell death in p31^{comet}-depleted cells, they behave differently regarding their mechanism. Depletion of p31^{comet} extends the duration of mitotic block in the presence of paclitaxel and shifts cell fate to accelerated cell death in the first mitosis. In contrast, p31^{comet} depletion shifts cell fate to accelerated post-mitotic death after the first cell cycle, in the presence of the apoptotic potentiator Navitoclax. Thus, in both contexts, cell death is enhanced and accelerated comparatively to individual treatment. We also show that p31^{comet} is overexpressed in NSCLC cell lines. Our data highlight the relevance of p31^{comet} as a drug target for cancer therapy.

We demonstrated that p31^{comet} targeting enhances cancer cells exposed to clinically relevant doses of paclitaxel, in an additive manner. Upon p31^{comet} depletion plus paclitaxel, cells were trapped in mitosis and arrested until death. This is in concordance with a previous work showing that p31^{comet} depletion promoted an increased duration of mitosis in the presence of paclitaxel that culminated with cell death in a colorectal carcinoma cell line (118). However, this result was achieved under a higher concentration of paclitaxel than that used in our study.

Paclitaxel inhibits tubulin depolymerization, impairing microtubule dynamics and leading to the permanent activation of SAC (70,125,276). However, SAC can be satisfied under low concentrations of paclitaxel, allowing mitosis to proceed in the presence of spindle abnormalities and congregation errors, which may increase the aggressiveness of malignant cells (291,297). Thus, by delaying SAC silencing, p31^{comet} knockdown enhances and accelerates cell death in the presence of low concentrations of paclitaxel, most probably by delaying mitotic slippage which favors the accumulation of apoptotic signals. Noteworthy, the precise mechanism of paclitaxel cytotoxicity is still debatable. In addition to its antimitotic-mediated chemotherapeutic effect, paclitaxel was shown to trigger a proinfammatory response by activation of innate immunity, providing an opportunity to explore its combination with immune checkpoint inhibitors (298). Interestingly, rather than inducing mitotic delay, low doses of paclitaxel promote chromosome missegregation and micronucleation which stimulates innate immunity response and promotes antitumor immune surveillance (299).

We found that the addition of the apoptosis potentiator Navitoclax to p31^{comet} depleted cells accelerated postmitotic death in NCI-H460 cells. These results are in line with previous reports demonstrating that Navitoclax plus antimitotics co-treatment potentiated cancer cell death (191,192). Surprisingly, although some studies have shown that Navitoclax in combination with MTAs prompted mitotic death by accelerating apoptosis in the mitotic-arrested cells (191,192), we demonstrated that Navitoclax shifted cell death from DiM to PMD in p31^{comet} depleted cells. This result is in line with another study that showed that inhibition of Bcl-xL by the BH3-mimetic WEHI-539 induces PMD in RKO cells in the presence of paclitaxel (297). We also found that Navitoclax promotes post-mitotic death of p31^{comet}-depleted cells after a short delay in mitosis. This suggests that cells that exit mitosis after a delay, here caused by p31^{comet} knockdown, are committed to dying due to Navitoclax-mediated inhibition of anti-apoptotic proteins. Indeed, Bcl-xL (a Navitoclax target) was shown to be crucial for cell survival following abnormal mitosis (297). Intriguingly, Navitoclax treatment alone resulted in a strong cytotoxic response (Figure 25b). However, Navitoclax showed limited single-agent activity in a completed phase II study, and current studies are focusing on combination therapies (300,301). In this perspective, we believe that its use to enhance/accelerate apoptotic signal accumulation in cancer cells treated with antimitotics could be beneficial by avoiding slippage from mitotic arrest. Mechanistically, the combination is much more aggressive in that it promotes rapid cell death, already at the first mitosis, while most of the cel- killing occurred at mitosis of the second cell cycle in individual treatments (Figure 25c). This is corroborated by the enhanced reduction of NCI-H460 cell survival (Figure 23a) and could be clinically relevant as it may offer higher efficacy while reducing repeated administration. Curiously, in the A549 line, cell survival decreased more significantly after Navitoclax individual treatment than in NCI-H460, and p31^{comet} knockdown did not significantly affect Navitoclax-treated A549 cells (Figure 23b). As the pro-survival Mcl-1 was underexpressed in A549 cells (Figure 24a), these cells could be less resistant to Navitoclax. Indeed, Navitoclax inhibits Bcl-2 and Bcl-xL, but only weakly Mcl-1 (294). Moreover, Mcl-1 has been considered as an indicator of resistance to Bcl2 inhibitors (190,302). Therefore, p31^{comet} knockdown/Navitoclax combination could provide conditions for maximal cytotoxicity in tumors with higher levels of Mcl-1.

p31^{comet} overexpression was previously associated with the abolishment of SAC-dependent mitotic arrest and subsequent mitotic slippage (118,169,303), as well as with increased resistance to apoptosis and to antimitotic drugs, such as paclitaxel in cancer cells (169). Furthermore, mRNA

screenings published in the oncomine database (www.oncomine.org) suggested that p31^{comet} is overexpressed in several cases of lung cancer as well as in other cancers. In line with those evidences, we confirmed that p31^{comet} was overexpressed at mRNA and protein level in three NSCLC cell lines when compared with a non-tumoral cell line, thus highlighting its potential value as a target for NSCLC therapy.

In conclusion, our data suggest that targeting SAC silencing components, such as p31^{comet}, can provide a means to block mitosis and, at the same time, to delay mitotic slippage, thereby providing maximal conditions to enhance the cytotoxicity of microtubule poisons and apoptosis-promoting agents. Therefore, targeting SAC silencing can provide a rationale for combination chemotherapy against cancer that deserves to be further explored to overcome problems of resistance and side effects.

CHAPTER IV

Depletion of p31^{comet} enhances the efficacy of paclitaxel and navitoclax in lung cancer spheroids

The information provided on this chapter was partially based in the following manuscript to be submitted:

Henriques, A.C.; Silva, P.M.A.; Sarmento, B.; Bousbaa, H.. " Depletion of p31^{comet} enhances the efficacy of paclitaxel and navitoclax in lung cancer spheroids". To be submitted.

1. Abstract

The spindle assembly checkpoint (SAC) has been pointed as an attractive target for the development of new antimitotic drugs for anticancer therapy. Moreover, drugs targeting SAC have been explored in combinatory therapeutic strategies, to overcome mitotic slippage associated with microtubule-targeting agents (MTAs) resistance. We previously found that depletion of the SAC silencer p31^{comet} enhanced the cytotoxic effect of low doses of paclitaxel and Navitoclax in 2D culture, through different mechanistic. Here we used monotypic non-small cell lung cancer (NSCLC) spheroids to investigate the impact of p31^{comet} knockdown in the treatment with paclitaxel and Navitoclax, to assess the efficacy of the treatment in a culture system that most resembles the three-dimensional architecture of the tumor. Under p31^{comet} knockdown plus clinically relevant concentrations of paclitaxel and Navitoclax, spheroid viability was significantly reduced, relative to the individual treatments. Interestingly, when comparing the results with previous data on 2D monolayers, lower doses of Navitoclax were required to induce a significant cytotoxic effect in 3D spheroids. Overall, the knockdown of the SAC silencer p31^{comet} improved the efficacy of the MTA paclitaxel and the pro-apoptotic Navitoclax in spheroids derived from NSCLC cells, which is in agreement with the outcomes obtained in 2D culture. The results emphasize the potential of targeting SAC silencing to improve the therapy with MTAs and pro-apoptotic drugs.

2. Introduction

Cancer accounted for one in six deaths in 2018, being the second leading cause of death worldwide (1), and chemotherapy is still a gold standard strategy for cancer treatment (304). Antimitotic drugs, which have been widely used for the treatment of several cancers, are mainly represented by MTAs, such as vinca alkaloids (vinblastine and vincristine) and taxanes (paclitaxel, docetaxel), (117). However, adverse effects and drug resistance associated with the action of MTAs in microtubules still limit their efficacy (70,125,126). Therefore, alternative antimitotic strategies such as those targeting spindle assembly checkpoint (SAC) have been investigated.

Spindle assembly checkpoint (SAC) is a control mechanism that prevents metaphase to anaphase transition until all chromosomes are perfectly attached to the microtubules of the mitotic spindle and bi-oriented in the metaphase plate. SAC acts through the mitotic checkpoint complex (MCC), which is formed by Bub3, BubR1, Mad2 and Cdc20. By sequestering Cdc20, MCC precludes the ubiquitination of cyclin B1 and securin by APC/C, and their consequent degradation by 26S proteasome, preventing premature mitotic exit (14,305,306). Small molecules targeting SAC components and regulators have been developed and tested (128). In addition, targeting of non-enzyme proteins has also been studied, such as spindly and the SAC-silencer $p31^{comet}$ (167–169,263,274). Some small molecules inhibiting proteasome have been approved (307). However, these inhibitors generally failed in clinical trials, which were frequently limited by side effects (62,133,134,141,142,152,160–162,308).

Moreover, the fact that most therapies with positive outcomes at the preclinical stage do not succeed in clinical trials may also be related to the type of preclinical models. The most frequently used are animal models, which can lead to biased results (14,309). Animal models allow to recreate complex systems and to assess pharmacokinetic parameters but display some limitations (14,309). For instance, animal models are not adequate to rebuild the tumor microenvironment (TEM), as the stroma is different and human cancer cells proliferate at higher rates in tumor xenografts (14,309). In this context, several advances have been made in the development of 3D cell culture models, which comprise spheroids, organoids, and organs-on-chips (14,310). For example, spheroids allow rebuilding the tridimensional architecture of the tumor, through the formation of heterogeneous regions made of proliferative cells (the most external layer), quiescent cells (intermediate layer), necrotic cells (the most inner layer). This conformation favors

the recreation of the O_2, nutrients, and pH gradients, which makes 3D spheroids trustworthy models. Therefore, 3D spheroids have emerged as attractive models to assess drug efficacy (14).

In the addition to the investment in more reliable models at preclinical studies, there is the constant need of developing innovative strategies that allow overcoming the constraints associated with side effects and drug resistance. In this regard, combination approaches involving conventional and new antimitotic drugs have been explored (143,167–169,263,274). The objective is either to arrest cells in mitosis until death or to promote aberrant mitosis that is incompatible with cell viability. Moreover, combination of antimitotics with pro-apoptotic drugs, such as BH3-mimetics, has been investigated (120,127,128,175,184,186,190,192,193,311). Considering the competing networks model (69,120,279), the cell fate of a mitotic-arrested cell can be shifted to death over slippage, either through delaying cyclin-b degradation, or by increasing death signals (see section 4.3.2 of Introduction).

The $p31^{comet}$ is involved in SAC silencing at least by two main mechanisms, one by preventing the activation of Mad2, and the other by promoting MCC disassembly (72,73,208,213,216–218,231,232,289). We previously showed that delaying slippage by antagonizing SAC silencing, through $p31^{comet}$ knockdown, enhanced the efficacy of paclitaxel and Navitoclax in 2D cultures of lung cancer cells (312). Mechanistically, $p31^{comet}$ knockdown increased mitotic block duration and, consequently, enhanced mitotic death in the presence of nanomolar concentrations of paclitaxel. Also, the BH3-mimetic Navitoclax accelerated post-mitotic death in the absence of $p31^{comet}$. In order to validate these results in an environment that is close to the in vivo tumor, here we evaluated the effect of the $p31^{comet}$ depletion + paclitaxel and p31 depletion + Navitoclax combinations on the viability of 3D spheroids of lung cancer cells. Spheroids allow mimicking the 3D conformation of cells in tumors, reproducing some traits that are responsible for drug resistance (14,266).

Here it is shown that $p31^{comet}$ knockdown enhances the cytotoxicity of clinically relevant doses of paclitaxel and Navitoclax in NSCLC spheroids. Therefore, this study validates the results previously obtained with NSCLC cells in a 2D model, highlighting the potential of targeting SAC silencing for the development of new therapeutic approaches for the treatment of lung cancer.

3. Material and methods

3.1. Cell lines and culture conditions

Cell culture was performed as described early (144). A549 (human adenocarcinoma alveolar basal epithelial) and NCI-H460 (human non-small cell lung cancer) were purchased from American Type Culture Collection. A549 cells were grown in DMEM culture medium with 10% fetal bovine serum (FBS, Biochrom) and 1% non-essential amino acids (Sigma Aldrich Co., Saint Louis, MO, USA), while NCI-H460 were grown in RPMI-1640 culture medium (Lonza, Basel, Switzerland) with 5% FBS. Cells were maintained at 37 ºC, in a 5% CO_2 humidified incubator.

3.2. 3D spheroid formation

Lung cancer spheroids were formed by seeding NCI-H460 and A549 cells in ultra-low attachment 96-well plate. Briefly, 100 µL of cell suspension was added to each well, and the following seeding densities were tested for each cell line: 1000, 2000, 3000, 5000, and 1000 cells/spheroid. NCI-NCI-H460 and A549 spheroids were cultured, respectively, in DMEM culture medium with 10% FBS, and RPMI-1640 culture medium 10% FBS. Culture media were exchanged every two days.

3.3. Spheroid size measurement

Spheroid size was determined at 2, 4, 7, and 10 days of culture. At the referred time-points, contrast-phase images were obtained using a Nikon TE 2000-U microscope (Amsterdam, Netherlands), with a DXM1200F digital camera (Amsterdam, Netherlands) and a Nikon ACT-1 software (version 2.62, Melville, NY, USA). Contrast phase images were analyzed using ImageJ software, and the average size was determined from two measurements of diameter per spheroid, measured in at least three spheroids. Three independent experiments were performed.

3.4. Cell Metabolic Activity of 3D spheroids

Cell viability was determined using CellTiter-Glo® 3D cell viability assay (promega), according to manufacturer instructions. Briefly, spheroids were transferred to an opaque 96-well plate. After equilibrating the reagent at 22 ºC, CellTiter-Glo® 3D reagent was added in an equal volume to each well, and mixed. Luminescence signal was recorded 30 min later, using an integration time of 1 second. For spheroids characterization, the assay was performed at 2, 4, 7, and 10 days of

culture. For siRNA transfection, 4-day-old spheroids, seeded at the density of 3000 cells/spheroid, were transfected, and cell viability was measured 48 h or 96 h later. For the treatment with paclitaxel or Navitoclax, spheroids were treated on the 4th day of culture, during 48 h or 72 h. In combination experiments, 4-day-old spheroids were transfected with siRNA and treated with paclitaxel or Navitoclax during 48 h or 72 h. In each case, three individual experiments were performed, with three spheroids per data point.

3.5. Histological Analysis of 3D spheroids

For histological analysis, 48 spheroids collected at 4 and 8 days of culture (seeding density = 3000 cells / spheroid) and fixed in PFA 4% (v/v in PBS 1x; 1 mL) for 1 h. Spheroids were then washed 2 times in PBS 1x and included in agarose 1.5% (w/v). Spheroids embedded in agarose were embedded in paraffin and processed in an automated system. Paraffin blocks were sectioned into 3 µM sections. Samples were deparaffinized in xylol, rehydrated in graded alcohol series, and stained with hematoxylin and eosin for general morphology analysis.

3.6. Immunohistochemistry of 3D spheroids

For immunohistochemistry, spheroids (4 and 8 days of culture, seeding density = 3000 cells/well) were first processed and embedded in paraffin, as described above. 3 µM sections were deparaffinized and rehydrated in decreasing concentrations of ethanol. Antigen retrieval was performed with citrate buffer (10×10^{-3} M, pH 6), at 98ºC, for 30 minutes. Following procedures were accomplished with Novolink™ Polymer Detection System (Leica, Biosystems), according to manufacturer instructions. Samples were incubated for 1 h, at room temperature, with ki-67 antibody (cat. no. sc-23900; Santa Cruz Biotechnology, Inc., Dallas, TX, USA). For antigen detection, a system that links H_2O_2-horseradish peroxidase (HRP) to the primary antibody was used, and the signal was obtained through the system of 3,3'-diaminobenzidine (DAB)-H_2O_2-horseradish peroxidase (HRP) At the end, sections were counterstained with Mayer's hematoxylin and dehydrated with increasing concentrations of ethanol.

3.7. RNA isolation and quantitative real-time PCR

RNA isolation was performed with PureZOL RNA Isolation Reagent (Bio-Rad Laboratories, Hercules, CA, USA), according to the manufacturer's instructions. In the case of 3D culture, RNA was extracted from, at least, 36 spheroids. For the analysis of $p31^{comet}$, Bcl2, Bcl-xL, and Mcl-1 expression in 3D *versus* 2D cultures, spheroids were collected on the 4^{th} day of culture. For the assessment of $p31^{comet}$ knockdown in 3D culture, 4-day-old spheroids were transfected and collected for RNA isolation two and four days after transfection. RNA was quantified by spectrophotometry, with NanoDrop 2000 (Thermo Scientifc, Waltham, MA, USA). cDNA synthesis was carried out with the iScript cDNA Synthesis Kit (Bio-Rad), according to the supplier's instructions. qRT-PCR was performed using the iQ SYBR Green Supermix Kit (Bio-Rad) and the iQ Termal Cycler (Bio-Rad) coupled to CFX Manager Sofware (version 3.1, Bio-Rad). The following amplification program was used: initial denaturing step at 95.0°C for 3 min; 40 cycles at 94.0°C for 20 s; 65.0°C ($p31^{comet}$ amplification) or 57°C (Bcl2, Bcl-xL, and Mcl-1 amplification) for 30 s and 72.0°C for 30 s. Temperatures from 65.0 to 95.0°C, with increments of 0.5°C for 5 s were included in the melt curves. Primers were used at final concentration of 0.1 µM. The following primer sequences were employed: $p31^{comet}$, 5'-AGTCCCTGATTTGGAGTGGT-3' (forward), 5'-GTAAACTGACAGCAGCCTTCC-3' (reverse); Mcl-1, 5'-CCAAGGCATGCTTCGGAAA-3' (forward), 5'-TCACAATCCTGCCCCAGTTT3' (reverse) (286); Bcl-2, 5'-ATCGCCCTGTGGATGACTGAGT-3' (forward), 5'-GCCAGGAGAAATCAAACAGAGGC-3' (reverse) (287); Bcl-xL, 5'-GCCACTTACCTGAATGACCACC-3' (forward), 5'-AACCAGCGGTTGAAGCGTTCCT-3' (reverse) (287) actin, 5'-AATCTGGCACCACACCTTCTA-3' (forward), 5'-ATAGCACAGCCTGGATAGCAA-3' (reverse) (144); GAPDH, 5'-ACAGTCAGC CGCATCTTC-3' (forward), 5'-GCCCAATACGACCAAATCC-3' (reverse) (288). The ΔΔCt method was used for relative quantification. Results were normalized against GAPDH and actin genes.

3.8. Spheroid transfection with siRNAs.

For siRNA transfection, 4-day-old spheroids (seeding density = 3000 cells/spheroid) were transfected using INTERFERin siRNA Transfection Reagent (PolyPlus, New York, USA). An alteration to the manufacturer instructions was tested: forming complexes between siRNA and the cationic complexes of INTERFERin in the presence of 10 % FBS (313). For each spheroid, 1 µL of INTERFERin per spheroid was used, and complexes were formed in 50 µL of RPMI with 10 %

FBS. After the formation of complexes, the 50 µL were added to a spheroid-containing well with 150 µL of RPMI with 5% FBS. The culture medium was removed 24 h after transfection. Different concentrations of a validated siRNA sequence against $p31^{comet}$ (205) were tested (50 to 300 nM). A validated negative control siRNA (AllStars Negative Control siRNA, Qiagen, Germantown MD, USA) was used.

3.9. Statistical analysis.

For statistical analysis, Unpaired Student t-test or ordinary two-way ANOVA with Tukey's multiple comparisons test, or Kruskal–Wallis with Dunn's multiple correction test were performed in GraphPad Prism version 7 (GraphPad software Inc., CA, USA). Data are shown as the means ± standard deviation (SD) of at least three independent experiments.

4. Results

4.1. Optimization and characterization of lung cancer monotypic spheroids

In order to obtain a tridimensional model of lung cancer cells, two NSCLC cells, NCI-H460 and A549, were tested at five seeding densities (1000 to 10000 cells per well). The diameter and viability of spheroids were monitored over 10 days post-culture (figure 26).

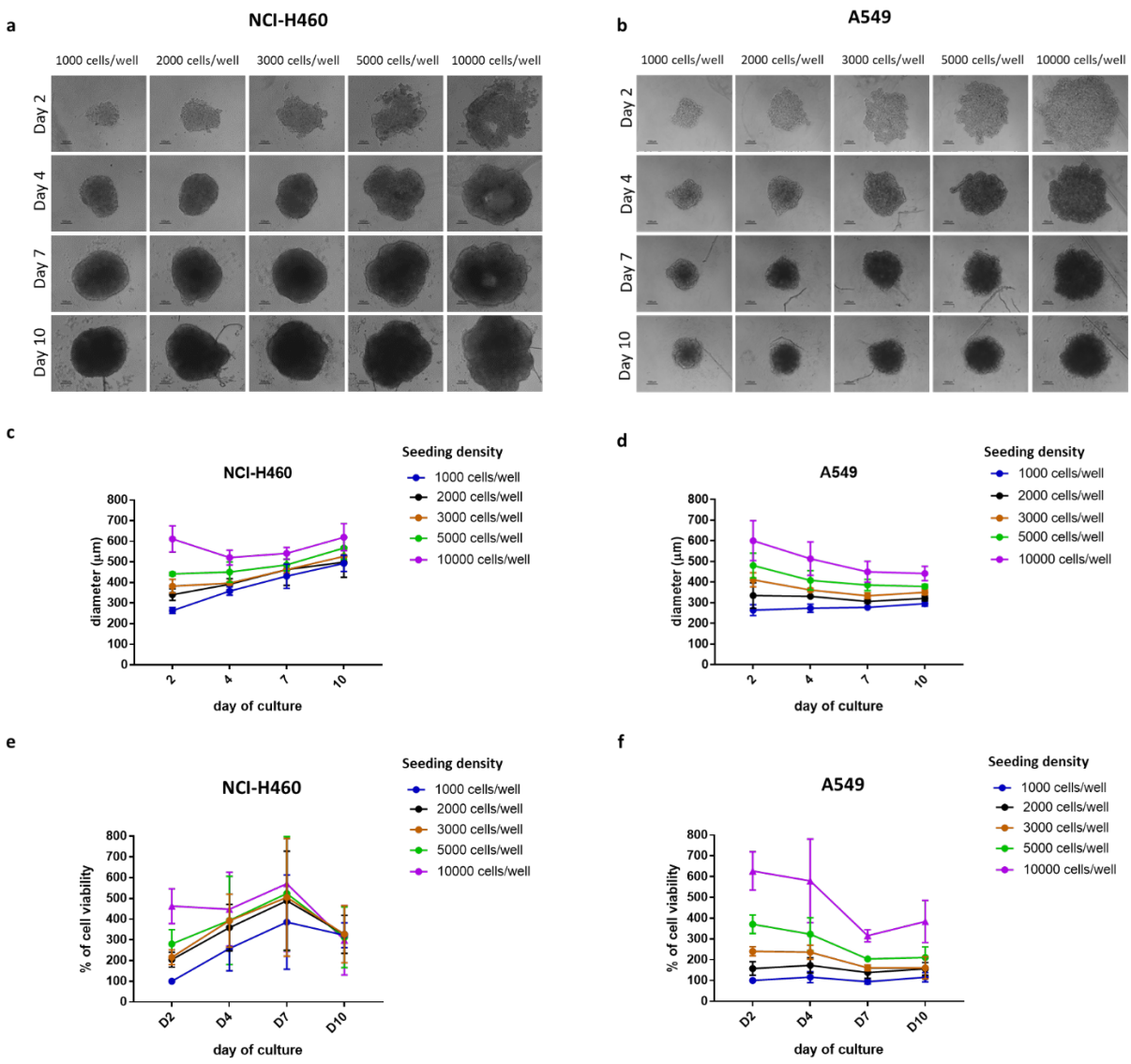

Figure 26. Characterization of lung cancer spheroids along ten days.

(**a**) Contrast phase images of NCI-H460 and (**b**) A549 monotypic spheroids with seeding densities from 1000 to 10000 cells/spheroid along ten days. (c) Diameter of NCI-H460 and (d) A549 spheroids seeded at different densities over time. (e) Viability evolution of NCI-H460 and (f) A549 spheroids over ten days, according to seeding densities. The viability results were normalized to the values obtained on the second day at the lowest density (1000 cells/well). The error bars represent the mean ± SD of at least 3 independent experiments.

Spheroids from both cell lines initially presented an irregular shape, particularly during the first four days of culture. However, they acquired a spheric and compact morphology over time. For NCI-H460 cells, the diameter increased for all seeding densities, except for the highest one (10000 cells/well) (figure 26a). On the other hand, A549 showed a size reduction until day seven, which accompanied the increasing compaction over the days (figure 26b). In general, the viability of NCI-H460 spheroids increased up to the seventh day of culture, and a reduction was observed from

that day to the tenth day (Figure 26e). On the other hand, in A549 spheroids, the viability decreased over time, but slightly increased from the seventh to the tenth day (Figure 26e). The fact that the viability of A549 spheroids decreased over the first week of culture and seemed to stabilize only around the tenth day, indicates that it would be necessary to wait roughly 10 days to use these spheroids in further assays. On the other hand, NCI-H460 spheroids revealed an active metabolic status at least, during the first seven days of culture, suggesting that these spheroids could be used for additional experiments during the first week of culture. Therefore, considering practical and logistic issues, NCI-H460 spheroids were selected to go on with the following experiments. According to the literature, spheroids with a diameter over 400 µm in generally exhibit a three-dimensional architecture typical of an *in vivo* solid tumor (314,315). With the increase of spheroid mass, gradients of nutrients and O_2 are formed, leading to the generation of a necrotic core, an intermediate region made of quiescent cells, and an external layer of proliferative cells. Hence, as NCI-H460 spheroids cultured at a seeding density of 3000 cells/well presented a diameter of approximately 400 µm at the fourth day of culture (Figure 26c), it was decided to use 4-day-old spheroids cultured at a seeding density of 3000 cells/well to start the following experiments. In order to confirm that those spheroids comprised the aimed three-dimensional morphology, an H&E coloration was performed in NCI-H460 spheroids with 4 and 8 days of culture, seeded at the density of 3000 cells/well. Spheroids with four (Figure 27a) and eight days of culture (Figure 27b) showed a core with few cells exhibiting micronucleation, and cell debris; an intermediate layer displaying more cells, but still showing micronucleation and some lack of cohesion; and a more cohesive external region. Positive immunostaining with ki-67 in this region was concordant with the presence of an external proliferative layer (figure 27). These results confirm that NCI-H460 spheroids seeded at the density of 3000 cells/well reproduce and maintain the morphologic traits characteristic of *in vivo* solid tumors during the first eight days of culture.

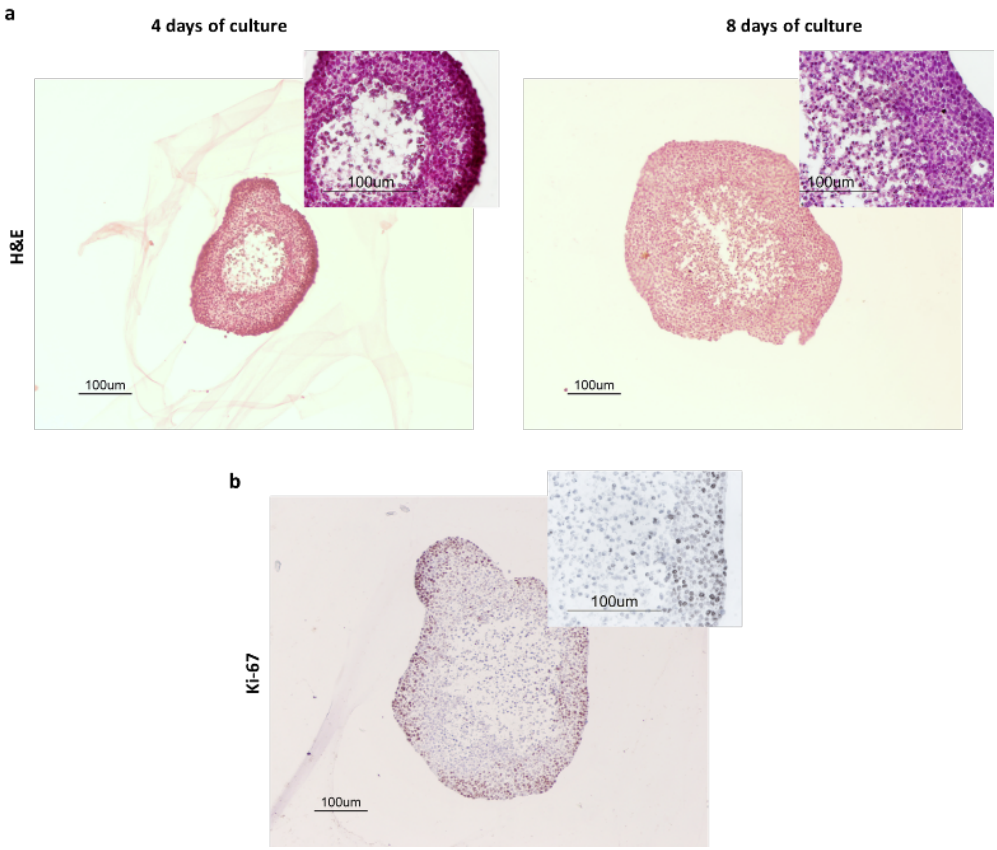

Figure 27. Representative images of sections from NCI-H460 spheroids with four and eight days of culture showing the morphology and cellular organization.
(a) H&E staining reveals higher cellular organization in the outer region, which is progressively lost as going to the center, where cell loss and micronucleation predominates. **(b)** Immunostaining for ki-67 targeting at day eight of culture confirms the presence of an external proliferative layer.

4.2. p31^{comet} knockdown

It was already established that p31^{comet} was overexpressed in NCI-H460 cells comparatively to the non-tumoral HPAEpiC cell line in a 2D model (312). We first evaluated whether the 3D conformation affected p31^{comet} expression, by comparing the mRNA levels of p31^{comet} between 4-day-old NCI-H460 spheroids and a 2D culture of NCI-H460 cells. We observed that there was no significant difference in p31^{comet} mRNA levels between 3D and 2D culture models (Figure 28).

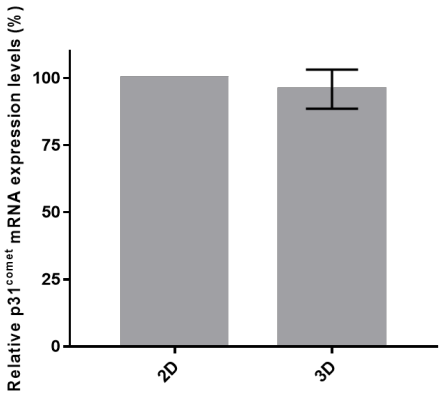

Figure 28. Relative expression of p31^{comet} mRNA levels in NCI-H460 cell line, under 2D or 3D culture, as determined by qRT-PCR. The error bars represent mean ± SD of three independent experiments.

We then wanted to investigate if p31^{comet} knockdown could affect cell viability in NCI-H460 spheroids. We could observe that when we transfected 4-day-old spheroids with 200 nM of sip31^{comet}, the levels of p31^{comet} RNA decreased about 40%, four days after transfection (Figure 29a). We then transfected spheroids with concentrations of sip31^{comet} ranging from 50 to 300 nM, and analyzed them for viability and diameter size, two and four days after transfection (Figure 29b and c). As Figure 29b shows, cell viability was mainly affected four days after transfection. Interestingly, the variation in viability was not accompanied by a diameter decrease, as a result of this treatment (Figure 29c). Therefore, in further combination assays with paclitaxel and Navitoclax, spheroid viability was assessed 96 h after sip31^{comet} transfection. This result could be due to a higher proportion of apoptotic or necrotic cells, which does not translate into a smaller diameter. As such, the determination of viability proved to be a more reliable method to assess the effect of the spheroid treatment with siRNA.

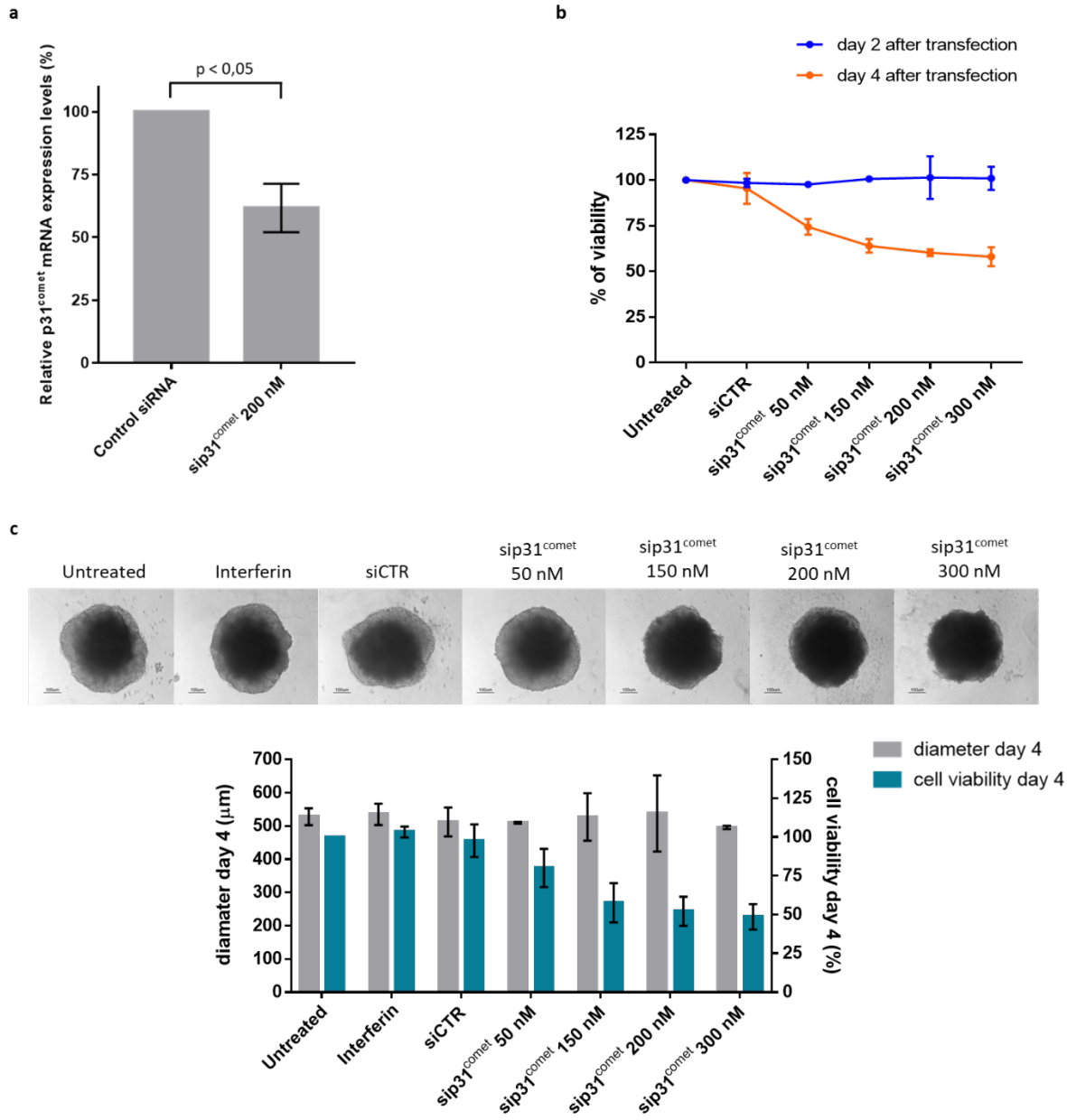

Figure 29. siRNA-mediated p31^{comet} knockdown in NCI-H460 spheroids.

(**a**) Relative expression of p31^{comet} RNA in NCI-H460 spheroids 96 h (4 days) after treatment with sip31^{comet} and siControl, as determined by qRT-PCR. Statistical analysis was performed through the Student t-test. (**b**) Cell viability in spheroids 2 and 4 days after transfection with different concentrations of sip31^{comet} *vs* siControl, as determined by CellTiter-Glo® 3D Cell Viability Assay. (**c**) Comparison between diameter and cell viability in spheroids 4 days after the treatment with different concentrations of sip31^{comet} *vs* siControl. Representative contrast phase images of spheroids are shown (above). Statistical analysis was performed through the Student t-test. The error bars represent the mean ± SD of at least 3 independent experiments.

4.3. p31^{comet} knockdown potentiate the cytotoxic activity of clinically relevant concentrations of paclitaxel and Navitoclax in lung cancer spheroids

We have previously reported in a 2D culture that p31^{comet} depletion enhanced paclitaxel cell death in an additive manner (312). This is relevant since paclitaxel is widely used in the treatment of several malignancies. On the other hand, p31^{comet} knockdown accelerated cell death in the presence of the BH3 mimetic Navitoclax (312). Hence, we wanted to investigate if p31^{comet} knockdown also potentiates cancer cell death in 3D spheroids treated with clinically relevant concentrations of paclitaxel and Navitoclax. First, we determined that the IC50 of paclitaxel was 50.50 nM ± 13.51, and 7.96 nM ± 2.26, after 48 and 72 h of treatment, respectively; and that the IC50 of Navitoclax was 1.82 µM±2.35 and 1.04 µM ± 0.52 after 48 and 72 h after treatment, respectively (Table 3). Considering these results, we opted to use drug concentrations nearly or slightly below the IC50 in further combination treatments with sip31^{comet}, in order to see in what extent p31^{comet} knockdown can increase paclitaxel and Navitoclax efficacy. Therefore, the concentrations of 2 nM paclitaxel and 1 µM Navitoclax were selected. A treatment interval of 72 h was chosen for the two drugs since it allows the use of lower concentrations at a time. We found that cell viability decreased to values near 70% either with 72 h paclitaxel treatment or 96 h after transfection with sip31^{comet} (Figure 30a). Notably, the cell viability of spheroids depleted of p31^{comet} and treated with 2 nM paclitaxel, significantly decreased (45.38% ± 2.51), compared to the individual treatment.

Table 3. IC50 values of 4-day-old spheroids treated with paclitaxel and Navitoclax during 48 h or 78 h.

Drug	Duration of treatment	IC50
paclitaxel	48 h	50.50 nM ± 13.51
	72 h	7.96 nM ± 2.26
Navitoclax	48 h	1.82 µM ± 2.35
	72 h	1.04 µM ± 0.52

When 72 h Navitoclax treatment was performed in sip31^{comet}-transfected spheroids, cell viability dropped to more than a half (45.00%±0.49) comparatively to Navitoclax only treated spheroids (83.99%±7.47) (Figure 30b).

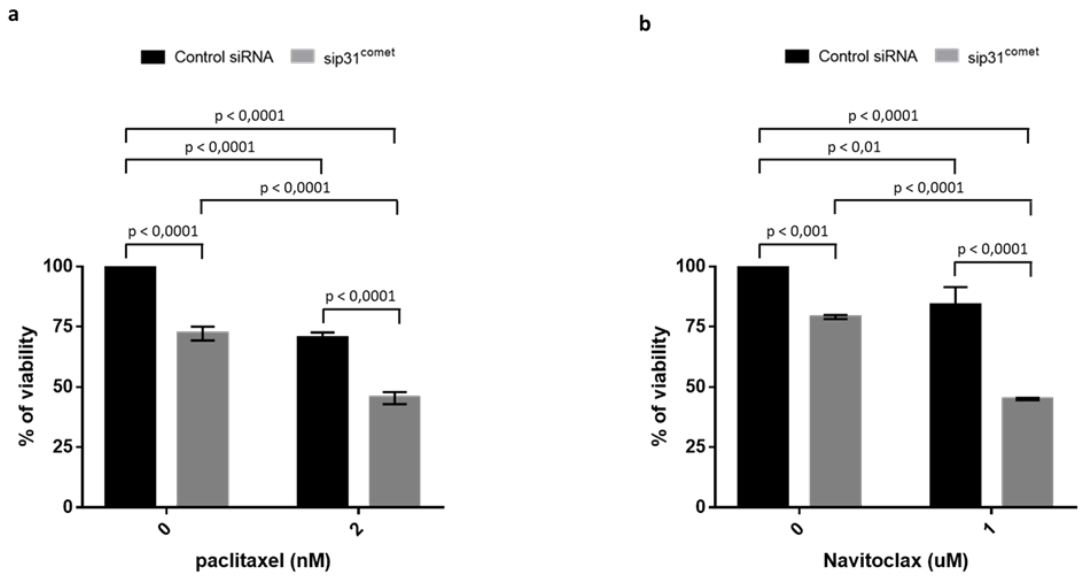

Figure 30. p31^{comet} knockdown enhances cytotoxicity in NCI-H460 spheroids, under low doses of paclitaxel and Navitoclax.

Cell viability was determined by CellTiter-Glo® 3D Cell Viability Assay. Twenty-four hours after transfection with sip31^{comet}, spheroids were treated with 2 nM paclitaxel (**a**) or 1 μM Navitoclax (**b**) for 72 hours. Statistical analysis was performed by two-way ANOVA with Tukey's multiple comparisons test. The error bars represent mean ± SD of three independent experiments.

The results suggested that spheroids could be more sensitive to Navitoclax than a 2D culture of NCI-H460 cells. Indeed, while previous results in 2D culture showed that 3.5 μM for 48 h were needed to inhibit long-term survival in ~ 75% (see section 4.3 of chapter III), 1.82 μM were needed to inhibit 50% of cell viability during 48 hours of treatment. To elucidate this difference, we compared the mRNA levels of the antiapoptotics Bcl-2, Bcl-xL, and Mcl-1, in 2D *vs* 3D cultures of NCI-H460. We observed that mRNA levels of the three antiapoptotics were significantly lower in spheroids (Figure 31). As Navitoclax inhibits Bcl-2 and Bcl-xL, this result helps to explain the lower resistance of 3D spheroids to Navitoclax, compared with 2D cultures.

…

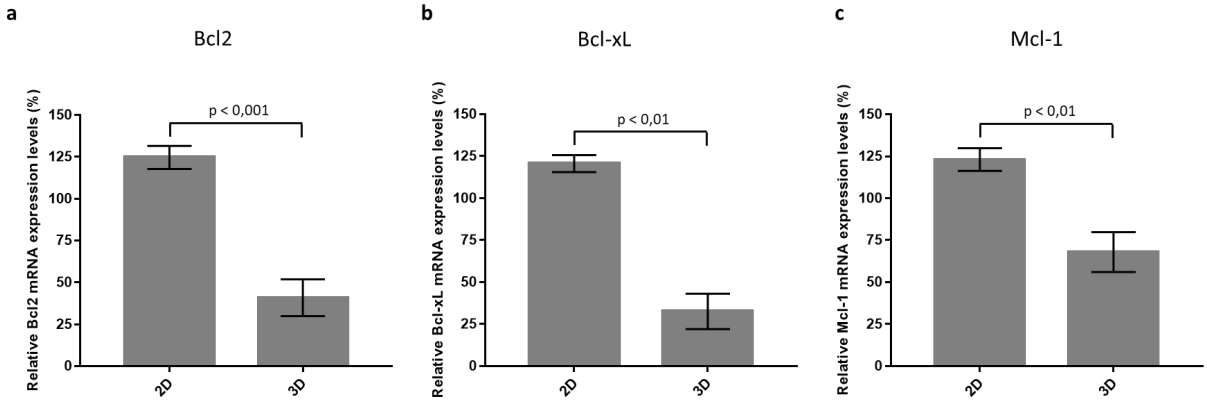

Figure 31. Relative expression of mRNA levels of Bcl2, Bcl-xL, and Mcl-1 genes in NCI-H460 cell line, in 2D or 3D culture.

All targets are underexpressed in 3D spheroids. Statistical analysis was performed through the Student t-test. The error bars represent mean ± SD of three independent experiments.

5. Discussion

In this study, we used lung cancer spheroids to demonstrate that knockdown of the SAC silencer p31^{comet} potentiates cell death in the presence of clinically relevant doses of paclitaxel and Navitoclax. In theory, the fate of a mitotic-arrested cell can be shifted to death either by delaying mitotic slippage or by increasing apoptotic signals (120,175). One way to delay mitotic slippage is through the impairment of SAC silencing (143,144,277). Therefore, we have explored the strategy of preventing SAC silencing in combination with a microtubule poison or with an apoptosis-promoting agent. In a previous work with 2D cultured NSCLC cells, we demonstrated that p31^{comet} knockdown potentiated mitotic arrest and mitotic death in the presence of paclitaxel, as well as accelerated post-mitotic death under Navitoclax treatment (see chapter III). Here, p31^{comet} knockdown was shown to significantly potentiate the cytotoxic activity of low doses of paclitaxel and Navitoclax in 3D spheroid.

3D spheroids allow to recreate the three-dimensional architecture of *in vivo* solid tumors and thus constitutes a more representative model than 2D culture (266).

Interestingly, spheroids seemed to be more sensitive to Navitoclax, compared to 2D cultured cells (see section 4.3 of the chapter III), and this could be in part explained by the lower levels of the pro-survivals Bcl2, Bcl-xL. and Mcl-1 in spheroids (Figure 31).

It was also found that the diameter of the spheroids did not decrease in the presence of the same sip31^{comet} concentrations that induced a decrease in viability. Although it is not clear why spheroid diameter did not decrease in the described conditions, we suspect that this fact may be related tothe presence of a higher proportion of apoptotic or necrotic cells or with the loss of spheroid integrity. Therefore, the evaluation of the spheroid diameter proved to be ineffective for the assessment of treatment efficacy.

It is important to refer that siRNA-mediated knockdown induced approximately 40% depletion of p31^{comet} in NCI-H460 spheroids. This result may be related with the type of methodology used to carry out the transfection. As an *in situ* delivery of siRNA to spheroids was performed, which presupposes the internalization of complexes formed by siRNA and cationic polymers in successive layers of cells (transfection was performed using INTERFERin® Polyplus – Materials and Methods section of this chapter). siRNAs are short double-stranded RNA molecules that have been widely used for transient inhibition of gene expression in basic and applied research, by blocking protein translation (316,317). However, due to its molecular weight, negative charge, and sensitivity to nuclease-degradation, its delivery to the cells can be challenging, particularly *in vivo* (316,317). Many cationic transfection reagents are successfully used in 2D culture cells, and some nanoparticles-based systems have been developed to improve *in vivo* siRNA delivery and to target cells and tissues (317). Nonetheless, efforts are still needed to increase the knockdown efficiency in solid tumors (317). Studies that perform spheroid transfection using commercial transfection reagents often involve the disruption of established spheroids before transfection and subsequent reseeding (313,318), or the transfection of the cells before spheroid formation (319). However, *in situ* transfection of spheroids allows recreating a scenario that better represents the treatment of *in vivo* tumors. Nevertheless, it is important to note that although the efficiency of the p31^{comet} knockdown had fallen short from the desired in this work, the cytotoxicity of paclitaxel and Navitoclax was potentiated in sip31^{comet}-transfected spheroids, in comparison with non-transfected spheroids. This result, which is in line with previous outcomes obtained in a 2D model (312), reinforces the potential of p31^{comet} inhibition to improve the efficacy of paclitaxel and Navitoclax treatment, lowering the effective doses of these drugs. Therefore, it would be interesting to explore more advanced methods of siRNA delivery to spheroid cells in the future. In fact, advances for *in situ* spheroid transfection have been recently reported, such as those using nanoparticle systems (for example, size-shrinkable matrix metallopeptidase-2-sensitive delivery nanosystem, nanodiamond-based drug delivery, and cation-free siRNA micelles), and peptides

that facilitate spheroid penetration (316,317,320,321). In addition, further experiments on heterotypic spheroids would also be useful to access the influence of the tumoral microenvironment in the treatment response.

Overall, this work confirms the cytotoxic efficacy of combining $p31^{comet}$ knockdown with low doses of paclitaxel and Navitoclax in a model that closely mimics the *in vivo* tumor microenvironment, such as monotypic spheroids of NSCLC cells. This highlights the potential of targeting SAC silencing in combination therapy for cancer treatment.

CHAPTER V

Clinical relevance of p31^{comet} targeting to oral cancer

The information provided on this chapter was partially based in the following manuscript to be submitted:

Henriques, A.C.; Silva, P.M.A.; Sarmento, B.; Bousbaa, H. "Clinical relevance of p31^{comet} targeting to oral cancer". To be submitted.

1. Abstract

Drug combination therapy against cancer has been explored as a strategy to overcome or, at least, to attenuate the constraints associated with resistance to chemotherapy. Cisplatin is a first-line chemotherapeutic drug used in the treatment of several cancers, including head and neck squamous cell carcinomas (HNSCC), such as oral squamous cell carcinomas (OSCC), and it is also used in combination with other drugs, including antimitotics, such as paclitaxel, a microtubule-targeting agent (MTA) that arrest cells in mitosis. Indeed, MTAs are also extensively used in cancer treatment but are still impaired by the development of resistance mechanisms, which are, in part, related to changes that occur at the microtubule level (for example, mutations occurring in tubulin sites that affect drug binding and/or GTPase activity). Therefore, targeting of mitotic components that do not interfere with microtubules, such as spindle assembly checkpoint (SAC) regulators, has been studied. Furthermore, some of these molecules are also deregulated in cancer cells. For instance, Bub3 and spindly, two molecules with important functions in the regulation of mitosis, were found to be overexpressed in OSCC cells, and Bub3 or spindly inhibition was demonstrated to sensitize these cells to the cisplatin effect. The present work explored the significance of the spindle assembly checkpoint (SAC) silencer p31^{comet} in oral cancer. In the first place, the clinical relevance of p31^{comet} as a biomarker for oral cancer was investigated. Secondly, the significance of p31^{comet} as a therapeutic target to potentiate the antitumoral activity of cisplatin in oral cancer, using OSCC cell lines was evaluated.

First, it was found that p31^{comet} was overexpressed in HNSCC cases analyzed through UALCAN web resource. Particularly, p31^{comet} upregulation was observed in HNSCC cases that revealed an altered chromatin status, or changes in mTOR and SWI/SNF pathways. However, the analysis of the p31^{comet} expression impact on the survival of HNSCC patients was not conclusive, and the possibility arises that this analysis should include the analysis of p31^{comet} partners. In agreement, Pearson correlation analysis demonstrated that p31^{comet} gene expression was positively correlated with the p31^{comet} interactors Mad2 and TRIP13, as well as with TP53 gene and E2F family members. In accordance with the data retrieved from UALCAN, *in vitro* results showed overexpression of p31^{comet} in two OSCC cell lines, compared to non-tumor oral keratinocytes. Remarkably, p31^{comet} knockdown potentiated the lethality of clinically relevant doses of cisplatin in OSCC cells. An interesting fact is that this result was more evident in the SCC09 cell line, which revealed a higher resistance to cisplatin treatment than the SCC25 cell line. Notably, despite being upregulated in

both OSCC cell lines, p31^{comet} expression was significantly higher in SCC25 cells, compared with the SCC09 cell.

In conclusion, the relevance of p31^{comet} as a clinical biomarker for survival oral cancer should be explored in a more global context that includes other factors, such as p31^{comet} interactors. Targeting of p31^{comet} potentiated the cytotoxicity of cisplatin in OSCC cell line that displayed more resistance to this drug. As p31^{comet} was moderately upregulated in these cells, p31^{comet} expression should not be used as an isolated factor for predicting the response to treatment. Therefore, the combination of p31^{comet} inhibition and cisplatin is a promising strategy that deserves to be explored for oral cancer in the context of cisplatin resistance.

2. Introduction

Chemotherapy has been increasingly investigated and applied to cancer treatment since the 1950s (322). Despite all the concerns related to therapeutic resistance and side effects, chemotherapy remains a key component in the therapeutic strategies against cancer (322,323).

One of the approaches used to impair the limitations associated with chemotherapy is to combine drugs (80). For instance, arresting cells in mitosis followed by the use of drugs that accelerate apoptosis, either by delaying mitotic slippage or by increasing death signals, is an interesting strategy proposed by Taylor and colleagues (120). The mitotic arrest of cancer cells can be achieved through the use of antimitotic drugs. Microtubule-targeting agents (MTAs) have been the gold standard of antimitotic drugs in cancer treatment. However, the efficacy of MTAs is still limited by drug resistance and side effects (80). The resistance to MTAs is, in part associated with mutations in tubulin sites that affect drug binding or GTPase activity (125). Therefore, alternative antimitotics drugs that do not target microtubules have been intensively explored (80). In this context, SAC regulators have emerged as promising microtubule-independent targets (80). The SAC silencer p31^{comet} has arisen as a new potential target to increase the mitotic duration and to potentiate the lethality of MTAs or pro-apoptotic drugs in cancer cells (118,312). Furthermore, SAC silencing was also demonstrated to sensitize oral squamous carcinoma (OSCC) cells to cisplatin, through inhibition of spindly (199).

Cisplatin main target is genomic DNA (gDNA), resulting in the formation of a variety of cisplatin-DNA adducts, and cisplatin-induced DNA damage can drive apoptosis through a set of different mechanisms (195,196). For instance, p53 activation via ATR and ATM may induce a set of processes that promote apoptosis either through intrinsic or extrinsic pathways; and the abrogation of the G1-S phase arrest induced by the activation of the cell cycle checkpoint kinases (CHK1 and CHK2) may force a premature re-entry in the cell cycle and the apoptosis through the DNA repair pathway (195). In addition to the direct-targeting, cisplatin induces the formation of reactive oxygen species (ROS), which can not only damage gDNA, but also cause mitochondrial DNA damage, and mitochondrial permeability transition, promoting the release of cytochrome C and pro-caspase 9, and the activation of apoptosis (195). Since cisplatin discovery in 1978, it remains a crucial chemotherapeutic drug for the treatment of a wide range of malignancies (324). This platinum-based drug is also the first-line chemotherapeutic drug for the treatment of the OSCC, which is very frequent among oral malignancies. Indeed, head and neck cancer was recently

referred to as the seventh most common cancer worldwide (325). This cancer type encompasses a heterogeneity of malignant tumors developing in the region of the head and neck (325). Head and neck squamous cell carcinomas (HNSCC) develop from the mucosal surfaces of the oral and sinonasal cavity, as well as larynx and pharynx, representing about 90% of head and neck malignancies (324–328). In fact, oral squamous cell carcinoma (OSCC) is the most common type of oral cancer, which is the sixth cause of cancer-related deaths on a global scale (329).

The preferred treatment for OSCC early stages (I and II) are surgery alone or radiotherapy alone, being the choice dependent on anatomical accessibility (325,329). For the late stages (III and IV), the main treatment is surgery – surgical resection of the oral cavity and elective neck resection, and adjuvant radiotherapy or chemoradiotherapy (325,329). Cisplatin is the first-line chemotherapeutic agent for OSCC (329), but due to toxicity issues, in some cases, it is replaced by carboplatin, although the later shows, in general, less efficacy (325). Furthermore, adjuvant systemic therapy may include not only platinum agents, but also taxanes, antifolates, and cetuximab (epidermal growth factor receptor antibody), either alone or in combination (325). Despite all the efforts that have been made, the development of resistance and/or cross-resistance continue to hamper the success of therapy (195,196).

In this chapter, the relevance of p31^{comet} as a prognostic biomarker in oral cancer is firstly addressed. This task is accomplished with the support of the web resource UALCAN, and involves: to access the existing data on p31^{comet} expression in HNSCC; to evaluate the association between p31^{comet} expression in HNSCC patients with changes in pathways that are often altered in cancer, as well as with clinicopathological features; the analysis of the correlation of p31^{comet} expression in HNSCC with the expression of genes that play an important role in p31^{comet} function or regulation; to investigate the effect of p31^{comet} expression on the survival of HNSCC patients. In the second part, the main aim is to evaluate the significance of p31^{comet} as a target to potentiate the cytotoxicity of cisplatin using OSCC cell lines. To achieve this objective: p31^{comet} expression is first analyzed in two OSCC cell lines compared to a non-tumor cell line of human keratinocytes; then, siRNA-mediated p31^{comet} knockdown is performed in OSCC cells; and finally, OSCC cells are subjected to the combined treatment of p31^{comet} siRNA and cisplatin, and viability assays are conducted to evaluate the impact of p31^{comet} depletion in cisplatin-treated cells.

3. Material and methods

3.1. UALCAN analysis

The UALCAN web resource (http://ualcan.path.uab.edu/) was used for the analysis of $p31^{comet}$ expression in HNSCC, and its association with clinicopathologic characteristics of HNSCC patients (258). Within UALCAN, transcriptomic data were retrieved from The Cancer Genome Atlas (TCGA), while proteomic data was obtained from Clinical Proteomic Tumor Analysis Consortium (CPTAC) (258,330). For transcriptomic data, the results were provided by UALCAN as transcripts per million, while in proteomic information, the results were expressed as Z-values, which represented standard deviations from the median across samples for HNSCC. For correlation analysis, UALCAN used Pearson correlation analysis and provided the Pearson correlation coefficient values. For survival plots, Kaplan-Meyer curves were generated to express HNSCC patient survival according to $p31^{comet}$ expression and clinicopathological features.

3.2. Cell lines and culture conditions

The cell lines used in this study were all grown at 37ºC, in a 5% CO_2 humidified incubator. Human oral keratinocytes (HOK) were cultured in a specific HOK medium (Innoprot, Derio, Biscaia, Spain), while for oral squamous carcinoma cell lines SCC09 and SCC25, DMEM-F12 culture medium (Biochrom, São Mamede de Infesta, Portugal), supplemented with 10% fetal bovine serum (FBS, Biochrom) and 40 ng/ml hydrocortisone (Sigma-Aldrich, St. Louis, MO, USA) was used.

3.3. RNA isolation and quantitative real time PCR

Total RNA isolation from culture cells and cDNA synthesis were performed as previous (312) using PureZOL RNA Isolation Reagent (Bio-Rad Laboratories, Hercules, CA, USA) and iScript cDNA Synthesis Kit (Bio-Rad), according to supplier's instructions. Amplification was performed with iQ SYBR Green Supermix Kit (Bio-Rad), on an iQ Termal Cycler (Bio-Rad) coupled to CFX Manager Sofware (version 3.1, Bio-Rad), as follows: initial denaturing step at 95.0°C for 3 min; 40 cycles at 94.0°C for 20 s; 65.0°C for 30 s and 72.0°C for 30 s. Temperatures from 65.0 to 95.0°C, with increments of 0.5°C for 5 s were included in the melt curves. The following primers were used: primers 5'-AGTCCCTGATTTGGAGTGGT-3' (forward), 5'-GTAAACTGACAGCAGCCTTCC-3' (reverse) for $p31^{comet}$ (312); 5'-AATCTGGCACCACACCTTCTA-3' (forward), 5'-ATAGCACAGCCTGGATAGCAA-3'

(reverse), for actin (144); GAPDH, 5'-ACAGTCAGCCGCATCTTC-3' (forward), 5'-GCCCAATACGACCAAATCC-3', for GAPDH (288). Triplicated experiments were performed, and results were analyzed through the ΔΔCT method, as previously described (312). GAPDH and actin were used as reference controls.

3.4. siRNAs transfection

Transfection was performed using INTERFERin siRNA Transfection Reagent (PolyPlus, New York, USA), according to the manufacturer's instructions. Briefly, 24 h after being seeded at the density of 0.12 x 10^6 cells/well, cells were transfected with 50 nM of a validated siRNA sequence against $p31^{comet}$ (205) or a validated negative control siRNA (AllStars Negative Control siRNA, Qiagen, Germantown MD, USA).

3.5. Cell extracts and Western blotting

Protein extraction and western blot analysis were carried out as previously described (312). Briefly, protein extracts were prepared with lysis buffer, in the presence of protease inhibitors cocktail (Sigma-Aldrich), and a total of 15 µg were separated by molecular weight using 12% SDS-PAGE gel and transferred to a nitrocellulose membrane. Rabbit anti-$p31^{comet}$ (abcam) and mouse anti-α-tubulin (Sigma-Aldrich) primary antibodies were diluted at 1:1000 and 1:5000, respectively. The secondary antibodies horseradish peroxidase (HRP)-conjugated secondary antibodies were diluted at 1:4000 (anti-mouse, Sigma-Aldrich) or at 1:1000 (anti-rabbit, Sigma-Aldrich). The intensity of the protein signal was quantified using ImageJ 1.4v software was used for. α-Tubulin expression levels were used for normalization.

3.6. Cell viability assay

To determine cell viability, the MTT (3-(4,5-dimethylthiazolyl-2)-2,5-diphenyltetrazolium bromide) assay (Sigma-Aldrich) was used. 24 h after being transfected with control or $p31^{comet}$ siRNA, cells were seeded in 96-well plates (cell density = 6000 cells per well), and 6 h later cisplatin was added at a range of concentrations from 0 to 100 µM. 24 h later, MTT assay was performed as described previously described (312). Measurements were performed in a microplate reader (Biotek Synergy 2, Winooski, VT, USA) coupled with the Gen5 software (version 1.07.5, Biotek, Winooski, VT, USA), at the optical density of 570 nm. Cell viability values were normalized

against control siRNA-treated cells. Three independent experiments were performed for each condition.

3.7. Colony forming assay

For colony formation assay, 24 h after transfection with control or p31^{comet} siRNA, cells were seeded in 6-well plated at the density of 1000 cells per well. 6 h after seeding, cisplatin was added at the concentrations of 0.25 and 0.5μM. 24 h later, cells were washed with PBS and allowed to grow in fresh medium for 10 days. Colonies were fixed with 3.7% (w/v) paraformaldehyde in PBS and stained with 0.05% (w/v) violet crystal (Merck Millipore, Billerica, MA, USA), as previous (312). Three independent experiments were performed on duplicate dishes for each condition. Plating efficiency (PE) was calculated as the percentage of the number of colonies over the number of cells seeded in control, and the survival fraction (the number of colonies over the number of cells seeded × 1/PE) was determined.

3.8. Statistical analysis

For statistical analysis, Unpaired Student t-test or ordinary two-way ANOVA with Tukey's multiple comparisons test were performed in GraphPad Prism version 7 (GraphPad software Inc., CA, USA). Data are shown as the means ± standard deviation (SD) of at least three independent experiments.

4. Results

4.1. p31^{comet} expression analysis in head and neck squamous carcinoma using UALCAN resource

Previous analysis on p31^{comet} mRNA using data retrieved from oncomine database revealed overexpression across several cancers, including head and neck - floor of the mouth carcinoma (www.oncomine.org) (102). This is in agreement with the data observed in the pan-cancer analysis performed using the web resource UALCAN (258), as shown in chapter I (Introduction). Transcript levels of p31^{comet} n HNSCC through UALCAN were assessed using data from TCGA (The Cancer Genome Atlas). p31^{comet} upregulation was observed in primary tumors of HNSCC at mRNA (median value of transcripts per million 1.59 times higher in tumor samples). p31^{comet} was also

overexpressed at protein levels, according to data from CPTAC (Clinical Proteomic Tumor Analysis Consortium) (UALCAN)(Figure 32).

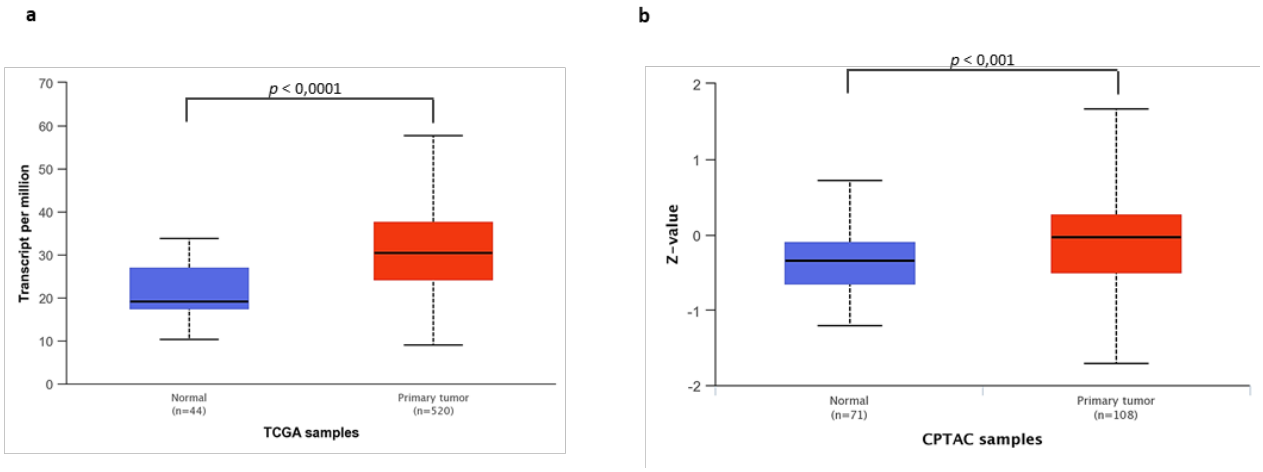

Figure 32. p31^{comet} is overexpressed in head and neck squamous cell carcinoma (HNSCC) tissue.

p31^{comet} expression in HNSCC at the mRNA (**a**) and protein (**b**) levels were assessed through UALCAN. Transcriptomic data was retrieved from The Cancer Genome Atlas (TCGA samples), while proteomics was provided by Clinical Proteomic Tumor Analysis Consortium (CPTAC samples). Boxplots were adapted from UALCAN. Statistical significance provided by UALCAN is represented as *p*-value.

Notably, p31^{comet} was also overexpressed across all tumor stages and grades relatively to normal samples, except for stage 2 at protein level (Figure 33 a-d). However, it is also worth noting that different cohorts were used for mRNA or protein analysis, as well as different size samples. For example, focusing on mRNA analysis (TCGA), 27 samples were evaluated from patients in stage 1, while the analysis of stage 4 comprised 264 samples. In the case of CPTAC samples (protein analysis), the n value was 71 in the normal cohort, and 7 in stage 1. On the other hand, considering stage 4, it was possible to observe a difference of 218 samples analyzed at mRNA (n = 264) or protein (n = 46) levels. Interestingly, p31^{comet} upregulation in HNSCC was more accentuated in males at mRNA levels (median value of transcripts per million 1.63 times higher relative to normal samples, and 1.11 times higher when compared to female samples), a result also confirmed at protein levels (Figure 33e and f).

Remarkably, p31^{comet} protein levels were higher in tumor samples with mammalian target of rapamycin (mTOR), SWItch/Sucrose Non-Fermentable (SWI/SNF), HIPPO, nuclear factor erythroid 2-related factor 2 (NRF2), receptor tyrosine kinases (RTK) or MYC/MYCN altered pathways.

Dysregulation of any of those pathways is frequently associated with cancer (331–335). Particularly, p31^{comet} was significantly increased in tumor samples with changes in mTOR and SWI/SNF mTOR pathways (Figure 33a and b). mTOR plays a key role in the modulation of metabolic pathways, being responsible for inducing several anabolic processes as a response to a wide range of environmental cues, and the mTOR pathway is frequently dysregulated in cancer (334). SWI/SNF are ATP-dependent chromatin remodeling complexes with reported functions in DNA damage repair, and numerous cancers present mutations in the genes encoding SWI/SNF subunits (335). p31^{comet} was also found to be up-regulated in HNSCC cases where chromatin-modifier status was altered, compared with HNSCC samples that did not present this condition (Figure 34c). This may be interesting since mutations in chromatin modifiers are associated with altered splicing profiles and contribute to carcinogenesis (336).

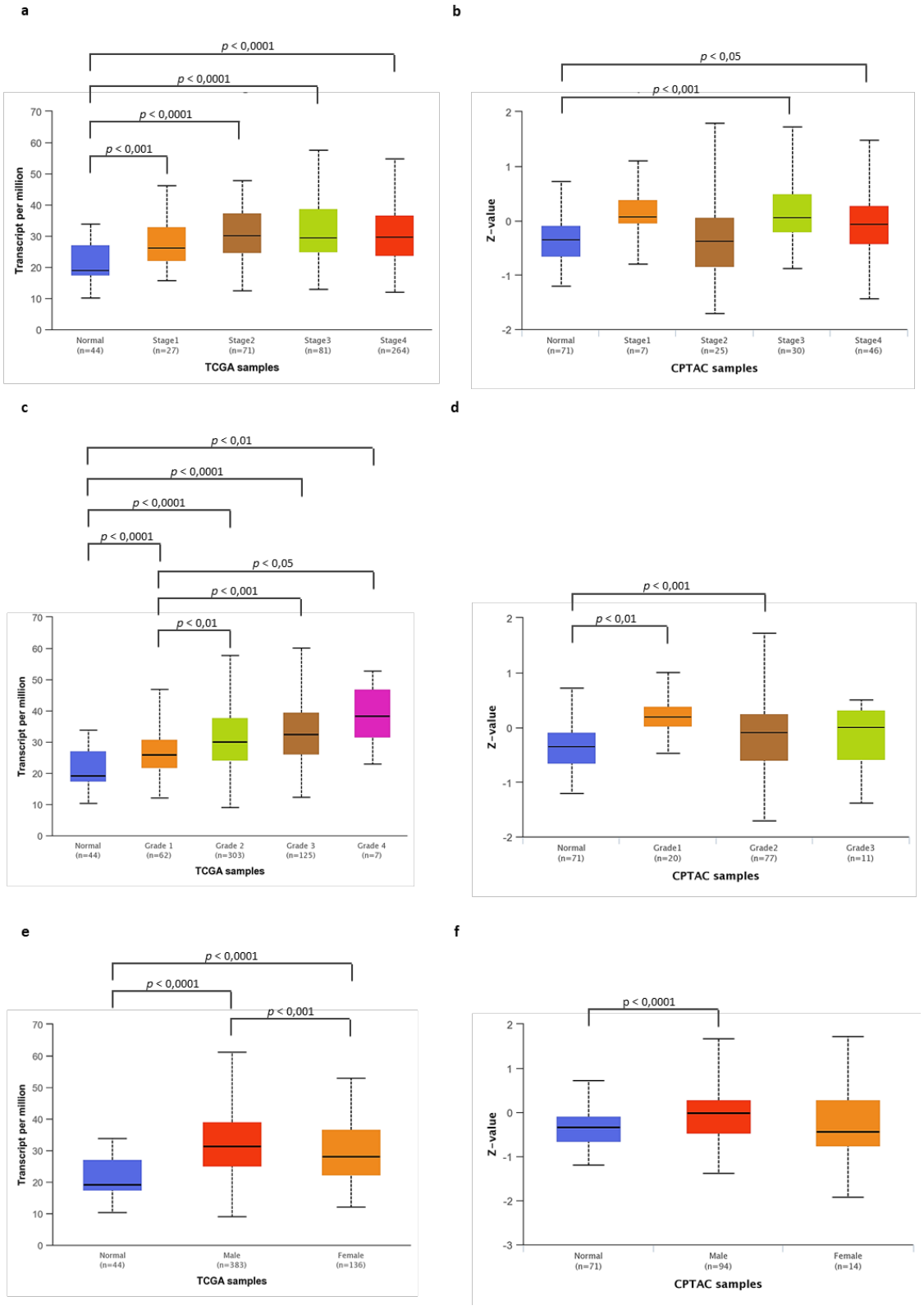

Figure 33. Relationship between p31^{comet} expression in HNSCC and clinicopathologic characteristics, assessed through UALCAN at mRNA (TCGA samples), and protein (CPTAC samples) levels.

p31^{comet} expression and tumor stage, tumor grade, and gender were analyzed at mRNA (**a, c, and e**) and protein (**b, d, f**) levels. Boxplots were adapted from UALCAN. Statistical significance provided by UALCAN is represented as *p*-value.

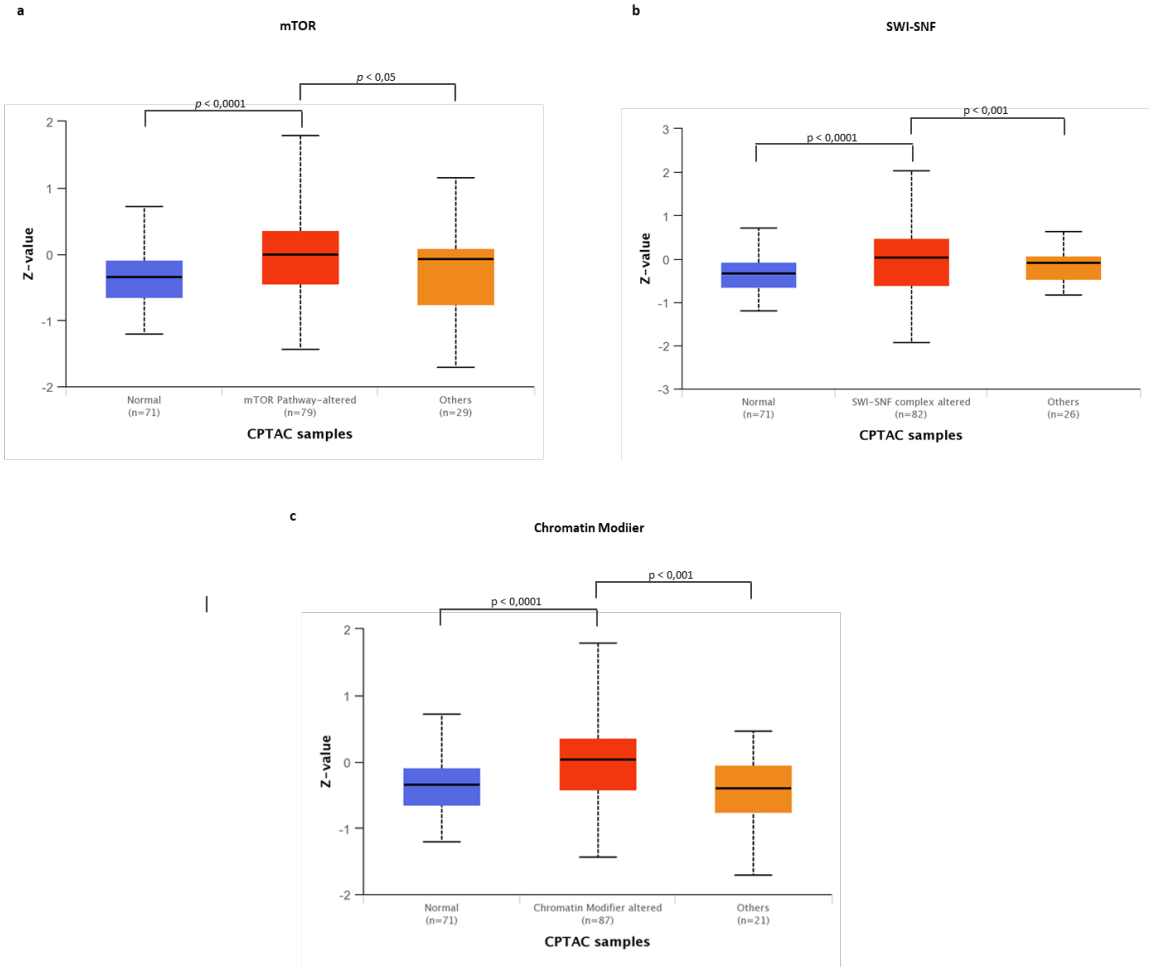

Figure 34. p31^{comet} is upregulated in HNSCC cases (protein expression, CPTAC samples) with altered cancer-related pathways, as determined through UALCAN.

(**a**) mTOR-altered pathway; (**b**) SWI-SNF-altered pathway; (**c**) chromatin-modified status. Boxplots were adapted from UALCAN. Statistical significance provided by UALCAN is represented as *p*-value.

Pearson correlation analysis

In addition to the aforementioned analysis of p31^{comet} expression, a Pearson correlation analysis was also performed in UALCAN with mRNA transcript levels from TCGA, and Pearson correlation coefficient (Pearson-CC) values were provided. Among the genes whose expression was positively correlated with p31^{comet}, are MAD2L1 (Pearson-CC = 0.33), TRIP13 (Pearson-CC = 0.30), TP53 (Pearson-CC = 0.30), E2F3 (Pearson-CC = 0.38), E2F6 (Pearson-CC = 0.35), E2F7 (Pearson-CC =

0.36), Ef38 (Pearson-CC = 0.30) genes. In fact, it was previously reported that senescence occurring in p53-proficient lung cancer cells after the induction of p31^{comet} overexpression was dependent on p53 status and also on p21 $^{Waf1/Cip}$ (261). Furthermore, the mechanism of action of p31^{comet} on SAC silencing is straightly connected to the interaction of p31^{comet} with Mad2 and TRIP13, as previously reviewed (206). It must be noted that both p31^{comet} and MAD2 expression are regulated by the Rb-E2F pathway (108). Indeed, the coordinated expression of p31^{comet} and MAD2 seems to be significant in cancer development and/or treatment, as p31^{comet}/Mad2 ratio was reported to be altered in some cancers, and different p31^{comet}/Mad2 ratios were proposed to be associated with the type of response of cancer cells to spindle poisons (sensitive *versus* resistant) (118).

The observed patterns of p31^{comet} expression point to it as an interesting candidate for therapeutic target in HNSCC. Patient survival as a function of p31^{comet} expression was then assessed.

p31^{comet} expression and survival of HNSCC patients

The survival probability of HNSCC patients over time, according to p31^{comet} expression and other clinicopathological characteristics was assessed through UALCAN. A Kaplan-Meier analysis was performed, based on TCGA data. Unexpectedly, HNSCC patients with high p31^{comet} expression showed better survival than those with low/medium p31^{comet} expression (Figure 35a). However, it is important to note that cohorts have different sizes (129 patients with high p31^{comet} expression, and 390 with low/medium p31^{comet} expression), a fact that might influence the results, as the group of HNSCC patients with high p31^{comet} expression is smaller. Furthermore, it is possible to observe different scenarios, if other variables are considered, such as tumor grade and gender (Figure 35b and c). For instance, a higher expression of p31^{comet} in samples from patients with tumor grade 2 is linked to worse survival, when compared with samples from tumor 2-grade patients with low/medium p31^{comet} expression, after 2000 days. In addition, female samples with high p31^{comet} expression had lower survival probability, compared to female samples with low/medium p31^{comet} expression, or with male samples in general. These data do not allow to conclude about the significance of p31^{comet} as a prognostic biomarker. However, it must be noted that p31^{comet} acts in concert with other molecules, such as Mad2 and TRIP13 (206). As such, it would not be surprising that a balance between these molecules could be more determinant in a clinical context than the individual expression of each of these partners. Therefore, the impact of

p31^{comet} expression in the survival of HNSCC patients should not be performed separately from these partners.

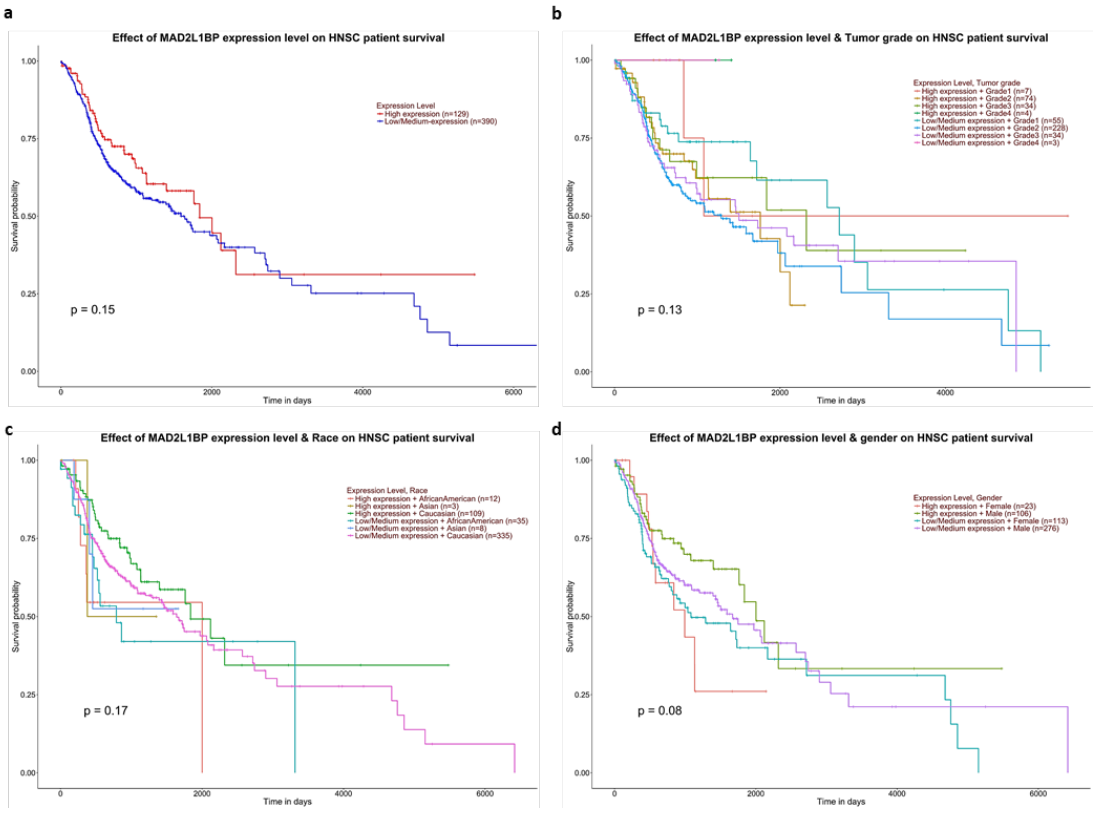

Figure 35. Kaplan-Meier curves for patient's survival according to p31^{comet} expression and/or clinicopathologic features.

(**a**) p31^{comet} expression; (**b**) p31^{comet} expression and tumor grade; (**c**) p31^{comet} expression and race; (**d**) p31^{comet} expression and gender. *p* value indicates statistical significance of survival correlation between groups.

These findings suggest that the possible role of p31^{comet} as a prognostic marker in HNSCC should be analyzed in a more global context and also include p31^{comet} interactors. Nevertheless, further experiments will be required to investigate this issue. However, it does not invalidate the therapeutic potential of p31^{comet} targeting. p31^{comet} targeting will be next investigated in OSCC cells.

4.2. p31^{comet} expression in OSCC cell lines

Cisplatin is the first-line chemotherapeutic drug in the treatment of OSCC but is still impaired by resistance and side effects (325). Combination therapy has been used as a strategy to overcome these issues, and cisplatin has been administered in combination with other drugs, including antimitotics, mostly MTAs (325). As MTAs also face limitations, in part due to the development of

resistance associated with their action on microtubules, alternative antimitotic approaches have been investigated, such as the targeting of SAC regulators (325,337). Therefore, we sought to investigate if p31^{comet} knockdown could be a valuable strategy to lower the effective dose of cisplatin in OSCC cancer. To this end, two human OSCC cell lines, SCC09 and SCC25 were used. p31^{comet} expression levels were first determined in both cell lines, in comparison with non-tumor human oral keratinocytes (HOK). Although both OSCC lines presented higher mRNA p31^{comet} levels than the non-tumor cell line, SCC25 showed a higher p31^{comet} expression than SCC09 (Figure 36a). These observations were consistent at protein levels (Figure 36b). In conclusion, p31^{comet} levels were upregulated in OSCC cells, a result that was significantly more pronounced in the SCC25 cell line. The p31^{comet} overexpression in OSCC cells is in line with the data obtained from UALCAN on HNSCC patients and reinforces the hypothesis that p31^{comet} targeting can be a valuable strategy in oral cancer.

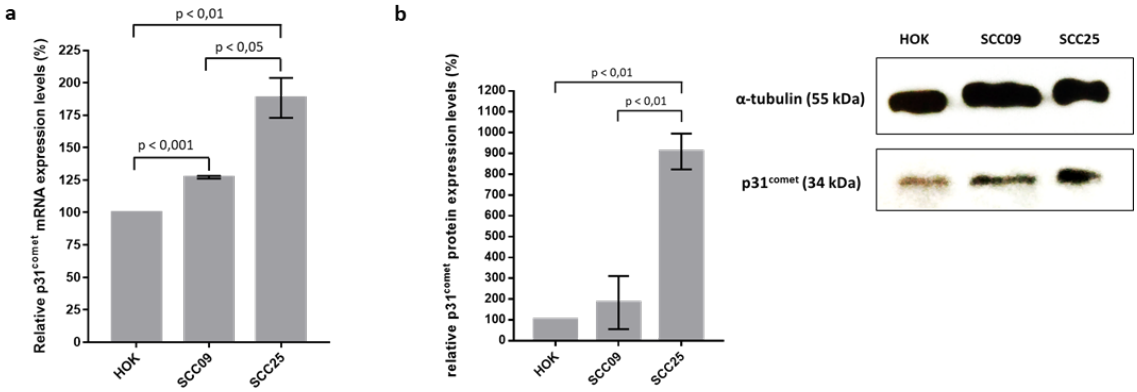

Figure 36. p31^{comet} is overexpressed in oral squamous cell carcinoma (OSCC) cells.

(**a**) Relative p31^{comet} mRNA expression levels were determined by qRT-PCR in OSCC cell lines SCC09 and SCC25 comparatively to non-tumor human oral keratinocytes (HOK). (**b**) Representative western blot (on the right) showing differential p31^{comet} protein expression levels were determined by western blot in cells analyzed in (**a**) and the respective quantification (on the left). α-tubulin was used as a loading control. Statistical analysis was performed through the Student t-test of three independent experiments. The error bars represent mean ± SD.

4.3. p31^{comet} knockdown in OSCC cell lines

As p31^{comet} overexpression in OSCC cell lines reinforced the relevance of targeting p31^{comet}, siRNA-mediated p31^{comet} knockdown was then performed. 48 hours after transfection with p31^{comet} siRNA (sip31^{comet}) (Figure 37), p31^{comet}-depletion levels were between 90 and 86% (90.38 ± 0.84 in SCC09 cells; 86.05 ± 1.58% in SCC25 cells) (Figure 37a and c) at the mRNA level, and between 56 and

52% in both cell lines (56.45 ± 17.22% in SCC09 cells; 52.40 ± 19.74% in SCC25 cells) at the protein levels (Figure 37b and d), when compared with p31^{comet} levels of cells transfected with Control siRNA. As the siRNA-mediated p31^{comet} knockdown was achieved in OSCC cells, it was next performed in combination with cisplatin treatment.

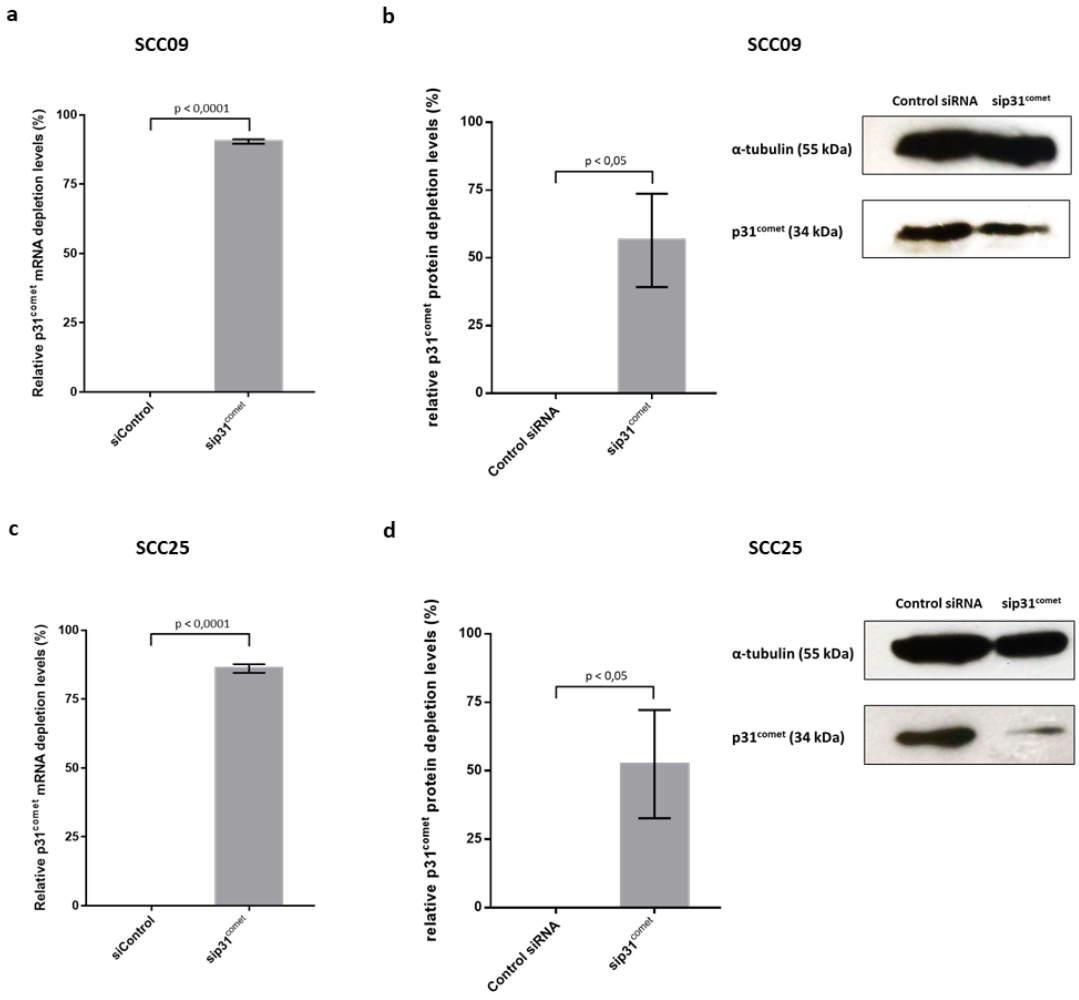

Figure 37. p31^{comet} knockdown in oral squamous cell carcinoma (OSCC) cells.

(**a**) p31^{comet} depletion in SCC09 cells at the mRNA level, as determined by qRT-PCR, and (**b**) at the protein level, as shown by the representative western blot (on the right) with the respective quantification results (on the left). In (**c**) and (**d**), the same analysis as in (**a**) and (**b**), respectively, was performed in SCC25 cells. mRNA and protein were extracted 48 h after transfection. Statistical analysis was performed through the Student t-test of three independent experiments. The error bars represent mean ± SD.

4.3. p31^{comet} knockdown potentiates cisplatin-mediated toxicity in SCC09 cells

After confirming the efficiency of siRNA-mediated p31^{comet} knockdown, it was investigated whether of p31^{comet} knockdown could potentiate the cytotoxic effect of cisplatin in the OSCC cell lines SCC09 and SCC25. For this purpose, 24 hours after transfection with control or p31^{comet} siRNA, cells were treated with cisplatin concentrations ranging from 0 to 100 μM and incubated for another 24 hours. The results from MTT assays demonstrated that p31^{comet} knockdown significantly decreased the viability of SCC09 cells exposed to 10 μM of cisplatin (a decrease of 22% or 23% relative to the individual treatment with cisplatin or sip31^{comet}, respectively; $p < 0.01$) (Figure 38a). In agreement, the IC50 value of cisplatin in SCC09 cells was lower under the treatment with sip31^{comet} plus cisplatin (19.24 μM), compared to the individual treatment with cisplatin, (29.12 μM) (Figure 38c). However, in SCC25 cells, the combined treatment of cisplatin and sip31^{comet} did not show efficacy in MTT assay, when compared with the individual treatments, at any cisplatin concentration (Figure 38b), a fact that was also reflected in the IC50 values (Figure 38d). Notably, in 10 days' colony formation assays, 0.5 μM of cisplatin were enough to significantly decrease the survival of SCC09 cells in combination with sip31^{comet}, compared with individual treatments with cisplatin (a decrease of 22%, $p < 0.01$) or sip31^{comet} (a decrease of 15%, $p < 0.05$) (Figure 38e). Regarding SCC25 cells, the combined treatment of sip31^{comet} plus 0.5 μM cisplatin decreased the survival compared to the individual treatment with cisplatin (a decrease of 12%), but the difference was not statistically significant (Figure 38f).

The MTT assay was used to evaluate the viability immediately after the removal of the drugs, and the colony formation assay to assess the survival ten days after drug removal. Therefore, as in colony formation assays lower cisplatin concentrations were needed (0.5 μM) to observe the efficacy of the combined treatment (sip31^{comet} plus cisplatin) compared to individual treatments, the effects of the treatment may not be completely manifested immediately after drug removal. Interestingly, when comparing the 48 h viability and 10 days' survival values of the two cell lines treated with cisplatin only, SCC09 cells presented higher values than SCC25 cells, for the same concentrations of cisplatin. This is evident, for example, at 50 μM of cisplatin in MTT assays (a difference of 22% in cell viability between both cell lines), as well as for 0.5 μM of cisplatin in clonogenic assays (a difference of 44% in cell survival between both cell lines) (Figure 39). This is also observable with the IC50 under cisplatin individual treatment (29.12 μM, SCC09; 17.57 μM, SCC25). These results suggest that the SCC09 cell line is more resistant than SCC25 to cisplatin.

Therefore, the results hint at the premise that targeting SAC silencing through p31^{comet} knockdown can be a valuable strategy, particularly in the OSCC cases that display resistance to cisplatin treatment.

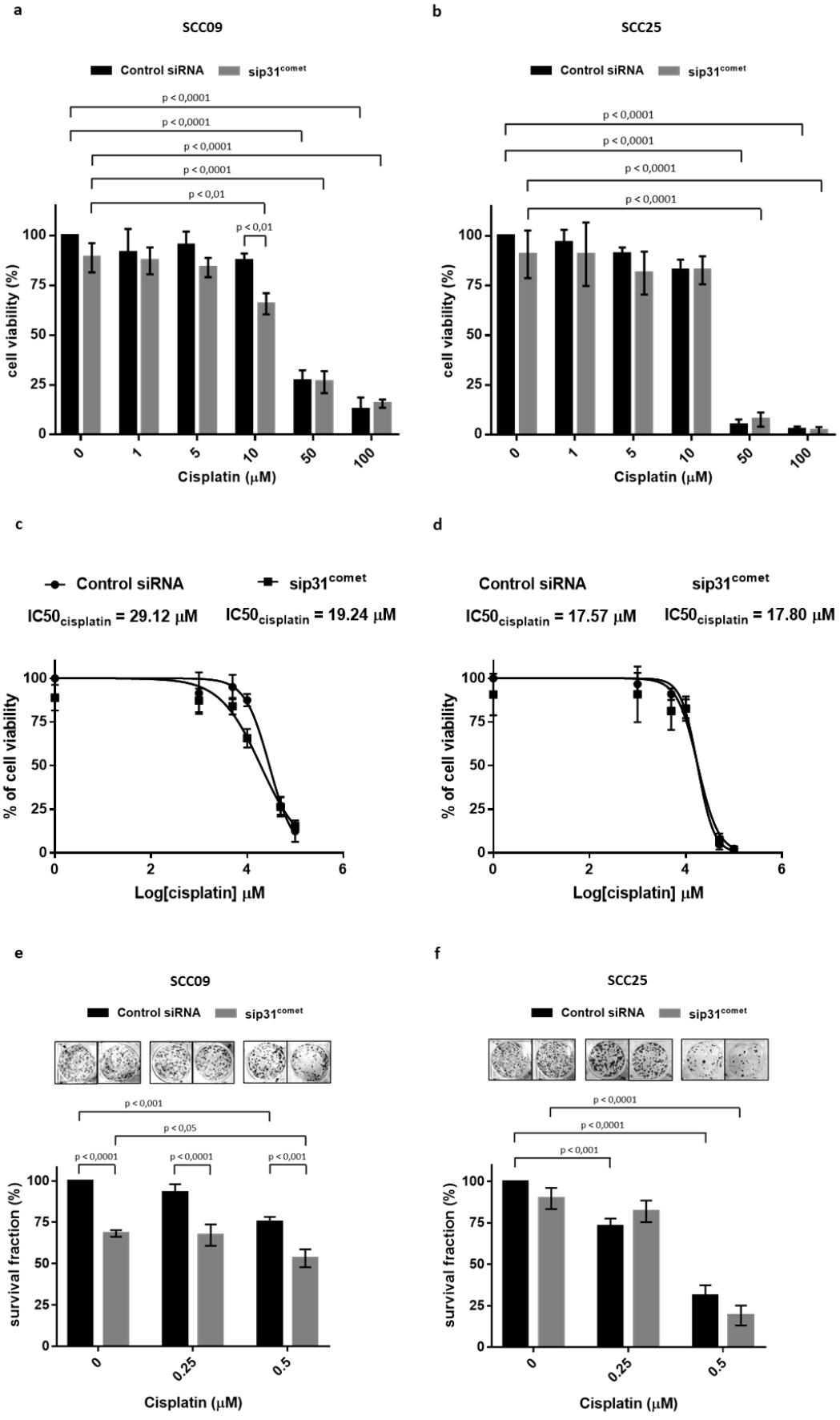

Figure 38. p31^{comet} knockdown enhances cisplatin-mediated toxicity in SCC09 cells under clinically relevant doses of cisplatin.

(**a**) Cell viability of SCC09 and (**b**) SCC25, as determined by MTT assay. Cisplatin was added to SCC09 (**a**) and SCC25 (**b**) cells at the indicated concentrations (0–100 μM) twenty-four hours after transfection with control or p31^{comet} siRNAs, and cells were incubated for an extra 24 h. (**c**) Dose response curves and IC50 values for cisplatin treatment of SCC09 and (**d**) SCC25 cells transfected with control or p31^{comet} siRNA-. (**e**) SCC09 and (**f**) SCC25 cells were treated as in (**a**) **and** (**b**), washed and allowed to grow for 10 days for colony formation assays. For each condition, representative images of surviving colonies (top) are shown. Results are the mean from three independent experiments, expressed as % of survival fraction. Statistical analysis was performed by two-way ANOVA with Tukey's multiple comparisons test. The error bars represent mean ± SD of three independent experiments.

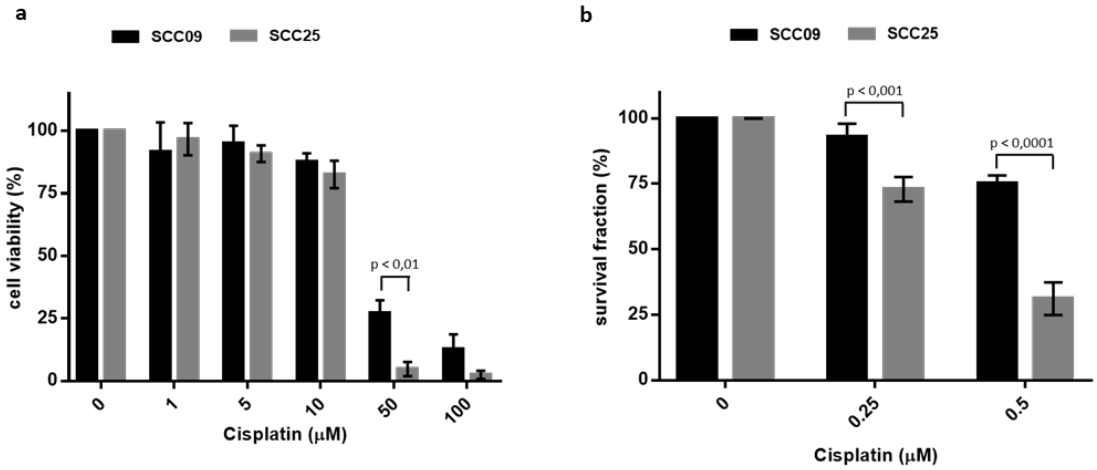

Figure 39. SCC09 cells exhibit more resistance to cisplatin than SCC25 cells.

The results of MTT and colony formation assays shown in Figure 26 were compared between SCC09 and SCC25 cells for the individual treatment with cisplatin. Statistical analysis was performed by two-way ANOVA with Tukey's multiple comparisons test. The error bars represent mean ± SD of three independent experiments.

5. Discussion

Squamous carcinomas represent the majority of the head and neck cancers, and oral squamous carcinoma cells are very common among oral cancers (329). When chemotherapy is needed, cisplatin is the first-line drug, although resistance is still a major concern (325). To overcome this problem, combined therapy with other drugs has been explored and applied, including the combination of cisplatin with MTAs. However, the efficacy of MTAs is still hindered by the development of resistance mechanisms and side effects, and cross-resistance still occurs after the combined treatment of cisplatin and MTAs (195,196). As, in part, the development of resistance to MTAs is related to their action on microtubules, antimitotics that do not directly interfere with

microtubules have been studied (80). For instance, targeting spindly or Bub3 was already found to sensitize OSCC cancer cells to clinically relevant doses of cisplatin (199).

In this context, p31^{comet} also emerges as an interesting target. p31^{comet} was previously demonstrated to potentiate the lethality of the pro-apoptotic Navitoclax, or the MTA paclitaxel in non-small cell lung cancer (NSCLC) cells (312). Therefore, this study sought to exploit the relevance of the SAC silencer p31^{comet} as a prognostic biomarker in oral cancer, and as a possible target to potentiate the efficacy of cisplatin in OSCC cell lines.

To investigate p31^{comet} significance as a biomarker, the UALCAN web resource was used to assess transcriptomics and proteomics data on HNSCC samples and to analyze its association with clinicopathological features. The fact that p31^{comet} was overexpressed across HNSCC samples at the mRNA and protein levels was in line with previous p31^{comet} transcriptomics analysis based on oncomine data (257). Moreover, p31^{comet} mRNA levels were upregulated in a wide range of cancers, according to data from oncomine (257), and from The Cancer Genome Atlas (TCGA) (see section 5.3 of introduction). In agreement, p31^{comet} was also overexpressed in the OSCC cell lines analyzed in this work. These results suggest a clinical relevance for p31^{comet} in oral cancer, either as a prognostic biomarker, or a therapeutic target. To reinforce this premise, it was also found that p31^{comet} overexpression in HNSCC cases coincided with alterations in pathways that are often associated with carcinogenesis, mainly in mTOR and SWI/SNF-altered pathways, and also with the presence of an altered chromatin-modified status.

Surprisingly, HNSCC samples with a low or medium expression of p31^{comet} were associated with poorer survival than those where p31^{comet} was upregulated. However, this result may also be influenced by other factors, such as gender and tumor grade. Curiously, preliminary results from our lab based on tissue microarray analysis (TMAs) of oral cancer samples also indicated that the cases with high p31^{comet} levels were related to a better prognosis [*unpublished data*]. Nevertheless, it should be noted that p31^{comet} function depends on the interaction with other partners, such as Mad2 and TRIP13, and that their expression should also be considered in survival analysis. Therefore, studying the changes occurring in the balance between those molecules can be more relevant than the analysis of their isolated expression. In agreement, p31^{comet}/Mad2-altered ratios were found in hepatocellular carcinoma and non-small cell lung cancer (NSCLC) cells (277). Moreover, the Pearson correlation analysis performed through UALCAN, demonstrated that p31^{comet} expression was positively correlated with the expression of its interactors MAD2 and

TRIP13, as well as with genes that may be involved in the regulation of its expression, like E2F genes (206). Notably, Mad2 mRNA levels were previously found to be upregulated in OSCC cells and immunohistochemistry analysis also revealed Mad2 overexpression in OSCC cases (338). In addition, immunoexpression analysis demonstrated overexpression of Mad2 in oral leukoplakias (339). Interestingly, it was also observed that a high expression of TRIP13 in HNSCC TMAs was associated with poor-free recurrence survival (340). These findings indicate that the significance of p31^{comet} as a prognostic biomarker requires further investigation and that the influence of p31^{comet} expression on the survival of HNSCC patients should not be analyzed separately, but also contemplates interactors. Nevertheless, although the relationship between p31^{comet} and HNSCC survival remains to be clarified, this finding does not invalidate the potential of p31^{comet} therapeutic targeting. Indeed, this study demonstrated that p31^{comet} knockdown was able to potentiate the cisplatin effect in the OSCC cell line SCC09. However, this effect was not observed in the SCC25 cell line, except for a slight decrease of cell survival in clonogenic experiments using sip31^{comet} and 0.5 μM of cisplatin. It would be expectable that this strategy would be well succeeded, as the targeting of SAC silencing through spindly knockdown was previously shown to sensitize both SCC25 and SCC09 cell lines to cisplatin. (199). On the other hand, SCC25 displayed more sensitivity to cisplatin than SCC09 cells, suggesting that SCC09 cells are more resistant to cisplatin. Another interesting fact was that the expression of p31^{comet} was significantly higher in the SCC25 cell line (~188% at mRNA level and ~449% at the protein level) than in the SCC09 line (~127% at mRNA level and ~183% at the protein level). Therefore, based on these results, it is not possible to associate the efficacy of silencing SAC through p31^{comet} targeting with the basal expression of p31^{comet}. Consequently, rather than p31^{comet} expression levels, other factors, including drug resistance, may dictate if p31^{comet} knockdown can be a useful strategy in the treatment of OSCC.

Therefore, the combination of p31^{comet} inhibition and cisplatin is a promising strategy that deserves to be explored for oral cancer in the context of cisplatin resistance, independently of p31^{comet} expression status.

In conclusion, p31^{comet} overexpression is frequently found in human oral cancer and shows association with alterations in cancer-related pathways. However, the impact of p31^{comet} overexpression in patient survival was not conclusive and should not be analyzed in separately. As such, the relevance of p31^{comet} as a prognostic biomarker for oral cancer must be further explored together with p31^{comet} interactors. Notably, p31^{comet} knockdown potentiated cisplatin

effect in the most resistant OSCC cell line. Although further studies are needed to confirm this finding, the results open the wind for an alternative antimitotic strategy to potentiate the cisplatin effect in oral cancer.

CHAPTER VI

Conclusions and future perspectives

Chemotherapy keeps being a point of reference in the treatment of several cancers, and MTAs are among the most used chemotherapeutic drugs. However, their efficacy is limited by resistance mechanisms, in part related to their action on microtubules. Therefore, in recent years, numerous efforts have been made to find alternative antimitotic strategies that could overcome the obstacles to the efficacy of the classical MTAs. In this context, SAC-related proteins have been regarded as attractive targets. Moreover, combination strategies have paved the way for promising approaches. For instance, combining antimitotics, or antimitotics with pro-apoptotics (such as BH3-mimetics) has been revealed to be interesting on overcoming mitotic slippage (63,143,149,165,274,277), one of the main problems associated with MTAs resistance.

In this work, the SAC silencer p31^{comet} has been explored as a target to potentiate the effect of anti-cancer drugs. In agreement with the competing network model, delaying mitotic slippage or accelerating apoptosis can shift the fate of a mitotic-arrested cell to death. Primarily, p31^{comet} knockdown was investigated in combination with the MTA paclitaxel and the BH3-mimetic Navitoclax, using NSCLC as a model. Furthermore, p31^{comet} targeting was also explored in OSCC in combination with cisplatin, a first-line chemotherapeutic drug used in cancer treatment.

The first main objective of this work "to explore the anti-tumoral potential of p31^{comet} knockdown in NSCLC cells in combination with paclitaxel and Navitoclax" has been achieved. In a 2D model, we were able to demonstrate that siRNA-mediated p31^{comet} knockdown was able to improve the anti-tumoral effect of clinically relevant doses of both drugs, through distinct mechanistic. It was revealed that, in the presence of clinically relevant doses of paclitaxel, p31^{comet} depleted cells were forced to arrest in mitosis until death. Although nanomolar concentrations of paclitaxel interfere with microtubule dynamics, generally SAC can still be satisfied in those conditions, and the mitosis procced (291,297). Notably, the mitotic delay induced by the absence of p31^{comet} shifted the fate of the paclitaxel-treated cells to death. On the other hand, cells died preferentially after mitosis, in the presence of Navitoclax. Moreover, when those cells were transfected with sip31^{comet}, post-mitotic death was anticipated. This was in line with previous findings suggesting that cells exposed to a mitotic blocker tend to be more dependent on Bcl-xL after mitosis, due to Mcl-1 degradation that occurred during the prolonged mitotic arrest (128). Therefore, the mitotic delay induced by p31^{comet} knockdown could result in an increased dependence on other pro-survival molecules, such as Bcl-xL and Bcl2, which could explain the anticipated cell mortality with Navitoclax. Interestingly, we could also observe that the combinatory strategy (sip31^{comet} plus

Navitoclax) was efficient in cells with higher levels of Mcl-1, which had shown a weaker response to Navitoclax individual treatment. Thus, this approach revealed the potential for the therapy of cancers overexpressing Mcl-1.

Regarding the second main objective, "To validate this strategy in 3D-cancer models, through the generation of tumor spheroids", p31^{comet} knockdown improved the cytotoxic ability of paclitaxel and Navitoclax clinically relevant concentrations, confirming the efficacy of the strategy in a 3D environment. Further investigation should proceed on heterotypic spheroids, which would include fibroblasts, immune cells, and endothelial cells. This would allow to recreate a microenvironment closer to that of the tumor and to evaluate in more accurately the efficacy of the strategy, before advancing to in vivo experiments. It should be noted, however, that *in situ* spheroid transfection is a challenging procedure, so the depletion of p31^{comet} fell short of the intended. Therefore, it would be interesting to exploit methods that allow performing a more efficient siRNA delivery, such as nanoparticle-based strategies. Overall, this study highlights the relevance of targeting SAC silencing as a strategy that deserves to be explored in the context of cancer treatment.

The third objective, covered in chapter V, sought to investigate the clinical relevance of p31^{comet} targeting to oral cancer. The first specific aim "to access the clinical relevance of p31^{comet} as a biomarker in oral cancer, by assessing p31^{comet} expression in HNSCC and the correlation with clinicopathological features of patients" was performed through the web resource UALCAN. Notably, p31^{comet} was overexpressed in HNSCC. Moreover, higher levels of p31^{comet} were observed in cases that revealed an altered chromatin status, and changes in pathways whose dysregulation is frequently associated with carcinogenesis. These data reinforced the clinical relevance of p31^{comet} in oral cancer. Curiously, and considering factors such as tumor grade and gender, the influence of p31^{comet} expression in the survival of HNSCC patients was not conclusive. In further studies, this analysis should also contemplate p31^{comet} interactors, such as Mad2 and TRIP13, as the balance between these molecules may assume a higher clinical relevance in oral cancer than the individual levels of each of these partners. In agreement, previous studies showed the presence of p31^{comet}/Mad2 altered ratios in cancer cells (277). The second specific objective was "to investigate the effect of p31^{comet} knockdown in combination with clinically relevant doses of cisplatin, using OSCC cells". In agreement with UALCAN data on HNSCC patients, p31^{comet} overexpression was also observed in OSCC cells, although it was subtler in one of the two cell lines analyzed. Remarkably, p31^{comet} knockdown potentiated cisplatin cytotoxicity in the OSCC cell line

that displayed more resistant cisplatin. As p31^{comet} levels were only slightly upregulated in this cell line, the results suggest that p31^{comet} basal levels do not correlate with the efficacy of this strategy in OSCC cells. Therefore, p31^{comet}-mediated SAC is a strategy that deserves to be explored in oral cancer. Further studies with a larger sample size would help not only to confirm this approach but also to clarify its relevance in the context of cisplatin resistance.

The outcomes presented here indicate that targeting of p31^{comet} is a promising strategy to potentiate the efficacy of chemotherapeutic drugs in NSCLC and OSCC. However, some aspects still need to be clarified. For instance, studies including a larger number of cell lines would be useful to confirm the relevance of the sip31^{comet} plus Navitoclax in NSCLC when the pro-survival Mcl-1 is overexpressed, as well as to elucidate the potential of using p31^{comet} knockdown to treat oral cancer in a situation of cisplatin-resistance. Moreover, the investigation of the combination strategies presented in this thesis would benefit from the use of 3D heterotypic spheroids that better mimic the tumor microenvironment. In this context, nanoparticle-based strategies would be advantageous. On the one hand, it could increase the efficiency of siRNA delivery, on the other hand, it could allow the specific targeting of cancer cells, as well as to overcome constraints associated with in vivo drug delivery.

In conclusion, SAC targeting through p31^{comet} knockdown opens the window for new strategies to potentiate the efficacy of anti-cancer drugs in NSCLC and oral cancer that deserves to be explored in further studies.

References

1. WHO. Cancer [Internet]. World Heath Organization. 2021 [cited 2021 May 24]. Available from: https://www.who.int/news-room/fact-sheets/detail/cancer

2. WHO WHO. WHO report on cancer: setting priorities, investing wisely and providing care for all [Internet]. 2020. Available from: https://www.who.int/publications/i/item/who-report-on-cancer-setting-priorities-investing-wisely-and-providing-care-for-all

3. Cao Y. Tumorigenesis as a process of gradual loss of original cell identity and gain of properties of neural precursor/progenitor cells. Cell Biosci [Internet]. 2017 Dec 7;7(1):61. Available from: https://cellandbioscience.biomedcentral.com/articles/10.1186/s13578-017-0188-9

4. Balani S, Nguyen L V., Eaves CJ. Modeling the process of human tumorigenesis. Nat Commun [Internet]. 2017 Aug 25;8(1):15422. Available from: http://dx.doi.org/10.1038/ncomms15422

5. Fouad YA, Aanei C. Revisiting the hallmarks of cancer. Am J Cancer Res [Internet]. 2017;7(5):1016–36. Available from: http://www.ncbi.nlm.nih.gov/pubmed/28560055

6. Vincent M. Cancer: A de-repression of a default survival program common to all cells? BioEssays [Internet]. 2012 Jan;34(1):72–82. Available from: http://doi.wiley.com/10.1002/bies.201100049

7. Paul D. The systemic hallmarks of cancer. J Cancer Metastasis Treat [Internet]. 2020 Aug 28;2020. Available from: https://jcmtjournal.com/article/view/3625

8. Hanahan D, Weinberg RA. The Hallmarks of Cancer. Cell [Internet]. 2000 Jan;100(1):57–70. Available from: https://linkinghub.elsevier.com/retrieve/pii/S0092867400816839

9. Hanahan D, Weinberg RA. Hallmarks of Cancer: The Next Generation. Cell [Internet]. 2011 Mar;144(5):646–74. Available from: https://linkinghub.elsevier.com/retrieve/pii/S0092867411001279

10. Ayob AZ, Ramasamy TS. Cancer stem cells as key drivers of tumour progression. J Biomed Sci [Internet]. 2018 Dec 6;25(1):20. Available from: https://jbiomedsci.biomedcentral.com/articles/10.1186/s12929-018-0426-4

11. Baghban R, Roshangar L, Jahanban-Esfahlan R, Seidi K, Ebrahimi-Kalan A, Jaymand M, et al. Tumor microenvironment complexity and therapeutic implications at a glance. Cell Commun Signal [Internet]. 2020 Dec 7;18(1):59. Available from: https://biosignaling.biomedcentral.com/articles/10.1186/s12964-020-0530-4

12. Spaw M, Anant S, Thomas SM. Stromal contributions to the carcinogenic process. Mol Carcinog [Internet]. 2017 Apr;56(4):1199–213. Available from: http://doi.wiley.com/10.1002/mc.22583

13. Elkhattouti A, Hassan M, Gomez CR. Stromal Fibroblast in Age-Related Cancer: Role in Tumorigenesis and Potential as Novel Therapeutic Target. Front Oncol [Internet]. 2015 Jul 27;5(JUL). Available from: http://journal.frontiersin.org/Article/10.3389/fonc.2015.00158/abstract

14. Pinto B, Henriques AC, Silva PMA, Bousbaa H. Three-Dimensional Spheroids as In Vitro Preclinical Models for Cancer Research. Pharmaceutics [Internet]. 2020 Dec 6;12(12):1186. Available from: https://www.mdpi.com/1999-4923/12/12/1186

15. Poltavets V, Kochetkova M, Pitson SM, Samuel MS. The Role of the Extracellular Matrix and Its Molecular and Cellular Regulators in Cancer Cell Plasticity. Front Oncol [Internet]. 2018 Oct 9;8. Available from: https://www.frontiersin.org/article/10.3389/fonc.2018.00431/full

16. Lu P, Weaver VM, Werb Z. The extracellular matrix: A dynamic niche in cancer progression. J Cell Biol [Internet]. 2012 Feb 20;196(4):395–406. Available from: https://rupress.org/jcb/article/196/4/395/36771/The-extracellular-matrix-A-dynamic-niche-in-cancer

17. Talib WH, Alsayed AR, Farhan F, Al Kury LT. Resveratrol and Tumor Microenvironment: Mechanistic Basis and Therapeutic Targets. Molecules [Internet]. 2020 Sep 18;25(18):4282. Available from: https://www.mdpi.com/1420-3049/25/18/4282

18. Li J, Stanger BZ. Cell Cycle Regulation Meets Tumor Immunosuppression. Trends Immunol [Internet]. 2020 Oct;41(10):859–63. Available from: https://linkinghub.elsevier.com/retrieve/pii/S1471490620301757

19. Oki T, Nishimura K, Kitaura J, Togami K, Maehara A, Izawa K, et al. A novel cell-cycle-indicator, mVenus-p27K–, identifies quiescent cells and visualizes G0–G1 transition. Sci Rep [Internet]. 2015 May 6;4(1):4012. Available from: http://www.nature.com/articles/srep04012

20. Cheung TH, Rando TA. Molecular regulation of stem cell quiescence. Nat Rev Mol Cell Biol [Internet]. 2013 Jun 23;14(6):329–40. Available from: https://www.ncbi.nlm.nih.gov/pmc/articles/PMC3624763/pdf/nihms412728.pdf

21. Wenzel ES, Singh ATK. Cell-cycle Checkpoints and Aneuploidy on the Path to Cancer. In Vivo (Brooklyn) [Internet]. 2018 Jan 2;32(1):1–5. Available from: http://iv.iiarjournals.org/content/32/1/1.abstract

22. Panagopoulos A, Altmeyer M. The Hammer and the Dance of Cell Cycle Control. Trends Biochem Sci [Internet]. 2021 Apr;46(4):301–14. Available from: https://doi.org/10.1016/j.tibs.2020.11.002

23. Musacchio A, Salmon ED. The spindle-assembly checkpoint in space and time. Nat Rev Mol Cell Biol [Internet]. 2007 May 11;8(5):379–93. Available from: http://www.nature.com/articles/nrm2163

24. Lim S, Kaldis P. Cdks, cyclins and CKIs: roles beyond cell cycle regulation. Development [Internet]. 2013 Aug 1;140(15):3079–93. Available from: https://journals.biologists.com/dev/article/140/15/3079/45823/Cdks-cyclins-and-CKIs-roles-beyond-cell-cycle

25. Sanchez Y, Wong C, Thoma RS, Richman R, Wu Z, Piwnica-worms H. Censervation of the Chkl Checkpoint Pathway in Mammals: Linkage of DNA Damage to Cdk Regulation Through Gdc25. 1997;277(5331):1497–501.

26. Darzynkiewicz Z, Gong J, Juan G, Ardelt B, Traganos F. Cytometry of cyclin proteins. Cytometry [Internet]. 1996 Sep 1;25(1):1–13. Available from: http://www.ncbi.nlm.nih.gov/pubmed/8875049

27. Stauffer S, Gardner A, Ungu DAK, López-Córdoba A, Heim M. Mitosis. In: Labster Virtual Lab Experiments: Basic Biology [Internet]. Berlin, Heidelberg: Springer Berlin Heidelberg; 2018. p. 11–26. Available from: http://link.springer.com/10.1007/978-3-662-57996-1_2

28. Lents NH, Baldassare JJ. Cyclins and Cyclin-Dependent Kinases. In: Encyclopedia of Cell Biology [Internet]. Elsevier; 2016. p. 423–31. Available from: http://dx.doi.org/10.1016/B978-0-12-394447-4.30057-8

29. Bower JJ, Vance LD, Psioda M, Smith-Roe SL, Simpson DA, Ibrahim JG, et al. Patterns of cell cycle checkpoint deregulation associated with intrinsic molecular subtypes of human breast cancer cells. npj Breast Cancer [Internet]. 2017 Dec 31;3(1):9. Available from: http://dx.doi.org/10.1038/s41523-017-0009-7

30. Smith HL, Southgate H, Tweddle DA, Curtin NJ. DNA damage checkpoint kinases in cancer. Expert Rev Mol Med [Internet]. 2020 Jun 8;22:e2. Available from: https://www.cambridge.org/core/product/identifier/S1462399420000034/type/journal_article

31. Gordon E, Ravicz J, Liu S, Chawla S, Hall F. Cell cycle checkpoint control: The cyclin G1/Mdm2/p53 axis emerges as a strategic target for broad-spectrum cancer gene therapy - A review of

molecular mechanisms for oncologists. Mol Clin Oncol [Internet]. 2018 Jun 14;115–34. Available from: http://www.spandidos-publications.com/10.3892/mco.2018.1657

32. Iyer D, Rhind N. The Intra-S Checkpoint Responses to DNA Damage. Genes (Basel) [Internet]. 2017 Feb 17;8(2):74. Available from: http://www.mdpi.com/2073-4425/8/2/74

33. Kondratova A, Watanabe T, Marotta M, Cannon M, Segall AM, Serre D, et al. Replication fork integrity and intra-S phase checkpoint suppress gene amplification. Nucleic Acids Res [Internet]. 2015 Mar 11;43(5):2678–90. Available from: http://academic.oup.com/nar/article/43/5/2678/2453179/Replication-fork-integrity-and-intraS-phase

34. Chao HX, Poovey CE, Privette AA, Grant GD, Chao HY, Cook JG, et al. Orchestration of DNA Damage Checkpoint Dynamics across the Human Cell Cycle. Cell Syst [Internet]. 2017 Nov;5(5):445-459.e5. Available from: https://doi.org/10.1016/j.cels.2017.09.015

35. Lee JH, Berger JM. Cell Cycle-Dependent Control and Roles of DNA Topoisomerase II. Genes (Basel) [Internet]. 2019 Oct 30;10(11):859. Available from: https://www.mdpi.com/2073-4425/10/11/859

36. Kaufmann WK. Decatenation G2 Checkpoint. In: Schwab M, editor. Encyclopedia of Cancer [Internet]. 2009th ed. Berlin, Heidelberg: Springer Berlin Heidelberg; 2009. p. 827–9. Available from: http://link.springer.com/10.1007/978-3-540-47648-1_1541

37. Ferreira LT, Maiato H. Prometaphase. Semin Cell Dev Biol [Internet]. 2021 Sep;117(xxxx):52–61. Available from: https://linkinghub.elsevier.com/retrieve/pii/S1084952121001555

38. Cooper GM. The Events of M Phase. In: The Cell: A Molecular Approach [Internet]. 2nd editio. Sunderland (MA): Sinauer Associates; 2000. Available from: https://www.ncbi.nlm.nih.gov/books/NBK9958/

39. McIntosh JR. Mitosis. Cold Spring Harb Perspect Biol [Internet]. 2016 Sep 1;8(9):a023218. Available from: http://cshperspectives.cshlp.org/lookup/doi/10.1101/cshperspect.a023218

40. Cheeseman IM, Desai A. Molecular architecture of the kinetochore–microtubule interface. Nat Rev Mol Cell Biol [Internet]. 2008 Jan;9(1):33–46. Available from: http://www.nature.com/doifinder/10.1038/nrm2310

41. Chavali PL, Peset I, Gergely F. Centrosomes and mitotic spindle poles: a recent liaison? Biochem Soc Trans [Internet]. 2015 Feb 1;43(1):13–8. Available from: https://portlandpress.com/biochemsoctrans/article/43/1/13/66180/Centrosomes-and-

mitotic-spindle-poles-a-recent

42. Reddy SK, Rape M, Margansky WA, Kirschner MW. Ubiquitination by the anaphase-promoting complex drives spindle checkpoint inactivation. Nature. 2007;446(7138):921–5.

43. Silva PMA, Reis RM, Bolanos-Garcia VM, Florindo C, Tavares ÁA, Bousbaa H. Dynein-dependent transport of spindle assembly checkpoint proteins off kinetochores toward spindle poles. FEBS Lett [Internet]. 2014 Aug 25;588(17):3265–73. Available from: http://doi.wiley.com/10.1016/j.febslet.2014.07.011

44. Silva P, Barbosa J, Nascimento A V., Faria J, Reis R, Bousbaa H. Monitoring the fidelity of mitotic chromosome segregation by the spindle assembly checkpoint. Cell Prolif. 2011;44(5):391–400.

45. Monda JK, Cheeseman IM. The kinetochore–microtubule interface at a glance. J Cell Sci [Internet]. 2018 Aug 15;131(16). Available from: https://journals.biologists.com/jcs/article/131/16/jcs214577/56961/The-kinetochore-microtubule-interface-at-a-glance

46. Biggins S, Walczak CE. Captivating Capture: How Microtubules Attach to Kinetochores. Curr Biol [Internet]. 2003 May;13(11):R449–60. Available from: https://linkinghub.elsevier.com/retrieve/pii/S0960982203003695

47. Craske B, Welburn JPI. Leaving no-one behind: how CENP-E facilitates chromosome alignment. DeLuca J, Fachinetti D, Dumont J, editors. Essays Biochem [Internet]. 2020 Sep 4;64(2):313–24. Available from: https://portlandpress.com/essaysbiochem/article/64/2/313/222869/Leaving-no-one-behind-how-CENP-E-facilitates

48. Kaul R, Risinger AL, Mooberry SL. Microtubule-Targeting Drugs: More than Antimitotics. J Nat Prod [Internet]. 2019 Mar 22;82(3):680–5. Available from: https://pubs.acs.org/doi/10.1021/acs.jnatprod.9b00105

49. Westermann S, Weber K. Post-translational modifications regulate microtubule function. Nat Rev Mol Cell Biol [Internet]. 2003 Dec;4(12):938–48. Available from: http://www.nature.com/articles/nrm1260

50. Walczak CE, Cai S, Khodjakov A. Mechanisms of chromosome behaviour during mitosis. Nat Rev Mol Cell Biol [Internet]. 2010 Feb 13;11(2):91–102. Available from: http://www.nature.com/articles/nrm2832

51. Forth S, Kapoor TM. The mechanics of microtubule networks in cell division. J Cell Biol [Internet]. 2017 Jun 5;216(6):1525–31. Available from:

https://rupress.org/jcb/article/216/6/1525/38948/The-mechanics-of-microtubule-networks-in-cell

52. McHugh T, Welburn JPI. Dynein at kinetochores: Making the connection. J Cell Biol [Internet]. 2017 Apr 3;216(4):855–7. Available from: https://rupress.org/jcb/article/216/4/855/52204/Dynein-at-kinetochores-Making-the-connectionDynein

53. Hara M, Fukagawa T. Dynamics of kinetochore structure and its regulations during mitotic progression. Cell Mol Life Sci [Internet]. 2020 Aug 12;77(15):2981–95. Available from: https://doi.org/10.1007/s00018-020-03472-4

54. Hayward D, Alfonso-Pérez T, Gruneberg U. Orchestration of the spindle assembly checkpoint by CDK1-cyclin B1. FEBS Lett [Internet]. 2019 Oct 13;593(20):2889–907. Available from: https://onlinelibrary.wiley.com/doi/abs/10.1002/1873-3468.13591

55. Varma D, Chandrasekaran S, Sundin LJR, Reidy KT, Wan X, Chasse DAD, et al. Recruitment of the human Cdt1 replication licensing protein by the loop domain of Hec1 is required for stable kinetochore–microtubule attachment. Nat Cell Biol [Internet]. 2012 Jun 13;14(6):593–603. Available from: http://www.nature.com/articles/ncb2489

56. Tanaka TU. Kinetochore–microtubule interactions: steps towards bi-orientation. EMBO J [Internet]. 2010 Dec 15;29(24):4070–82. Available from: http://emboj.embopress.org/cgi/doi/10.1038/emboj.2010.294

57. Cheeseman IM. The Kinetochore. Cold Spring Harb Perspect Biol [Internet]. 2014 Jul 1;6(7):a015826–a015826. Available from: http://www.ncbi.nlm.nih.gov/pubmed/24984773

58. Saurin AT, Kops GJPL. Studying Kinetochore Kinases. In 2016. p. 333–47. Available from: http://link.springer.com/10.1007/978-1-4939-3542-0_21

59. Rieder CL, Maiato H. Stuck in Division or Passing through. Dev Cell [Internet]. 2004 Nov;7(5):637–51. Available from: https://linkinghub.elsevier.com/retrieve/pii/S1534580704003016

60. Sullivan M, Morgan DO. Finishing mitosis, one step at a time. Nat Rev Mol Cell Biol [Internet]. 2007 Nov;8(11):894–903. Available from: http://www.nature.com/articles/nrm2276

61. Lin C-C, Su W-C, Yen C-J, Hsu C-H, Su W-P, Yeh K-H, et al. A phase I study of two dosing schedules of volasertib (BI 6727), an intravenous polo-like kinase inhibitor, in patients with advanced solid malignancies. Br J Cancer [Internet]. 2014 May 22;110(10):2434–40. Available from: http://www.nature.com/articles/bjc2014195

62. Stadler WM, Vaughn DJ, Sonpavde G, Vogelzang NJ, Tagawa ST, Petrylak DP, et al. An open-label,

single-arm, phase 2 trial of the polo-like kinase inhibitor volasertib (BI 6727) in patients with locally advanced or metastatic urothelial cancer. Cancer [Internet]. 2014 Apr 1;120(7):976–82. Available from: http://doi.wiley.com/10.1002/cncr.28519

63. Gjertsen BT, Schöffski P. Discovery and development of the Polo-like kinase inhibitor volasertib in cancer therapy. Leukemia [Internet]. 2015 Jan 16;29(1):11–9. Available from: http://www.nature.com/articles/leu2014222

64. Etemad B, Kops GJ. Attachment issues: kinetochore transformations and spindle checkpoint silencing. Curr Opin Cell Biol [Internet]. 2016 Apr;39:101–8. Available from: https://linkinghub.elsevier.com/retrieve/pii/S0955067416300230

65. Howell BJ, McEwen BF, Canman JC, Hoffman DB, Farrar EM, Rieder CL, et al. Cytoplasmic dynein/dynactin drives kinetochore protein transport to the spindle poles and has a role in mitotic spindle checkpoint inactivation. J Cell Biol [Internet]. 2001 Dec 24;155(7):1159–72. Available from: https://rupress.org/jcb/article/155/7/1159/32688/Cytoplasmic-dyneindynactin-drives-kinetochore

66. Gassmann R, Holland AJ, Varma D, Wan X, Civril F, Cleveland DW, et al. Removal of Spindly from microtubule-attached kinetochores controls spindle checkpoint silencing in human cells. Genes Dev [Internet]. 2010 May 1;24(9):957–71. Available from: http://genesdev.cshlp.org/cgi/doi/10.1101/gad.1886810

67. Chan YW, Fava LL, Uldschmid A, Schmitz MHA, Gerlich DW, Nigg EA, et al. Mitotic control of kinetochore-associated dynein and spindle orientation by human Spindly. J Cell Biol [Internet]. 2009 Jun 1;185(5):859–74. Available from: https://rupress.org/jcb/article/185/5/859/35349/Mitotic-control-of-kinetochoreassociated-dynein

68. Barisic M, Sohm B, Mikolcevic P, Wandke C, Rauch V, Ringer T, et al. Spindly/CCDC99 Is Required for Efficient Chromosome Congression and Mitotic Checkpoint Regulation. Doxsey S, editor. Mol Biol Cell [Internet]. 2010 Jun 15;21(12):1968–81. Available from: https://www.molbiolcell.org/doi/10.1091/mbc.e09-04-0356

69. Foss KM, Robeson AC, Kornbluth S, Zhang L. Mitotic phosphatase activity is required for MCC maintenance during the spindle checkpoint. Cell Cycle [Internet]. 2016 Jan 17;15(2):225–33. Available from: http://dx.doi.org/10.1080/15384101.2015.1121331

70. Schmidt M, Bastians H. Mitotic drug targets and the development of novel anti-mitotic anticancer drugs. Drug Resist Updat [Internet]. 2007 Aug;10(4–5):162–81. Available from:

https://linkinghub.elsevier.com/retrieve/pii/S1368764607000441

71. Thompson SL, Bakhoum SF, Compton DA. Mechanisms of Chromosomal Instability. Curr Biol [Internet]. 2010 Mar;20(6):R285–95. Available from: https://linkinghub.elsevier.com/retrieve/pii/S096098221000076X

72. Yang M, Li B, Tomchick DR, Machius M, Rizo J, Yu H, et al. p31comet Blocks Mad2 Activation through Structural Mimicry. Cell [Internet]. 2007 Nov;131(4):744–55. Available from: https://linkinghub.elsevier.com/retrieve/pii/S0092867407011993

73. Ye Q, Rosenberg SC, Moeller A, Speir JA, Su TY, Corbett KD. TRIP13 is a protein-remodeling AAA+ ATPase that catalyzes MAD2 conformation switching. Elife. 2015;2015(4):1–44.

74. Hellmuth S, Gómez-H L, Pendás AM, Stemmann O. Securin-independent regulation of separase by checkpoint-induced shugoshin–MAD2. Nature [Internet]. 2020 Apr 8;580(7804):536–41. Available from: http://www.nature.com/articles/s41586-020-2182-3

75. Mansfeld J, Collin P, Collins MO, Choudhary JS, Pines J. APC15 drives the turnover of MCC-CDC20 to make the spindle assembly checkpoint responsive to kinetochore attachment. Nat Cell Biol [Internet]. 2011 Oct 18;13(10):1234–43. Available from: http://www.nature.com/articles/ncb2347

76. Uzunova K, Dye BT, Schutz H, Ladurner R, Petzold G, Toyoda Y, et al. APC15 mediates CDC20 autoubiquitylation by APC/CMCC and disassembly of the mitotic checkpoint complex. Nat Struct Mol Biol [Internet]. 2012 Nov 24;19(11):1116–23. Available from: http://www.ncbi.nlm.nih.gov/pmc/articles/PMC3498062/

77. Nijenhuis W, Vallardi G, Teixeira A, Kops GJPL, Saurin AT. Negative feedback at kinetochores underlies a responsive spindle checkpoint signal. Nat Cell Biol [Internet]. 2014 Dec 17;16(12):1257–64. Available from: http://www.nature.com/articles/ncb3065

78. Weaver BAA, Cleveland DW. Decoding the links between mitosis, cancer, and chemotherapy: The mitotic checkpoint, adaptation, and cell death. Cancer Cell [Internet]. 2005 Jul;8(1):7–12. Available from: https://linkinghub.elsevier.com/retrieve/pii/S1535610805001972

79. Hanahan D, Weinberg RA. Hallmarks of cancer: The next generation. Cell [Internet]. 2011;144(5):646–74. Available from: http://dx.doi.org/10.1016/j.cell.2011.02.013

80. Henriques AC, Ribeiro D, Pedrosa J, Sarmento B, Silva PMA, Bousbaa H. Mitosis inhibitors in anticancer therapy: When blocking the exit becomes a solution. Cancer Lett [Internet]. 2019;440–441(September 2018):64–81. Available from: https://doi.org/10.1016/j.canlet.2018.10.005

81. Levine MS, Holland AJ. The impact of mitotic errors on cell proliferation and tumorigenesis. Genes

Dev [Internet]. 2018 May 1;32(9–10):620–38. Available from: http://genesdev.cshlp.org/lookup/doi/10.1101/gad.314351.118

82. Duijf PHG, Schultz N, Benezra R. Cancer cells preferentially lose small chromosomes. Int J Cancer [Internet]. 2013 May 15;132(10):2316–26. Available from: http://doi.wiley.com/10.1002/ijc.27924

83. Sarkar S, Sahoo PK, Mahata S, Pal R, Ghosh D, Mistry T, et al. Mitotic checkpoint defects: en route to cancer and drug resistance. Chromosom Res [Internet]. 2021 Jun 6;29(2):131–44. Available from: https://link.springer.com/10.1007/s10577-020-09646-x

84. Cahill DP, Lengauer C, Yu J, Riggins GJ, Willson JK V., Markowitz SD, et al. Mutations of mitotic checkpoint genes in human cancers. Nature [Internet]. 1998 Mar;392(6673):300–3. Available from: http://www.nature.com/articles/32688

85. Gemma A, Seike M, Seike Y, Uematsu K, Hibino S, Kurimoto F, et al. Somatic mutation of the hBUB1 mitotic checkpoint gene in primary lung cancer. Genes Chromosomes Cancer [Internet]. 2000 Nov;29(3):213–8. Available from: http://www.ncbi.nlm.nih.gov/pubmed/10992296

86. Collin P, Nashchekina O, Walker R, Pines J. The spindle assembly checkpoint works like a rheostat rather than a toggle switch. Nat Cell Biol [Internet]. 2013 Nov 6;15(11):1378–85. Available from: http://www.nature.com/articles/ncb2855

87. Shichiri M, Yoshinaga K, Hisatomi H, Sugihara K, Hirata Y. Genetic and epigenetic inactivation of mitotic checkpoint genes hBUB1 and hBUBR1 and their relationship to survival. Cancer Res [Internet]. 2002 Jan 1;62(1):13–7. Available from: http://www.ncbi.nlm.nih.gov/pubmed/11782350

88. Imai Y, Shiratori Y, Kato N, Inoue T, Omata M. Mutational Inactivation of Mitotic Checkpoint Genes, hsMAD2 and hBUB1 , Is Rare in Sporadic Digestive Tract Cancers. Japanese J Cancer Res [Internet]. 1999 Aug;90(8):837–40. Available from: http://doi.wiley.com/10.1111/j.1349-7006.1999.tb00824.x

89. Tsukasaki K, Miller CW, Greenspun E, Eshaghian S, Kawabata H, Fujimoto T, et al. Mutations in the mitotic check point gene, MAD1L1, in human cancers. Oncogene [Internet]. 2001 May 22;20(25):3301–5. Available from: http://www.nature.com/articles/1204421

90. Guo Y, Zhang X, Yang M, Miao X, Shi Y, Yao J, et al. Functional evaluation of missense variations in the human MAD1L1 and MAD2L1 genes and their impact on susceptibility to lung cancer. J Med Genet [Internet]. 2010 Sep 1;47(9):616–22. Available from: https://jmg.bmj.com/lookup/doi/10.1136/jmg.2009.074252

91. Zhong R, Chen X, Chen X, Zhu B, Lou J, Li J, et al. MAD1L1 Arg558His and MAD2L1 Leu84Met interaction with smoking increase the risk of colorectal cancer. Sci Rep [Internet]. 2015 Dec 17;5(1):12202. Available from: http://www.nature.com/articles/srep12202

92. Hanks S, Coleman K, Reid S, Plaja A, Firth H, FitzPatrick D, et al. Constitutional aneuploidy and cancer predisposition caused by biallelic mutations in BUB1B. Nat Genet [Internet]. 2004 Nov 10;36(11):1159–61. Available from: http://www.nature.com/articles/ng1449

93. Suijkerbuijk SJE, van Osch MHJ, Bos FL, Hanks S, Rahman N, Kops GJPL. Molecular Causes for BUBR1 Dysfunction in the Human Cancer Predisposition Syndrome Mosaic Variegated Aneuploidy. Cancer Res [Internet]. 2010 Jun 15;70(12):4891–900. Available from: http://cancerres.aacrjournals.org/lookup/doi/10.1158/0008-5472.CAN-09-4319

94. Yost S, de Wolf B, Hanks S, Zachariou A, Marcozzi C, Clarke M, et al. Biallelic TRIP13 mutations predispose to Wilms tumor and chromosome missegregation. Nat Genet [Internet]. 2017 Jul 29;49(7):1148–51. Available from: http://www.nature.com/articles/ng.3883

95. Sun Q, Zhang X, Liu T, Liu X, Geng J, He X, et al. Increased expression of Mitotic Arrest Deficient-Like 1 (MAD1L1) is associated with poor prognosis and insensitive to Taxol treatment in breast cancer. Breast Cancer Res Treat [Internet]. 2013 Jul 17;140(2):323–30. Available from: http://link.springer.com/10.1007/s10549-013-2633-8

96. Mondal G, Sengupta S, Panda CK, Gollin SM, Saunders WS, Roychoudhury S. Overexpression of Cdc20 leads to impairment of the spindle assembly checkpoint and aneuploidization in oral cancer. Carcinogenesis [Internet]. 2007 Jan 1;28(1):81–92. Available from: https://academic.oup.com/carcin/article-lookup/doi/10.1093/carcin/bgl100

97. Gayyed MF, El-Maqsoud NMRA, Tawfiek ER, El Gelany SAA, Rahman MFA. A comprehensive analysis of CDC20 overexpression in common malignant tumors from multiple organs: its correlation with tumor grade and stage. Tumor Biol [Internet]. 2016 Jan 6;37(1):749–62. Available from: http://link.springer.com/10.1007/s13277-015-3808-1

98. Murray S, Briasoulis E, Linardou H, Bafaloukos D, Papadimitriou C. Taxane resistance in breast cancer: Mechanisms, predictive biomarkers and circumvention strategies. Cancer Treat Rev [Internet]. 2012 Nov;38(7):890–903. Available from: https://linkinghub.elsevier.com/retrieve/pii/S0305737212000497

99. McGrogan B, Phelan S, Fitzpatrick P, Maguire A, Prencipe M, Brennan D, et al. Spindle assembly checkpoint protein expression correlates with cellular proliferation and shorter time to recurrence in ovarian cancer. Hum Pathol [Internet]. 2014 Jul;45(7):1509–19. Available from:

https://linkinghub.elsevier.com/retrieve/pii/S004681771400121X

100. Bargiela-Iparraguirre J, Fernandez-Fuente M, Herrera L., Sanchez Perez I. MAD2 in the Spotlight as a Cancer Therapy Regulator. Int J Cancer Oncol [Internet]. 2016;3(2):1–8. Available from: http://www.ommegaonline.org/article-details/MAD2-in-the-Spotlight-as-a-Cancer-Therapy-Regulator/889

101. Wang L, Wang J, Jin Y, Zheng J, Yang Y, Xi X. Downregulation of Mad2 and BubR1 increase the malignant potential and nocodazole resistance by compromising spindle assembly checkpoint signaling pathway in cervical carcinogenesis. J Obstet Gynaecol Res [Internet]. 2019 Dec 15;45(12):2407–18. Available from: https://onlinelibrary.wiley.com/doi/abs/10.1111/jog.14120

102. Rhodes DR, Yu J, Shanker K, Deshpande N, Varambally R, Ghosh D, et al. ONCOMINE: A Cancer Microarray Database and Integrated Data-Mining Platform. Neoplasia [Internet]. 2004 Jan;6(1):1–6. Available from: https://linkinghub.elsevier.com/retrieve/pii/S1476558604800472

103. Fagerberg L, Hallström BM, Oksvold P, Kampf C, Djureinovic D, Odeberg J, et al. Analysis of the Human Tissue-specific Expression by Genome-wide Integration of Transcriptomics and Antibody-based Proteomics. Mol Cell Proteomics [Internet]. 2014 Feb;13(2):397–406. Available from: http://www.mcponline.org/lookup/doi/10.1074/mcp.M113.035600

104. Dai W, Wang Q, Liu T, Swamy M, Fang Y, Xie S, et al. Slippage of Mitotic Arrest and Enhanced Tumor Development in Mice with BubR1 Haploinsufficiency. Cancer Res [Internet]. 2004 Jan 15;64(2):440–5. Available from: http://cancerres.aacrjournals.org/lookup/doi/10.1158/0008-5472.CAN-03-3119

105. Hernando E, Nahlé Z, Juan G, Diaz-Rodriguez E, Alaminos M, Hemann M, et al. Rb inactivation promotes genomic instability by uncoupling cell cycle progression from mitotic control. Nature [Internet]. 2004 Aug;430(7001):797–802. Available from: http://www.nature.com/articles/nature02820

106. Sotillo R, Hernando E, Díaz-Rodríguez E, Teruya-Feldstein J, Cordón-Cardo C, Lowe SW, et al. Mad2 Overexpression Promotes Aneuploidy and Tumorigenesis in Mice. Cancer Cell [Internet]. 2007 Jan;11(1):9–23. Available from: https://linkinghub.elsevier.com/retrieve/pii/S1535610806003710

107. Schvartzman J-M, Duijf PHG, Sotillo R, Coker C, Benezra R. Mad2 Is a Critical Mediator of the Chromosome Instability Observed upon Rb and p53 Pathway Inhibition. Cancer Cell [Internet]. 2011 Jun;19(6):701–14. Available from: https://linkinghub.elsevier.com/retrieve/pii/S1535610811001619

108. Date DA, Burrows AC, Venere M, Jackson MW, Summers MK. Coordinated regulation of p31Cometand Mad2 expression is required for cellular proliferation. Cell Cycle. 2013;12(24):3824–32.

109. Kent LN, Leone G. The broken cycle: E2F dysfunction in cancer. Nat Rev Cancer [Internet]. 2019 Jun 3;19(6):326–38. Available from: http://www.nature.com/articles/s41568-019-0143-7

110. Li G-Q, Li H, Zhang H-F. Mad2 and p53 expression profiles in colorectal cancer and its clinical significance. World J Gastroenterol [Internet]. 2003 Sep;9(9):1972–5. Available from: http://www.wjgnet.com/1007-9327/full/v9/i9/1972.htm

111. Chun ACS, Jin D-Y. Transcriptional Regulation of Mitotic Checkpoint Gene MAD1 by p53. J Biol Chem [Internet]. 2003 Sep;278(39):37439–50. Available from: https://linkinghub.elsevier.com/retrieve/pii/S0021925820833043

112. Wan J, Block S, Scribano CM, Thiry R, Esbona K, Audhya A, et al. Mad1 destabilizes p53 by preventing PML from sequestering MDM2. Nat Commun [Internet]. 2019 Dec 4;10(1):1540. Available from: http://www.nature.com/articles/s41467-019-09471-9

113. Choi E, Zhang X, Xing C, Yu H. Mitotic Checkpoint Regulators Control Insulin Signaling and Metabolic Homeostasis. Cell [Internet]. 2016 Jul;166(3):567–81. Available from: https://linkinghub.elsevier.com/retrieve/pii/S0092867416307218

114. Cayrol C, Cougoule C, Wright M. The β2-adaptin clathrin adaptor interacts with the mitotic checkpoint kinase BubR1. Biochem Biophys Res Commun [Internet]. 2002 Nov;298(5):720–30. Available from: https://linkinghub.elsevier.com/retrieve/pii/S0006291X02025226

115. O'Neill TJ, Zhu Y, Gustafson TA. Interaction of MAD2 with the carboxyl terminus of the insulin receptor but not with the IGFIR. Evidence for release from the insulin receptor after activation. J Biol Chem [Internet]. 1997 Apr 11;272(15):10035–40. Available from: http://www.jbc.org/lookup/doi/10.1074/jbc.272.15.10035

116. Wood KW, Cornwell WD, Jackson JR. Past and future of the mitotic spindle as an oncology target. Curr Opin Pharmacol. 2001;1(4):370–7.

117. Rowinsky EK, Donehower RC. Paclitaxel (Taxol). Wood AJJ, editor. N Engl J Med [Internet]. 1995 Apr 13;332(15):1004–14. Available from: http://www.nejm.org/doi/full/10.1056/nejm199504133321507

118. Ma HT, Chan YY, Chen X, On KF, Poon RYC. Depletion of p31 comet Protein Promotes Sensitivity to Antimitotic Drugs. J Biol Chem [Internet]. 2012 Jun 15;287(25):21561–9. Available from:

http://www.jbc.org/lookup/doi/10.1074/jbc.M112.364356

119. Brito DA, Rieder CL. Mitotic Checkpoint Slippage in Humans Occurs via Cyclin B Destruction in the Presence of an Active Checkpoint. Curr Biol [Internet]. 2006 Jun;16(12):1194–200. Available from: https://linkinghub.elsevier.com/retrieve/pii/S0960982206015405

120. Topham CH, Taylor SS. Mitosis and apoptosis: How is the balance set? Curr Opin Cell Biol [Internet]. 2013;25(6):780–5. Available from: http://dx.doi.org/10.1016/j.ceb.2013.07.003

121. Huang Y, Yao Y, Xu H-Z, Wang Z-G, Lu L, Dai W. Defects in chromosome congression and mitotic progression in KIF18A-deficient cells are partly mediated through impaired functions of CENP-E. Cell Cycle [Internet]. 2009 Aug 15;8(16):2643–9. Available from: http://www.tandfonline.com/doi/abs/10.4161/cc.8.16.9366

122. Bekier ME, Fischbach R, Lee J, Taylor WR. Length of mitotic arrest induced by microtubule-stabilizing drugs determines cell death after mitotic exit. Mol Cancer Ther [Internet]. 2009 Jun;8(6):1646–54. Available from: http://mct.aacrjournals.org/lookup/doi/10.1158/1535-7163.MCT-08-1084

123. Mansoori B, Mohammadi A, Davudian S, Shirjang S, Baradaran B. The Different Mechanisms of Cancer Drug Resistance: A Brief Review. Adv Pharm Bull [Internet]. 2017 Sep 25;7(3):339–48. Available from: http://apb.tbzmed.ac.ir/Abstract/APB_386_20170226104729

124. Rebucci M, Michiels C. Molecular aspects of cancer cell resistance to chemotherapy. Biochem Pharmacol [Internet]. 2013 May;85(9):1219–26. Available from: https://linkinghub.elsevier.com/retrieve/pii/S0006295213001214

125. Dumontet C, Jordan MA. Microtubule-binding agents: a dynamic field of cancer therapeutics. Nat Rev Drug Discov [Internet]. 2010 Oct 1;9(10):790–803. Available from: http://www.nature.com/articles/nrd3253

126. Jordan MA, Wilson L. Microtubules as a target for anticancer drugs. Nat Rev Cancer [Internet]. 2004 Apr;4(4):253–65. Available from: http://www.nature.com/articles/nrc1317

127. Keen N, Taylor S. Mitotic drivers—inhibitors of the Aurora B Kinase. Cancer Metastasis Rev [Internet]. 2009 Jun 3;28(1–2):185–95. Available from: http://link.springer.com/10.1007/s10555-009-9184-9

128. Bennett A, Sloss O, Topham C, Nelson L, Tighe A, Taylor SS. Inhibition of Bcl-xL sensitizes cells to mitotic blockers, but not mitotic drivers. Open Biol. 2016;6(8).

129. Sawin KE, LeGuellec K, Philippe M, Mitchison TJ. Mitotic spindle organization by a plus-end-

directed microtubule motor. Nature [Internet]. 1992 Oct;359(6395):540–3. Available from: http://www.nature.com/articles/359540a0

130. Zitouni S, Nabais C, Jana SC, Guerrero A, Bettencourt-Dias M. Polo-like kinases: structural variations lead to multiple functions. Nat Rev Mol Cell Biol [Internet]. 2014 Jul 23;15(7):433–52. Available from: http://www.nature.com/articles/nrm3819

131. Weaver BAA, Silk AD, Montagna C, Verdier-Pinard P, Cleveland DW. Aneuploidy Acts Both Oncogenically and as a Tumor Suppressor. Cancer Cell [Internet]. 2007 Jan;11(1):25–36. Available from: https://linkinghub.elsevier.com/retrieve/pii/S1535610806003680

132. Chung V, Heath EI, Schelman WR, Johnson BM, Kirby LC, Lynch KM, et al. First-time-in-human study of GSK923295, a novel antimitotic inhibitor of centromere-associated protein E (CENP-E), in patients with refractory cancer. Cancer Chemother Pharmacol [Internet]. 2012 Mar 22;69(3):733–41. Available from: http://link.springer.com/10.1007/s00280-011-1756-z

133. Yim H. Current clinical trials with polo-like kinase 1 inhibitors in solid tumors. Anticancer Drugs [Internet]. 2013 Nov;24(10):999–1006. Available from: https://journals.lww.com/00001813-201311000-00002

134. Melichar B, Adenis A, Lockhart AC, Bennouna J, Dees EC, Kayaleh O, et al. Safety and activity of alisertib, an investigational aurora kinase A inhibitor, in patients with breast cancer, small-cell lung cancer, non-small-cell lung cancer, head and neck squamous-cell carcinoma, and gastro-oesophageal adenocarcinoma: a five-arm ph. Lancet Oncol [Internet]. 2015 Apr;16(4):395–405. Available from: https://linkinghub.elsevier.com/retrieve/pii/S1470204515700513

135. Wood KW, Lad L, Luo L, Qian X, Knight SD, Nevins N, et al. Antitumor activity of an allosteric inhibitor of centromere-associated protein-E. Proc Natl Acad Sci [Internet]. 2010 Mar 30;107(13):5839–44. Available from: http://www.pnas.org/cgi/doi/10.1073/pnas.0915068107

136. Marcus AI, Peters U, Thomas SL, Garrett S, Zelnak A, Kapoor TM, et al. Mitotic Kinesin Inhibitors Induce Mitotic Arrest and Cell Death in Taxol-resistant and -sensitive Cancer Cells. J Biol Chem [Internet]. 2005 Mar;280(12):11569–77. Available from: https://linkinghub.elsevier.com/retrieve/pii/S002192582080862X

137. Brier S, Lemaire D, DeBonis S, Forest E, Kozielski F. Molecular Dissection of the Inhibitor Binding Pocket of Mitotic Kinesin Eg5 Reveals Mutants that Confer Resistance to Antimitotic Agents. J Mol Biol [Internet]. 2006 Jul;360(2):360–76. Available from: https://linkinghub.elsevier.com/retrieve/pii/S0022283606005560

138. Tcherniuk S, van Lis R, Kozielski F, Skoufias DA. Mutations in the human kinesin Eg5 that confer resistance to monastrol and S-trityl-l-cysteine in tumor derived cell lines. Biochem Pharmacol [Internet]. 2010 Mar;79(6):864–72. Available from: https://linkinghub.elsevier.com/retrieve/pii/S0006295209009654

139. Bu Y, Yang Z, Li Q, Song F. Silencing of Polo-Like Kinase (Plk) 1 via siRNA Causes Inhibition of Growth and Induction of Apoptosis in Human Esophageal Cancer Cells. Oncology [Internet]. 2008;74(3–4):198–206. Available from: https://www.karger.com/Article/FullText/151367

140. Spänkuch B, Heim S, Kurunci-Csacsko E, Lindenau C, Yuan J, Kaufmann M, et al. Down-regulation of Polo-like Kinase 1 Elevates Drug Sensitivity of Breast Cancer Cells In vitro and In vivo. Cancer Res [Internet]. 2006 Jun 1;66(11):5836–46. Available from: http://cancerres.aacrjournals.org/lookup/doi/10.1158/0008-5472.CAN-06-0343

141. Blagden SP, Molife LR, Seebaran A, Payne M, Reid AHM, Protheroe AS, et al. A phase I trial of ispinesib, a kinesin spindle protein inhibitor, with docetaxel in patients with advanced solid tumours. Br J Cancer [Internet]. 2008 Mar 4;98(5):894–9. Available from: http://www.nature.com/articles/6604264

142. El-Nassan HB. Advances in the discovery of kinesin spindle protein (Eg5) inhibitors as antitumor agents. Eur J Med Chem [Internet]. 2013 Apr;62:614–31. Available from: https://linkinghub.elsevier.com/retrieve/pii/S0223523413000597

143. Visconti R, Della Monica R, Palazzo L, D'Alessio F, Raia M, Improta S, et al. The Fcp1-Wee1-Cdk1 axis affects spindle assembly checkpoint robustness and sensitivity to antimicrotubule cancer drugs. Cell Death Differ [Internet]. 2015 Sep 6;22(9):1551–60. Available from: http://www.nature.com/articles/cdd201513

144. Silva PMA, Ribeiro N, Lima RT, Andrade C, Diogo V, Teixeira J, et al. Suppression of spindly delays mitotic exit and exacerbates cell death response of cancer cells treated with low doses of paclitaxel. Cancer Lett. 2017;394(February):33–42.

145. D'Angiolella V, Mari C, Nocera D, Rametti L, Grieco D. The spindle checkpoint requires cyclin-dependent kinase activity. Genes Dev [Internet]. 2003 Oct 15;17(20):2520–5. Available from: http://www.genesdev.org/cgi/doi/10.1101/gad.267603

146. Visconti R, Palazzo L, Della Monica R, Grieco D. Fcp1-dependent dephosphorylation is required for M-phase-promoting factor inactivation at mitosis exit. Nat Commun [Internet]. 2012 Jan 12;3(1):894. Available from: http://www.nature.com/articles/ncomms1886

147. Wang K, Sturt-Gillespie B, Hittle JC, Macdonald D, Chan GK, Yen TJ, et al. Thyroid hormone receptor interacting protein 13 (TRIP13) AAA-ATPase is a novel mitotic checkpoint-silencing protein. J Biol Chem. 2014;289(34):23928–37.

148. Ma HT, Poon RYC. TRIP13 Functions in the Establishment of the Spindle Assembly Checkpoint by Replenishing O-MAD2. Cell Rep [Internet]. 2018 Feb;22(6):1439–50. Available from: https://doi.org/10.1016/j.celrep.2018.01.027

149. Janssen A, Kops GJPL, Medema RH. Elevating the frequency of chromosome mis-segregation as a strategy to kill tumor cells. Proc Natl Acad Sci [Internet]. 2009 Nov 10;106(45):19108–13. Available from: http://www.pnas.org/cgi/doi/10.1073/pnas.0904343106

150. Kops GJPL, Weaver BAA, Cleveland DW. On the road to cancer: aneuploidy and the mitotic checkpoint. Nat Rev Cancer [Internet]. 2005 Oct;5(10):773–85. Available from: http://www.nature.com/articles/nrc1714

151. Lengauer C, Kinzler KW, Vogelstein B. Genetic instabilities in human cancers. Nature [Internet]. 1998 Dec 17;396(6712):643–9. Available from: http://www.nature.com/articles/25292

152. Dominguez-Brauer C, Thu KL, Mason JM, Blaser H, Bray MR, Mak TW. Targeting Mitosis in Cancer: Emerging Strategies. Mol Cell [Internet]. 2015 Nov;60(4):524–36. Available from: http://dx.doi.org/10.1016/j.molcel.2015.11.006

153. Marques S, Fonseca J, Silva P, Bousbaa H. Targeting the Spindle Assembly Checkpoint for Breast Cancer Treatment. Curr Cancer Drug Targets [Internet]. 2015 May 18;15(4):272–81. Available from: http://www.eurekaselect.com/openurl/content.php?genre=article&issn=1568-0096&volume=15&issue=4&spage=272

154. Teixeira JH, Silva PM, Reis RM, Moura IM, Marques S, Fonseca J, et al. An Overview of the Spindle Assembly Checkpoint Status in Oral Cancer. Biomed Res Int [Internet]. 2014;2014:1–8. Available from: http://www.hindawi.com/journals/bmri/2014/145289/

155. Diogo V, Teixeira J, Silva PMA, Bousbaa H. Spindle Assembly Checkpoint as a Potential Target in Colorectal Cancer: Current Status and Future Perspectives. Clin Colorectal Cancer [Internet]. 2017 Mar;16(1):1–8. Available from: http://dx.doi.org/10.1016/j.clcc.2016.06.006

156. Kollareddy M, Zheleva D, Dzubak P, Brahmkshatriya PS, Lepsik M, Hajduch M. Aurora kinase inhibitors: Progress towards the clinic. Invest New Drugs [Internet]. 2012 Dec 18;30(6):2411–32. Available from: http://link.springer.com/10.1007/s10637-012-9798-6

157. Colombo R, Caldarelli M, Mennecozzi M, Giorgini ML, Sola F, Cappella P, et al. Targeting the

Mitotic Checkpoint for Cancer Therapy with NMS-P715, an Inhibitor of MPS1 Kinase. Cancer Res [Internet]. 2010 Dec 15;70(24):10255–64. Available from: http://cancerres.aacrjournals.org/cgi/doi/10.1158/0008-5472.CAN-10-2101

158. Jemaà M, Galluzzi L, Kepp O, Senovilla L, Brands M, Boemer U, et al. Characterization of novel MPS1 inhibitors with preclinical anticancer activity. Cell Death Differ [Internet]. 2013 Nov;20(11):1532–45. Available from: http://www.ncbi.nlm.nih.gov/pubmed/23933817

159. Liu Y, Lang Y, Patel NK, Ng G, Laufer R, Li S-W, et al. The Discovery of Orally Bioavailable Tyrosine Threonine Kinase (TTK) Inhibitors: 3-(4-(heterocyclyl)phenyl)-1 H -indazole-5-carboxamides as Anticancer Agents. J Med Chem [Internet]. 2015 Apr 23;58(8):3366–92. Available from: https://pubs.acs.org/doi/10.1021/jm501740a

160. Huszar D, Theoclitou M-E, Skolnik J, Herbst R. Kinesin motor proteins as targets for cancer therapy. Cancer Metastasis Rev [Internet]. 2009 Jun 21;28(1–2):197–208. Available from: http://link.springer.com/10.1007/s10555-009-9185-8

161. Löwenberg B, Muus P, Ossenkoppele G, Rousselot P, Cahn J-Y, Ifrah N, et al. Phase 1/2 study to assess the safety, efficacy, and pharmacokinetics of barasertib (AZD1152) in patients with advanced acute myeloid leukemia. Blood [Internet]. 2011 Dec 1;118(23):6030–6. Available from: https://ashpublications.org/blood/article/118/23/6030/29094/Phase-12-study-to-assess-the-safety-efficacy-and

162. Komlodi-Pasztor E, Sackett D, Wilkerson J, Fojo T. Mitosis is not a key target of microtubule agents in patient tumors. Nat Rev Clin Oncol [Internet]. 2011 Apr 1;8(4):244–50. Available from: http://www.nature.com/articles/nrclinonc.2010.228

163. Tang A, Gao K, Chu L, Zhang R, Yang J, Zheng J. Aurora kinases: novel therapy targets in cancers. Oncotarget [Internet]. 2017 Apr 4;8(14):23937–54. Available from: https://www.oncotarget.com/lookup/doi/10.18632/oncotarget.14893

164. Tao Y, Zhang P, Frascogna V, Lecluse Y, Auperin A, Bourhis J, et al. Enhancement of radiation response by inhibition of Aurora-A kinase using siRNA or a selective Aurora kinase inhibitor PHA680632 in p53-deficient cancer cells. Br J Cancer [Internet]. 2007 Dec 20;97(12):1664–72. Available from: http://www.nature.com/articles/6604083

165. Ma Y, Cao H, Lou S, Shao X, Lv W, Qi X, et al. Sequential treatment with aurora B inhibitors enhances cisplatin-mediated apoptosis via c-Myc. J Mol Med [Internet]. 2015 Apr 21;93(4):427–38. Available from: http://link.springer.com/10.1007/s00109-014-1228-0

166. Baron AP, von Schubert C, Cubizolles F, Siemeister G, Hitchcock M, Mengel A, et al. Probing the catalytic functions of Bub1 kinase using the small molecule inhibitors BAY-320 and BAY-524. Elife [Internet]. 2016 Feb 17;5. Available from: https://elifesciences.org/articles/12187

167. Choi E, Yu H. Phosphorylation propels p31comet for mitotic exit. Cell Cycle. 2015;14(13):1997–8.

168. Hagan RS, Manak MS, Buch HK, Meier MG, Meraldi P, Shah J V., et al. P31 Comet Acts To Ensure Timely Spindle Checkpoint Silencing Subsequent To Kinetochore Attachment. Mol Biol Cell. 2011;22(22):4236–46.

169. Habu T, Matsumoto T. p31comet inactivates the chemically induced Mad2-dependent spindle assembly checkpoint and leads to resistance to anti-mitotic drugs. Springerplus. 2013;2(1):1–15.

170. Wu D, Wang L, Yang Y, Huang J, Hu Y, Shu Y, et al. MAD2-p31comet axis deficiency reduces cell proliferation, migration and sensitivity of microtubule-interfering agents in glioma. Biochem Biophys Res Commun [Internet]. 2018 Mar;498(1):157–63. Available from: https://linkinghub.elsevier.com/retrieve/pii/S0006291X18302341

171. Lauzé E, Stoelcker B, Luca FC, Weiss E, Schutz AR, Winey M. Yeast spindle pole body duplication gene MPS1 encodes an essential dual specificity protein kinase. EMBO J [Internet]. 1995 Apr;14(8):1655–63. Available from: http://doi.wiley.com/10.1002/j.1460-2075.1995.tb07154.x

172. Liu X, Winey M. The MPS1 Family of Protein Kinases. Annu Rev Biochem [Internet]. 2012 Jul 7;81(1):561–85. Available from: http://www.annualreviews.org/doi/10.1146/annurev-biochem-061611-090435

173. Tambe M, Pruikkonen S, Mäki-Jouppila J, Chen P, Elgaaen BV, Straume AH, et al. Novel Mad2-targeting miR-493-3p controls mitotic fidelity and cancer cells' sensitivity to paclitaxel. Oncotarget [Internet]. 2016 Mar 15;7(11):12267–85. Available from: https://www.oncotarget.com/lookup/doi/10.18632/oncotarget.7860

174. Furlong F, Fitzpatrick P, O'Toole S, Phelan S, McGrogan B, Maguire A, et al. Low MAD2 expression levels associate with reduced progression-free survival in patients with high-grade serous epithelial ovarian cancer. J Pathol [Internet]. 2012 Apr;226(5):746–55. Available from: http://doi.wiley.com/10.1002/path.3035

175. Gascoigne KE, Taylor SS. Cancer Cells Display Profound Intra- and Interline Variation following Prolonged Exposure to Antimitotic Drugs. Cancer Cell. 2008;14(2):111–22.

176. Antonio C, Ferby I, Wilhelm H, Jones M, Karsenti E, Nebreda AR, et al. Xkid, a Chromokinesin Required for Chromosome Alignment on the Metaphase Plate. Cell [Internet]. 2000

Aug;102(4):425–35. Available from:
https://linkinghub.elsevier.com/retrieve/pii/S0092867400000489

177. Sackton KL, Dimova N, Zeng X, Tian W, Zhang M, Sackton TB, et al. Synergistic blockade of mitotic exit by two chemical inhibitors of the APC/C. Nature [Internet]. 2014 Oct 30;514(7524):646–9. Available from: http://www.ncbi.nlm.nih.gov/pubmed/25156254

178. Zeng X, Sigoillot F, Gaur S, Choi S, Pfaff KL, Oh D-C, et al. Pharmacologic Inhibition of the Anaphase-Promoting Complex Induces A Spindle Checkpoint-Dependent Mitotic Arrest in the Absence of Spindle Damage. Cancer Cell [Internet]. 2010 Oct 19;18(4):382–95. Available from: http://www.ncbi.nlm.nih.gov/pubmed/20951947

179. Wang L, Zhang J, Wan L, Zhou X, Wang Z, Wei W. Targeting Cdc20 as a novel cancer therapeutic strategy. Pharmacol Ther [Internet]. 2015 Jul;151:141–51. Available from: https://linkinghub.elsevier.com/retrieve/pii/S0163725815000777

180. Lub S, Maes A, Maes K, De Veirman K, De Bruyne E, Menu E, et al. Inhibiting the anaphase promoting complex/cyclosome induces a metaphase arrest and cell death in multiple myeloma cells. Oncotarget [Internet]. 2016 Jan 26;7(4):4062–76. Available from: https://www.oncotarget.com/lookup/doi/10.18632/oncotarget.6768

181. Dou Q, Zonder J. Overview of Proteasome Inhibitor-Based Anti-cancer Therapies: Perspective on Bortezomib and Second Generation Proteasome Inhibitors versus Future Generation Inhibitors of Ubiquitin-Proteasome System. Curr Cancer Drug Targets [Internet]. 2014 Aug 31;14(6):517–36. Available from: http://www.eurekaselect.com/openurl/content.php?genre=article&issn=1568-0096&volume=14&issue=6&spage=517

182. Adams J. The proteasome: a suitable antineoplastic target. Nat Rev Cancer [Internet]. 2004 May;4(5):349–60. Available from: http://www.nature.com/articles/nrc1361

183. Skaar JR, Pagan JK, Pagano M. SCF ubiquitin ligase-targeted therapies. Nat Rev Drug Discov [Internet]. 2014 Dec 14;13(12):889–903. Available from: http://www.nature.com/articles/nrd4432

184. Delbridge ARD, Strasser A. The BCL-2 protein family, BH3-mimetics and cancer therapy. Cell Death Differ [Internet]. 2015;22(7):1071–80. Available from: http://dx.doi.org/10.1038/cdd.2015.50

185. Opferman JT, Kothari A. Anti-apoptotic BCL-2 family members in development. Cell Death Differ [Internet]. 2018 Jan 3;25(1):37–45. Available from: http://www.nature.com/articles/cdd2017170

186. Billard C. BH3 Mimetics: Status of the Field and New Developments. Mol Cancer Ther [Internet]. 2013 Sep;12(9):1691–700. Available from: http://mct.aacrjournals.org/lookup/doi/10.1158/1535-7163.MCT-13-0058

187. Wong RS. Apoptosis in cancer: from pathogenesis to treatment. J Exp Clin Cancer Res [Internet]. 2011 Dec 26;30(1):87. Available from: https://jeccr.biomedcentral.com/articles/10.1186/1756-9966-30-87

188. Barbosa J, Nascimento AV, Faria J, Silva P, Bousbaa H. The spindle assembly checkpoint: perspectives in tumorigenesis and cancer therapy. Front Biol (Beijing) [Internet]. 2011 Apr 5;6(2):147–55. Available from: http://link.springer.com/10.1007/s11515-011-1122-x

189. Oltersdorf T, Elmore SW, Shoemaker AR, Armstrong RC, Augeri DJ, Belli BA, et al. An inhibitor of Bcl-2 family proteins induces regression of solid tumours. Nature [Internet]. 2005 Jun 15;435(7042):677–81. Available from: http://www.nature.com/articles/nature03579

190. Leverson JD, Zhang H, Chen J, Tahir SK, Phillips DC, Xue J, et al. Potent and selective small-molecule MCL-1 inhibitors demonstrate on-target cancer cell killing activity as single agents and in combination with ABT-263 (navitoclax). Cell Death Dis [Internet]. 2015 Jan 15;6(1):e1590–e1590. Available from: http://www.nature.com/articles/cddis2014561

191. Shi J, Zhou Y, Huang H-C, Mitchison TJ. Navitoclax (ABT-263) Accelerates Apoptosis during Drug-Induced Mitotic Arrest by Antagonizing Bcl-xL. Cancer Res [Internet]. 2011 Jul 1;71(13):4518–26. Available from: http://cancerres.aacrjournals.org/cgi/doi/10.1158/0008-5472.CAN-10-4336

192. Tan N, Malek M, Zha J, Yue P, Kassees R, Berry L, et al. Navitoclax enhances the efficacy of taxanes in non-small cell lung cancer models. Clin Cancer Res. 2011;17(6):1394–404.

193. Bah N, Maillet L, Ryan J, Dubreil S, Gautier F, Letai A, et al. Bcl-xL controls a switch between cell death modes during mitotic arrest. Cell Death Dis [Internet]. 2014 Jun 12;5(6):e1291–e1291. Available from: http://www.nature.com/articles/cddis2014251

194. Wong M, Tan N, Zha J, Peale F V., Yue P, Fairbrother WJ, et al. Navitoclax (ABT-263) Reduces Bcl-x L –Mediated Chemoresistance in Ovarian Cancer Models. Mol Cancer Ther [Internet]. 2012 Apr;11(4):1026–35. Available from: http://mct.aacrjournals.org/lookup/doi/10.1158/1535-7163.MCT-11-0693

195. Ghosh S. Cisplatin: The first metal based anticancer drug. Bioorg Chem [Internet]. 2019 Jul;88(October 2018):102925. Available from: https://doi.org/10.1016/j.bioorg.2019.102925

196. Cocetta V, Ragazzi E, Montopoli M. Mitochondrial Involvement in Cisplatin Resistance. Int J Mol Sci

[Internet]. 2019 Jul 10;20(14):3384. Available from: https://www.mdpi.com/1422-0067/20/14/3384

197. Belur Nagaraj A, Kovalenko O, Avelar R, Joseph P, Brown A, Surti A, et al. Mitotic Exit Dysfunction through the Deregulation of APC/C Characterizes Cisplatin-Resistant State in Epithelial Ovarian Cancer. Clin Cancer Res [Internet]. 2018 Sep 15;24(18):4588–601. Available from: http://clincancerres.aacrjournals.org/lookup/doi/10.1158/1078-0432.CCR-17-2885

198. Dasari S, Bernard Tchounwou P. Cisplatin in cancer therapy: Molecular mechanisms of action. Eur J Pharmacol [Internet]. 2014 Oct;740:364–78. Available from: https://linkinghub.elsevier.com/retrieve/pii/S0014299914005627

199. Silva PMA, Delgado ML, Ribeiro N, Florindo C, Tavares ÁA, Ribeiro D, et al. Spindly and Bub3 expression in oral cancer: Prognostic and therapeutic implications. Oral Dis [Internet]. 2019 Jul 4;25(5):1291–301. Available from: https://onlinelibrary.wiley.com/doi/10.1111/odi.13089

200. Patel RP, Kuhn S, Yin D, Hotz JM, Maher FA, Robey RW, et al. Cross-resistance of cisplatin selected cells to anti-microtubule agents: Role of general survival mechanisms. Transl Oncol [Internet]. 2021 Jan;14(1):100917. Available from: https://pubmed.ncbi.nlm.nih.gov/33129114/

201. Iwasaki I, Sugiyama H, Kanazawa S, Hemmi H. Establishment of cisplatin-resistant variants of human neuroblastoma cell lines, TGW and GOTO, and their drug cross-resistance profiles. Cancer Chemother Pharmacol [Internet]. 2002 Jun 1;49(6):438–44. Available from: http://link.springer.com/10.1007/s00280-002-0452-4

202. Stordal B, Hamon M, McEneaney V, Roche S, Gillet J-P, O'Leary JJ, et al. Resistance to Paclitaxel in a Cisplatin-Resistant Ovarian Cancer Cell Line Is Mediated by P-Glycoprotein. Bishop AJR, editor. PLoS One [Internet]. 2012 Jul 11;7(7):e40717. Available from: https://dx.plos.org/10.1371/journal.pone.0040717

203. Januchowski R, Wojtowicz K, Sujka-Kordowska P, Andrzejewska M, Zabel M. MDR Gene Expression Analysis of Six Drug-Resistant Ovarian Cancer Cell Lines. Biomed Res Int [Internet]. 2013;2013:1–10. Available from: http://www.hindawi.com/journals/bmri/2013/241763/

204. Novais P, Silva PMA, Amorim I, Bousbaa H. Second-generation antimitotics in cancer clinical trials. Pharmaceutics. 2021;13(7).

205. Westhorpe FG, Tighe A, Lara-Gonzalez P, Taylor SS. p31comet-mediated extraction of Mad2 from the MCC promotes efficient mitotic exit. J Cell Sci [Internet]. 2011 Nov 15;124(22):3905–16. Available from: http://jcs.biologists.org/cgi/doi/10.1242/jcs.093286

206. Henriques AC, Silva PMA, Sarmento B, Bousbaa H. The Mad2-Binding Protein p31comet as a Potential Target for Human Cancer Therapy. Curr Cancer Drug Targets [Internet]. 2021 Jul 5;21(5):401–15. Available from: https://www.eurekaselect.com/190869/article

207. Gene [MAD2L1BP (MAD2L1 binding protein)] [Internet]. Bethesda (MD): National Library of Medicine (US), National Center for Biotechnology Information. [cited 2020 May 25]. Available from: https://www.ncbi.nlm.nih.gov/gene/9587

208. Habu T, Kim SH, Weinstein J, Matsumoto T. Identification of a MAD2-binding protein, CMT2, and its role in mitosis. EMBO J. 2002;21(23):6419–28.

209. Nucleotide [MAD2L1-binding protein isoform 1]. Accession No. NM_001003690.1, Homo sapiens MAD2L1 binding protein (MAD2L1BP), transcript variant 1, mRNA [Internet]. Bethesda (MD): National Library of Medicine (US), National Center for Biotechnology Information. [cited 2020 May 25]. Available from: https://www.ncbi.nlm.nih.gov/nuccore/NM_001003690.1

210. Nucleotide [MAD2L1-binding protein isoform 2]. Accession No. NM_014628.3, Homo sapiens MAD2L1 binding protein (MAD2L1BP), transcript variant 2, mRNA [Internet]. Bethesda (MD): National Library of Medicine (US), National Center for Biotechnology Information. [cited 2020 May 20]. Available from: https://www.ncbi.nlm.nih.gov/nuccore/NM_014628.3

211. Rosenberg SC, Corbett KD. The multifaceted roles of the HORMA domain in cellular signaling. J Cell Biol [Internet]. 2015 Nov 23;211(4):745–55. Available from: https://rupress.org/jcb/article/211/4/745/38616/The-multifaceted-roles-of-the-HORMA-domain-in

212. Hegemann B, Hutchins JRA, Hudecz O, Novatchkova M, Rameseder J, Sykora MM, et al. Systematic Phosphorylation Analysis of Human Mitotic Protein Complexes. Sci Signal [Internet]. 2011 Nov 8;4(198):rs12–rs12. Available from: https://www.ncbi.nlm.nih.gov/pmc/articles/PMC3624763/pdf/nihms412728.pdf

213. Eytan E, Wang K, Miniowitz-Shemtov S, Sitry-Shevah D, Kaisari S, Yen TJ, et al. Disassembly of mitotic checkpoint complexes by the joint action of the AAA-ATPase TRIP13 and p31comet. Proc Natl Acad Sci U S A. 2014;111(33):12019–24.

214. Date DA, Burrows AC, Summers MK. Phosphorylation regulates the p31comet-mitotic arrest-deficient 2 (Mad2) interaction to promote spindle assembly checkpoint (SAC) activity. J Biol Chem. 2014;289(16):11367–73.

215. Kaisari S, Shomer P, Ziv T, Sitry-Shevah D, Miniowitz-Shemtov S, Teichner A, et al. Role of Polo-

like kinase 1 in the regulation of the action of p31comet in the disassembly of mitotic checkpoint complexes. Proc Natl Acad Sci U S A. 2019;116(24):11725–30.

216. Mapelli M, Filipp F V., Rancati G, Massimiliano L, Nezi L, Stier G, et al. Determinants of conformational dimerization of Mad2 and its inhibition by p31comet. EMBO J. 2006;25(6):1273–84.

217. Teichner A, Eytan E, Sitry-Shevah D, Miniowitz-Shemtov S, Dumin E, Gromis J, et al. p31comet promotes disassembly of the mitotic checkpoint complex in an ATP-dependent process. Proc Natl Acad Sci U S A. 2011;108(8):3187–92.

218. Xia G, Luo X, Habu T, Rizo J, Matsumoto T, Yu H. Conformation-specific binding of p31comet antagonizes the function of Mad2 in the spindle checkpoint. EMBO J. 2004;23(15):3133–43.

219. Balboni M, Yang C, Komaki S, Brun J, Schnittger A. COMET Functions as a PCH2 Cofactor in Regulating the HORMA Domain Protein ASY1. Curr Biol [Internet]. 2020 Nov;30(21):4113-4127.e6. Available from: https://linkinghub.elsevier.com/retrieve/pii/S0960982220311489

220. Ji J, Tang D, Shen Y, Xue Z, Wang H, Shi W, et al. P31comet, a member of the synaptonemal complex, participates in meiotic DSB formation in rice. Proc Natl Acad Sci U S A. 2016;113(38):10577–82.

221. Giacopazzi S, Vong D, Devigne A, Bhalla N. PCH-2 collaborates with CMT-1 to proofread meiotic homolog interactions. Libuda DE, editor. PLOS Genet [Internet]. 2020 Jul 30;16(7):e1008904. Available from: https://dx.plos.org/10.1371/journal.pgen.1008904

222. Sarangi P, Clairmont CS, Galli LD, Moreau LA, D'Andrea AD. p31 comet promotes homologous recombination by inactivating REV7 through the TRIP13 ATPase. Proc Natl Acad Sci [Internet]. 2020 Oct 27;117(43):26795–803. Available from: http://www.pnas.org/lookup/doi/10.1073/pnas.2008830117

223. De Antoni A, Pearson CG, Cimini D, Canman JC, Sala V, Nezi L, et al. The Mad1/Mad2 Complex as a Template for Mad2 Activation in the Spindle Assembly Checkpoint. Curr Biol [Internet]. 2005 Feb;15(3):214–25. Available from: https://www.sciencedirect.com/science/article/pii/S0960982205000734

224. Sudakin V, Chan GKT, Yen TJ. Checkpoint inhibition of the APC/C in HeLa cells is mediated by a complex of BUBR1, BUB3, CDC20, and MAD2. J Cell Biol [Internet]. 2001 Sep 3;154(5):925–36. Available from: http://www.jcb.org/lookup/doi/10.1083/jcb.200102093

225. Vink M, Simonetta M, Transidico P, Ferrari K, Mapelli M, De Antoni A, et al. In Vitro FRAP Identifies

the Minimal Requirements for Mad2 Kinetochore Dynamics. Curr Biol. 2006;16(8):755–66.

226. Lok TM, Wang Y, Xu WK, Xie S, Ma HT, Poon RYC. Mitotic slippage is determined by p31comet and the weakening of the spindle-assembly checkpoint. Oncogene [Internet]. 2020 Mar 6;39(13):2819–34. Available from: http://dx.doi.org/10.1038/s41388-020-1187-6

227. Ma HT, Poon RYC. How protein kinases co-ordinate mitosis in animal cells. Biochem J [Internet]. 2011 Apr 1;435(1):17–31. Available from: https://portlandpress.com/biochemj/article/435/1/17/88356/How-protein-kinases-coordinate-mitosis-in-animal

228. Tipton AR, Wang K, Oladimeji P, Sufi S, Gu Z, Liu ST. Identification of novel mitosis regulators through data mining with human centromere/kinetochore proteins as group queries. BMC Cell Biol [Internet]. 2012;13(1):1. Available from: ???

229. Miniowitz-Shemtov S, Eytan E, Kaisari S, Sitry-Shevah D, Hershko A. Mode of interaction of TRIP13 AAA-ATPase with the Mad2-binding protein p31comet and with mitotic checkpoint complexes. Proc Natl Acad Sci [Internet]. 2015 Sep 15;112(37):11536–40. Available from: http://www.pnas.org/lookup/doi/10.1073/pnas.1515358112

230. Ma HT, Poon RYC. TRIP13 Regulates Both the Activation and Inactivation of the Spindle-Assembly Checkpoint. Cell Rep [Internet]. 2016;14(5):1086–99. Available from: http://dx.doi.org/10.1016/j.celrep.2016.01.001

231. Ye Q, Kim DH, Dereli I, Rosenberg SC, Hagemann G, Herzog F, et al. The AAA + ATP ase TRIP 13 remodels HORMA domains through N-terminal engagement and unfolding . EMBO J. 2017;36(16):2419–34.

232. Alfieri C, Chang L, Barford D. Mechanism for remodelling of the cell cycle checkpoint protein MAD2 by the ATPase TRIP13. Nature. 2018;559(7713):274–8.

233. Brulotte ML, Jeong B-C, Li F, Li B, Yu EB, Wu Q, et al. Mechanistic insight into TRIP13-catalyzed Mad2 structural transition and spindle checkpoint silencing. Nat Commun [Internet]. 2017 Dec 5;8(1):1956. Available from: http://dx.doi.org/10.1038/s41467-017-02012-2

234. Marks DH, Thomas R, Chin Y, Shah R, Khoo C, Benezra R. Mad2 Overexpression Uncovers a Critical Role for TRIP13 in Mitotic Exit. Cell Rep [Internet]. 2017 May;19(9):1832–45. Available from: http://dx.doi.org/10.1016/j.celrep.2017.05.021

235. Nelson CR, Hwang T, Chen PH, Bhalla N. TRIP13PCH-2 promotes Mad2 localization to unattached kinetochores in the spindle checkpoint response. J Cell Biol. 2015;211(3):503–16.

236. Défachelles L, Russo AE, Nelson CR, Bhalla N. PCH-2 TRIP13 regulates spindle checkpoint strength. Skop AR, editor. Mol Biol Cell [Internet]. 2020 Jul 22;mbc.E20-05-0310. Available from: https://www.molbiolcell.org/doi/10.1091/mbc.E20-05-0310

237. Uzunova K, Dye BT, Schutz H, Ladurner R, Petzold G, Toyoda Y, et al. APC15 mediates CDC20 autoubiquitylation by APC/CMCC and disassembly of the mitotic checkpoint complex. Nat Struct Mol Biol [Internet]. 2012 Nov 24;19(11):1116–23. Available from: http://www.nature.com/articles/nsmb.2412

238. Jia L, Li B, Warrington RT, Hao X, Wang S, Yu H. Defining pathways of spindle checkpoint silencing: Functional redundancy between Cdc20 ubiquitination and p31 comet. Mol Biol Cell. 2011;22(22):4227–35.

239. Richeson K V., Bodrug T, Sackton KL, Yamaguchi M, Paulo JA, Gygi SP, et al. Paradoxical mitotic exit induced by a small molecule inhibitor of APC/CCdc20. Nat Chem Biol [Internet]. 2020; Available from: http://dx.doi.org/10.1038/s41589-020-0495-z

240. Densham RM, Morris JR. Moving Mountains—The BRCA1 Promotion of DNA Resection. Front Mol Biosci [Internet]. 2019 Sep 3;6. Available from: https://www.frontiersin.org/article/10.3389/fmolb.2019.00079/full

241. Setiaputra D, Durocher D. Shieldin – the protector of DNA ends. EMBO Rep. 2019 May 4;20(5).

242. Tipton AR, Wang K, Link L, Bellizzi JJ, Huang H, Yen T, et al. BUBR1 and closed MAD2 (C-MAD2) interact directly to assemble a functional mitotic checkpoint complex. J Biol Chem. 2011;286(24):21173–9.

243. Yun MY, Sang BK, Park S, Chul JH, Han YH, Sun HY, et al. Mutation analysis of p31 comet gene, a negative regulator of Mad2, in human hepatocellular carcinoma. Exp Mol Med. 2007;39(4):508–13.

244. Garber ME, Troyanskaya OG, Schluens K, Petersen S, Thaesler Z, Pacyna-Gengelbach M, et al. Diversity of gene expression in adenocarcinoma of the lung. Proc Natl Acad Sci [Internet]. 2001 Nov 20;98(24):13784–9. Available from: http://www.pnas.org/cgi/doi/10.1073/pnas.241500798

245. Bhattacharjee A, Richards WG, Staunton J, Li C, Monti S, Vasa P, et al. Classification of human lung carcinomas by mRNA expression profiling reveals distinct adenocarcinoma subclasses. Proc Natl Acad Sci [Internet]. 2001 Nov 20;98(24):13790–5. Available from: http://www.pnas.org/cgi/doi/10.1073/pnas.191502998

246. Curtis C, Shah SP, Chin S-F, Turashvili G, Rueda OM, Dunning MJ, et al. The genomic and

transcriptomic architecture of 2,000 breast tumours reveals novel subgroups. Nature [Internet]. 2012 Jun 18;486(7403):346–52. Available from: http://www.nature.com/articles/nature10983

247. Haqq C, Nosrati M, Sudilovsky D, Crothers J, Khodabakhsh D, Pulliam BL, et al. The gene expression signatures of melanoma progression. Proc Natl Acad Sci [Internet]. 2005 Apr 26;102(17):6092–7. Available from: http://www.pnas.org/cgi/doi/10.1073/pnas.0501564102

248. Riker AI, Enkemann SA, Fodstad O, Liu S, Ren S, Morris C, et al. The gene expression profiles of primary and metastatic melanoma yields a transition point of tumor progression and metastasis. BMC Med Genomics [Internet]. 2008 Dec 28;1(1):13. Available from: http://bmcmedgenomics.biomedcentral.com/articles/10.1186/1755-8794-1-13

249. Morrison C, Farrar W, Kneile J, Williams N, Liu-Stratton Y, Bakaletz A, et al. Molecular Classification of Parathyroid Neoplasia by Gene Expression Profiling. Am J Pathol [Internet]. 2004 Aug;165(2):565–76. Available from: https://linkinghub.elsevier.com/retrieve/pii/S0002944010633214

250. Sanchez-Carbayo M, Socci ND, Lozano J, Saint F, Cordon-Cardo C. Defining Molecular Profiles of Poor Outcome in Patients With Invasive Bladder Cancer Using Oligonucleotide Microarrays. J Clin Oncol [Internet]. 2006 Feb 10;24(5):778–89. Available from: http://ascopubs.org/doi/10.1200/JCO.2005.03.2375

251. Gutmann DH, Hedrick NM, Li J, Nagarajan R, Perry A, Watson MA. Comparative gene expression profile analysis of neurofibromatosis 1-associated and sporadic pilocytic astrocytomas. Cancer Res [Internet]. 2002 Apr 1;62(7):2085–91. Available from: http://www.ncbi.nlm.nih.gov/pubmed/11929829

252. Pyeon D, Newton MA, Lambert PF, den Boon JA, Sengupta S, Marsit CJ, et al. Fundamental Differences in Cell Cycle Deregulation in Human Papillomavirus-Positive and Human Papillomavirus-Negative Head/Neck and Cervical Cancers. Cancer Res [Internet]. 2007 May 15;67(10):4605–19. Available from: http://cancerres.aacrjournals.org/cgi/doi/10.1158/0008-5472.CAN-06-3619

253. Yusenko M V, Kuiper RP, Boethe T, Ljungberg B, van Kessel AG, Kovacs G. High-resolution DNA copy number and gene expression analyses distinguish chromophobe renal cell carcinomas and renal oncocytomas. BMC Cancer [Internet]. 2009 Dec 18;9(1):152. Available from: http://bmccancer.biomedcentral.com/articles/10.1186/1471-2407-9-152

254. Maia S, Haining WN, Ansén S, Xia Z, Armstrong SA, Seth NP, et al. Gene Expression Profiling Identifies BAX-δ as a Novel Tumor Antigen in Acute Lymphoblastic Leukemia. Cancer Res

[Internet]. 2005 Nov 1;65(21):10050–8. Available from: http://cancerres.aacrjournals.org/lookup/doi/10.1158/0008-5472.CAN-05-1574

255. Tomlins SA, Mehra R, Rhodes DR, Cao X, Wang L, Dhanasekaran SM, et al. Integrative molecular concept modeling of prostate cancer progression. Nat Genet [Internet]. 2007 Jan 17;39(1):41–51. Available from: http://www.nature.com/articles/ng1935

256. Quade BJ, Wang T-Y, Sornberger K, Cin PD, Mutter GL, Morton CC. Molecular pathogenesis of uterine smooth muscle tumors from transcriptional profiling. Genes, Chromosom Cancer [Internet]. 2004 Jun;40(2):97–108. Available from: http://doi.wiley.com/10.1002/gcc.20018

257. Iacobuzio-Donahue CA, Maitra A, Olsen M, Lowe AW, Van Heek NT, Rosty C, et al. Exploration of Global Gene Expression Patterns in Pancreatic Adenocarcinoma Using cDNA Microarrays. Am J Pathol [Internet]. 2003 Apr;162(4):1151–62. Available from: https://linkinghub.elsevier.com/retrieve/pii/S0002944010639119

258. Chandrashekar DS, Bashel B, Balasubramanya SAH, Creighton CJ, Ponce-Rodriguez I, Chakravarthi BVSK, et al. UALCAN: A Portal for Facilitating Tumor Subgroup Gene Expression and Survival Analyses. Neoplasia [Internet]. 2017 Aug;19(8):649–58. Available from: https://linkinghub.elsevier.com/retrieve/pii/S1476558617301793

259. Sarangi P, Clairmont CS, D'Andrea AD. Disassembly of the Shieldin Complex by TRIP13. Cell Cycle [Internet]. 2020 Jul 2;19(13):1565–75. Available from: https://www.tandfonline.com/doi/full/10.1080/15384101.2020.1758435

260. Schuyler SC, Wu Y-FO, Chen H-Y, Ding Y-S, Lin C-J, Chu Y-T, et al. Peptide inhibitors of the anaphase promoting-complex that cause sensitivity to microtubule poison. Bhattacharjya S, editor. PLoS One [Internet]. 2018 Jun 8;13(6):e0198930. Available from: https://dx.plos.org/10.1371/journal.pone.0198930

261. Miyong Y, Han YH, Sun HY, Hee YK, Kim BY, Ju YJ, et al. p31comet Induces cellular senescence through p21 accumulation and Mad2 disruption. Mol Cancer Res. 2009;7(3):371–82.

262. Shin HJ, Park ER, Yun SH, Kim SH, Jung WH, Woo SR, et al. P31comet-induced cell death is mediated by binding and inactivation of Mad2. PLoS One. 2015;10(11):1–17.

263. Wu D, Wang L, Yang Y, Huang J, Hu Y, Shu Y, et al. MAD2-p31comet axis deficiency reduces cell proliferation, migration and sensitivity of microtubule-interfering agents in glioma. Biochem Biophys Res Commun [Internet]. 2018;498(1):157–63. Available from: https://doi.org/10.1016/j.bbrc.2018.02.011

264. Kim BC, Yoo HJ, Lee HC, Kang K-A, Jung SH, Lee H-J, et al. Evaluation of premature senescence and senescence biomarkers in carcinoma cells and xenograft mice exposed to single or fractionated irradiation. Oncol Rep [Internet]. 2014 May;31(5):2229–35. Available from: https://www.spandidos-publications.com/10.3892/or.2014.3069

265. Schosserer M, Grillari J, Breitenbach M. The Dual Role of Cellular Senescence in Developing Tumors and Their Response to Cancer Therapy. Front Oncol [Internet]. 2017 Nov 23;7. Available from: http://journal.frontiersin.org/article/10.3389/fonc.2017.00278/full

266. Zanoni M, Pignatta S, Arienti C, Bonafè M, Tesei A. Anticancer drug discovery using multicellular tumor spheroid models. Expert Opin Drug Discov [Internet]. 2019 Mar 4;14(3):289–301. Available from: https://www.tandfonline.com/doi/full/10.1080/17460441.2019.1570129

267. Arrowsmith J, Miller P. Phase II and Phase III attrition rates 2011–2012. Nat Rev Drug Discov [Internet]. 2013 Aug 1;12(8):569–569. Available from: http://www.nature.com/articles/nrd4090

268. Teicher BA. Tumor models for efficacy determination. Mol Cancer Ther [Internet]. 2006 Oct;5(10):2435–43. Available from: http://mct.aacrjournals.org/lookup/doi/10.1158/1535-7163.MCT-06-0391

269. Zhong S, Jeong J-H, Chen Z, Chen Z, Luo J-L. Targeting Tumor Microenvironment by Small-Molecule Inhibitors. Transl Oncol [Internet]. 2020 Jan;13(1):57–69. Available from: https://linkinghub.elsevier.com/retrieve/pii/S1936523319304966

270. Jing X, Yang F, Shao C, Wei K, Xie M, Shen H, et al. Role of hypoxia in cancer therapy by regulating the tumor microenvironment. Mol Cancer [Internet]. 2019 Dec 11;18(1):157. Available from: https://molecular-cancer.biomedcentral.com/articles/10.1186/s12943-019-1089-9

271. Tesei A, Sarnelli A, Arienti C, Menghi E, Medri L, Gabucci E, et al. In vitro irradiation system for radiobiological experiments. Radiat Oncol [Internet]. 2013 Dec 1;8(1):257. Available from: https://ro-journal.biomedcentral.com/articles/10.1186/1748-717X-8-257

272. Zanoni M, Piccinini F, Arienti C, Zamagni A, Santi S, Polico R, et al. 3D tumor spheroid models for in vitro therapeutic screening: a systematic approach to enhance the biological relevance of data obtained. Sci Rep [Internet]. 2016 May 11;6(1):19103. Available from: http://www.nature.com/articles/srep19103

273. Ruan W, Lim HH, Surana U. Mapping Mitotic Death: Functional Integration of Mitochondria, Spindle Assembly Checkpoint and Apoptosis. Front Cell Dev Biol [Internet]. 2019 Jan 10;6. Available from: https://www.frontiersin.org/article/10.3389/fcell.2018.00177/full

274. Silva PMA, Ribeiro N, Lima RT, Andrade C, Diogo V, Teixeira J, et al. Suppression of spindly delays mitotic exit and exacerbates cell death response of cancer cells treated with low doses of paclitaxel. Cancer Lett. 2017;394(March):33–42.

275. Kang J, Yu H. Kinase Signaling in the Spindle Checkpoint. J Biol Chem [Internet]. 2009 Jun 5;284(23):15359–63. Available from: http://www.jbc.org/lookup/doi/10.1074/jbc.R900005200

276. Jordan MA, Wilson L. Microtubules as a target for anticancer drugs. Nat Rev Cancer [Internet]. 2004 Apr 1;4(4):253–65. Available from: http://linkinghub.elsevier.com/retrieve/pii/S0960982206015405

277. Ma HT, Chan YY, Chen X, On KF, Poon RYC. Depletion of p31 comet protein promotes sensitivity to antimitotic drugs. J Biol Chem. 2012;287(25):21561–9.

278. Sacristan C, Kops GJPL. Joined at the hip: Kinetochores, microtubules, and spindle assembly checkpoint signaling. Trends Cell Biol [Internet]. 2015;25(1):21–8. Available from: http://dx.doi.org/10.1016/j.tcb.2014.08.006

279. Mapelli M, Musacchio A. MAD contortions: conformational dimerization boosts spindle checkpoint signaling. Curr Opin Struct Biol. 2007;17(6):716–25.

280. Izawa D, Pines J. The mitotic checkpoint complex binds a second CDC20 to inhibit active APC/C. Nature. 2015;517(7536):631–4.

281. Haschka MD, Soratroi C, Kirschnek S, Häcker G, Hilbe R, Geley S, et al. The NOXA–MCL1–BIM axis defines lifespan on extended mitotic arrest. Nat Commun [Internet]. 2015 Nov 29;6(1):6891. Available from: http://www.nature.com/articles/ncomms7891

282. Wan L, Tan M, Yang J, Inuzuka H, Dai X, Wu T, et al. APCCdc20 Suppresses Apoptosis through Targeting Bim for Ubiquitination and Destruction. Dev Cell [Internet]. 2014 May;29(4):377–91. Available from: http://linkinghub.elsevier.com/retrieve/pii/S1534580714002421

283. Wang P, Lindsay J, Owens TW, Mularczyk EJ, Warwood S, Foster F, et al. Phosphorylation of the Proapoptotic BH3-Only Protein Bid Primes Mitochondria for Apoptosis during Mitotic Arrest. Cell Rep [Internet]. 2014 May;7(3):661–71. Available from: https://linkinghub.elsevier.com/retrieve/pii/S2211124714002472

284. Díaz-Martínez LA, Karamysheva ZN, Warrington R, Li B, Wei S, Xie X, et al. Genome-wide si RNA screen reveals coupling between mitotic apoptosis and adaptation . EMBO J. 2014;33(17):1960–76.

285. Marshall OJ. PerlPrimer: cross-platform, graphical primer design for standard, bisulphite and real-

time PCR. Bioinformatics [Internet]. 2004 Oct 12;20(15):2471–2. Available from: https://academic.oup.com/bioinformatics/article-lookup/doi/10.1093/bioinformatics/bth254

286. Cerella C, Muller F, Gaigneaux A, Radogna F, Viry E, Chateauvieux S, et al. Early downregulation of Mcl-1 regulates apoptosis triggered by cardiac glycoside UNBS1450. Cell Death Dis [Internet]. 2015 Jun 11;6(6):e1782–e1782. Available from: http://www.nature.com/articles/cddis2015134

287. Delbandi A-A, Mahmoudi M, Shervin A, Heidari S, Kolahdouz-Mohammadi R, Zarnani A-H. Evaluation of apoptosis and angiogenesis in ectopic and eutopic stromal cells of patients with endometriosis compared to non-endometriotic controls. BMC Womens Health [Internet]. 2020 Dec 6;20(1):3. Available from: https://bmcwomenshealth.biomedcentral.com/articles/10.1186/s12905-019-0865-4

288. Pagano F, Angelini F, Castaldo C, Picchio V, Messina E, Sciarretta S, et al. Normal versus Pathological Cardiac Fibroblast-Derived Extracellular Matrix Differentially Modulates Cardiosphere-Derived Cell Paracrine Properties and Commitment. Stem Cells Int [Internet]. 2017;2017:1–9. Available from: https://www.hindawi.com/journals/sci/2017/7396462/

289. Westhorpe FG, Tighe A, Lara-Gonzalez P, Taylor SS. p31comet-mediated extraction of Mad2 from the MCC promotes efficient mitotic exit. J Cell Sci [Internet]. 2011 Nov 15;124(22):3905–16. Available from: http://jcs.biologists.org/cgi/doi/10.1242/jcs.093286

290. Silva PMA, Tavares ÁA, Bousbaa H. Co-silencing of human Bub3 and dynein highlights an antagonistic relationship in regulating kinetochore-microtubule attachments. FEBS Lett. 2015;589(23):3588–94.

291. Zasadil LM, Andersen KA, Yeum D, Rocque GB, Wilke LG, Tevaarwerk AJ, et al. Cytotoxicity of Paclitaxel in Breast Cancer Is due to Chromosome Missegregation on Multipolar Spindles. Sci Transl Med [Internet]. 2014 Mar 26;6(229):229ra43-229ra43. Available from: https://stm.sciencemag.org/lookup/doi/10.1126/scitranslmed.3007965

292. Huisman C, Ferreira CG, Bröker LE, Rodriguez JA, Smit EF, Postmus PE, et al. Paclitaxel triggers cell death primarily via caspase-independent routes in the non-small cell lung cancer cell line NCI-H460. Clin Cancer Res. 2002;8(2):596–606.

293. Olaussen KA, Postel-Vinay S. Predictors of chemotherapy efficacy in non-small-cell lung cancer: A challenging landscape. Ann Oncol. 2016;27(11):2004–16.

294. Tse C, Shoemaker AR, Adickes J, Anderson MG, Chen J, Jin S, et al. ABT-263: A potent and orally bioavailable Bcl-2 family inhibitor. Cancer Res. 2008;68(9):3421–8.

295. Han B, Park D, Li R, Xie M, Owonikoko TK, Zhang G, et al. Small-Molecule Bcl2 BH4 Antagonist for Lung Cancer Therapy. Cancer Cell [Internet]. 2015 Jun;27(6):852–63. Available from: https://linkinghub.elsevier.com/retrieve/pii/S1535610815001439

296. Borgovan T, Bellistri J-PS, Slack KN, Kopelovich L, Desai M. Inhibition of BCL2 expression and activity increases H460 sensitivity to the growth inhibitory effects of polyphenon E. J Exp Ther Oncol [Internet]. 2009;8(2):129–144. Available from: https://www.ncbi.nlm.nih.gov/pmc/articles/PMC6361110/

297. Topham C, Tighe A, Ly P, Bennett A, Sloss O, Nelson L, et al. MYC Is a Major Determinant of Mitotic Cell Fate. Cancer Cell [Internet]. 2015;28(1):129–40. Available from: http://dx.doi.org/10.1016/j.ccell.2015.06.001

298. Serpico AF, Visconti R, Grieco D. Exploiting immune-dependent effects of microtubule-targeting agents to improve efficacy and tolerability of cancer treatment. Cell Death Dis [Internet]. 2020 May 12;11(5):361. Available from: http://www.nature.com/articles/s41419-020-2567-0

299. Mitchison TJ, Pineda J, Shi J, Florian S. Is inflammatory micronucleation the key to a successful anti-mitotic cancer drug? Open Biol [Internet]. 2017 Nov 15;7(11):170182. Available from: https://royalsocietypublishing.org/doi/10.1098/rsob.170182

300. Rudin CM, Hann CL, Garon EB, Ribeiro de Oliveira M, Bonomi PD, Camidge DR, et al. Phase II Study of Single-Agent Navitoclax (ABT-263) and Biomarker Correlates in Patients with Relapsed Small Cell Lung Cancer. Clin Cancer Res [Internet]. 2012 Jun 1;18(11):3163–9. Available from: http://clincancerres.aacrjournals.org/cgi/doi/10.1158/1078-0432.CCR-11-3090

301. Montero J, Letai A. Why do BCL-2 inhibitors work and where should we use them in the clinic? Cell Death Differ [Internet]. 2018 Jan 27;25(1):56–64. Available from: http://www.nature.com/articles/cdd2017183

302. Li Y, Zhou D, Xu S, Rao M, Zhang Z, Wu L, et al. DYRK1A suppression restrains Mcl-1 expression and sensitizes NSCLC cells to Bcl-2 inhibitors. Cancer Biol Med [Internet]. 2020;17(2):387–400. Available from: http://www.cancerbiomed.org/index.php/cocr/article/view/1607

303. On KF, Chen Y, Ma HT, Chow JPH, Poon RYC. Determinants of mitotic catastrophe on abrogation of the G2 DNA damage checkpoint by UCN-01. Mol Cancer Ther. 2011;10(5):784–94.

304. Bukowski K, Kciuk M, Kontek R. Mechanisms of Multidrug Resistance in Cancer Chemotherapy. Int J Mol Sci [Internet]. 2020 May 2;21(9):3233. Available from: https://www.mdpi.com/1422-0067/21/9/3233

305. Kops GJPL, Gassmann R. Crowning the Kinetochore: The Fibrous Corona in Chromosome Segregation. Trends Cell Biol [Internet]. 2020 Aug;30(8):653–67. Available from: https://linkinghub.elsevier.com/retrieve/pii/S0962892420300921

306. Dou Z, Prifti D, Gui P, Liu X, Elowe S, Yao X. Recent Progress on the Localization of the Spindle Assembly Checkpoint Machinery to Kinetochores. Cells [Internet]. 2019 Mar 23;8(3):278. Available from: https://www.mdpi.com/2073-4409/8/3/278

307. Caravita T, de Fabritiis P, Palumbo A, Amadori S, Boccadoro M. Bortezomib: efficacy comparisons in solid tumors and hematologic malignancies. Nat Clin Pract Oncol [Internet]. 2006 Jul;3(7):374–87. Available from: http://www.nature.com/articles/ncponc0555

308. Jackson RS, Placzek W, Fernandez A, Ziaee S, Chu C-Y, Wei J, et al. Sabutoclax, a Mcl-1 Antagonist, Inhibits Tumorigenesis in Transgenic Mouse and Human Xenograft Models of Prostate Cancer. Neoplasia [Internet]. 2012 Jul;14(7):656-IN24. Available from: http://linkinghub.elsevier.com/retrieve/pii/S1476558612800996

309. Ni D, Ding H, Liu S, Yue H, Bao Y, Wang Z, et al. Superior Intratumoral Penetration of Paclitaxel Nanodots Strengthens Tumor Restriction and Metastasis Prevention. Small [Internet]. 2015 Jun;11(21):2518–26. Available from: https://onlinelibrary.wiley.com/doi/10.1002/smll.201403632

310. Lee S-J, Lee H-A. Trends in the development of human stem cell-based non-animal drug testing models. Korean J Physiol Pharmacol [Internet]. 2020 Nov 1;24(6):441–52. Available from: http://www.kjpp.net/journal/view.html?doi=10.4196/kjpp.2020.24.6.441

311. Oltersdorf T, Elmore SW, Shoemaker AR, Armstrong RC, Augeri DJ, Belli BA, et al. An inhibitor of Bcl-2 family proteins induces regression of solid tumours. Nature [Internet]. 2005 Jun 15;435(7042):677–81. Available from: http://www.nature.com/articles/nature03579

312. Henriques AC, Silva PMA, Sarmento B, Bousbaa H. Antagonizing the spindle assembly checkpoint silencing enhances paclitaxel and Navitoclax-mediated apoptosis with distinct mechanistic. Sci Rep [Internet]. 2021;11(1):1–12. Available from: https://doi.org/10.1038/s41598-021-83743-7

313. Morgan RG, Chambers AC, Legge DN, Coles SJ, Greenhough A, Williams AC. Optimized delivery of siRNA into 3D tumor spheroid cultures in situ. Sci Rep [Internet]. 2018 Dec 21;8(1):7952. Available from: http://dx.doi.org/10.1038/s41598-018-26253-3

314. Gebhard C, Gabriel C, Walter I. Morphological and Immunohistochemical Characterization of Canine Osteosarcoma Spheroid Cell Cultures. Anat Histol Embryol [Internet]. 2016 Jun 19;45(3):219–30. Available from: https://onlinelibrary.wiley.com/doi/10.1111/ahe.12190

315. Kunz-Schughart LA, Freyer JP, Hofstaedter F, Ebner R. The Use of 3-D Cultures for High-Throughput Screening: The Multicellular Spheroid Model. J Biomol Screen [Internet]. 2004 Jun 1;9(4):273–85. Available from: http://journals.sagepub.com/doi/10.1177/1087057104265040

316. Al-Husaini K, Elkamel E, Han X, Chen P. Therapeutic potential of a cell penetrating peptide (CPP, NP1) mediated siRNA delivery: Evidence in 3D spheroids of colon cancer cells. Can J Chem Eng [Internet]. 2020 Jun 26;98(6):1240–54. Available from: https://onlinelibrary.wiley.com/doi/10.1002/cjce.23743

317. Xu J, Gu M, Hooi L, Toh TB, Thng DKH, Lim JJ, et al. Enhanced penetrative siRNA delivery by a nanodiamond drug delivery platform against hepatocellular carcinoma 3D models. Nanoscale [Internet]. 2021;13(38):16131–45. Available from: http://xlink.rsc.org/?DOI=D1NR03502A

318. CHEN X, WEI B, HAN X, ZHENG Z, HUANG J, LIU J, et al. LGR5 is required for the maintenance of spheroid-derived colon cancer stem cells. Int J Mol Med [Internet]. 2014 Jul;34(1):35–42. Available from: https://www.spandidos-publications.com/10.3892/ijmm.2014.1752

319. Min S, Choe C, Roh S. AQP3 Increases Intercellular Cohesion in NSCLC A549 Cell Spheroids through Exploratory Cell Protrusions. Int J Mol Sci [Internet]. 2021 Apr 20;22(8):4287. Available from: https://www.mdpi.com/1422-0067/22/8/4287

320. Wen J, Qiu N, Zhu Z, Bai P, Hu M, Qi W, et al. A size-shrinkable matrix metallopeptidase-2-sensitive delivery nanosystem improves the penetration of human programmed death-ligand 1 siRNA into lung-tumor spheroids. Drug Deliv [Internet]. 2021 Jan 1;28(1):1055–66. Available from: https://www.tandfonline.com/doi/full/10.1080/10717544.2021.1931560

321. Jiang T, Qiao Y, Ruan W, Zhang D, Yang Q, Wang G, et al. Cation-Free siRNA Micelles as Effective Drug Delivery Platform and Potent RNAi Nanomedicines for Glioblastoma Therapy. Adv Mater [Internet]. 2021 Nov 18;33(45):2104779. Available from: https://onlinelibrary.wiley.com/doi/10.1002/adma.202104779

322. Patel B V., Hotaling JM. Impact of chemotherapy on subsequent generations. Urol Oncol Semin Orig Investig [Internet]. 2020;38(1):10–3. Available from: https://doi.org/10.1016/j.urolonc.2019.02.011

323. Wei G, Wang Y, Yang G, Wang Y, Ju R. Recent progress in nanomedicine for enhanced cancer chemotherapy. Theranostics. 2021;11(13):6370–92.

324. Zhang J, Ye Z wei, Tew KD, Townsend DM. Cisplatin chemotherapy and renal function. In: Advances in Cancer Research [Internet]. 1st ed. Elsevier Inc.; 2021. p. 305–27. Available from:

http://dx.doi.org/10.1016/bs.acr.2021.03.008

325. Chow LQ. Head and neck cancer. N Engl J Med. 2020;382(1):60–72.

326. Johnson DE, Burtness B, Leemans CR, Lui VWY, Bauman JE, Grandis JR. Head and neck squamous cell carcinoma. Nat Rev Dis Prim [Internet]. 2020 Dec 26;6(1):92. Available from: http://www.nature.com/articles/s41572-020-00224-3

327. Alfouzan AF. Radiation therapy in head and neck cancer. Saudi Med J. 2021;42(3):247–54.

328. Bos T, Ratti JA, Harada H. Targeting Stress-Response Pathways and Therapeutic Resistance in Head and Neck Cancer. Front Oral Heal [Internet]. 2021 Jun 23;2. Available from: https://www.frontiersin.org/articles/10.3389/froh.2021.676643/full

329. Cheng Y, Li S, Gao L, Zhi K, Ren W. The Molecular Basis and Therapeutic Aspects of Cisplatin Resistance in Oral Squamous Cell Carcinoma. Front Oncol. 2021;11(October):1–16.

330. Chen F, Chandrashekar DS, Varambally S, Creighton CJ. Pan-cancer molecular subtypes revealed by mass-spectrometry-based proteomic characterization of more than 500 human cancers. Nat Commun [Internet]. 2019;10(1):1–15. Available from: http://dx.doi.org/10.1038/s41467-019-13528-0

331. Dey A, Varelas X, Guan K-L. Targeting the Hippo pathway in cancer, fibrosis, wound healing and regenerative medicine. Nat Rev Drug Discov [Internet]. 2020 Jul 17;19(7):480–94. Available from: http://www.nature.com/articles/s41573-020-0070-z

332. Rojo de la Vega M, Chapman E, Zhang DD. NRF2 and the Hallmarks of Cancer. Cancer Cell [Internet]. 2018 Jul;34(1):21–43. Available from: https://linkinghub.elsevier.com/retrieve/pii/S1535610818301272

333. Bachmann AS, Geerts D. Polyamine synthesis as a target of MYC oncogenes. J Biol Chem [Internet]. 2018 Nov;293(48):18757–69. Available from: https://linkinghub.elsevier.com/retrieve/pii/S0021925820311832

334. Murugan AK. mTOR: Role in cancer, metastasis and drug resistance. Semin Cancer Biol [Internet]. 2019 Dec;59:92–111. Available from: https://linkinghub.elsevier.com/retrieve/pii/S1044579X18301354

335. Ribeiro-Silva C, Vermeulen W, Lans H. SWI/SNF: Complex complexes in genome stability and cancer. DNA Repair (Amst) [Internet]. 2019 May;77:87–95. Available from: https://linkinghub.elsevier.com/retrieve/pii/S1568786418303057

336. Sciarrillo R, Wojtuszkiewicz A, Assaraf YG, Jansen G, Kaspers GJL, Giovannetti E, et al. The role of alternative splicing in cancer: From oncogenesis to drug resistance. Drug Resist Updat [Internet]. 2020 Dec;53:100728. Available from: https://linkinghub.elsevier.com/retrieve/pii/S1368764620300571

337. De Blasio A, Vento R, Di Fiore R. Mcl-1 targeting could be an intriguing perspective to cure cancer. J Cell Physiol [Internet]. 2018 Nov 24;233(11):8482–98. Available from: https://onlinelibrary.wiley.com/doi/10.1002/jcp.26786

338. Teixeira J, Silva P, Faria J, Ferreira I, Duarte P, Delgado M, et al. Clinicopathologic significance of BubR1 and Mad2 overexpression in oral cancer. Oral Dis [Internet]. 2015 Sep;21(6):713–20. Available from: https://onlinelibrary.wiley.com/doi/10.1111/odi.12335

339. Monteiro L, Silva P, Delgado L, Amaral B, Garcês F, Salazar F, et al. Expression of spindle assembly checkpoint proteins BubR1 and Mad2 expression as potential biomarkers of malignant transformation of oral leukoplakia: an observational cohort study. Med Oral Patol Oral y Cir Bucal [Internet]. 2021;e719–28. Available from: http://www.medicinaoral.com/medoralfree01/aop/24511.pdf

340. Banerjee R, Liu M, Bellile E, Schmitd LB, Goto M, Hutchinson M-KND, et al. Phosphorylation of TRIP13 at Y56 induces radiation resistance but sensitizes head and neck cancer to cetuximab. Mol Ther [Internet]. 2022 Jan;30(1):468–84. Available from: https://linkinghub.elsevier.com/retrieve/pii/S1525001621003154

APPENDIX

Supplementary table and figures

Movie legends

Supplementary tables

CHAPTER III. ANTAGONIZING THE SPINDLE ASSEMBLY CHECKPOINT SILENCING ENHANCES PACLITAXEL AND NAVITOCLAX MEDIATED APOPTOSIS WITH DISTINCT MECHANISTIC

Summplementary table S1. Primers used to test the amplification of the transcript variants 1 and 2 of p31^{comet}. Primers were designed using PerlPrimer Software v1.1.21.

Transcript variant	Primer sequence (5' →3')	Amplicon size (bp)
1	CTCTGCCTCAGTTTCTTCCC	174
	CCACTCCAAATCTATAATCTCAGC	
2	AGTCCCTGATTTGGAGTGGT	179
	GTAAACTGACAGCAGCCTTCC	

Supplementary figures

CHAPTER III. ANTAGONIZING THE SPINDLE ASSEMBLY CHECKPOINT SILENCING ENHANCES PACLITAXEL AND NAVITOCLAX MEDIATED APOPTOSIS WITH DISTINCT MECHANISTIC

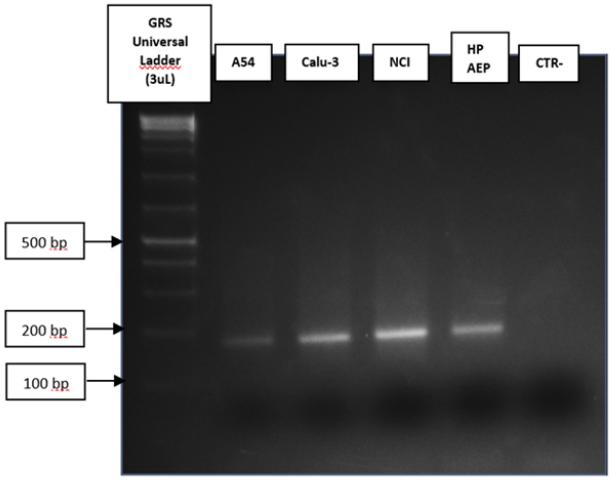

Supplementary figure S1. End-point PCR products resulting from the amplification with primers directed to the transcript variant 2, using an annealing temperature of 65 °C. Electrophoresis was performed in a 2 % agarose gel, at 120 V, 40 min.

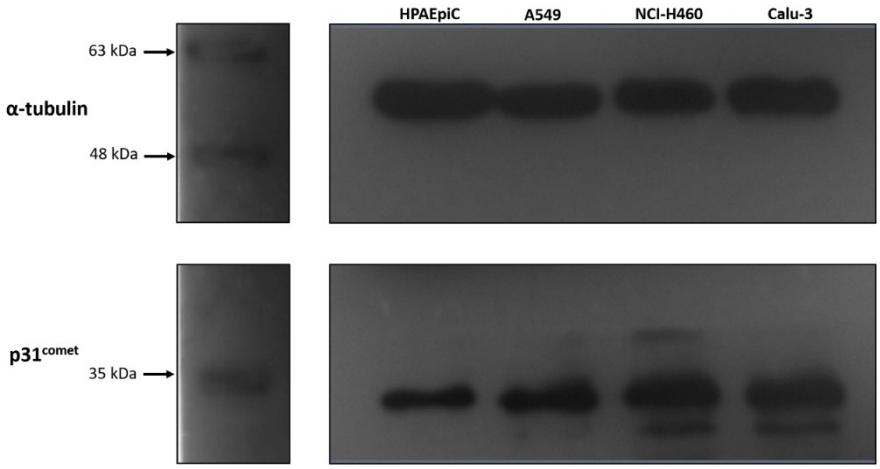

Supplementary Figure S2. Full-length blots of p31^{comet} expression in HPAEpiC, A549, NCI-H460, and Calu-3 cell lines. The two blots are from the same membrane but were separated to avoid oversaturation of tubulin signal, because α-tubulin needed short exposure time, while p31^{comet} protein needed a long exposure time

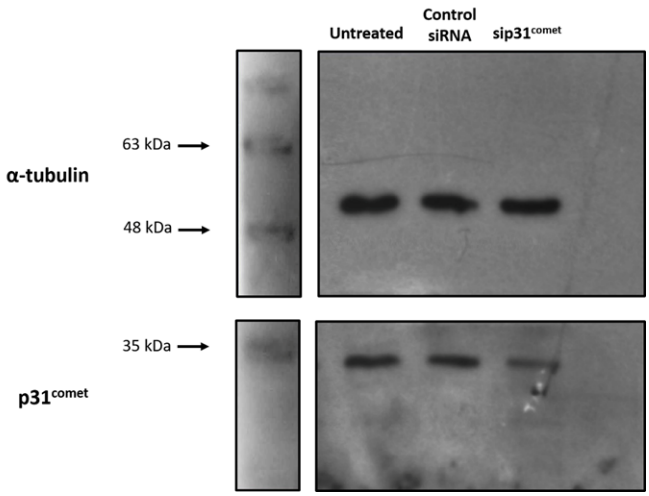

Supplementary Figure S3. Full-length blots of p31^{comet} siRNA-mediated knockdown in NCI-H460 cells. The two blots are from the same membrane but were separated to avoid oversaturation of tubulin signal, because α-tubulin needed short exposure time, while p31^{comet} protein needed a long exposure time

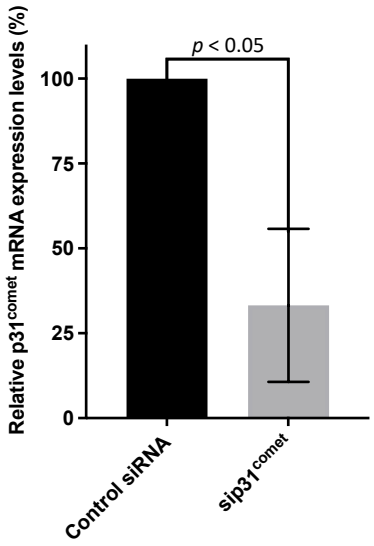

Supplementary figure S4. Relative expression of p31^{comet} mRNA in control siRNA and in sip31^{comet}-treated A549 cells, as determined by qRT-PCR. RNA was extracted 48 h after transfection. Statistical analysis was performed through the Student t-test. The error bars represent mean ± SD of three independent experiments.

Movie legends

CHAPTER III. ANTAGONIZING THE SPINDLE ASSEMBLY CHECKPOINT SILENCING ENHANCES PACLITAXEL AND NAVITOCLAX MEDIATED APOPTOSIS WITH DISTINCT MECHANISTIC

Movie 1. Time-lapse sequence (DIC microscopy) from Control siRNA transfected NCI-H460 cells, showing a 30-minute mitosis. Time is shown in hours:minutes.

Movie 2. Time-lapse sequence (DIC microscopy) from NCI-H460 cells treated with paclitaxel (10nM), showing a paclitaxel-treated cell spending 1 h and 30 min in mitosis. Time is shown in hours:minutes.

Movie 3. Time-lapse sequence (DIC microscopy) from sip31^{comet}-transfected NCI-H460 cells. A sip31^{comet}-transfected cell dies through PMD, and an increase of only 20 min in mitosis duration relative to the Control siRNA-treated cell is enough to trigger death. One of the daughter-cell survives and divides, but her daughter cells die after mitosis. Time is shown in hours:minutes.

Movie 4. Time-lapse sequence (DIC microscopy) from NCI-H460 cells treated with sip31^{comet} and paclitaxel (10nM). A cell treated with sip31^{comet} plus paclitaxel is trapped in mitosis and undergoes membrane blebbing after 5 h. Time is shown in hours:minutes.

Movie 5. Time-lapse sequence (DIC microscopy) from NCI-H460 cells treated with Navitoclax (3.5 μM). A Navitoclax-treated cell spends the same time in mitosis as the Control siRNA-treated cell (30 min), and the first daughter cell (1) dies 23 h after division. Time is shown in hours:minutes

Movie 6. Time-lapse sequence (DIC microscopy) from NCI-H460 cells treated with sip31^{comet} and Navitoclax (3.5 μM). A cell spends only 30 min in mitosis (20 min less than the cell only transfected with sip31^{comet}), and both the daughter-cells die approximately 2 h after cell division, 21 h or 11 h less than cells individually treated with Navitoclax or sip31^{comet}, respectively. Time is shown in hours: minutes.